

**OBJECT-BASED CLASSIFICATION  
USING MULTI-RESOLUTION IMAGE  
FUSION**

**A THESIS**

**Submitted to the Delhi Technological University  
for the award of the degree of**

**DOCTOR OF PHILOSOPHY  
in  
CIVIL ENGINEERING**

**by**

**RUBEENA**

**(2K13/PHDCE/03)**



**DEPARTMENT OF CIVIL ENGINEERING  
DELHI TECHNOLOGICAL UNIVERSITY  
DELHI-110042 (INDIA)**

**OCTOBER, 2019**

**COPYRIGHT NOTICE**

**© DELHI TECHNOLOGICAL UNIVERSITY-2019**

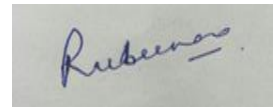
**ALL RIGHTS RESERVED**

## ***Declaration***

I hereby declare that this Ph.D thesis entitled “**Object-based classification using multi-resolution image fusion**” was carried out by me for the degree of Doctor of Philosophy under the supervision of Dr. K.C.Tiwari, Professor, Department of Civil Engineering, Delhi Technological University (D.T.U) Delhi.

This thesis is a presentation of my original research work. Wherever contributions of others are involved, every effort has been made to indicate this clearly.

For the present thesis, which I am submitting to the University, no degree or diploma has been conferred on me before, either in this or in any other University.



**Rubeena**  
Research Scholar  
(2K13/PHDCE/03)  
Delhi Technological University

**DELHI TECHNOLOGICAL UNIVERSITY**  
(Formerly Delhi College of Engineering)  
Shahbad Daultapur, Bawana Road, Delhi-110042, India



*Certificate*

This is to certify that the thesis entitled “Object based classification using multi-resolution image fusion ” submitted to the Delhi Technological University, Delhi-110042, in fulfilment of the requirement for the award of the degree of **Doctor of Philosophy** by the candidate **RUBEENA**, (Reg. No.: 2K13/PHDCE/03) under the supervision of **Prof. K.C. Tiwari**. It is further certified that the work embodied in this thesis has neither partially nor fully submitted to any other university or institution for the award of any degree or diploma.

**Prof. K.C. Tiwari**  
(Supervisor)  
Professor, Civil Engineering  
Delhi Technological University

**Prof. Nirendra Dev**  
Head of the Department, Civil Engineering  
Delhi Technological University

## *Acknowledgements*

First, *thanks to the Almighty*, for it is he who disposes what we record as our achievements. May *the Almighty* be with everyone in their human endeavours. I owe a deep sense of gratitude to his *All-Pervading Spirit* whose *Divine Light* provided me the perseverance, guidance, inspiration, faith and strength to carry on even when the going was tough.

This thesis is the result of continuous four years of research work after the finalization of the research objectives in June 2015 during my SRC in Civil Engineering Department, Delhi Technological University, New Delhi. Throughout this journey, I have been accompanied and supported by many people. I am elated that I now have the opportunity to express my gratitude towards all of them.

I would like to express my gratitude to my supervisor *Dr. K.C. Tiwari* for his proficient guidance and continued encouragement for the fulfillment of the research work. With great pleasure, I express my heartfelt gratitude for his valuable advice, fruitful discussions, numerous suggestions, constructive criticism, and constant support throughout the period of my research.

I gratefully acknowledge the unceasing support provided by *Civil Engineering Department* and *Post-Graduation Ph.D Section* of Delhi Technological University, Delhi. I would like to thank *my Fellow Researchers of Multi-Disciplinary Centre of Geoinformatics*, Delhi Technological University, Delhi who have always been the source of motivation during my research work.

I lay my indebtedness to my current organisation where I am working, *Bharati Vidyapeeth's College of Engineering (BVCOE)*, New Delhi for exhibiting a faith in me and supporting me throughout the process of carrying out my research work along with my professional responsibilities in the organisation. I owe my deep sense of gratitude to *HOD-*

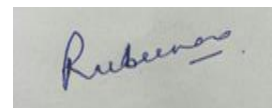
*ECE and all Professors of BVCOE, New Delhi* for their help during the entire period of my research.

I express my sincere thanks to all my research colleagues from different research areas who have always supported and helped me in clearing my doubts and assisting me in my research work whenever required. I owe my thanks to *Dr. Mona Aggarwal (Associate Prof. at North Campus University, New Delhi)* and several others for their help.

For my research work, I have used two data sets – one from IEEE GRSS Contest (2014), which is a multisensory data and another is AVIRIS-NG Hyperspectral data. Under a campaign, ISRO in conjunction with NASA captured the aerial AVIRIS-NG hyperspectral data. I acknowledge both the organizations for the data sets that have been used for research work.

My sincerest, heartfelt gratitude also goes to *my son Rudra Vohra, my husband, my mother, my father, my sister, my brother-in-law and my in-laws* who never complained about the time that I could not spend with them. I am also indebted to my relatives and friends for their sincere prayers, constant encouragement and blessings.

Finally, I thank all those who helped and supported me. Thank you so much!

A rectangular box containing a handwritten signature in blue ink that reads "Rubeena".

**Date:** 29-7-20

**(Rubeena)**

**Place:** New Delhi

## ***Abstract***

Multisource remote sensing data has recently gained much greater attention of researchers for urban land-cover classification because it is increasingly being realized that the complimentary characteristics of different types of remote sensing data can significantly enhance and aid the identification of natural and man-made objects in an urban landscape. However while on one hand, it improves the classification accuracy, on the other, it also increases the data volume including noise, redundant information and uncertainty between the datasets. Therefore, it is essential to extract selected input features and combine them from the multisource data to achieve the highest possible classification accuracy. The other challenging tasks while dealing with multisource data are the development of the data processing and classification techniques to exploit the advantages of multisource data sets. The objective of this thesis is to improve the urban land-cover classification process by using multisource remote sensing data and exploring various spectral and spatial features with recent image processing and classification algorithms and techniques for improvement in classification accuracy of urban land cover objects.

This work proposes a methodological approach for classifying natural (*i.e.*, vegetation, trees and soil) and man-made (*i.e.*, buildings and roads) objects using multisource datasets (*i.e.*, Long Wave Infrared (LWIR) Hyperspectral and High Spatial Resolution Visible RGB data). The spatial, spectral and spatial-structural features, such as textural (*i.e.*, contrast and homogeneity), Normalized Difference Vegetation Index (NDVI), Morphological Building Index (MBI) are extracted and incorporated on the connected components of each class under the category of natural and man-made objects. The feature knowledge set formed consisting of different domains of spectral and spatial attributes are trained and tested using one-against-one Support Vector Machine (SVM) classifier network. The decisions of the classifier network are finalized using fusion technique *i.e.*, majority vote contributed by each feature set. The results

obtained from the classification approach using decision level fusion show that majority vote by NDVI feature in SVM classifier network has contributed in achieving good confidence measures for classes, building (100%), vegetation (91.6%), soil (91%) and road (79.3%). From these results, it may be inferred that NDVI feature gives better results for almost all classes. Since, NDVI is calculated using mean spectral information of thermal bands from hyperspectral data and red bands from VIS RGB data, therefore, the mean spectral information from the thermal hyperspectral bands can be explored for studying the natural and man-made objects in urban land-cover. Also, the feature level fusion of multisource datasets *i.e.*, the fusion of long wave thermal bands from hyperspectral data and red bands from very high resolution visible RGB data has resulted in achieving good classification accuracy of objects in an urban area.

A decision level strategy has also been derived using the combination of textural, NDVI and MBI features using weighted majority voting fusion technique to enhance the classification results of natural and man-made objects. The comparative analysis of decision level fusion of each feature set and the combination of all features reveal that the overall confidence measure of the classified objects has improved from 57.1% to 98.2% (for all classes except for building). Hence, it is seen that the proposed weighted majority voting strategy of combined spectral and spatial features derived from multisensory data improves the classification accuracy of urban land-cover objects.

The capabilities of non-parametric classifiers, such as Artificial Neural Network (ANN) and Support Vector Machine (SVM), have been investigated using LWIR and Visible RGB data with the methodological approach derived using spectral and spatial features and decision level fusion strategy. The results have shown that SVM classifier network gives better generalisation results than ANN for identification of natural and man-made objects. The



statistics obtained show that in comparison to neural networks, SVM requires less training data for a decent performance.

This research also explores the benefit of using wide range hyperspectral data *i.e.*, Airborne Visible/Infrared Imaging Spectrometer-Next Generation (AVIRIS-NG). The spectral channels of hyperspectral data ranging from 325-nm to 2500-nm have been investigated for extracting the useful wavelengths for forming the spectral indices which in turn can be used for identifying the components /constituents of natural and man-made objects of an urban area. The Optimum Index Factor (OIF) is computed by evaluating different standard deviation and correlation values. The wavelength values for which the best OIF is obtained are selected to form the spectral indices. Various spectral indices (namely, Normalised Difference Vegetation Index (NDVI), Infrared Percentage Vegetation Index (IPVI), Difference Vegetation Index (DVI)-wavelengths (in nanometers-1077.65, 666.94), Normalised Difference Building Index (NDBI)-wavelengths (in nanometers-1788.88, 892.33), Normalised Difference Soil Index (NDSI)-wavelengths (in nanometers-1763.84, 396.47), Clay Mineral Index-wavelengths (in nanometers-2164.54, 1713.75) have been formulated by using the significant wavelengths derived from OIF. Two indices, namely Clay Mineral Index and NDBI have resulted in significantly improving the classification of components/constituents in soil (*i.e.*, Producers' Accuracy of Arid Soil-92.13% and Non-Arid Soil-93.84%) and man-built (*i.e.*, Producers' Accuracy of Concrete -83.41% and Asphalt-93.09%) structures.

Besides, the research also focuses on improving the classification accuracy of linearly structured man-made object *i.e.*, roads in an urban area by exploring the spatial shape attributes using a very high spatial resolution VIS RGB data. A new approach has been proposed in for calculating the spatial shape features. The results have shown that it is beneficial to study the pixel shape features which can be extended to object level in order to improve the classification accuracy. The classification accuracy achieved through this study for class "road" is 97.3%

which is the enhanced in comparison to the results achieved so far with other experiments in this research work.

Several important conclusions have been drawn from this study regarding improvement in classification accuracy of urban objects and certain new approaches for the same have been recommended. The study also gives suggestions for undertaking future research in certain areas such as for exploring more number of spatial structural features in identifying man made features and use of combination of spectral and spatial features in identification of subclasses or different levels of classification in natural and man-made objects in an urban environment.

# *Table of Contents*

<b>Declaration</b>	i
<b>Certificate</b>	ii
<b>Acknowledgements</b>	iii
<b>Abstract</b>	v
<b>Table of Contents</b>	ix
<b>List of Publications</b>	xiv
<b>List of Figures</b>	xv
<b>List of Tables</b>	xviii
<b>List of Abbreviations</b>	xxi

## **CHAPTER 1- OBJECT-BASED CLASSIFICATION USING** 1-23

### **REMOTE SENSING DATA**

1.1	Motivation	01
1.2	Introduction to Remote Sensing	03
1.2.1	Remote Sensing Data Acquisition	04
1.2.2	Elements of Digital Image Processing	07
1.3	Remote Sensing Data and Object-Based Urban Land-Cover Classification	09
1.3.1	Issues of High-Resolution Remote Sensing Data For Urban Land-Cover Classification	12
1.4	Fusion Strategy in Classification Task	14
1.5	Research Gaps	18
1.6	Research Objectives	19
1.7	Organization of Thesis	21

## **CHAPTER 2- BACKGROUND INFORMATION** 24-51

2.1	Image Analysis	24
2.2	Segmentation of Image Objects-Connected Component Analysis	26
2.2.1	Bounding Box	28
2.3	Feature Extraction	29
2.3.1	Feature Extraction in Spectral Domain for Hyperspectral Image	30

2.3.1.1	Band Ratios	31
2.3.1.2	Normalised Difference Vegetation Index	32
2.3.2	Feature Extraction in Spatial Domain- High-Resolution Multispectral Image	34
2.3.2.1	Textural Analysis	34
2.3.2.2	Gray Level Cooccurrence Matrix and Two-Order Statistical Parameters	35
2.3.3	Shape Features	37
2.3.3.1	Pixel Shape Index	37
2.3.4	Feature Extraction in Spectral-Spatial Domain-High-Resolution Multispectral Image	39
2.3.4.1	Morphological Building Index	40
2.4	Classification	41
2.4.1	Classification Techniques	42
2.4.1.1	Support Vector Machine	44
2.4.1.2	Artificial Neural Network	46
2.4.1.3	Spectral Angle Mapper	49
2.4.1.4	Spectral Information Divergence	50
<b>CHAPTER 3- DATA SETS</b>		<b>52-60</b>
3.1	General	52
3.2	Data Set-1: Longwave Infrared Hyperspectral And Visible RGB Data	52
3.2.1	Acquisition and Characteristics of Data Set-1	53
3.3	Data Set-2: AVIRIS-NG Hyperspectral Data	55
3.3.1	Acquisition of Data	56
3.3.2	Characteristics of Data Set-2	57
3.3.3	Ground Data Collection	59
<b>CHAPTER 4- THERMAL INFRARED HYPERSPECTRAL AND VIS RGB DATA FOR EXTRACTION OF NATURAL AND MAN-MADE OBJECTS</b>		<b>61-91</b>
4.1	Introduction to the Problem	61
4.2	Experimental Data Set	66

4.3	Methodology	67
4.3.1	Charateristics of Images in Data Set-1	67
4.3.2	Choice of Feature Extraction	69
4.3.2.1	Spectral Feature Set	69
4.3.2.2	Spectral-Structural Feature Set	70
4.3.2.3	Spatial Feature	72
4.3.3	Segmentation	72
4.3.4	Classifier Network	73
4.4	Implementation	74
4.5	Results and Discussions	77
4.5.1	Spectral-Spatial Feature Extraction	77
4.5.2	Regions of Interest	81
4.5.3	Connected Component Analysis and Bounding Box	82
4.5.4	Extraction of Features Knowledge Database in Bounding Box	82
4.5.5	Resizing Bounding Box and Generation of Training and Testing Samples	83
4.5.6	SVM Classifier	84
4.5.7	Decision Level Fusion on Multi-class SVM Classifier	86
4.5.8	Classification Map	89
4.6	Summary	90

**CHAPTER 5- CLASSIFICATION OF NATURAL AND MAN MADE** 92-108

**OBJECTS USING WEIGHTED MAJORITY VOTING FUSION**

5.1	Introduction to the Problem	92
5.2	Experimental Data Set	95
5.3	Theoretical Modelling	96
5.3.1	Majority Voting Rule	97
5.3.2	Weighted Majority Voting	98
5.4	Methodology and Implementation	98
5.4.1	Fusion Strategy	100
5.4.1.1	Stage1-Multiclass binary SVMs decision using individual features	101
5.4.1.2	Stage2-Proposed strategy of multiclass binary SVMs decision using combined features	102

5.5	Results and Discussions	104
5.6	Summary	107
<b>CHAPTER 6- LAND-COVER CLASSIFICATION USING</b>		109-125
<b>NON-PARAMETRIC CLASSIFIERS IN MULTISENSORY IMAGES</b>		
6.1	Introduction to the Problem	109
6.2	Experimental Data Set	114
6.3	Methodology and Implementation	114
	6.3.1 Artificial Neural Network	116
6.4	Results and Discussions	119
	6.4.1 Desigh Parameters-LM-ANN	120
	6.4.2 Design Parameters-Support Vector Machine	120
6.5	Summary	125
<b>CHAPTER 7- IDENTIFICATION OF OPTIMAL SPECTRAL WAVELENGTHS</b>		126-148
<b>FOR CLASSIFICATION OF LAND FEATURES</b>		
<b>USING HYPERSPECTRAL IMAGERY</b>		
7.1	Introduction to the Problem	126
7.2	Experimental Data Set	130
7.3	Theoretical Background	131
	7.3.1 Spectral indices for depicting the features of natural class: Water	132
	7.3.2 Spectral indices for depicting features of natural class: Barren land	133
	7.3.3 Spectral indices for depicting features of natural class: Vegetation	134
	7.3.4 Spectral indices for depicting features of natural class: Geological Minerals	135
	7.3.5 Spectral indices for depicting features of man-built class: Developed Land and Impervious Surfaces	136
7.4	Methodology and Implementation	137
	7.4.1 Implementation Steps of Methodological Approach	138
	7.4.1.1 Pre-processing of the Data Set	138
	7.4.1.2 Spectral Indices Development from Field Spectroscopy Data	139
	7.4.1.3 Training and Validation Data	140
	7.4.1.4 SVM classifier network	140
7.5	Results and Discussions	141

7.6	Summary	146
<b>CHAPTER 8- SPATIAL SHAPE DESCRIPTORS FOR IDENTIFICATION</b>		<b>149-172</b>
<b>OF LINEAR OBJECTS IN AN URBAN AREA USING</b>		
<b>HIGH SPATIAL RESOLUTION IMAGERY</b>		
8.1	Introduction to the Problem	149
8.2	Experimental Data Set	152
8.3	Theoretical Background	152
8.3.1	Homogeneity analysis in spatial domain	152
8.3.2	Spatial shape feature	153
8.3.3	Gray level co-occurrence matrix	153
8.4	Methodology and Implementation	154
8.4.1	Experiment I-Influence of Parameters of Spatial Shape Features) on Bounding Box of Connected Regions	156
8.4.2	Experiment II-To Compare the Classification Accuracy Obtained From Different Spatial and Spectral Features using Different Classifiers	162
8.5	Results and Discussions	162
8.5.1	Experiment I-SVM classification of engineered objects using spatial shape features on bounding box of connected regions	163
8.5.2	Experiment II-Compare the Classification Accuracy Obtained from Different Spatial and Spectral Features using Different Classifiers	166
8.6	Summary	171
<b>CHAPTER 9- CONCLUSIONS AND MAJOR CONTRIBUTIONS</b>		<b>173-180</b>
9.1	General	173
9.2	Objectives	173
9.3	Overview of Methodology	174
9.4	Conclusions	175
9.5	Major Contributions	178
9.6	Recommendations	179
9.7	Further Work	180
<b>References</b>		<b>182</b>
<b>Web References</b>		<b>189</b>
<b>Appendix I-IV</b>		
<b>Brief Biodata of the Author</b>		

## ***List of Publications***

### **A. International Journals**

- Rubeena Vohra & K.C.Tiwari (2017), “Object based Classification using Multisensor Data Fusion and Support Vector Algorithm”, International Journal of Image and Data Fusion, Taylor and Francis, DOI: 10.1080/19479832.2017.1372524.
- Rubeena Vohra & K.C.Tiwari (2019), “Spatial Shape Feature Descriptors in Classification of Engineered Objects Using High Spatial Resolution Remote Sensing Data”, Evolving Systems, Springer, DOI: 10.1007/s12530-019-09275-8.
- Rubeena Vohra & K.C.Tiwari (2015), “A Review and Assessment of Fusion Algorithms on Gray Scale Images International Journal of Electronics, Electrical and Computational System, IJEECS, Volume 4.

### **B. Communicated Research Work in International Journals**

- Rubeena Vohra & K.C.Tiwari, “Comparative Analysis of SVM and ANN Classifiers using Multilevel Fusion of Multi-Sensor data in Urban Land Classification”, Sensing and Imaging, Springer.
- Rubeena Vohra & K.C.Tiwari, “Multisensory Data Fusion for Urban Land Classification”, Special Issue for Recent Patents of Computer Science”, Bentham Publications.

### **C. International Conference**

- Rubeena Vohra & K.C.Tiwari (2016), “Multisensor Multiresolution Data Fusion for Improvement in Classification”, Multispectral, Hyperspectral, and Ultraspectral Remote Sensing Technology, Techniques and Applications VI, Proc. of SPIE Vol. 9880, 2016 SPIE, DOI: 10.1117/12.2222164.



## *List of Figures*

<b>Figure No.</b>	<b>Title</b>	<b>Page No.</b>
1.1	Remote sensing systems for data acquisition	05
1.2	Two aspects of classification of remote sensing data	09
1.3	Hyperspectral data cube showing spectral variability	14
1.4	Mixed Pixels	15
1.5	Organization of thesis	23
2.1	Image analysis for object-based feature extraction classification	25
2.2	Pixel connectivity	26
2.3	Connected component analysis	27
2.4	Bounding box coordinates	28
2.5	NDVI range for object identification	33
2.6	Spectral curves of vegetation, soil, and water	33
2.7	Classification of remote sensing data	41
2.8	Concept of SVM hyperplane	45
2.9	Simple neural network	47
2.10	Feedforward Network	48
2.11	Feedback Network	48
2.12	Spectral angle mapping	50
3.1	Area of Thetford Mines, Canada	53

3.2	Data Set-1: Thermal hyperspectral and VIS RGB data	54
3.3	Major components of the AVIRIS-NG airborne flight package	56
3.4	AVIRIS – NG Sensor	57
3.5	Data Set-2: RGB display of AIRIS-NG hyperspectral data, Udaipur	58
4.1	Hyperspectral and Multispectral Data	66
4.2	Spectral response curve	68
4.3	Flowchart of object-based classification using LWIR HS and VIS RGB data	76
4.4	False color composite image of NDVI spectral Index	78
4.5	MBI Image	79
4.6	Regions of interest polygons of natural and man-made objects	81
4.7	Classification maps for natural and man-made objects	90
5.1	Structure of multiclass classifier fusion	99
5.2	Structure of Stage II - Fusion strategy	104
6.1	Parameters for study on two non-parametric classifiers	115
6.2	Flowline of the implementation steps	116
6.3	State diagram (Training) – LM Algorithm	119
7.1	Subset of the original AVIRIS-NG data	131
7.2	Implementation of the methodological approach	141
7.3	Spectral index images	143
7.4	Sub-division classified map of soil	144
7.5	Sub-division classified map of materials in man-built structures	145

8.1	VIS RGB imagery	152
8.2	Flowline of the experiment conducted	155
8.3	Flowchart for depicting connected regions	156
8.4	Direction lines	158
8.5	Flowchart for shape and size features calculation	159
8.6	Dividing 25x25 bounding box in 5x5 boxes/windows	160
8.7	Directions for feature computation	160
8.8	Flowchart for classification	161
8.9	Classification map of engineered objects <i>i.e.</i> , buildings and roads generated using spatial shape features	165
8.10	Classification map of engineered objects <i>i.e.</i> , buildings and roads using textural features	168
8.11	Classification map of engineered objects <i>i.e.</i> , buildings and roads using mean spectra	169
8.12	Classification map of engineered objects <i>i.e.</i> , buildings and roads using mean spectra	169

## *List of Tables*

<b>Table No.</b>	<b>Title</b>	<b>Page No.</b>
1.1	Characteristics of sensors	06
1.2	Classification of imaging systems in terms of spatial resolution	06
1.3	Classification of imaging systems in terms of spectral resolution	06
2.1	Various tasks performed through image analysis	25
2.2	Eight elements of image interpretation	29
2.3	Techniques of texture analysis	35
2.4	Second order statistical texture features	36
2.5	A taxonomy of remote sensing image classification techniques	43-44
3.1	Categorization of land-cover classes	55
3.2	Meta data information of AVIRIS-NG HIS	58-59
4.1	Summary of data set-1	66-67
4.2	Subset of MBI Matrix	80
4.3	Total number of pixels in each class of natural and man-made objects	82
4.4	Total number of connected components in each class of natural and man-made objects	82
4.5	Total number of training and testing bounding boxes for each class	83
4.6	Feature size for training and testing samples for each class	84
4.7	Confidence measure of one class against another class using NDVI feature	85
4.8	Confidence measure of one class against another class using MBI feature	85

4.9	Confidence measure of one class against another class using Textural feature	86
4.10	Confidence measure of natural and man-made objects by decision level fusion of SVM classifiers using NDVI, MBI and Textural features	87
5.1	Structure of Stage I- Multiclass SVM classifier network	102
5.2	Confidence measure of SVM classifier network for natural and man-made objects using weighted majority voting fusion strategy	105
6.1	Dimensions of LM ANN based on NDVI, MBI and Textural Features	120
6.2	SVM classifier results using majority voting fusion on spectral and spatial features	121
6.3	ANN classifier results using majority voting fusion on spectral and spatial features	122
6.4	Comparative assessment of classification accuracy of natural and man-made objects	122
7.1	Level-wise categorization of natural and man-built class features	132
7.2	Spectral indices for computing features of water at different categorization level	133
7.3	Spectral Indices for computing features of barren land at different categorization level	134
7.4	Spectral Indices for computing features of natural vegetation at different categorization level	135
7.5	Geologically important wavelength regions in EM spectrum	136
7.6	Spectral Indices for computing features of minerals	136
7.7	Spectral Indices for computing features of man built-up features at different categorization level	137
7.8	Informative spectral bands and OIFs	142
7.9	Total number of pixels for sub-classes	143

7.10	Training and Testing Samples	144
7.11	Classification accuracy of sub-classes obtained from Clay Mineral Index and NDBI	145
8.1	Calculation of correctly predicted objects <i>wrt</i> threshold	164
8.2	Training and testing samples	164
8.3	Training and testing SSF	165
8.4	Design parameters of SVM for spatial shape features	165
8.5	Accuracy assessment for spatial shape features	166
8.6	Training and testing textural features	167
8.7	Design parameters of SVM for textural features	168
8.8	Accuracy Assessment of Spectral Classifiers	170
8.9	Classification Accuracy of Spatial and Spectral Features	170

## *List of Abbreviations*

ANN	Artificial Neural Network
AVIRIS-NG	Airborne Visible/Infrared Imaging Spectrometer
BAEI	Built-Up Extraction Index
CCA	Connected Component Analysis
CRF	Conditional Random Field
DAIS	Digital Airborne Imaging System
DEM	Digital Elevation Model
DL	Direction Line
DMP	Differential Morphological Profile
DVI	Difference Vegetation Index
EM	ElectroMagnetic
ENVI	Environment for Visualizing Images
FOV	Field-Of-View
FTS	Fourier Transform Spectrometer
GLCM	Gray Level Co-occurrence Matrix
GRVI	Green Ratio Vegetation Index
GSD	Ground Sampling Data
HS	Hyperspectral
HYSI	Hyperspectral Imaging
IFOV	Instantaneous Field-Of -View

IPVI	Infrared Percentage Vegetation Index
ISODATA	Iterative Self-Organizing Data Analysis Technique
ISRO	Indian Space Research Organization
LDA	Linear Discriminant Analysis
Landsat OLI	Landsat Operational Land Imager
LULC	Land Use Land Cover
LWEA	Length-Width Extraction Algorithm
LWIR	Long Wave Infrared
MCS	Multiple Classifier Systems
MDC	Minimum Distance Classifier
MBI	Morphological Building Index
MIR	Middle Infrared
MLC	Minimum Likelihood Classifier
MNDWI	Modified Normalised Difference Water Index
MNF	Minimum Noise Fraction
MNLI	Modified Non-Linear Index
MRF	Markov Random Field
MP	Morphological Profile
MS	Multispectral
MSRSI	Multi-Spectral Remote Sensing Imagery
MV	Majority Voting



NASA	National Aeronautics and Space Administration
NBAI	Normalized Built-Up Area Index
NDBI	Normalized Difference Built-Up Index
NDCI	Normalized Difference Clay Index
NDISI	Normalized Difference Impervious Surface Index
NDMI	Normalized Difference Moisture Index
NDSI	Normalized Difference Snow Index
NDVI	Normalized Difference Vegetation Index
NDWI	Normalized Difference Water Index
NIR	Near-Infrared
OA	Overall Accuracy
OBC	On-Board Calibrator
OBIA	Object-based Image Analysis
OIF	Optimum Index Factor
OSAVI	Optimized Soil Adjusted Vegetation Index
PA	Producer's Accuracy
PAN	Panchromatic
PCA	Principal Component Analysis
PSI	Pixel Shape Index
QP	Quadratic Programming
ROI	Regions of Interest

RDVI	Renormalized Difference Vegetation Index
RS	Remote Sensing
RSI	Remote Sensing Imagery
SAM	Spectral Angle Mapper
SAR	Synthetic Aperture Radar
SAVI	Soil Adjusted Vegetation Index
SID	Spectral Information Divergence
SE	Structuring Element
SOM	Self-Organizing Map
SRCI	Simple Ratio Clay Index
SSF	Spatial Shape Features
SVM	Support Vector Machine
SWIR	Short Wave Infrared
TIR	Thermal Infrared
UA	User's Accuracy
VIS	Visible
VHR	Very High Resolution
VNIR	Visible and Near Infrared
WMV	Weighted Majority Voting
W-TH	White Top-Hat



# *Chapter 1*

## *Object-Based Classification Using*

### *Remote Sensing Data*

#### **1.1 Motivation**

Ever since the advent of satellite technology, remote sensing has grown in leaps and bounds simultaneously keeping pace with the development in sensor technology. Today, these integrated technologies equip us with the capability to remotely acquire information about the ground surface and study various Earth features and phenomena occurring on it such as water, soil, minerals, agriculture, urban growth and various other geographical features and phenomena. Remote sensing and its associated technologies, with its humble beginnings in traditional surveying, has over last 150 years transformed itself significantly and emerged as a very powerful tool for studying the Earth's surface. The advancement in these technologies and the immense potential that it offers has motivated the researchers to exploit these technologies and gain greater insights into it for the benefit of the mankind.

One of the major issues affecting mankind and its continued progression as well survival on planet Earth today is the growth in urbanisation that has led to various environmental and climatic changes. Land-cover planning and management using remotely sensed images has therefore become a very helpful tool in identification and classification of various features of the urban land surfaces. In many studies, high spectral resolution data has been explored for classification of land features in urban environment. The high spectral resolution data is largely characterised by the radiance parameters captured from different land-covers in a large number of bands of the electromagnetic spectrum. Many a times, it may not have an optimal spatial resolution, therefore, it may be inadequate for a specific identification and classification task despite of its good spectral resolution. On the

other hand, in a high spatial resolution remote sensing data, while geometric features can easily get recognized but shadow of various land features and the spatial adjacencies between the features may lead to ambiguities and lower the classification accuracy.

A lot of work has been reported in literature in identification and classification of physical features of land surfaces using multispectral remote sensing data, but uncertainty still exists on many issues such as the use of single source remote sensing data, handling of ambiguities that may arise due to spatial adjacencies between the various land cover features, tall trees and buildings or spectral similarities shown by many land-covers feature etc. Though, the classification of urban land features has been well investigated and adequately reported in the literature there still exists a lot of scope for exploring multisource remote sensing data, exploiting radiation spectrum other than visible spectrum, and also the combination of spatial and spectral features for improved classification accuracy. Several advanced image processing techniques are also being explored for enhancing the classification accuracies in estimation of urban land cover features.

Similarly, while all types of remote sensing data such as Panchromatic (PAN), Multispectral (MS) and Hyperspectral (HS) data are suitable for urban land feature classification, all of them have their advantages and limitations. Most physical urban land-cover features either show similar spectral radiance or are combination of mixed pixels, therefore the classification of land features becomes difficult to be handled by low resolution or single source remote sensing data, it may require either data with fine spatial resolution or data with high spectral resolution. The desired data may not always be available and where available, there may be a requirement of analytical tools to facilitate urban land cover feature classification. For example, hyperspectral data is known to be rich in information content due to its high spectral resolution but traditional classification algorithms using hyperspectral data are still under different stages of investigations. The

classification unit in the algorithms are either pixels or a group of pixels and in practice, most land-cover features are known to exhibit either spectral or spatial similarity. Therefore, there is a requirement of exploring efficient ways of handling the hyperspectral data for urban land feature classification. Similarly, while most land features occurring on land surface may now get captured in different electromagnetic spectrums simultaneously and the information is available in wider range, yet classification algorithms deal with the spectral range information for land cover features separately and this may lead to lower classification accuracy. The issue again merits investigation.

Remote sensing data may be useful in classification of various physical features on urban land surfaces. For example, the idea of combining the multisource remote sensing data seems to strengthen the urban land-cover classification. Similarly, long wave infra-red thermal hyperspectral data may possibly aid in detection of natural and man-made land features. There, however, appears limited indigenous effort in exploitation of spectral and spatial features from multisource airborne and satellite based remote sensing data. The motivation of this research originates from an urge to explore some of these possibilities discussed here.

## **1.2 Introduction to Remote Sensing**

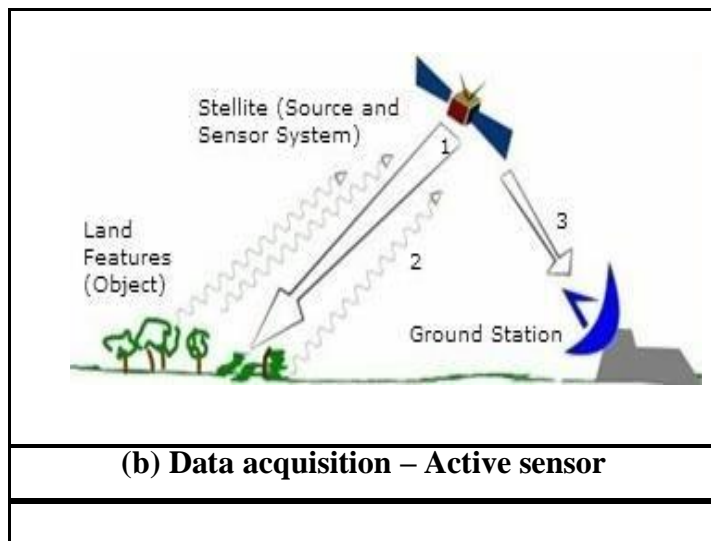
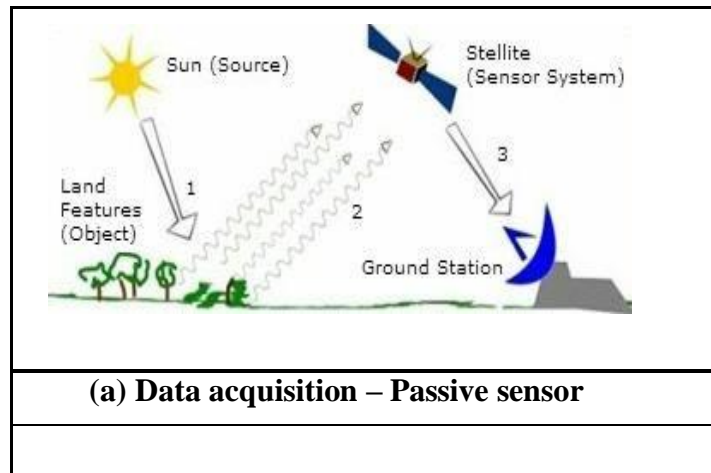
Remote sensing plays a vital role in field of surveying as it provides the on-site information of the objects on Earth's surface from the distance that can be well analysed and interpreted for various applications [1,2]. In field surveying, it is necessary to visit different locations on the ground in order to capture the on-site information of any object area which now-a-days seems time consuming and impractical. Even the traditional methods that are being used in field surveying for capturing the information seem to be

impractical and inefficient. Hence, the use of remote sensing data appears to be attractive as it makes the whole process faster and accurate [3].

During the last decade, the advent in space borne sensor technologies have created a possibility of acquiring very high-resolution remote sensing images. These technologies have provided an improved spatial resolution data which lies in the range of 4-m to 1.65-m for multispectral band and from 1-m to sub meters (0.41-m) for panchromatic band [4]. Also, the airborne sensors are now capable of simultaneously providing color and infrared images at a resolution of up to 2-cm. The multi-sensor MS and HS remote sensing imagery with finer spatial and spectral resolution can be well explored for various applications.

### **1.2.1 Remote Sensing Data Acquisition**

Remote sensing is the science and art which involves the acquisition of remote sensing data and understanding it for extracting the relevant information. The acquisition of data in an appropriate wavelength range is highly important for extracting the information of various objects on the ground. Most objects on ground reflect a part of the electromagnetic energy radiated towards it from the sun or emit some energy due to their own temperatures [5]. The remote sensing sensors that are classified as passive and active sensors record the information about an object by measuring the electromagnetic energy in the form of reflectance or emittance. The data acquisition by the remote sensing sensors is illustrated in Figure-1.1.



**Figure 1.1 – Remote sensing systems for data acquisition**

The extraction of information using remote sensing data depends upon sensor resolution which is described broadly in four domains *i.e.*, spatial, spectral, radiometric and temporal [6]. The characteristics of these four types of sensor resolutions are explained in Table-1.1[7]. These resolutions are characterised by the sensors deployed on the platform for capturing the wavelength bands of the objects of interest on ground. Certain salient details of sensors based on spatial and spectral resolutions are given in Table-1.2 and Table-1.3 [7,8].



**Table 1.1 - Characteristics of sensors**

<b>Types of Resolution</b>	<b>Explanation</b>
Spectral resolution	Represents the wavelength interval acquired by panchromatic/multi-spectral or hyper-spectral sensor. Narrow wavelength range of a channel or band symbolizes better spectral resolution.
Radiometric resolution	Illustrates the potential of the sensor to discriminate the slightest differences in the energy. The more the sensitivity of detecting the reflected or emitted energy differences, the finer is the radiometric resolution.
Spatial resolution	The area/region of the Earth is represented by the number of pixels deployed to detect the size of the smallest possible feature.
Temporal resolution	Represents the repeated observations over the surface of Earth with respect to the time interval between consequent observations.

**Table 1.2 - Classification of imaging systems in terms of spatial resolution**

<b>Types of Imaging Systems</b>	<b>Range of Spatial Resolution</b>
Low resolution sensor	Nearly 1-km or more
Medium resolution sensor	Nearly 100-m to 1-km
High resolution sensor	Nearly 5-m to 100-m
Very-high resolution sensor	Nearly 5-m or less

**Table 1.3 - Classification of imaging systems in terms of spectral resolution**

<b>Types of Imaging Systems</b>	<b>Number of Spectral Bands</b>
Optical imaging sensors (including electromagnetic ranges in visible, near infrared, and shortwave infrared regions)	Panchromatic (1-band) – IKONOS PAN, SPOT PAN <i>etc.</i> Multispectral (3-10 bands)– Landsat TM, IKONOS MS
Thermal imaging sensors	<i>etc.</i> Hyperspectral (100s or 1000s)– MODIS, MERIS
Synthetic Aperture Radar (SAR) imaging system	Radarsat (C-band), Terra SAR (X-band)

### 1.2.2 Digital Image Processing

Several algorithms and methodologies are continuously being evolved to extract information of Earth's objects recorded by the remote sensing sensors in least possible time with as high accuracy as possible. Most research-oriented applications related to the fields of defence, agriculture, environment, intelligence, commerce *etc.* rely on the appropriate and effective interpretation of remote sensing data. The interpretation and analysis of remote sensing data for extracting land features *i.e.*, natural and man-made objects is largely facilitated by digital image processing techniques and algorithms. The abstraction of information about the objects includes the recognition and computation of the interested objects in an area of an image. There exist two leading methods for extracting and deciphering the information about the objects of interest from remote sensing imageries [7],

- (i) **Visual Comprehension:** The identification of natural and man-made objects performed by humans is mainly based on the knowledge of feature tone (color), repetitive patterns, shape and structure, texture and appearance, shadow and association of the objects in an image.
- (ii) **Digital Image Processing and its Interpretation:** The analysis of remote sensing data is computer-aided, and the algorithms are used to enhance information from the data. This is also used to assess and correct the image, automate the process of identification of objects, extract the useful information, to delineate and categorize different land-cover features in an image. Thus, for the analysis of data, particularly, for classification of urban land-cover, there exist four basic domains, where image processing tools can be applied,
  - (a) Pre-processing

- (b) Image Enrichment
- (c) Image Transformation
- (d) Image Classification and Analysis

The analysis of remote sensing data for urban land-cover classification requires pre-processing functions in its initial stage. It includes the corrections in the distortions that may occur due to imaging conditions. Though, some correction procedures are done after the data collection, before handling it to the user. These procedures include radiometric and geometric corrections in the captured data. The radiometric corrections are done in the situation where there is a requirement of correcting uneven sensor response. The geometric corrections are done to correct the geometric distortions that arises due to the rotation of the Earth which leads to different orientations and different imaging conditions due to different viewing angles (such as oblique viewing) [8]. At few stages in the analysis, the need for enhancing the image becomes necessary. This is done using image enhancement techniques that translates the information of original imagery for better interpretation in either spectral domain for quality spectral feature extraction or in spatial domain to extract features such as edges and boundaries [9]. Next is image transformation, that involves the processing of data simultaneously from multiple spectral bands. The purpose of this transformation is highly applicable in hyperspectral data. The image transformation techniques help in lowering the dimensional burden (*i.e.*, the number of bands) in the data. This leads to the compression of the information in the original bands and highlights the information into fewer useful bands. Finally, after these stages the remotely sensed MS/HS data is quantitatively analysed for categorizing the individual pixels or group of pixels considered as objects to certain identifiable class. The classification of remotely sensed MS/HS data is performed using classification algorithms based on supervised and unsupervised learning procedures [10]. The idea is to classify the unknown samples or

objects in an image as per the algorithm rules. Once the classification is done, it is necessary to assess the performance in terms of accuracy measurements. This is done by registering the groupings on the classified images with that of known regions of interest or ground samples. The result of the analysis may consist of classification maps (or images), statistics or a report.

### 1.3 Object-Based Urban Land-Cover Classification

Amongst many applications, classification of various urban land-cover objects using remote sensing data is highly in demand, though, the classification of land-cover objects is one of the most difficult tasks. This is because of the complex arrangements in land-cover types and the diversity of natural and man-built structures like various vegetation or buildings, roads and pavements in urban areas. Land-cover classification aims at distinguishing the urban objects, materials and vegetation in complex and diverse pattern of an urban area. The classification unit for analysis is either pixel-based or object-based, hence, the classification in remote sensing imagery can either be carried as pixel-based approach or object-based approach. The classification scheme of both approaches is shown below in Figure-1.2.

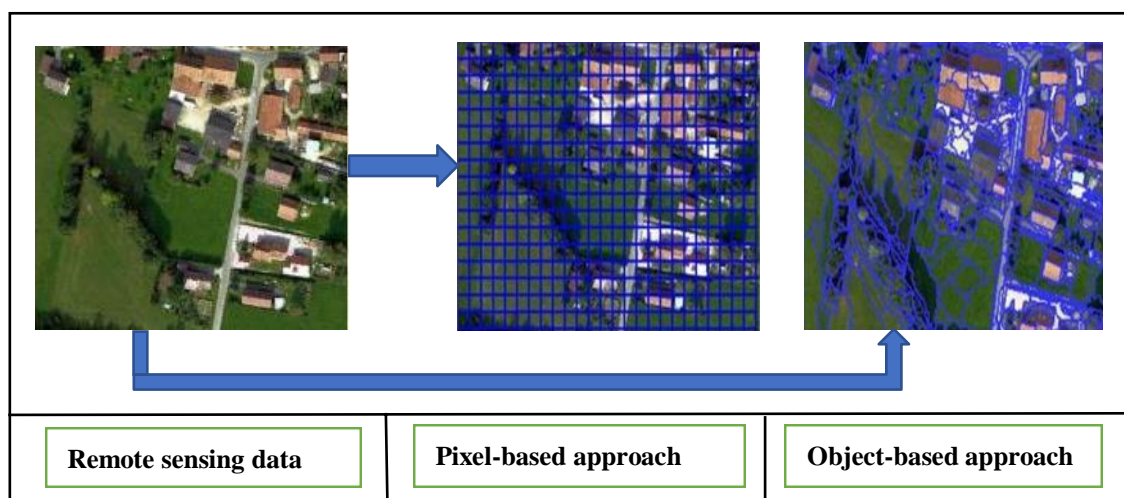


Figure 1.2- Two aspects of classification of remote sensing data

In general, pixel-based approach assigns each pixel to a class based on the digital values of each band. The pixel-based approach is largely used as it is conceptually simpler and computationally faster. This approach got the popularity due to its applicability in many LANDSAT imageries [11]. The data has medium spectral and low spatial resolution and it is largely characterised by its spectral properties only. The limitation of pixel-based approach is that it makes use of only one element of image interpretation and therefore, leads to within class spectral variations and this lowers the classification accuracy of complex land features such as buildings and roads. In object-based approach, pixels are grouped together and are characterised by the spatial properties which contribute as the complimentary information to the spectral observations and thus improve the classification accuracy [12]. Since, urban land surface is amalgamation of impervious surfaces *i.e.*, artificial cover and structures such as pavement, roads, buildings, residential and industrial hubs which are constructed from concrete, stone and other man-made impenetrable materials and types of vegetation, therefore, it seems significant to study and interpret the objects on the land surfaces from remote sensing data using object-based approach.

Traditional pixel-based image classification approach creates square classified pixels. These have been found to produce low classification accuracies particularly in applications related to urban areas [13]. Object-based image classification is very different from traditional pixel-based classification as object-based approach creates objects of dissimilar shape and scale [14]. This approach groups the homogeneous pixels which forms the “image objects”, the process is popularly known as multi-resolution segmentation. The information about the object can be obtained at different scales from an image simultaneously. The objects by this manner appear to convey more meaningful information than the traditional pixel-based segmentation approach as objects can now be classified based on spatial information extracted from object’s texture, shape, and geometry. Multi-

resolution segmentation and classification using object-based image analysis (OBIA) assist the use of multiple bands in an image [15]. This means that texture, elevation or existing shape attributes can altogether be computed from multiple bands that have contextual relationship with each other to classify image objects. This context may appear as in proximity in pixel intensities, neighbourhood relationships, and distance between layers *etc.* [16]. From literature, it is seen that OBIA techniques perform better as compared to pixel-based approaches for land-cover classification using high-resolution remote sensing imagery [15].

An object-based classification approach is superior to pixel-based approach and can contribute significantly in improving the classification accuracy for many reasons as given below,

- (i) The conceptual categorization of image objects in an image is similar in a way as done by the humans. Hence, the comprehension of the partitioned land-cover features is easier to understand as it matches closely to human interpretations [17];
- (ii) The approach allows to investigate the use of spatial features in addition to spectral features. Image objects makes use of textural statistics and contextual properties with the neighbouring objects to form the spatial features. It also enables the use of shape and geometric features (*e.g.* shape, size and geo-morphology) for extracting the information [18,19]; and
- (iii) The classification of image objects may be combined at distinct abstraction levels (*i.e.* different scales) and these levels can be used to represent contextual relationship at multiple bands in an analysis system [20].

The advantages of using object-based classification approach have been demonstrated in many previous research studies [21-28]. The discussion of few studies is presented here, [26] adopted OBIA for classifying urban land-cover features in Wuhan City, China, from high-spatial resolution imagery with spatial resolution of 2.4-m and four MS bands using multi-feature and multi-scale segmentation technique. The experimental results show satisfactory delineation of urban roads, buildings, woods, farmland and waters in an image. In [18], vegetation classification was performed using object-based features on an image acquired by Digital Airborne Imaging System (DAIS). The imagery has four MS bands with high spatial resolution of 1-m. The airborne data consists of an area at National Seashore Park in northern California, USA. The experimental results demonstrated that the use of object-based classification approach overcame the problem of the salt-and-pepper effects that are found in the classification results obtained from traditional pixel-based classification approaches and thus improves the classification accuracy. In [28], a study of mapping large-scale vegetation communities of Dunedin City, New Zealand is performed using IKONOS imagery by object-based classification approach. The experimental results demonstrate the feasibility of extracting ecologically significant classes using the object-based approach. Although, the approach does not provide the detail mapping of an area as generated by interpreting the aerial photographs manually. But the results confirm that the object-based approach is an efficient way to generate precise classified maps.

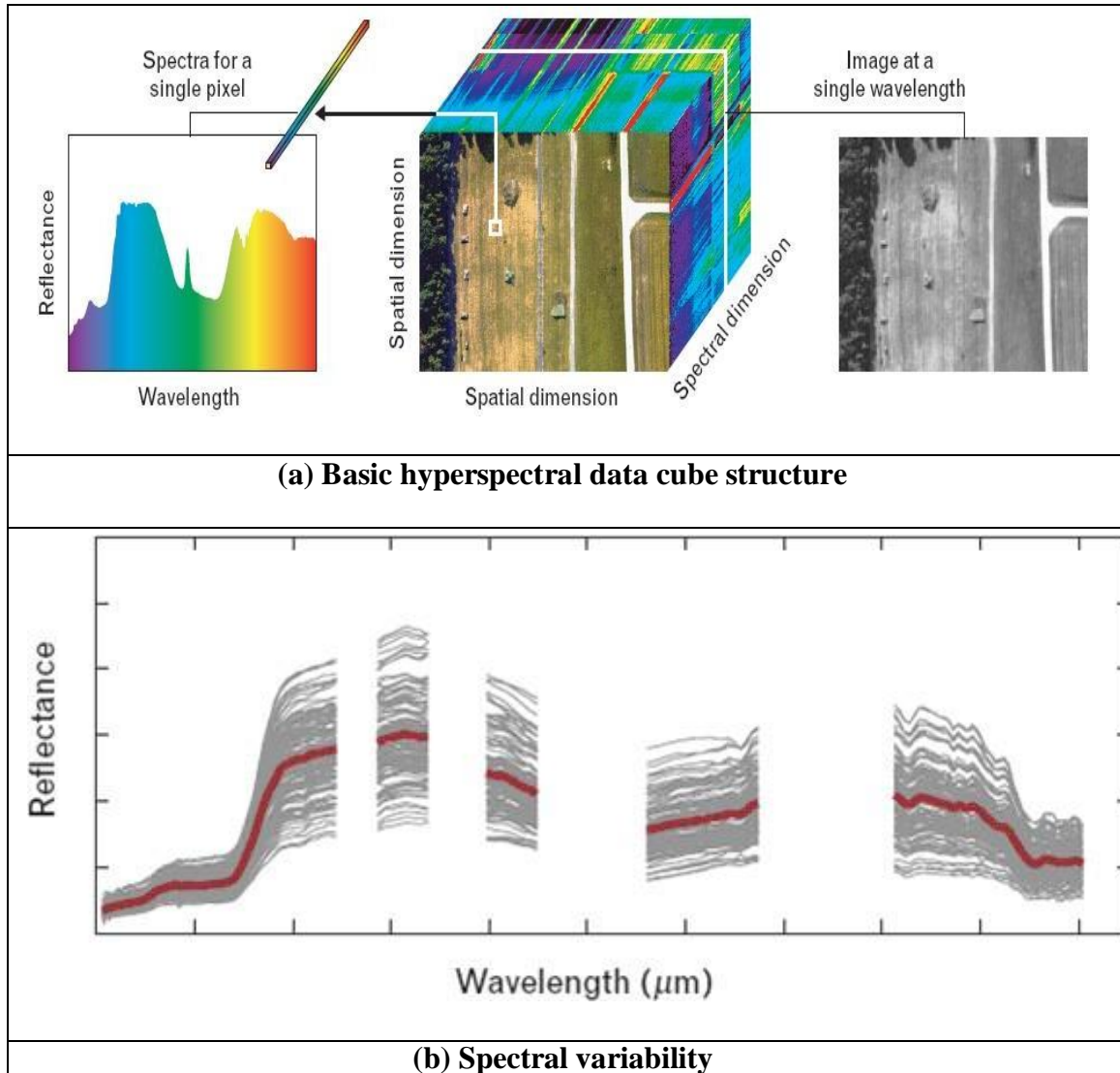
### **1.3.1 Issues of High-Resolution RS Data for Urban Land-Cover Classification**

In the past, coarse spectral resolution data often failed to classify several objects and materials of interest on the surface of the earth. Hyperspectral sensors can image the Earth's surface in hundreds of narrow contiguous spectral bands and are rich in information

content due to which these are now increasingly being advocated for classifying land-cover objects in an urban area [29,30].

Although, the data captured by hyperspectral sensors can detect various objects of urban land-cover, there are few major challenges. The processing of hyperspectral data involves high computational complexity due to high data dimensionality and redundancy. This requires use of appropriate dimensionality reduction techniques via feature extraction, namely, Linear Discriminant Analysis (LDA) and Principal Component Analysis (PCA). The other challenge relates to the spectral behaviour exhibited by various materials and objects under complex pattern of an urban area. In optical remote sensing, the reflectance from a given object in different bands constitutes its spectra. Most traditional classification algorithms are based on exploiting the target spectra of various objects. However, the spectrum of any material of an object is never found to be same even in laboratory conditions [31,32]. This variation in the spectra is referred to as spectral variability. Figure-1.3 (a) [32] provides an illustration of a basic hyperspectral data cube with the number of spectral bands shown along z-axis. Most objects in nature are known to have varying reflectance's in different spectral bands known as spectral variability. Figure-1.3 (b) [32] illustrates spectral variability. The reasons for this variability may be atmospheric interference as well as the environment and illumination conditions. Therefore, conversion of radiance to reflectance is an important step in spectral analysis in optical remote sensing, particularly in hyperspectral images.

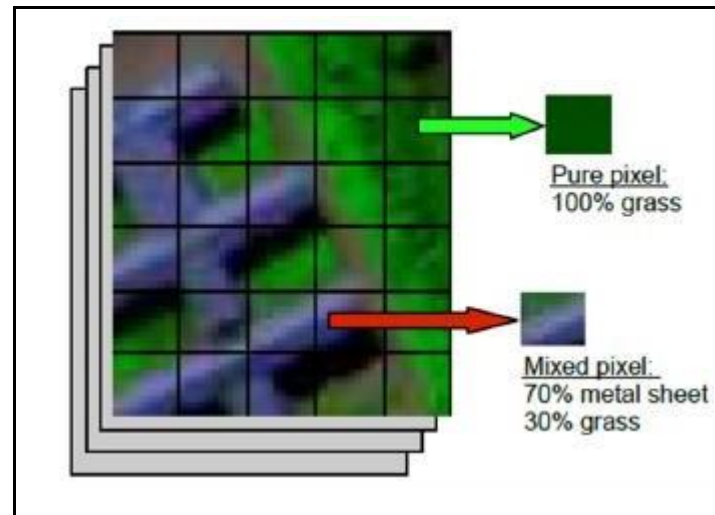




**Figure 1.3 – Hyperspectral data cube showing spectral variability [32]**

Although high resolution hyperspectral data provides better spectral resolution, but the spatial resolution simultaneously may not be equally high. The use of spatial data is highly important in urban land-cover classification as it signifies the positional characteristics and defines the size, structure and shape of an object (such as road, pavement, building, water bodies *etc.*) on Earth’s surface. The relatively low spatial resolution data can lead to the challenging problem of mixed pixels in classification. The illustration of mixed pixels in urban land-cover classification is shown in Figure-1.4 [33]. The low spatial resolution data leads to inevitable loss of information because several land-

cover objects tend to fall in same pixel which results in inaccurate mapping of objects in an urban area [33]. Also, even if the spatial resolution is high, a hyperspectral image generally shows a combination of pure and mixed pixels.



**Figure 1.4 – Mixed Pixel**

Besides, in case of high spatial resolution multispectral data, the issues related with the mixed pixels are largely reduced but the lower spectral information leads to spectral confusion among different land-cover objects such as buildings, roads, pedestrians *etc.* as they show similar spectral characteristics and this lead to lower classification accuracy. Due to the shadows from tall buildings or from tree crowns the information of many objects get occluded and the lower spectral values of the actual land-cover objects result in inaccuracies in land-cover classification. Despite these issues, the use of traditional pixel-based spectral classifiers for land-cover classification often leads to high spatial frequency noises as in this approach each pixel is designated to a class individually [34].

From the discussion presented, it is evident that usually, because of technical constraints or cost considerations, remote sensing imaging systems can either provide high spectral resolution data associated with a low spatial resolution or vice versa. Hence, the analysis of multiresolution and multi-sensor remote sensing imagery needs to be explored

altogether for achieving higher classification accuracy in an urban environment. The analysis can be encouraged by exploring spatial as well as spectral characteristics of high-resolution multispectral and hyperspectral remote sensing imagery simultaneously for extracting objects in an urban area for classification. Further, the object-based classification algorithms can be used for better understanding and interpretation of various land-cover objects.

#### **1.4 Fusion Strategy in Classification Task**

The spectral or spatial features extracted from the remote sensing data aid in obtaining information of natural and man-made objects, but they alone might be insufficient to obtain reliable classification results in an urban environment. Instead, the combination of characteristics derived from spectral and spatial domain from multiple sources can contribute to a comprehensive interpretation of the land-cover objects [35,36]. As explained earlier in the text that from hyperspectral data the information from spectral signatures are extracted for classifying the objects. The differentiation of man-made objects based on spectral information that consists of the same material (*e.g.* buildings and roads) may become difficult to assess, while that may be easily distinguished by exploring their linear structure geometry properties. On the other hand, spatial features obtained from a high spatial resolution data alone may fail to discriminate the objects that are quite heterogeneous in nature (*e.g.* grass field and swimming pool) but they exhibit similar geometry. Hence, fusion techniques can be used to improve the classification accuracies in such cases. These techniques involve the combination of spectral and spatial properties from multi-sensor data [36]. This can be achieved by extracting the features either from each individual feature space and then concatenating them into one vector space for classification. Although this technique seems to be simple, but it sometimes creates several problems and using a single feature may give an impression of giving better information.

It happens so because many a times the feature vector space consists of different feature analytical values and therefore, makes the concatenated feature vector space unbalanced. Hence, the representation of information contained by different feature vector space makes the analysis of the data difficult. By concatenating the feature vector space, there are chances of redundancy of information which results in ambiguous decisions. Also, the computational burden may increase due to the dimensionality of concatenated feature vector space. It is evident that though fusion techniques enrich the information content, but efficient handling of data is still an issue and requires detailed analysis while exploring it for remote sensing data.

The fusion of different spatial and spectral resolution data sets has been widely investigated in the literature [e.g.37,38]. The fusion techniques in remote sensing are carried at three different levels,

- (i) At observation level, the most popular advantage of using fusion technique is it results in Pan-Sharpening. It includes merging of high-resolution Panchromatic (PAN) image with low resolution MS image to produce high resolution MS image. A review of such fusion techniques can be found in [39].
- (ii) Feature level fusion techniques demonstrated in [40-42] shows the effects of combining the features from different sources for classification. In [41], a Conditional Random Field (CRF) model is proposed for detection of buildings using In-SAR and orthophoto features.
- (iii) At decision level as demonstrated in [43], different classifiers maps are merged to obtain the accurate information of heterogeneous data sets.

The type of remote sensing fusion technique used is highly application dependent and depends on the type of the datasets involved. A deep insight is desired for exploring the potential of remote sensing and image processing techniques with high spectral and spatial

resolution images in identification/classification task of complex morphological associated areas such as urban areas, heterogeneous vegetated areas or agricultural areas.

## **1.5 Research Gaps**

The present study proposes to address several research gaps identified through extensive literature survey. Following point-wise discussion summarises the research gaps which have been considered for investigation,

- (i) The use of single source data for classifying urban land-cover features seem to be inefficient for extracting enough information about natural and man-made objects.
- (ii) The misclassification of occluded objects in an urban scene which arises due to spectral similarities and spatial adjacencies between various kinds of objects. The possibility of combining spectral and spatial features using advanced algorithms needs to be explored.
- (iii) The use of thermal range data has scarcely been used in research study involving urban environment, though it has a potential of extracting information of man-made objects regardless of illumination conditions in an urban area.
- (iv) Inadequate efforts in extracting the spatial information using high spatial resolution imagery in extracting the linear structured land-cover features in an urban area.
- (v) Most studies have either used the simple classifier, namely, nearest neighbour classifier or traditional parametric classifier such as the Maximum Likelihood Classifier (MLC) or the Minimum Distance Classifier (MDC) for urban land-cover classification. The recently developed classification algorithms based on machine learning need to be tested using combination of spectral and spatial

features. Also, the rule-based classifiers need to be investigated on multi-sensor data features.

- (vi) Many prevailing studies have not explored an approach to build up features from distinct set of spatial and spectral features in the form of establishing image objects. Creating image objects for all classes from all possible spectral and spatial features is necessary to remove the information redundancy that may exist among the features, including spectral, textual/contextual and shape/geometric features.
- (vii) Finally, most data fusion methods reported in the literature utilize passive optical remote sensing data ranging from the visible to the near infrared for land cover classification (that is, from 400-nm to 1100-nm). The use of ultraviolet to long infrared range needs to be explored for material identification of urban land features.

## **1.6 Research Objectives**

Based on the discussions, it is seen that analysis of remote sensing data using image processing and advanced algorithms for urban land-cover classification needs improvement. The idea of combining the multi-sensor remote sensing data seems to strengthen the possibility of classifying natural and man-made objects in an urban area. For this purpose, in this study, a new coarser spatial resolution Long Wave Infrared (LWIR) hyperspectral is explored along with a high spatial resolution Visible (VIS) RGB data. From multi-sensor remote sensing data, it seems possible to explore and extract features in spectral as well as spatial domain. From a high spatial resolution data, a large set of features characterising objects such as spatial, textural and contextual properties can be derived as a complimentary information to spectral information derived from hyperspectral data for conducting urban land-cover classification. Further, the use of remote sensing image fusion

techniques can be explored for complementing the multi-sensor datasets for improved classification accuracy in diverse and complex urban land-cover types. Also, a set of shape features can be explored and studied for extracting the linear structured man-made objects from a very high-resolution VIS RGB data. Various probabilistic classifier techniques can be compared and studied using the spatial and spectral features on multi-sensor data for analysing the performance parameters of the features on the classifiers. The focus here will be on the use of fusion techniques on different probabilistic classifiers for finding its possibility in classification of natural and man-made objects. Hyperspectral data ranging from near ultra-violet to near infra-red data is explored for formulating the spectral indices using informative wavelengths for extracting the materials of urban land-cover.

The main aim of this research is to develop approaches for improving the classification accuracy of natural and man-made objects in an urban land-cover and to explore useful wavelength bands to formulate spectral indices for material identification. For the former objective, object-based spatial and spectral features are explored from multisource data. A decision-based fusion of features is proposed for multi-sensor classification. Various classifiers' also have been studied and tested on different set of features with a decision-based fusion rules. For the latter objective, hyperspectral data with a wide range is explored for investigating the possible wavelengths in formulating the spectral indices for identifying various objects and materials in an urban area. The methodologies have been designed and proposed for the objectives to support the research gaps. Following are the research objectives,

- (i) To perform fusion of thermal infrared hyperspectral and VIS RGB data for extraction of natural and man-made objects.
- (ii) To improve classification accuracy based on the decision level fusion of high-resolution VIS RGB and hyperspectral data for object extraction.

- (iii) Comparative analysis to show the effects of spectral-spatial fusion of multi-resolution and multisensory images for object-based classification.
- (iv) To study and establish the database of indices from spectral index formulations using hyperspectral data and generation of the region of interest pixels from established indices which would assist in identification of maximal sub-classes.
- (v) To enhance the classification accuracy of linearly structured man-made objects *i.e.*, buildings and roads with the addition of the spatial shape descriptors using high spatial resolution imagery and non-parametric classifier.

## 1.7 Organisation of Thesis

The thesis has been organized into **Nine Chapters**. A layout of Chapter organization is shown in Figure-1.5. **Chapter-1** introduces the basic concepts of remote sensing data and its processing using digital image techniques. It also describes the possible exploration of remote sensing data for object-based land-cover classification, issues related to classification using the data, fusion strategy on classification task with a brief review of the literature on object-based classification and remote sensing image fusion. It also identifies the research gaps which lead to formation of objectives of this research.

**Chapter-2** is devoted to background information related to various spectral and spatial feature extractions from remote sensing data. It also describes the concept of connected component labeling for extraction of object's information. Various parametric and non-parametric classifier algorithms are also discussed. **Chapter-3** describes the salient features of the datasets that have been used to obtain the desired objectives.

The problem statements, description of tasks carried out on each objective along with the methodology and its implementation steps, observations and discussion of results of objectives are highlighted in four chapters *i.e.*, Chapter 4-Chapter 8. **Chapter-4** shows



the feature extracted decision level multi-sensory classification using LWIR HS and VIS RGB data. **Chapter-5** focuses on the improvement in classification accuracy of natural and man-made objects using weighted decision strategy of combined spectral and spatial features on multi-sensory data. **Chapter-6** provides the study and comparative analysis of two classifiers on classification of land-cover objects. The comparative analysis highlights the effects on different classifiers with the use of spectral and spatial features and the fusion strategy. **Chapter-7** shows the formulation of spectral indices by identifying significant wavelengths from hyperspectral data and the use of formulated spectral indices for material classification. **Chapter-8** explores the shape features for identification of linear structured man-made objects from a high spatial resolution data.

Finally, **Chapter-9** provides a summary of the recommendations, major contributions of this research and the future scope of research.

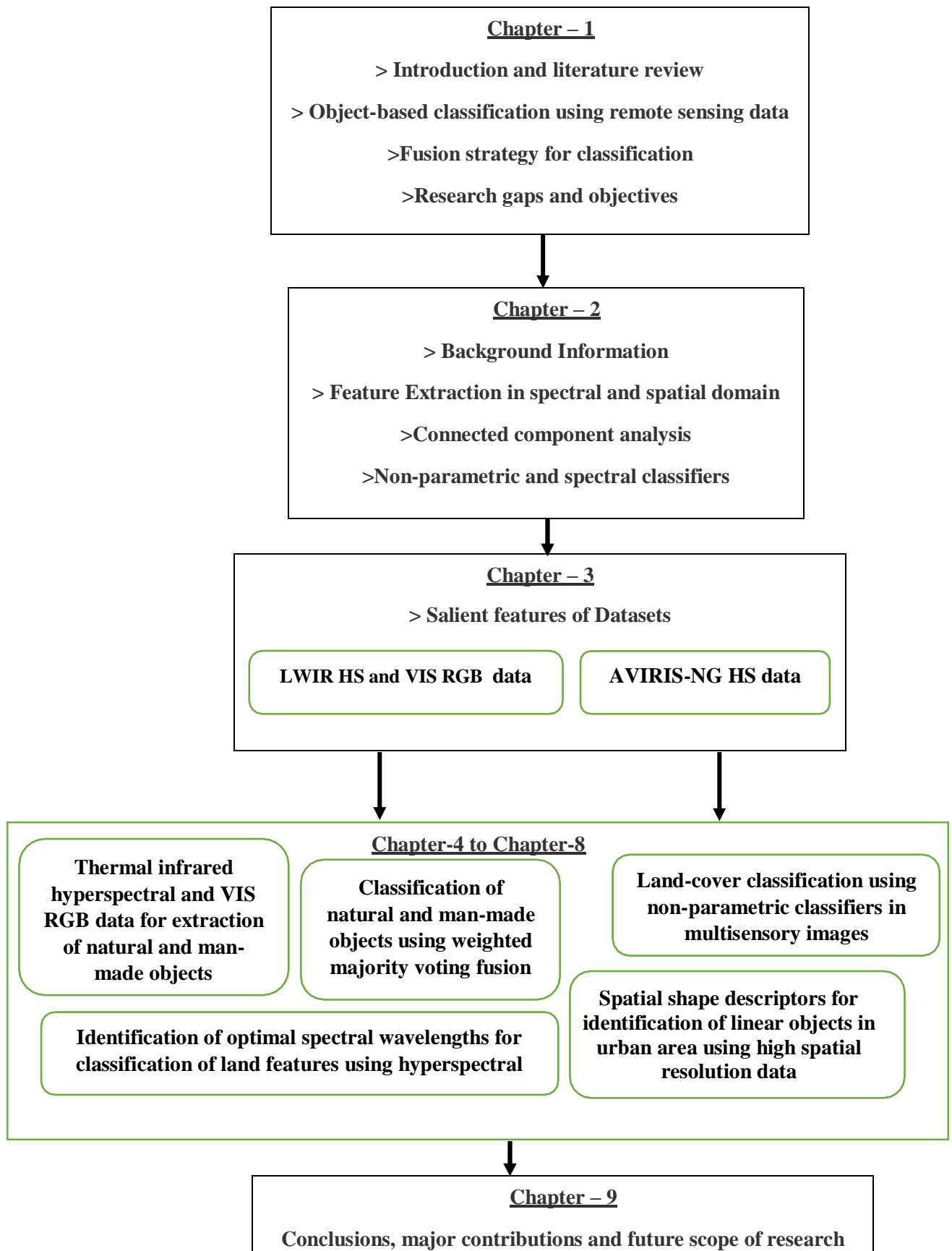


Figure 1.5 - Flow chart: Organization of thesis

## *Chapter 2*

### *Background Information*

In the earlier Chapter, an overview to object-based classification of urban land-cover features using remote sensing imagery is presented. It highlights the importance of using remote sensing data over ground survey data for processing the information for urban-land cover classification with greater accuracy. It also highlights the brief literature survey on various methodological approaches that had been used for analysing the remote sensing data. The literature survey has helped in chalking out the research gaps and to build the objectives for research in the area of classification using remote sensing data.

In view of the above, this Chapter discusses the background information of various topics involved in proceeding steps of the methodological approaches designed to support the outlined research objectives.

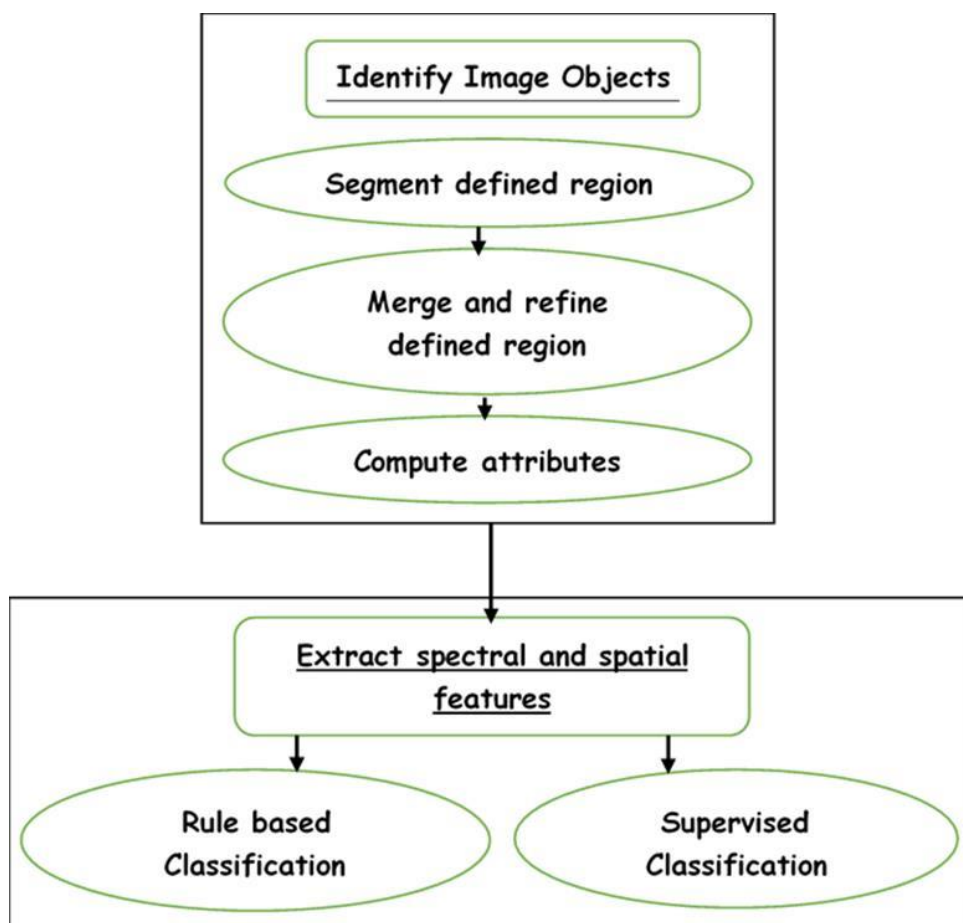
#### **2.1 Image Analysis**

Image analysis is the fundamental tool for numerical/graphical analysis of the image [44]. The characteristics analysed from Multispectral (MS) and Hyperspectral (HS) imagery are effectively used in performing various tasks which are illustrated in Table-2.1[45]. The analysis of an image for distinguishing the objects (homogeneous regions of interest or ROIs) from the background and producing quantitative information from MS/HS imagery is subsequently used for classification or prediction of some of the quality properties of the imaged object.

**Table 2.1 – Various tasks performed through image analysis**

<b>Task</b>	<b>Brief Description</b>
Classification	Assign an object, feature, or area to a class
Detection	Determine the presence or absence of a feature
Recognition	Assign an object or feature to a general class or category
Identification	Identify an object with confidence to assign it to a very specific class
Enumeration	List or count a discrete item visible on an image
Mensuration	Measure an object and feature in terms of distance, height, volume, or area
Delineation	Draw boundary around distinct region of the image characterized by specific tone or texture

Object-based image analysis of MS/HS imagery using machine vision interpretation is shown in Figure-2.1. It gives a general flow of steps/operations needed for extracting application oriented quantitative information from the data.



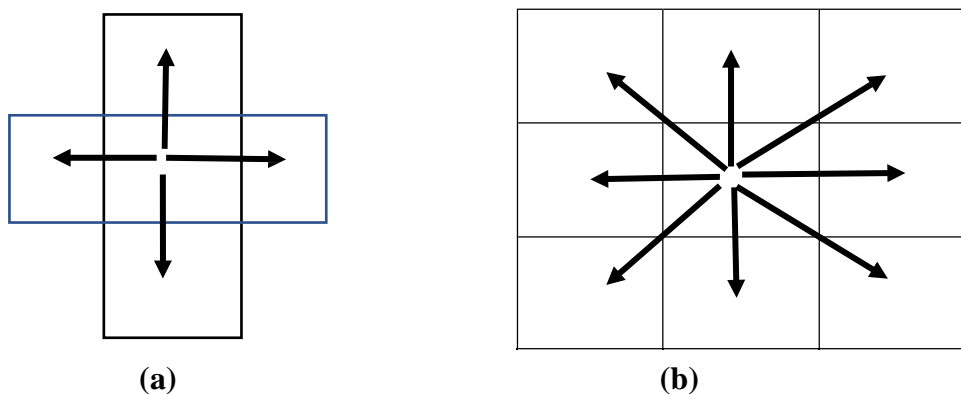
**Figure 2.1 – Image analysis for object-based feature extraction classification**

The processing of the machine vision for object-based classification generally consists of three major operations,

- (i) **Image segmentation:** divides the digital image into two regions, namely, disjoint and non-overlapping regions;
- (ii) **Feature extraction:** measures the characteristics of objects in the image in the form of its color, tone, geometry, size, shape and texture;
- (iii) **Classification:** identifies the objects and classifies them into distinct groups or classes.

## 2.2 Segmentation of Image Objects - Connected Component Analysis

Connected Component Analysis (CCA) is a procedure used for differentiating and identifying varying objects in an image by allocating a unique label to the pixels that refer to the same object. It is, therefore, a prerequisite in image analysis for object identification process. Connected components are clusters of pixels (and is called an “object”) in which each pixel is connected to all other pixels through *4-pixel*, or *8-pixel* connectivity rule which is shown in Figure-2.2. The set of connected components partition an image into segments/objects.



**Figure 2.2 – Pixel connectivity: (a) 4-pixel and (b) 8-pixel connectivity**

Assume a binary image of size  $N \times N$ , where, value '1' is assigned to foreground or object pixels and '0' is assigned to background pixels. In an image, with  $(x, y)$  coordinates, the pixel  $d(x, y)$  lies in the range of  $0 \leq x \leq N-1$  and  $0 \leq y \leq N-1$ . Then, the *4-neighbor* connectivity for the pixel  $d(x, y)$  are at  $d(x-1, y)$ ,  $d(x, y-1)$ ,  $d(x+1, y)$ , and  $d(x, y+1)$  coordinate positions. These *4-neighbors* together with the four pixels at coordinate positions  $d(x-1, y-1)$ ,  $d(x+1, y-1)$ ,  $d(x-1, y+1)$ , and  $d(x+1, y+1)$  are called the *8-neighbors* of the pixel. Two foreground or object pixels  $p$  and  $q$  are said to be *8-connected* or *4-connected* if there exist a path which consists of foreground or object pixels  $a_1, a_2, \dots, a_n$  such that  $a_1 = p$  and  $a_n = q$ , and for all  $1 \leq i \leq n-1$ ,  $a_i$  and  $a_{i+1}$  are *8-neighbor* or *4-neighbor* for each other. This concept is explained in an example shown in Figure-2.3. Figure-2.3(a) shows the *8-pixel* connectivity of foreground or object pixels  $p$  and  $q$ .

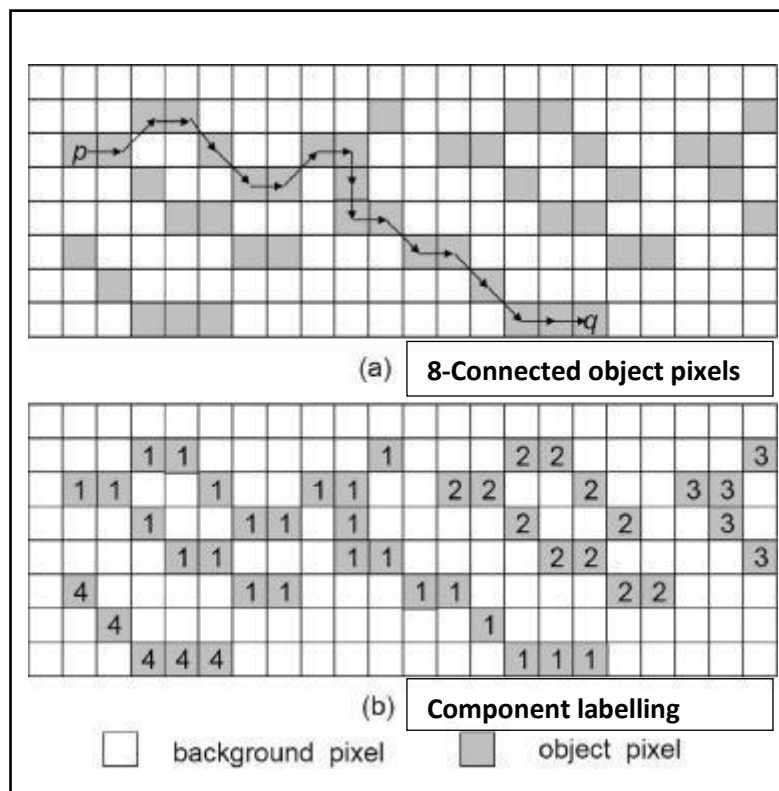


Figure 2.3 – Connected component analysis

A component labelling algorithm counts all connected components in an image and assigns a unique label (as shown in Figure-2.3 (b)) to all pixel points that display either 4-*pixel*, or 8-*pixel* connectivity. Connected component labelling is often followed by an analysis step, where for the connected components/objects a feature vector usually based on the shape properties or the region properties are derived for each label. These feature vectors or the region properties of the objects can then be used for subsequent classification.

### 2.2.1 Bounding Box

Bounding box obtains the region properties of the connected components in the binary image. It is represented by a smallest rectangle whose dimensions are the top-most and left-most pixel, along with width and height containing the region, which is illustrated in Figure-2.4. Hence, bounding box is specified by the location of the upper left corner of the connected component along with the width and height of the label matrix. Bounding box not only helps in identification of an object of interest in an image but also provides the knowledge of the position/coordinates of the bounding box for an object in an image. Bounding box enclosing the image objects can be used as a development stage in classification applications.



**Figure 2.4 – Bounding box coordinates**

### 2.3 Feature Extraction

Humans are extraordinarily proficient at identifying features and extracting information from the objects in an image. From the literature, it has been found that there exist eight elements of image interpretation which are listed by human image interpreters, illustrated in Table 2.2 [46].

**Table 2.2 - Eight elements of image interpretation**

<b>Elements of image</b>	<b>Explanation</b>
Tone	Describes the lightness or darkness in an image. Land-cover objects such as vegetation, soil, water reflect certain proportions of energy in electro-magnetic spectrum. Human interprets the amount of energy reflected by the object to create spectral signature. These spectral signatures help in understanding the shading of gray element (tone) in an object. The object that reflects less light appears dark in an image.
Texture	Describes the homogeneity or heterogeneity in an image. It is characterised by the arrangement of certain repetitions of tone. Texture is a product of scale. The texture appears smoother with smaller scale.
Shadow	Highlights the information about the length/size of an object which cannot be discerned from an overhead view alone. Humans interpret the shadows cast by an object from remotely sensed data for extracting the size and shape of the object. The shadow's length is vital for identification of the object as the length of the shadow defines the height of the object.
Pattern	Spatial arrangement of natural and man-made objects in the landscape. The objects arranged in distinctive recurring patterns, such as buildings in an industrial complex or arranged in systematic patterns, such as fruit trees in an orchard.
Association	Occurrence of certain activity/feature of an object in an image that helps in inferring the presence of associated object nearby. In an image, a large shopping complex may be associated with multiple buildings, parking lots and a major road.
Shape	Humans interprets the uniquely shaped man-made and natural features by their shape characteristics in an image.
Size	Humans interprets the objects based on the relative size of an object, which aids in the recognition of objects that are less easily recognized otherwise.
Site	Refers to the unique physical characteristics of topography. It helps in understanding socioeconomic characteristics like it provides the information of about which crops are suitable for growth on hillsides or near large water bodies.



The interpretation of high resolution multispectral/hyperspectral imagery for a specific task illustrated in Table-2.1 depends on the selections of the appropriate band combinations or extracting spatial attributes for computing the features of interest.

Feature extraction is a way of obtaining information in different resolutions from panchromatic, multispectral or hyperspectral imagery. The term “feature” in spatial resolution refers to the information derived from the spatial characteristic of an object whereas, in spectral resolution the feature may not be the original spectral measurement (*e.g.*, reflectivity) of an object [47]. In spectral resolution, the feature is potentially the information derived from spectral measurements using linear or nonlinear transformations on the information derived from the original data. As discussed earlier in Chapter-1 in section-1.3, an object-based approach provides more flexibility in extracting features of different objects. The spectral and spatial feature extraction and its analysis for object-based classification (flowchart illustration is given in Figure-2.1) forms an important processing step after pre-processing of high-resolution panchromatic or multispectral/hyperspectral imagery as it provides the necessary attributes of the defined region under study. The attributes obtained from features form the knowledge database of wide variety of land-cover objects such as buildings, roads, soil, bridges, lakes and fields for its identification in supervised classification.

### **2.3.1 Feature Extraction in Spectral Domain for Hyperspectral Image**

Spectral indices are used to highlight specific features on Earth’s surface, such as vegetation, water, geological features in remotely sensed imagery. The spectral indices are established by using ratios between bands, hence, transforming the spectral data into meaningful information. The establishment of indices support the interpretation of remotely sensed imagery broadly in three ways,

- (i) To highlight the spectral properties of land-cover objects to foresee its growth and senescence.
- (ii) To compensate for background effects which arises due to the domination of the response of any land-cover object over the other in urban environment.
- (iii) To compensate for the issues arising due to atmospheric distortion that degrades the identification process.

#### **2.3.1.1 Band Ratios**

The spectral enhancement in MS/HS imageries can be done by one of the most common technique *i.e.*, by band ratios. It is obtained by dividing one spectral band by another to produce a relative band intensity value. An image obtained through the relative band intensity value enhances the spectral differences between the bands. The ratio of two bands removes the undesirable effects on the analysis of spectral radiance values which may occur because of varying illumination or due to varying topography. Also, various other aspects of spectral reflectance curves of different land-cover objects can be brought out by band ratios. The two main issues handled by the band ratio images *i.e.*, the reduction of topographic effects and correlation between ratio values help in obtaining the shape of spectral reflectance curves that enable its widespread usage in identification of land-cover objects for classification. In literature, various band ratios had been developed using significant spectral bands for identification for natural and man-made objects. But, with the advent in the availability of large spectral wavelength band MS/HS remote sensing data, many significant wavelengths can still be well explored using band ratio techniques for material classification in land-cover types.

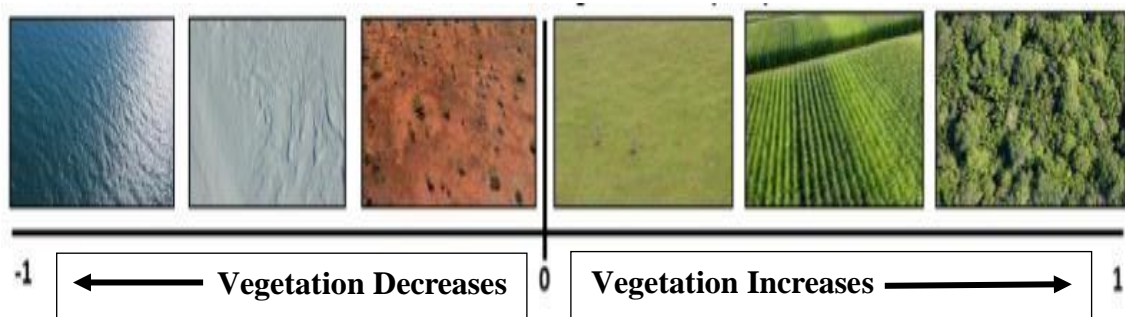
In land-cover classification, an urban area generally consists of various types of vegetation, buildings and roads, therefore, it becomes evident to explore normalised difference vegetation index which is one of the most common and popular spectral indexes.

### **2.3.1.2 Normalised Difference Vegetation Index**

Normalized Difference Vegetation Index (NDVI) utilizes MS/HS remote sensing data to find vegetation, water bodies (such as ponds, lakes, wetlands *etc.*), open fields, scrub and sparse vegetated areas, hilly and agricultural land, dense and thin forest useful combinations of few bands of remotely sensed data [48]. Identification of land-cover objects are highly facilitated with spectral index, namely, NDVI for land-cover classification. NDVI quantifies vegetation by difference measurements of Near-Infrared (NIR) (which is strongly reflected by healthy vegetation) and red bands (which is absorbed by vegetation) of MS/HS imagery. In the literature, it has been found that the resultant value scale of NDVI ranges from -1 to 1, where positive values typically represent vegetation (where thick vegetation is closer to 1) and negative values represent no vegetation (the prominent classes may be bare soil, snow, water, *etc.*) [49]. The class identification range from NDVI is illustrated in Figure-2.5 that corresponds to barren land comprising of rocks, sand, soil, quarries or snow for low values *i.e.*, 0.1 and below. Moderate values *i.e.*, 0.2 and 0.3 represent shrub and grassland, while high value ranging 0.6 - 0.8 indicates temperate and tropical rainforests. The NDVI values close '0' represent bare soil and negative values represent water bodies [50]. Mathematically, the spectral band ratio of NDVI is defined as [50],

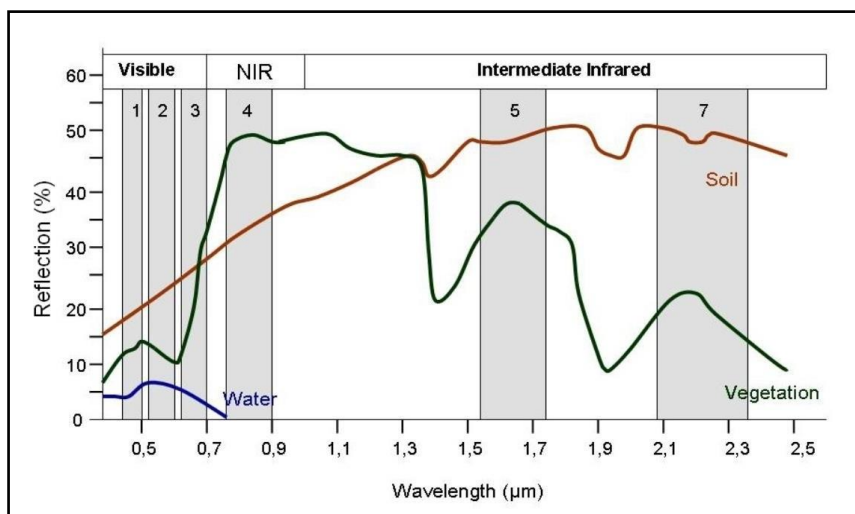
$$NDVI = \frac{NIR-RED}{NIR+RED} \quad (2.1)$$

where RED is Visible Red reflectance band, and NIR is Near Infrared reflectance band. The wavelength range in electromagnetic spectrum for NIR band is 750-1300 nm and for RED band is 600-700 nm [51].



**Figure 2.5 – NDVI range for object identification**

The vegetation reflectance is low in the red band but reflects highly in the NIR band. In case of dense vegetation, NIR reflectance is higher and red reflectance is lower, therefore, the numerator ( $NIR - RED$ ) gives a positive value, and the denominator ( $NIR + RED$ ) has a similar positive value, giving a resultant value close to 1. In case of bare soil, the red reflectance is almost equal to NIR, hence, the numerator gives a value close to 0 and a similar value on the denominator, gives a resultant value closer to 0. Finally, in case of water, the reflectance is higher in the red band than NIR, hence, gives a value close to -1 [52]. The explanation deduced from equation 2.1 is illustrated in Figure-2.6.



**Figure 2.6 - Spectral curves of vegetation, soil, and water**

## **2.3.2 Feature Extraction in Spatial Domain for High-Resolution Multispectral Image**

The interpretation of land-cover objects using spatial information seems to be more sophisticated and important information to quantify in high resolution multispectral images than spectral information. This is so because, spatial information involves measurements related to spatial variability that helps in studying the pattern, shape, structure and size for a set of pixels to define objects. In view of this, various important spatial features are discussed below which are used in this study to classify natural and man-made objects in the urban areas.

### ***2.3.2.1 Texture Analysis***

Texture defines the surface property of any object, which may be used to highlight the characteristics of land-cover objects. The information of the surface property may be considered as an important attribute in spatial domain for identifying objects or homogeneous regions of interest in multispectral images. It is a descriptor that refers to variation in local brightness in the neighbouring pixels over a small region of an image. Since, the composition of land-cover objects is complicated, and their actual sizes are larger than the acquired information gained in the form of spatial resolution of the sensors, therefore, the objects texture can be quantitatively represented in form of its coarseness. The coarseness in an object is seen due to the repetition of the spatial arrangement in its local structure [53]. Based on the spatial resolution of the multispectral image, different mathematical models are devised to effectively analyse the spatial arrangement of objects in an imagery and these models differ from each other by the way they are used for extracting textural features. Four different methods of extracting textural features are found in literature: Statistical methods, Structural methods, Model-based methods and

Transform-based methods [54,55]. A short categorical description of these models is given in Table-2.3 [56].

**Table 2.3 - Techniques of texture analysis**

<b>Techniques</b>	<b>Description</b>
Statistical based	Describe the texture in terms of region's grayscale histograms in high-order moments.
Structural based	Define texture as the configuration of well-defined texture components.
Model-based	Create experimental model for each pixel in the image which is described by weighted average of pixel intensities in its neighbourhood.
Transform-based	Spatial frequency property of intensity of each pixel is explored to describe a new image.

Statistical methods are effective in identification of land-cover objects as the features extracted from second order statistics help in solving the issues related to spectral heterogeneity and complex spatial distribution of the homogeneous pixels considered as objects in the image.

### ***2.3.2.2 Gray Level Co-Occurrence Matrix and Two-Order Statistical Parameters***

The texture is studied using altering gray value intensities of the pixel in the spatial position. This change in value develops definite spatial relationship connecting two neighbouring pixels that are separated by a certain distance in the image. The spatial correlation of neighbouring pixels described by gray scale values which are obtained by Gray Level Co-Occurrence Matrix (GLCM) calculations describe the information of the transformed image in terms of extent in variation and direction of adjoining pixels. GLCM transforms the spatial information of MS image to perform spectral classification by transforming gray scale values into a co-occurrence matrix space and thereby facilitating to obtain varied statistical transformed images. GLCM is based on frequency count of grayscale values of two pixels in a certain spatial relationship. The frequency either

represents the local consistency or the relativity between the two pixels in the image. For coarse texture, GLCM changes slowly and for fine texture, the values change rapidly. GLCM is defined as a square matrix that defines the relationship of occurrence of gray level value  $p_1$  to another gray level value  $p_2$ . Both the gray level values are distanced at a fixed spatial neighbouring positions described in terms of size and direction. Assume,  $f(i, j)$  is used to define any 2D gray-scale image, with  $P$  as a set of pixels such that there exist certain spatial relation between the set of pixels in the defined region and  $S$  referring to the GLCM, then the spatial statistic of the pixel can be expressed as [57],

$$(i, j) = \frac{[(i_1, j_1), (i_2, j_2)] \in S | (i_1, j_1) = g_1 \& f(i_2, j_2) = g_2}{S} \quad (2.2)$$

The textural features using GLCM computes two-order statistical parameters. In literature, [58] proposed 14 types of spatial statistical features to describe the texture of an image. Particularly, for high spatial resolution remote sensing images, four kinds of feature statistics can be considered *i.e.*, energy, contrast, homogeneity and entropy for extracting the textural information. The mathematical expression of these feature statistics is given in Table-2.4 [59].

**Table 2.4 - Second order statistical texture features**

<b>Textural feature - Formulae</b>	
Energy	$\sum_{i=0}^{N-1} \sum_{j=0}^{N-1} p(i, j)^2$
Contrast	$\sum_{i=0}^{N-1} \sum_{j=0}^{N-1} p(i, j)  i - j $
Homogeneity	$\sum_{i=0}^{N-1} \sum_{j=0}^{N-1} \frac{p(i, j)}{1 +  i - j }$
Entropy	$\sum_{i=0}^{N-1} \sum_{j=0}^{N-1} p(i, j) \log p(i, j)$
where, $(i, j)$ are the coordinates of GLCM matrix, N is the dimension of co-occurrence matrix	

### **2.3.3 Shape Features**

Shape information about land-cover objects is one of the main features that can be extracted from remote sensing images. In urban land-cover classification, it sometimes become difficult to extract information of few land-cover objects from textural and spectral features. It happens owing to complicated arrangement of features in spatial space and heterogenous demonstration of spectral features within classes under man-made objects [59,60]. Moreover, many man-made objects in an urban area reflects similar spectral signatures, hence, it becomes difficult to classify those objects based on spectral information only [61,62]. So, in order to overcome these issues and problems, the information related to the shapes of an object is highly important. In literature, many methods are found in respect of discovering shape information that involves area, perimeter, and other structural parameters or the establishment of pixel shape index based on length and width of the objects. In this study, pixel shape index (PSI) is explored as it contemplates the information of homogeneous area in terms of shape and size and selects other suitable parametrical spatial features.

#### ***2.3.3.1 Pixel Shape Index***

A spatial feature index, PSI is used to extract the shape attribute in a neighbouring region surrounding a pixel. PSI is a pixel-based shape characteristic acquired by calculating gray similarity distance measurements in every direction. The shape features obtained in a pixel-by-pixel approach characterizes the contextual statistics along all the directions around the central pixel [63].

The shape feature extraction by PSI algorithm involves the calculation of three parameters [64],



- (i) Calculation of up to which pixel should the direction lines be extended is based on similar gray level values of neighbouring pixels around the central pixel;
- (ii) Measurement of the length and width parameters of analogous gray level values along each direction line;
- (iii) Computation of PSI.

The measurement of length and width direction line values gives the contextual feature along the horizontal and vertical directions around the central pixel. Direction Line (DL) histograms [65] are used to compute the values of length and width of the spatially similar objects. Mathematically, these features are defined as [66],

$$\text{For length spatial feature: } L = \max (d_i(c)) \quad (2.3)$$

$$\text{For width spatial feature: } W = \min (d_i(c)) \quad (2.4)$$

where,  $d_i$  is the direction line,  $c$  is the central pixel. The spectral homogeneity is evaluated involving the central and the neighbouring pixels along each chosen direction. The calculations are performed to decide whether the central pixel lies in the similar region or not. The homogeneity expression for a direction line is defined as [63],

$$PH_i = \sum_{s=1}^n |p_s(cen) - p_s(surr)| \quad (2.5)$$

where,  $PH_i$  signifies the spectral homogeneity of the  $i^{th}$  direction between the central and its neighbouring pixels, the number of spectral bands is represented by  $n$ ,  $p_s(cen)$  represents the spectral value of the central pixel and  $p_s(surr)$  represents the spectral value of neighbouring pixel, which is on the chosen direction line. After determining the values in all direction lines  $D$ , the length of each direction line  $d_i$  is evaluated. Finally, the total length of all direction lines gives the shape index of the central pixel, which is defined as [63],

$$PSI = \sum_{i=1}^D d_i \quad (2.6)$$

where,  $PSI$  signifies the shape index of the central pixel. The shape index of the complete object is as given below [63],

$$PSI = \sum_{i=1}^D d_i / D \quad (2.7)$$

For calculating  $PSI$ , three parameters which are required to be dealt are,

- (i) the total number of directions  $D$ ;
- (ii) the extension of the direction line;
- (iii) threshold  $T$  for pixel shape homogeneity which is required to be evaluated for better extraction of man-made objects in urban land-cover.

### **2.3.4 Feature Extraction in Spectral-Spatial Domain for High-Resolution Multispectral Image**

The basic idea of feature extraction in spectral-spatial domain is to construct an association between the implicit descriptions of an object (*i.e.*, brightness, contrast, and size of different classes such as roads, buildings and soil as they have similar spectral characteristics) and the morphological operators. The generally employed morphological operators are opening and closing. The opening operator is used to dilate an erode object in an image and the closing operator erodes a dilated object to obtain the initial shape of the structures that have been dilated. The filtering process transforms to isolate bright (opening) and dark (closing) structures of the objects in the image, where bright/dark means the contrast of pixels that separate it from the surrounding background in the image. For extracting the feature property, a morphological transformation called top-hat and inverse top-hat (or bot-hat) [67] is used. This method uses a non-Euclidean metric known as filtering by reconstruction [68,69]. The reconstruction approach helps in preserving the

shape of an object as it uses the shapes of the structure of the object in the image for filtering.

Buildings, roads and soil extraction in the urban areas is a difficult task because these structures have complex pattern and cover a very small area on the land surface. In addition, the reflectance of buildings, roads and soil are almost similar in satellite/aerial images which result in faulty identification in digital classification. Keeping this in view, it is reasonable to exploit some additional features like morphological features for increasing the accuracy of these objects from satellite/aerial images. In respect to this concern, Morphological Building Index (MBI) is used in the study as these objects (*i.e.*, buildings, road and soil) tend to show high local contrast in most directions of morphological transformations.

#### **2.3.4.1 Morphological Building Index**

MBI has recently been used for automatically detecting the buildings from high resolution images. MBI is used to relate the implied characteristics of the building with the morphological operators *e.g.*, top-hat reconstruction and directionality [70]. The buildings are categorized by high brightness values whereas the shadow areas have lower values due to the lower spectral reflectance. White/black top hat transformation is used to indicate bright/dark structures with a determined size to indicate the buildings/shadows. MBI algorithm is used to find the local contrast in the buildings by extracting the most popular multiresolution feature fusion approach by differential morphological profile of white-top hat transformed data [71]. Mathematically,

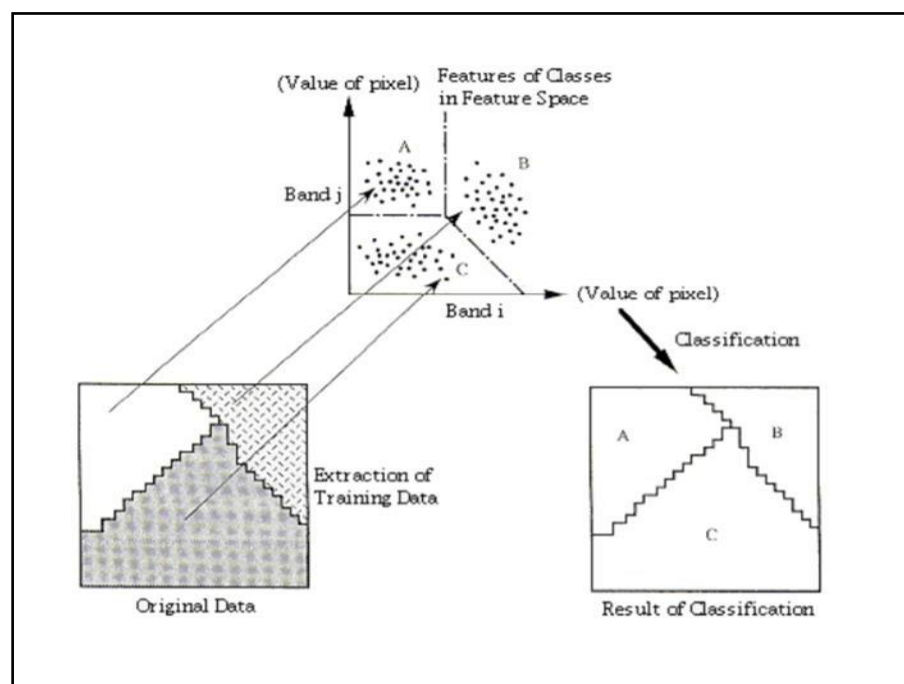
$$MBI = \frac{\sum DMP W-TH (d,)}{(D*S)} \quad (2.8)$$

where,  $D$  and  $S$  is number, and scale of directions applied to the linear structuring element.  $S$  is calculated as  $((s_{max} - s_{min})/\Delta s) + 1$  where  $s$  is defined the length of linear structuring element (SE) and  $d$  is the direction of linear SE.

## 2.4 Classification

Image classification is the process of sorting the spectral and spatial arrangements in an image to define a set of informational classes. The main aim of classification is to discriminate several objects from each other within the image. The fundamental nature of remote sensing image classification is to distribute objects into several different categories by extracting the descriptors of dissimilar objects and exploring accurate similarity measurement combining criteria [72] (few of those have been discussed in above section).

Figure-2.7 shows the general concept of classification of remote sensing data.



**Figure 2.7- Classification of remote sensing data**

Particularly, the categorization of mosaic in urban land-cover classification using remote sensing imageries broadly covers man-made and natural objects, such as buildings, roads, pavements, soil, vegetation and waterbodies. Based on different spectral reflectance

and spatial properties, the identification of various land-cover objects is carried out through the classification process. The basic classification procedure for urban land classification consists of the following steps [73],

- (i) Acquire remotely sensed imagery (MS/HS) and design the classification scheme for extracting information classes such as buildings, roads, pavements, residential hub, vegetated areas *etc.*
- (ii) Ground data and other ancillary information of the area under study is collected for forming the knowledge database.
- (iii) Pre-process the image which includes corrections such as, radiometric, geometric, atmospheric and topographic, enhancements in an image using techniques such as pan-sharpening, and initial image segmentation or clustering.
- (iv) From the image, the regions of interest are selected for generating clustering/segmentation results or creating training signatures for further analysis.
- (v) Select appropriate image classification algorithm.
- (vi) Post-process the classification procedure to remove noise effects by filtering process.
- (vii) Perform accuracy assessment of classified land-cover objects and compare classification results with field studies.

#### **2.4.1 Classification Techniques**

In the literature, several classification methods have been reported and widely used in urban land-cover classification [74]. They can be grouped as supervised and unsupervised or parametric and non-parametric to non-metric, or hard and soft (fuzzy), or

pixel and object-based classification [75]. A brief description of the classification techniques is given in Table-2.5 [76].

**Table 2.5 - A taxonomy of remote sensing image classification techniques**

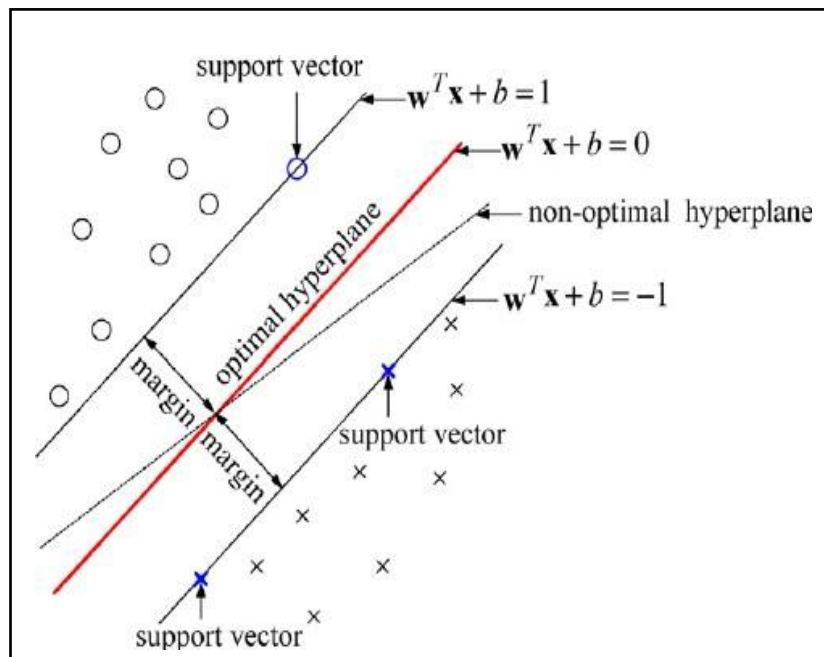
<b>Techniques</b>	<b>Characteristics</b>	<b>Examples</b>
Parametric	A learning model that summarizes data with a fixed training size. They are simpler to understand and interpret results with good computational speed. They can even work with less training samples. But they are highly constrained to some specified functional methods. They are well suited for simpler problems.	Logistic Regression Models; Linear Discriminant Analysis; Naïve Bayes; Simple Neural Networks
Non-Parametric	A learning model that does not make assumptions about knowledge features. They are adaptable in learning any functional method from the training data. These models are flexible as they have the capability of fitting large number of functional models. These models need more training data and are a bit slower to train. Some issues related to overfitting the training data is reported.	K-Nearest Neighbours; Decision Tree; Support Vector Machines (SVM); Artificial Neural Network (ANN)
Non-Metric	A model includes both real-valued and small scaled data for statistical analysis in recognition problems.	Decision tree; Rule based methods; Hierarchical Classifier
Supervised	A model in which analyst identifies training sites/features to represent the class and the testing sites are classified based on statistical analysis.	Maximum Likelihood; Minimum Distance; Parallelepiped; SVM; ANN; Spectral Angle Mapper (SAM); Spectral Information Divergence (SID)
Unsupervised	A model in which no prior ground information is known. Analogous spectral characteristics of pixels are grouped together according to some specific statistical criteria.	K-means; Iterative Self-Organizing Data Analysis Technique (ISODATA)

<b>Techniques</b>	<b>Characteristics</b>	<b>Examples</b>
Hard (Parametric)	A model that gives a definite decision for a pixel to be assigned to one and only one category.	Supervised and Unsupervised classification models
Soft or Fuzzy (Non-Parametric)	A model in which each pixel is assigned a measure of the degree of similarity for each class.	ANN; Fuzzy logic; Decision tree; Genetic Algorithms
Pixel-based	A model in which pixel is the fundamental unit of classification. It uses class characterization properties that are well-defined.	Maximum likelihood; Minimum-distance-to-mean; Minimum-Mahalanobis-distance
Object-based	A model in which a group of homogeneous pixels called an object forms the classification unit. The information is extracted in the form of spatial relationship with the surrounding pixels.	Nearest-neighbour Classification

In this study, object-based classification approach is used for exploring and unravelling the shape, textural and morphological characteristics from high resolution MS and HS imagery in addition to the spectral information for better classification of urban land-cover objects. Various popular classification algorithms such as SVM, ANN, SAM and SID are used to study the object-based approach using spatial and spectral features. These classification algorithms are discussed below.

#### ***2.4.1.1 Support Vector Machine***

Support Vector Machine (SVM) is a classifier that discriminates the data based on the statistical learning of features. SVM is used to generate a model that determines the decision boundaries for optimal separation of classes [77] defined by a separating hyperplane which is shown in Figure-2.8.



**Figure 2.8 – Concept of SVM hyperplane**

For a two-class identification problem, if the classes are linearly separable, linear decision boundary is selected by SVM to minimize the generalization error. The selected decision boundary provides the maximum margin between the two separated classes. The margin between the two classes is sum of the distances from the closest data points of the two classes to the hyperplane [77]. Generally, the standard Quadratic Programming (QP) optimization techniques are used for maximizing the margin distance. The data points that are used to find the margin and are closest to the hyperplane are termed as “support vectors”. The second case, if the two classes are non-linearly separable, then hyperplane is selected by SVM in such a way that the margin gets maximized and the number of misclassification errors gets minimised. The trade-off is required between margin and misclassification errors and this is controlled by a user-defined constant [77,78].

SVMs were primarily proposed for binary (two-class) problems but with the improvement in algorithm it is now possible to deal with multiple classes. To implement this a strategy is used in which there are  $n$  classifiers, where  $n$  is the number of classes. This strategy is described as ‘one against the rest’. In this strategy, the class that matches to the

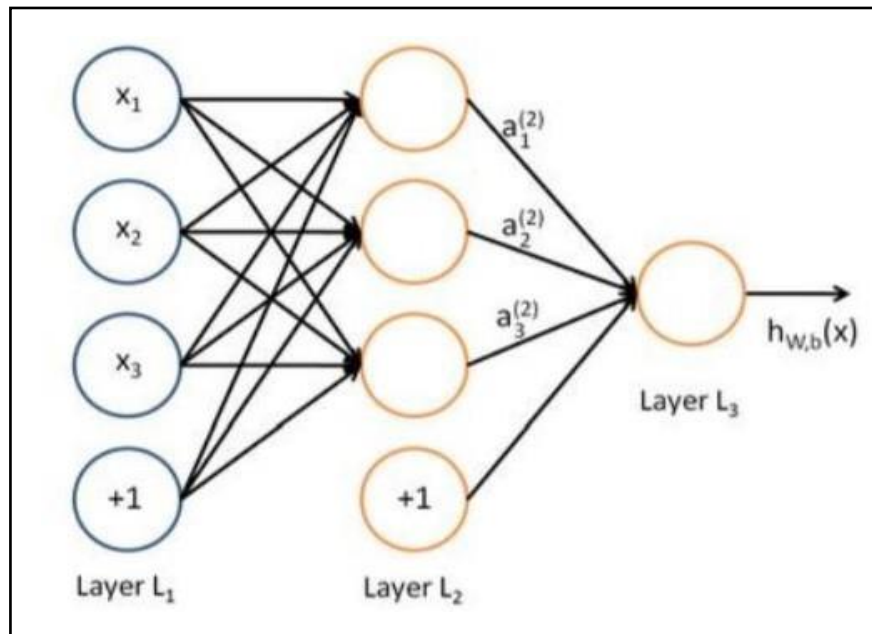


SVM with the largest margin results in the final decision of final output, as defined above in Figure-2.8. For multi-class classification one must resolve problem by determining  $n$  hyperplanes. Since, this problem is addressed with multiple hyperplanes, thus it requires  $n$  QP optimization solutions for separating each class from the remaining classes. Another method to resolve this issue lies in combining the decision of several classifiers to obtain the final output for a class. This strategy is defined as ‘one against one’ class discrimination. In this strategy, [79] pair-wise association between all  $n$  classes is performed. All possible two-class classifier networks are assessed from the training set of  $n$  classes. Each pair of classifier network is trained on two out of  $n$  classes, resulting in  $n(n-1)/2$  classifiers. The classifier network is applied to the testing samples to obtain the vote for the winning class. The label of the class with most votes is assigned to the testing sample.

#### ***2.4.1.2 Artificial Neural Network***

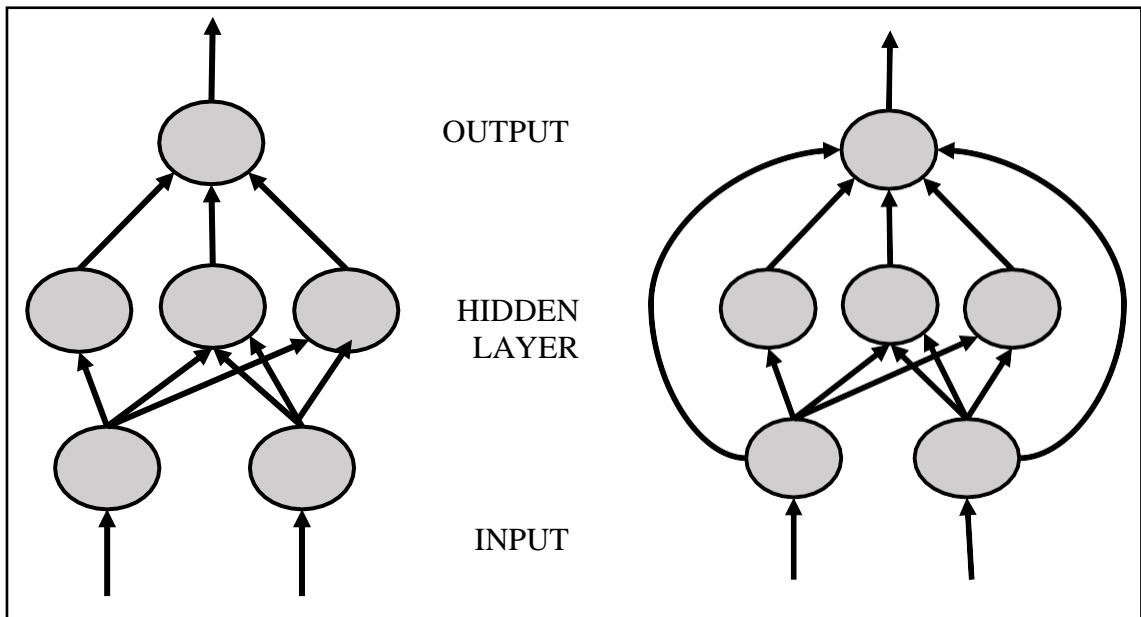
An Artificial Neural Network (ANN) is a nonlinear statistical paradigm inspired by biological nervous systems. It is an artificial network which consist of certain functions known as parameters, which are termed as “neurons”. These parameters have inherent capability to learn and tune itself from the instances provided by the data to resolve specific problems. Neuron is a function parameter which produces certain output after gathering knowledge from one or multiple inputs. The outputs obtained at one layer are passed to the next layer of neurons. Next layer of neurons takes them as their own function inputs and produce further outputs. These outputs are then further passed on to the next layer of neurons. The process continues for all layer of neurons until the terminal neurons are receiving their input for further evaluations. The final terminal neurons, outputs the result for the established network model. Figure-2.9 shows a visual representation of such a network. The neural network shown in the figure has 3 input units, 3 hidden units, and 1 output unit. The circle labelled as "+1" is called bias units with the leftmost layer of the

network called the input layer, and the rightmost layer of the network as the output layer. The middle layer of nodes is called the hidden layer as their values are not observed in the training set.



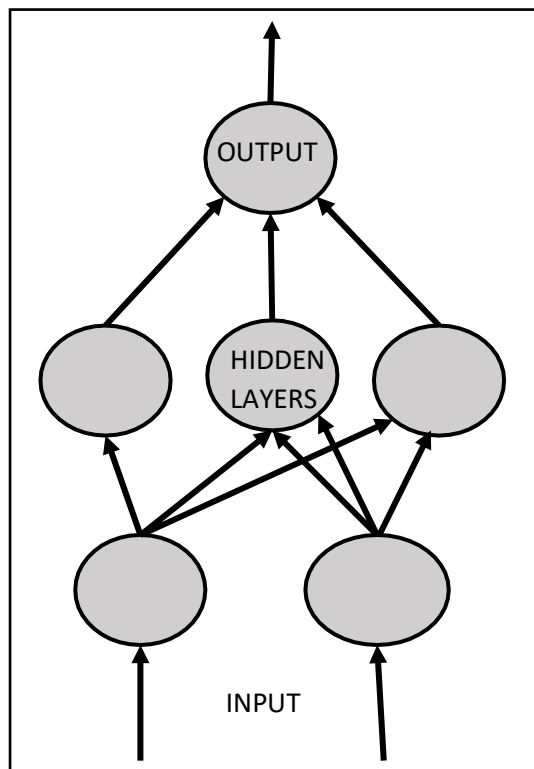
**Figure 2.9 – Simple neural network**

In literature, two ANN topologies exist, one being Feedforward and other is Feedback. In a Feedforward ANN (illustrated in Figure-2.10), the input receives the response quickly when the connections between units is established. The flow of information is unidirectional. The information from a unit is send to the other input that has not received any information earlier. The network does not contain the feedback loops. They are used in pattern generation, recognition and classification. The number of inputs and outputs are fixed in the network.



**Figure 2.10 – Feedforward Network**

Feedback networks (illustrated in Figure-2.11) are bidirectional, therefore, they have indicators in both directions. Details about feedback networks can be found in literature [80].



**Figure 2.11 – Feedback Network**

ANN approach has an apparent advantage over other statistical classification approaches in a way that they are non-parametric and require little or no *a priori* knowledge of input data in its learning model. Few additional advantages of ANN include parallel computation, the ability to estimate the non-linear relationship between the input data and desired outputs, and fast generalization capability [80]. The algorithm of neural network used in this study is discussed in detail in Chapter-6 under the section-6.3.1.

### 2.4.1.3 Spectral Angle Mapper

In multi-dimensional MS/HS imageries, a pixel vector  $x$  defined in the coordinate system of spectral space has both magnitude (length) and an angle [81]. Spectral Angle Mapper (SAM) uses the angular information of the spectral space for identifying pixel spectra which is shown in Figure-2.12. SAM technique assumes that the number of bands acquired as spectral reflectance represents the dimensionality of the data. It calculates the spectral angle between image pixel spectrum and training spectrum [82-84]. The spectral angle  $\theta$  is defined as [85],

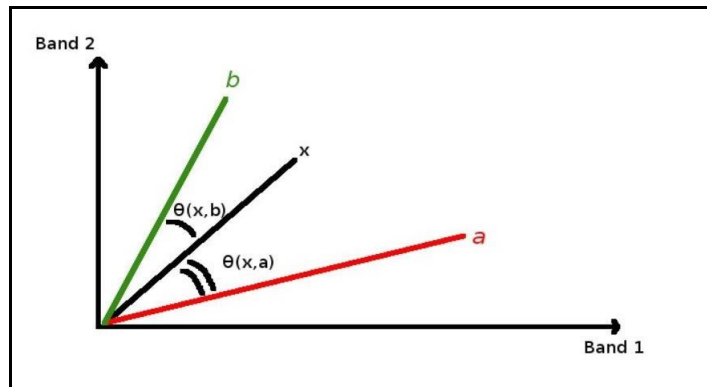
$$\theta(x, y) = \cos^{-1} \left( \frac{\sum_{i=1}^n x_i y_i}{\left( \sum_{i=1}^n x_i^2 \right)^{\frac{1}{2}} \left( \sum_{i=1}^n y_i^2 \right)^{\frac{1}{2}}} \right) \quad (2.9)$$

where,  $x$  is image pixel spectral signature vector;  $y$  is training spectral signature and  $n$  is the number of spectral bands.

The small angles represent a close match to training spectrum. The spectra are considered to be matched if the spectral angle is smaller than a given tolerance level. An image pixel belonging to the class have the smallest angle, that is,

$$x \in C_k \Leftrightarrow \theta(x, y_k) < \theta(x, y_j) \quad \forall k \neq j \quad (2.10)$$

where,  $C_k$  is defined land-cover class  $k$ ;  $y_k$  is spectral signature of class  $k$  and  $y_j$  is spectral signature of class  $j$ .



**Figure 2.12 – Spectral angle mapping**

The pixels are excluded from classification if they do not lie in the specified maximum angle threshold. The threshold mathematically is defined as,

$$x \in C_k \Leftrightarrow \theta(x, y_k) < \theta(x, y_j) \quad \forall k \neq j \text{ and} \quad (2.11)$$

$$\theta(x, y_k) < T_i \quad (2.12)$$

SAM is an influential classification approach as it limits the issue of shading effects that occur within land-cover objects and thereby emphasizing the training reflectance spectrum characteristics. To achieve good separation based on angular information, it is necessary that different classes show different pixel spectra. However, the mixed pixels may pose problems in identification which may be due to the assumption that endmembers represent the pure spectra of a reference object.

#### **2.4.1.4 Spectral Information Divergence**

Spectral Information Divergence (SID) is a stochastic similarity measure algorithm which is based on information entropy. SID is used to model the spectrum of MS/HS image pixel in terms of probability distribution that observes the variations or divergence measures in pixel. The divergence measure matches the pixel values to the reference

spectra. If the divergence is less, then the pixels are considered similar in nature. The divergence measure ranges from zero to some user-defined threshold and if this measure is greater than the specified maximum divergence threshold, then the pixels are not classified. SID measure [86] calculates the distance between the probability distributions produced by the spectral signatures of two pixels which is defined as,

$$SID(r_i, r_j) = D(r_i // r_j) + D(r_j // r_i) \quad (2.13)$$

where,

$$D(r_i // r_j) = \sum_{l=1}^L p_l D_l(r_i // r_j) = \sum_{l=1}^L p_l (I_l(r_j) - I_l(r_i)) \quad (2.14)$$

$$= \sum_{l=1}^L \log \left( \frac{p_l}{q_l} \right) \quad (2.15)$$

and

$$D(r_j // r_i) = \sum_{l=1}^L q_l D_l(r_j // r_i) = \sum_{l=1}^L q_l (I_l(r_i) - I_l(r_j)) \quad (2.16)$$

$$= \sum_{l=1}^L \log \left( \frac{q_l}{p_l} \right) \quad (2.17)$$

The equations are derived from two probability vectors  $p = (p_1, p_2, \dots, p_L)^T$  and  $q = (q_1, q_2, \dots, q_L)^T$  for the spectral signatures of two pixel vectors  $s_i$  and  $s_j$  where,  $p_k = \frac{s_{ik}}{\sum_{l=1}^L s_{il}}$

and  $q_k = \frac{s_{jk}}{\sum_{l=1}^L s_{jl}}$ . Similarity measures  $I_l(r_j) = -\log q_l$  and  $I_l(r_i) = -\log p_l$  are referred to

as the self-information of  $r_j$  and  $r_i$  for band  $l$  [87,88]. The equations 2.14 – 2.17 represent the relative entropy of  $r_j$  with respect to  $r_i$ .

## ***Chapter 3***

### ***Data Set***

#### **3.1 General**

This Chapter provides the information regarding the characteristics of various data sets that have been used in this research work. There are two distinctive data sets that have been used for classifying different urban areas. The first set of data comprises of airborne multisensory data which consist of two images, where, one imagery covers the thermal range and the other imagery includes the visible range of electromagnetic spectrum. The other set of data is spectroscopic hyperspectral airborne image that covers a wide spectral range from ultraviolet to long infrared electromagnetic range. Both data sets comprise of natural and man-made objects of urban land-cover. Further details of the data sets have been described below in the subsequent sections of this chapter.

#### **3.2 Data Set – 1: Long Wave Infrared Hyperspectral and Visible RGB Data**

It has been reported in the research gap that the use of single sensor might be insufficient, unreliable or imprecise, therefore, fusion of multi-sensors seems to be a better approach in remote sensing classification as compared with the single-source remote sensing image classification. Keeping this and other research gaps in view, for the research objectives (i), (ii) and (iii) outlined in section-1.6 of Chapter-1, the utility of the long-wave infrared (LWIR) information as a complementary spectral source for Very High Resolution (VHR) classification is examined in urban land-cover classification. The acquisition and the essential characteristics of multisensory data sets used in this study are discussed below.

### 3.2.1 Acquisition and Characteristics of Data Set-1

On 21 May 2013, two airborne data were acquired by Telops Inc., Québec, Canada. The airborne data was collected over a small city in Black Lake area of Thetford Mines, province of Québec, Canada (46.047927N, 71.366893W). The image of the region is shown in Figure-3.1[89].



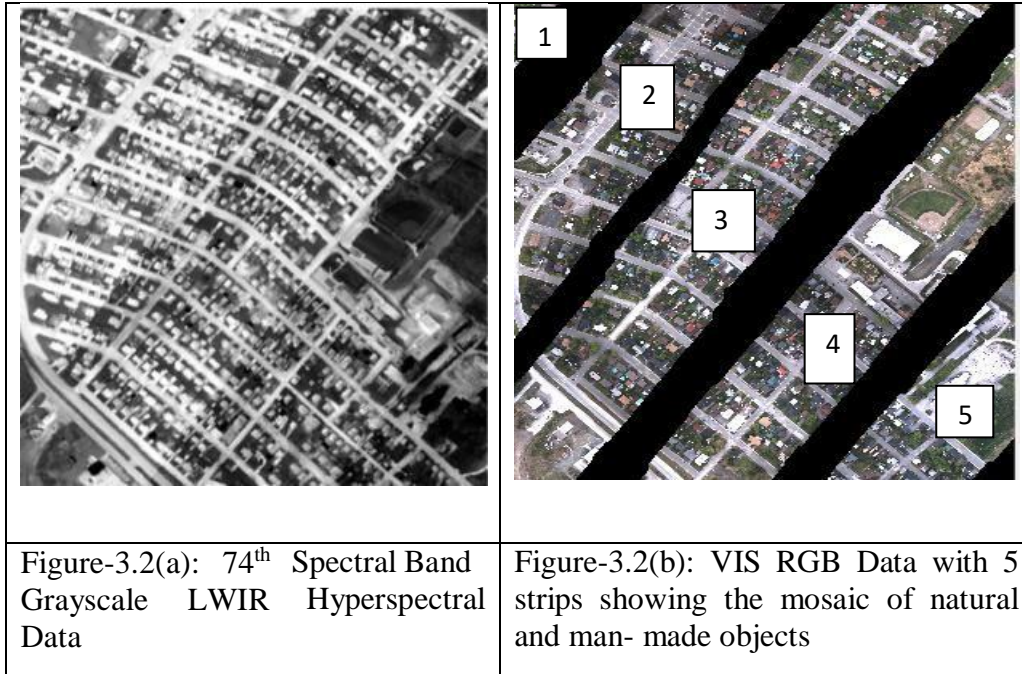
**Figure 3.1 – Area of Thetford Mines, Canada [89]**

The datasets include the low-density portions of an urban area in the neighbourhood of an open pit mining area and forest areas. The urban region in an area in the mosaic indicated in Figure-3.2 includes residential and industrial hubs comprising of a variety of natural and man-made objects. The data set has been provided by IEEE GRSS in 2014 and it comprises of the following images [89],

- (i) Long Wavelength Infra-Red hyperspectral dataset of the city in the range 7800nm-11500nm.



- (ii) High resolution Visible RGB data of the same area in the range 400nm-700nm.



**Figure 3.2 – Data Set-1: Thermal hyperspectral and VIS RGB data**

The first airborne data set shown in Figure-3.2 (a) has been captured using the Telops' Hyper-Cam. It is a Fourier-Transform Spectrometer (FTS) consisting of long-wave infrared hyperspectral imager. The airborne LWIR hyperspectral imagery captured consists of 84 spectral bands covering a spectral range of 7.8- $\mu\text{m}$  to 11.5- $\mu\text{m}$ , with a spectral resolution of 6  $\text{cm}^{-1}$  (full-width-half-maximum). The data has been calibrated to at-sensor spectral radiance units, in  $\text{W}/(\text{m}^2 \text{sr cm}^{-1})$ . Another airborne data is visible imagery shown in Figure-3.2 (b). It consists of uncalibrated, high spatial resolution, digital data covering a spectral range of 0.4- $\mu\text{m}$  to 0.7- $\mu\text{m}$  with sparse ground coverage. Both airborne measurements were taken over the same place. The hyperspectral imager and a digital color camera (2-megapixels) were integrated to a gyro-stabilized platform inside a fixed-wing aircraft to acquire simultaneously a LWIR and visible imagery data set. Both airborne data

sets are georeferenced images that are mutually registered. The average spatial resolution of LWIR hyperspectral imagery is approximately 1-m and 0.2-m for the visible imagery.

In this study, from Data Set-1 shown in Figure-3.2, a variety of urban land-cover classes has been identified and classified under the category of natural and man-made objects which are summarised in Table-3.1.

**Table 3.1 – Categorization of land-cover classes**

<b>Object-1</b>	<b>Class-1</b>	<b>Class-2</b>	<b>Class-3</b>
<b>Natural</b>	Vegetation	Soil	Trees
<b>Object-2</b>	<b>Class-4</b>	<b>Class-5</b>	
<b>Man-made</b>	Buildings	Roads	

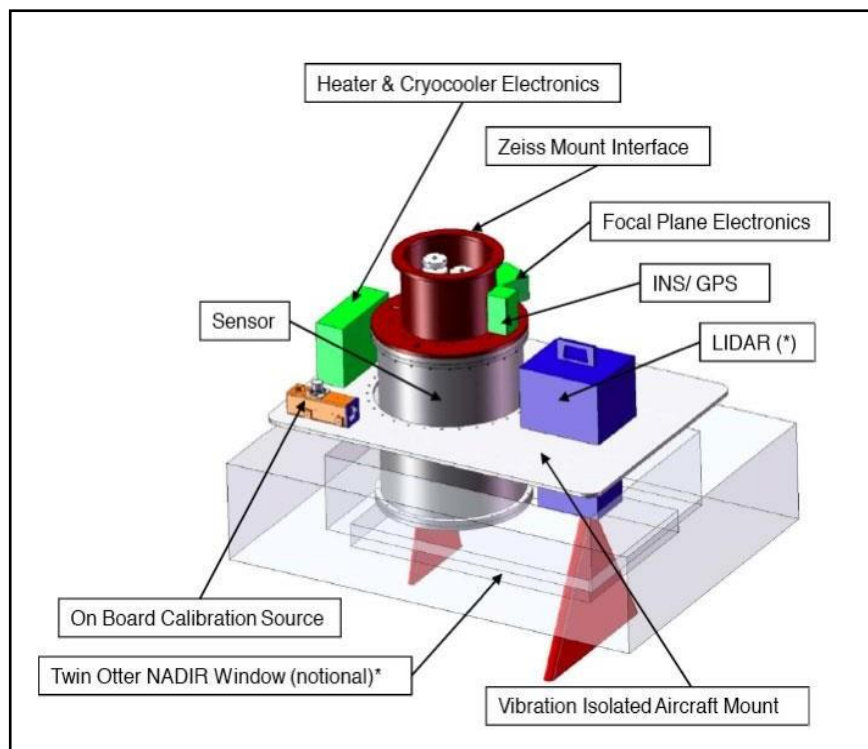
Out of the five listed research objectives in section-1.8 of Chapter-1, the results of the first, second and third research objectives have been formed using two imageries of Data Set-1 (*i.e.*, Figure-3(a) and Figure-3(b)) and for the fifth research objective, the results have been formulated using high resolution VIS RGB imagery shown in Figure-3(b).

### **3.3 Data Set – 2: AVIRIS-NG Hyperspectral Data**

Airborne Visible/Infrared Imaging Spectrometer-Next Generation (AVIRIS-NG) imaging spectrometer was used to capture an area over a 22,840 sq. km across 57 sites in India during 84 days from 16<sup>th</sup> December 2015 to 6<sup>th</sup> March 2016. AVIRIS-NG airborne campaign was organized under the Indian Space Research Organisation (ISRO) and National Aeronautics and Space Administration (NASA) joint initiative for Hyper-Spectral Imaging (HSI) programme. Under this campaign field and ground measurements were also taken up to capture and generate the data that could be used in various applications related to crop, soil, forest, geology, coastal, ocean, river water, snow, urban, *etc.*

### 3.3.1 Acquisition of Data

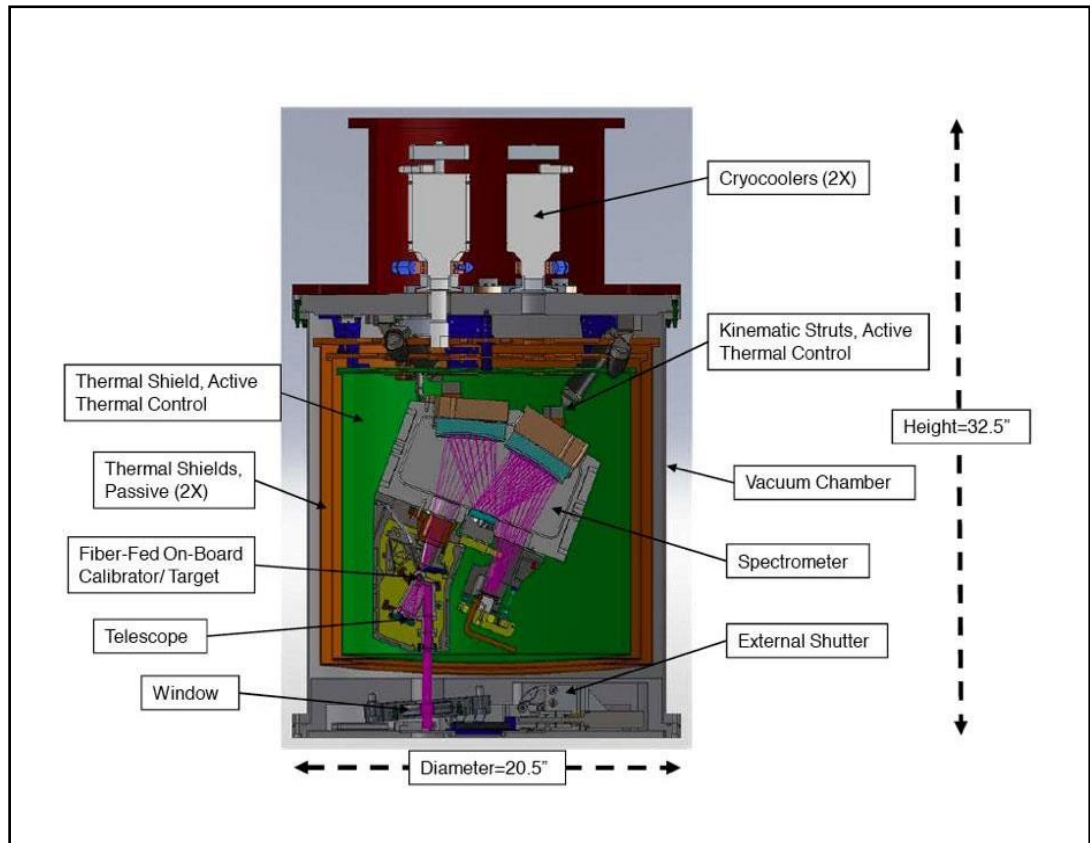
AVIRIS-NG is created to be compatible with all-encompassing aircraft platforms, such as NASA's ER-2 jet, the Twin Otter turboprop, and the B200 King Air. AVIRIS-NG flight package consist of major components, that include, the sensor encased in a vacuum enclosure, the meticulous INS/GPS, the focal plane electronics, the On-Board Calibrator (OBC) electronics source, the heater and cryocooler boxes, and a vibration isolating aircraft mount. Figure-3.3 shows the major components of AVIRIS-NG flight package.



**Figure 3.3 - Major components of the AVIRIS-NG airborne flight package**

The CAD model of the AVIRIS-NG sensor is shown in Figure-3.4. The height of the sensor is approximately 33" by 20" in diameter. Various major parts of sensor include the optical telescope and spectrometer benches, the detector, the source for OBC and kinematic struts which suspend the assembly from the instrument backplate. The sensor is held in a vacuum container with three thermal shields that are operated at temperatures of

down to -40 degrees C at the detector. It is vital to maintain a stable temperature across the instrument to minimize the thermal distortions which could affect optical alignment. The effective temperature is maintained by the help of two cyro-coolers.



**Figure 3.4 - AVIRIS – NG Sensor**

### 3.3.2 Characteristics of Data Set-2

AVIRIS-NG airborne hyperspectral phase-1 campaign was carried from 31<sup>st</sup> January to 5<sup>th</sup> February 2016 that covered eight sites of Udaipur, imaging an area of 3697-sq. km. The salient features of AVIRIS-NG data set are such that, it covers the spectral range from 380 to 2510-nm at 5-nm sampling with a ground sampling distance ranging from 4-m to 8-m. The spectroscopic signatures captured are intended to discriminate surface types and retrieve physical and compositional parameters for the study of land-cover features and atmospheric properties.

For research study (*i.e.*, objective (iv)), listed in section-1.6 of Chapter-1, the data captured under AVIRIS-NG campaign over the city of Udaipur, Rajasthan is potentially explored. The RGB band display of the dataset is shown in Figure-3.5 [90] which covers an urban area of the city. The dataset consists of a variety of natural and man-made objects. The dataset is used for discriminating the materials for classification in an urban area.



**Figure 3.5 – Data Set-2: RGB display of AVIRIS-NG hyperspectral data, Udaipur [90]**

The following Table-3.2 shows the metadata information of the hyperspectral imagery of the captured site of urban land-cover of the city.

**Table 3.2 – Meta data information of AVIRIS-NG HSI**

<b>Features</b>	<b>Parameters</b>
Samples	724
Lines	9946
Bands	425
Spectral Range	376nm-2500nm
File Type	ENVI
Data Type	4
Interleave	BIL
Coordinate System	WGS84
Zone	43 North
Wavelengths (unit)	Nanometers
Spatial Resolution	8.1 m
Spectral Resolution	5nm



AVIRIS-NG data set offers a hyperspectral data that can be explored for identification of more materials or surface object types such as minerals, rocks, vegetation etc. as the data captures a wide range of spectral signatures related to the composition of various materials on land surfaces. The other benefits of this dataset are that it includes the measures of absorption strength that can be related to the abundance of the materials present on land surfaces. Also, the sub-pixel abundance estimates for different materials captured by the sensors can be used to derive the composition of man-made objects in an urban area.

### **3.3.3 Ground Data Collection**

The ground data was collected in the first week of July 2017 after the completion of AVIRIS-NG phase-I data under joint campaign of ISRO with NASA (which has been discussed in this Chapter).

The spectral evolution spectroradiometer consisting of 2151 channels was utilized for the measurement of radiance/reflectance of various natural and man-made surfaces at different locations of Udaipur. The area under the study was captured using contact probe and gun for measuring the spectral signatures of aforesaid surfaces. A 5x5 inch Spectralon plate was used for capturing the reference intensity after recording two to three spectral signatures of the objects under particular site area. Further, a total of 1132 spectras of different samples were recorded between the time period of 1000 hrs to 0300 hrs. Out of 1132 spectral signatures collected, 604 spectral signatures belong to man-made surfaces while 528 spectral signatures belong to natural surfaces. The captured spectral signatures under man-made surfaces were further categorized into different material classes belonging to roads, pavements and roofs. In the same manner, the captured spectral signatures under natural surfaces were further classified into different types of vegetation, soil and water

bodies. These spectral signatures along with site information have been used for accuracy assessment and validation of classification / detection results.

All the spectral signatures of 2151 channels are re-sampled with respect to hyperspectral imagery of similar region for analysis purpose. Since, in this study 387 channels are selected as good bands, therefore *in-situ* spectras of aforesaid channels have been resampled using nearest neighbour algorithm. A spectral library of different man-made and natural surfaces has also been created in Environment for Visualizing Images (ENVI-5.3) software for further analysis.

# *Thermal Infrared Hyperspectral and VIS RGB Data for Extraction of Natural and Man-made Objects*

### 4.1 Introduction to the Problem

With the advent in technology remote sensing sensors can now obtain high-resolution imageries in different specific bands which seem useful in identifying and categorizing various land-cover classes. The categorization of land-cover classes provides significant information which is used in applications related to land use planning such as, suburban sprawl, urban growth trends, management policy regulations and inducements. These applications require authentic information on Land Use / Land Cover (LULC) classification patterns which in turn help in facilitating the balanced interaction between the humans and the environment through developers of LULC information [91]. Not limited to this, the information appreciably develops the association of geospatial technologies along with the development of technological product with the available resources in least possible time. Each of these applications of urban land-cover classification highlight two important aspects of research study, first being the acquisition and availability of high-quality sensor data and second being the advanced methodological processing techniques for retrieving the valuable information from the sensor data.

In literature, it has been seen that remotely sensed images attained by various several sensors are explored for land-cover classification applications, such as, images acquired by the Landsat Operational Land Imager (OLI) have been explored globally for classification of fast-developing towns across the world [92,93]. However, the use of medium spatial resolution Multi-Spectral Remote Sensing Imagery (MSRSI) for



identification of land-cover physical features leads to lower accuracy. For example, the land-cover classes categorized under man-built surface in an urban area could comprise of both industrial and residential hub, but the processing of medium spatial resolution data may categorize them under a single class of man-built objects.

High spatial resolution MSRSI provide both spectral and textural information of physical features in an urban area, therefore, it seems promising data source for classification of complex and diversified urban land-cover [94,95,96]. The processing of high spatial resolution MSRSI by different spectral-spatial classification approaches have been discussed in literature to extract and identify urban land-cover classes. The popular method is to add spatial attributes such as textural statistics [97,98], structural and shape features [99] and morphological features [100] into the spectral observations derived from the spectral bands of high spatial resolution Remote Sensing Imagery (RSI). In [101], Bayesian network is used to classify building objects into various classes on the knowledge of spatial and spectral-spatial attributes *i.e.*, morphological, geometric, and contextual information. Another approach includes object-based classification, in which physical coverage pattern of urban land is interpreted using high spatial resolution RSI. The spatial metrics of different classes are extracted in the form of textural statistics, and nearest-neighbour relationships between one land-cover class and the other to identify the urban features [102,103].

Besides, the numerous benefits obtained through these spectral-spatial approaches, some limitations remain that degrades the classification accuracy of physical features of urban land-cover. The limitation is due to the fact that an urban land-cover is a mix of natural and man-made classes that consist of objects whose information is varied or mixed in their spectral and textural characteristics, therefore, it becomes challenging to differentiate them correctly using classification algorithms based on spatial characteristics

alone. Also, the spectral mixing is another probable limitation of MSRSI that degrades the accurate classification of urban land-cover. In relation to this, Hyperspectral (HS) images obtain narrowband contiguous spectral information for the same area, and therefore, provide richer spectral information that enables more accurate discrimination of urban physical features [104]. In [105], the research study demonstrates the use of aerial HS imagery for developing the spectral index and the extraction of asbestos cement roofs is shown. In [106], the classification of soil using AVIRIS-NG HS data is shown using SVM classification technique. HS data has been explored for various applications such as differentiating vegetation classes in mountain areas [107,108] in urban areas [109,110,111,112,113]. The study of HS data also facilitates the interpretation of vegetation conditions using spectral indices [114]. Despite the numerous applications of exploring HS data for remote sensing applications, it suffers a well-known curse of dimensionality and Hughes phenomenon affect [115].

In addition to high resolution spatial and spectral remote sensing data, the choice of classification algorithms also plays a major role in extracting the accurate information from the data. Many algorithms for classification of multispectral data are available. The various traditional distance measure classifiers (such as, Mahalanobis and minimum distance classifiers) are used exhaustively but their applicability in classification of hyperspectral data is still limited due high dimensionality and redundancy of hyperspectral data [116]. With the development of advanced and efficient classification algorithms such as angle measure classifiers, probability divergence measure classifiers and machine learning classifiers *e.g.*, Support Vector Machine (SVM), it is now possible to analyse hyperspectral data efficiently.

From the above discussions, it is seen that high resolution spatial or spectral MS/HS remote sensing imageries have certain issues pertaining to spatial or spectral similarities of

heterogeneous objects found in an urban area. Therefore, it appears that for improving the classification accuracy in an urban environment, the fusion of high resolution spatial and spectral imageries seems to be a promising way of enhancing the information. In relation to this, the information derived from multi-sensor and multiresolution data are getting popular these days. The fusion techniques aim at combining various spatial and spectral characteristics to extract the desired information for the given application. Some of the salient features of fusion have been reported in the literature, such as, pan-sharpening the data using high spatial resolution PAN and low spatial resolution multispectral data for exploring the detailed structures within the objects, land-cover classification using LANDSAT data for classifying residential areas, wetland areas, agricultural land, *etc.* [117] and different temporal observations for surface change detection [118]. Many examples of fusion of the LIDAR, microwave or Panchromatic data with hyperspectral data for classification of urban land-cover have been reported. Most of the examples that have been reported indicate that multi-sensor fusion contributes to the geometric information which is useful in segmentation and classification [117,118]. These examples also report the existence of ambiguities in object identification that occur due to spectral similarities and spatial adjacencies between various kinds of objects in an urban area. However, the usefulness of fusion techniques in distinguishing natural and man-made objects for urban land-cover need to be explored.

In view of the foregoing discussion on the identification and extraction of objects in an urban area, the present study focusses on the potential use of Long Wave Infrared Hyperspectral (LWIR) and Visible (VIS) RGB data for selection of spectral and spatial features and delineation of urban land-cover objects using advanced classifier *i.e.*, SVM. The use of Thermal Infrared (TIR) imaging is scarcely used in fusion techniques though the data is highly relevant for urban land-cover classification. TIR imagery can describe

surface-emitted energy differences caused by human activity [119], therefore, helpful in acquiring the information about the location and shape of objects even in darkness. For this reason, TIR imagery is getting popular and can be used for identification of natural or man-made objects in an urban area.

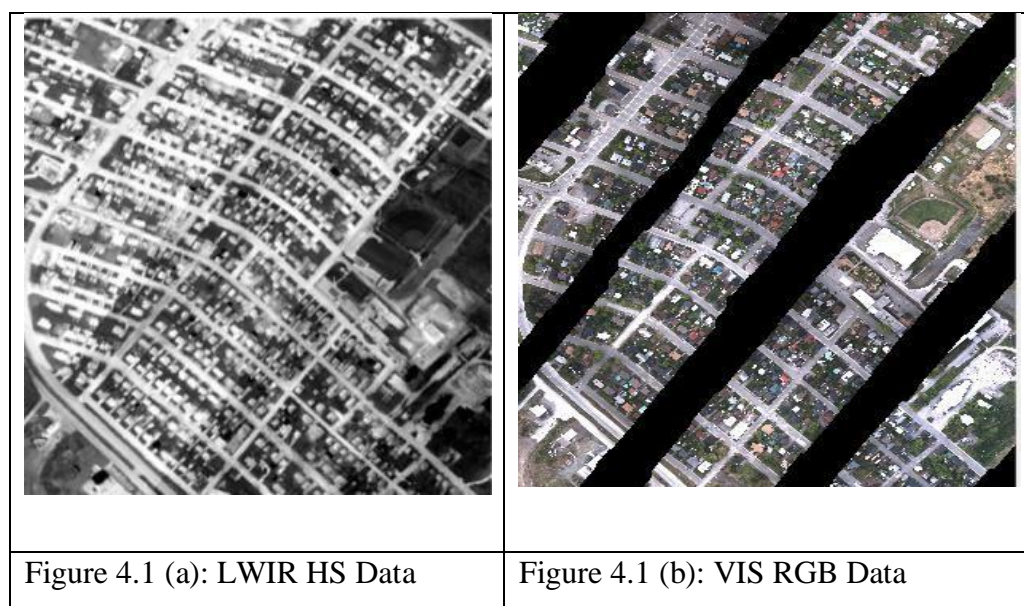
The objective of this study is to extract natural and man-made objects by computing features from coarse resolution hyperspectral (1-m) LWIR and fine resolution (20-cm) VIS RGB data. The study emphasizes the preservation of spectral and spatial characteristics from hyperspectral and high-resolution spatial data for classifying five classes under natural and man-made objects. Under the category of natural objects; the classes that have been extracted are, vegetation, trees and soil, and under the category of man-made objects; roads and buildings have been extracted. Feature oriented object-based classification is performed to generate the classification map that highlights the natural (soil, trees, and vegetated area) and man-made objects (roads and buildings) in the given dataset. This chapter discusses the various tasks that have been formulated and investigated. Following are the investigations/tasks that have been carried out,

- (i) Explore the possibility of multi-sensor data for preserving the spectral and spatial characteristics of various land-cover objects for classification.
- (ii) Explore the effectiveness of fusion in multi-sensor data i.e., thermal infrared hyperspectral and VIS RGB data.
- (iii) Extract the spatial and spectral features for extraction of natural and man-made objects.
- (iv) Segment the features on bounding box of each class under investigation.
- (v) Classify the data based on the feature analysis using one-class vs. one-class SVM classification scheme.

- (vi) Generate the classification maps of the land-cover classes under natural and man-made objects.

## 4.2 Experimental Data Set

In the present experiment, Data Set-1 is used which is mentioned in Chapter-3 under the section-3.2. It consists of two airborne data sets of urban area at Thetford Mines, Canada acquired at different spectral and spatial resolutions. The data *i.e.*, LWIR HS and VIS RGB is shown below in Figure-4.1. The data set includes the residential and commercial buildings, roads and green vegetated area of an urban area. The brief summary of salient features of the two data sets is given in Table-4.1.



**Figure 4.1 – Hyperspectral and Multispectral Data**

**Table 4.1- Summary of data set-1**

Data Set-1	Data set Type	Features	Parameters
4.1(a)	LWIR Hyperspectral Data	Samples and Lines	751 x 874
		Bands	84
		File Type	ENVI
		Spectral Range	7800 -11500 nm
		Spatial Resolution	1m

*Table 4.1-.....Contd.*

4.1(b)	Visible RGB Data	Samples and Lines	3769 x 4386
		Bands	3
		File Type	ENVI
		Spectral Range	400 -700 nm
		Spatial Resolution	0.2m

### 4.3 Methodology

The primary task in classification of HS/MS RSI is to understand and study the characteristics of the data. In present study, since we are using LWIR HS and VIS RGB images which are multiresolution and multi-sensor, therefore, it is necessary to investigate the possible synergies between the two images of Data Set-1. The study of the images in Data Set-1 are well explored to identify the possible characteristics that can be extracted in spectral and spatial domain for identification of the classes under natural and man-made objects. The characteristics and the attributes can be segmented on high resolution data for obtaining the knowledge-based dataset. Finally, the identification and implementation of advanced classifier network is done using knowledge data base for correct delineation of objects in an urban area.

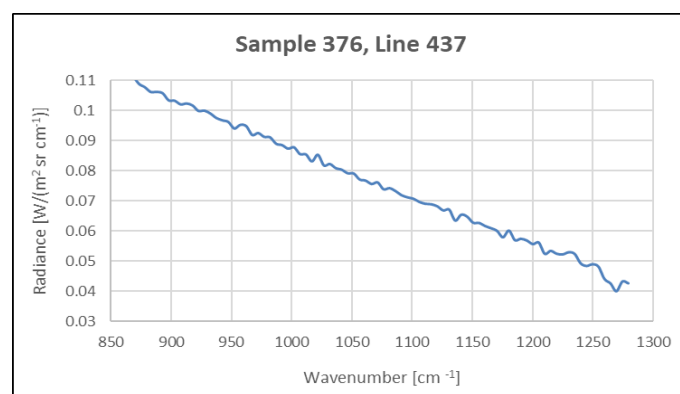
#### 4.3.1 Characteristics of Images in Data Set-1

For object-based classification, it is necessary to explore the two datasets *i.e.*, LWIR thermal hyperspectral and VIS RGB data to understand the challenges posed by them so that the proper procedural processing can be done in land-cover classification of natural and man-made objects. From the two datasets following important information is drawn,

- (i) LWIR thermal hyperspectral data is comparatively a low spatial resolution data with more spectral channels *i.e.*, 84 spectral bands. Due to large number of spectral bands, the data is likely to have higher spectral redundancy, that is, the

linear correlation between the spectral bands may exist which may lead to erroneous results in depicting the objects.

- (ii) As the thermal data shows the radiant energy of man-made objects, the spectral response curves are required to be studied. It is found that the maximum radiant energy is quite low, which is less than 0.12 that is shown in Figure-4.2. Lower radiant energy of man-made objects may lead to lesser precision in extraction of these objects.
- (iii) The challenge posed by VIS RGB dataset is that there are large gaps between the given strips of the entire scene which are highlighted in Figure-3.2(b) (refer Chapter-3 under the section-3.2). The spatial descriptors performance can be corrupted due to these gaps in between the strips.
- (iv) Furthermore, some of the spectral bands of LWIR data show little information about the scene; therefore, it is necessary to choose the useful spectral bands for studying the spectral signatures of the objects for classification. Only the useful spectral bands can enhance the spectral characteristics in defining the objects in the classification process.



**Figure 4.2 – Spectral response curve**

The challenges that have been discussed above are dealt during the processing of the data which are explained below in section-4.4 under the implementation section.

Despite the challenges posed by the two datasets, they have been used in present study to explore the possibility of using information through the properties that can be attained both in spectral and spatial domain for classification which otherwise are difficult to retrieve if using a single image. HS data contains significant spectral information but contains little or no spatial information. The spatial resolution data used for urban land-cover classification contains the spectral and structural information but spectral information for the objects in the scene is very limited. Consequently, a combination of spectral and spatial resolution dataset is needed in classification of urban land-cover area and to achieve this a different approach of implementation is proposed.

### **4.3.2 Choice of Feature Extraction**

The characteristic study of both images of Data Set-1 has helped in identifying the spectral and spatial features for various classes in the data.

#### ***4.3.2.1 Spectral Feature Set***

The acquisition of information regarding vegetation is captured in the form of electromagnetic wave reflectance spectra [120]. The spectral reflectance or emission characteristics of vegetation is determined by biophysical and morphological characteristics of the surface of plants or leaves [120]. The important reflectance bands that capture the various categories of vegetation are : (i) the visible spectra, which are composed of the blue (450-495-nm), green (495-570-nm), and red (620-750-nm) wavelength regions; and (ii) the near and mid infrared band (850-1700-nm) [121,122]. Many vegetation study



related applications are dependent on the reflectivity peaks or overtones of reflectance spectra within the visible and near/mid infrared regions [123,124]. Plant reflectivity in the thermal infrared spectral range (8-14- $\mu\text{m}$ ) follows the blackbody radiation law [125], which interprets the plant emission in relation to plant temperature. Hence, indices obtained from this spectra range can be used as a proxy to assess the dynamics of various categories of the vegetation in an urban area such as ground grass, trees and shrubs.

Since, LWIR HS imagery comprises of spectral channel band ranging from 7800-nm to 11500-nm and VIS RGB band ranging from 400-nm to 700-nm, therefore, NDVI spectral feature is computed using the bands from the multi-sensor data. In this study, 4 classes out of 5 are either the types of vegetation, soil or building and the morphological and biophysical characteristics of buildings, soil and green plants is high in infrared spectral bands, therefore, it becomes relevant to compute NDVI. Mathematical description of NDVI is explained in Chapter-2 under the section-2.3.1.2. In this study, the average of LWIR channels are extracted from LWIR HS data and red channels from VIS RGB data to compute NDVI feature (as given in equation (4.1)).

$$NDVI = \frac{R_{\text{AVERAGE OF LWIR CHANNELS (LWIR HS)}} - R_{\text{RED CHANNELS (VIS RGB)}}}{R_{\text{AVERAGE OF LWIR CHANNELS (LWIR HS)}} + R_{\text{RED CHANNELS (VIS RGB)}}} \quad (4.1)$$

#### **4.3.2.2 Spectral – Structural Feature**

The categorization of man-made objects in an urban area is getting popular with the availability of high-resolution imageries. This is so because it has been reported in various literature surveys that the spectral information of man-made objects exhibits similar characteristics, thereby, making it inefficient in distinguishing the classes. The knowledge of spectral-structural characteristics of such objects from high resolution imageries is highly useful in extracting the important attributes that may lead to correct identification. MBI is recently developed algorithm which is used for the extraction of buildings from

high resolution imageries. Since, the present study involves the classification of buildings, roads and soil, therefore, it becomes relevant to extract MBI to have the information in spectral-structural domain of the mentioned classes as they exhibit similar spectral characteristics. The concept of MBI is discussed in Chapter-2 under the section-2.3.4.1 and is reproduced here with its mathematical explanation [70].

The visible channels in the data provide significant contribution of spectral information of man-made objects, particularly, for buildings. Therefore, the brightness of pixel is computed from all channels of VIS RGB data. The brightness of pixel from each band is recorded as,

$$(x) = \max_{1 \leq k \leq K} (band_k(x)) \quad (4.2)$$

where,  $band_k(x)$  is the spectral value of pixel  $x$  at the  $k^{th}$  spectral band and  $K$  is 3 expressing RGB bands. Next, local contrast information for man-made objects is captured through Differential Morphological Profiles (DMP) of the White Top-Hat by reconstruction (W-TH) using a series of linear Structuring Elements (SE), describing the size and directionality of objects, such as buildings, roads and soil. Mathematically, it is defined as,

$$W - TH(d, s) = b - \gamma_b^{r_e}(d, s) \quad (4.3)$$

where,  $s$  and  $d$  indicate length and direction of a linear SE, respectively. Morphological Profile (MP) of the white top-hat is defined as,

$$MP_{W-TH}(d, s) = W - TH(d, s) \quad (4.4)$$

$$MP_{W-}(d, 0) = b \quad (4.5)$$

The DMP of the white top-hat is defined as,

$$DMP_{W-TH}(d, s) = |MP_{W-TH}(d, s + \Delta s) - MP_{W-TH}(d, s)| \quad (4.6)$$

where,  $\Delta s$  is the interval of the profiles and  $s_{min} \leq s \leq s_{max}$ .

Finally, MBI is constructed as the average of DMP of the white top-hat,

$$MBI = \frac{\sum DMP W - TH (d, s)}{(D * S)} \quad (4.7)$$

where,  $D$  and  $S$  denote the numbers of directionality and scale of the profiles, respectively.

Four directions are considered in this study *i.e.*,  $D$  is kept 4, since increase of  $D$  did not result in higher accuracy for building detection. The sizes of SE ( $x$ ,  $s_{min}$ ,

*and*  $\Delta s$  should be determined according to the spatial characteristics of buildings and the spatial resolution (in this study,  $s_{min} = 2$ ,  $s_{max} = 52$ , and  $\Delta s = 5$ ). The number of scales is calculated by  $((s_{max} - s_{min})/\Delta s) + 1$ . The larger values obtained in MBI vector refer to man-made structures since these structures show larger values in most of the directions of DMPs.

#### **4.3.2.3 Spatial Feature**

In the present study, VIS RGB data has been used for extracting cooccurrence statistics as the spatial resolution of the data is 0.2-m. The statistics are calculated using GLCMs which have been discussed in Chapter-2 under the section-2.3.2. The contrast and homogeneity features are extracted from each band of VIS RGB data. The feature vector using GLCM characterizes the texture of the objects in the scene by calculating the number of pixel pairs in the neighbourhood with the specified spatial intensity and then extracting the statistical measures from the matrix consisting of specific spatial relationship.

### **4.3.3 Segmentation**

The regions of interest polygons for all classes are obtained from VIS RGB data which is a high spatial resolution imagery. Since, VIS RGB data has five strips which does not contain any information, therefore, no polygons have been obtained from the strips.

The connectivity of the polygons is retrieved through *8-pixel* neighbourhood rule followed by assigning a label to the connected object of all regions of interest classes. Bounding box created around the connected objects leads to the object identification for image analysis in classification of objects in an urban area. The concepts related to connected component analysis and bounding box has been explained in Chapter-2 under the section-2.2.

#### 4.3.4 Classifier Network

In the present study, SVM classifier network is used which is a popular method of supervised classification. SVM with one-vs-one approach is built because of its effective processing and the ability to handle unbalanced training datasets. The concept of SVM discussed in Chapter-2 under the section-2.4.1.1 has been reproduced here to show and understand the mathematical approach of SVM network used in the present study. SVM classifiers [126] of the form  $f(x) = w \cdot \Phi(x) + b$  are made to learn from the data  $\{x_i, y_i\}$ , where  $x_i$  is an  $n$ - dimensional input feature vector,  $f(x)$  denotes the hyperplane that separates the class labels on the basis of the support vectors on the hyperplane  $y_i = \pm 1$  on each side,  $w$  and  $b$  are the parameters *i.e.*, weights and bias of the hyperplane. The hyperplane calculation can be optimized as follows,

$$\min_{w, b} \frac{1}{2} \|w\|^2 + C \sum_{i=0}^N \varepsilon_i \quad (4.8)$$

where  $C$  is a regularization parameter and  $\varepsilon_i$  is slack variable. SVM separates the objects/classes based on separating hyper plane [127]. For a given a set of training data, support vectors for the concerned objects/classes are generated near or far from the hyper plane. The larger the distance of the support vectors from the hyper plane the better is the separation of the objects/classes from the other set of objects/classes [127,128]. Few distinct features of using SVMs in the present study for multiresolution and multi-sensor data classification is that the SVM classifier networks are capable of using the hyperspectral

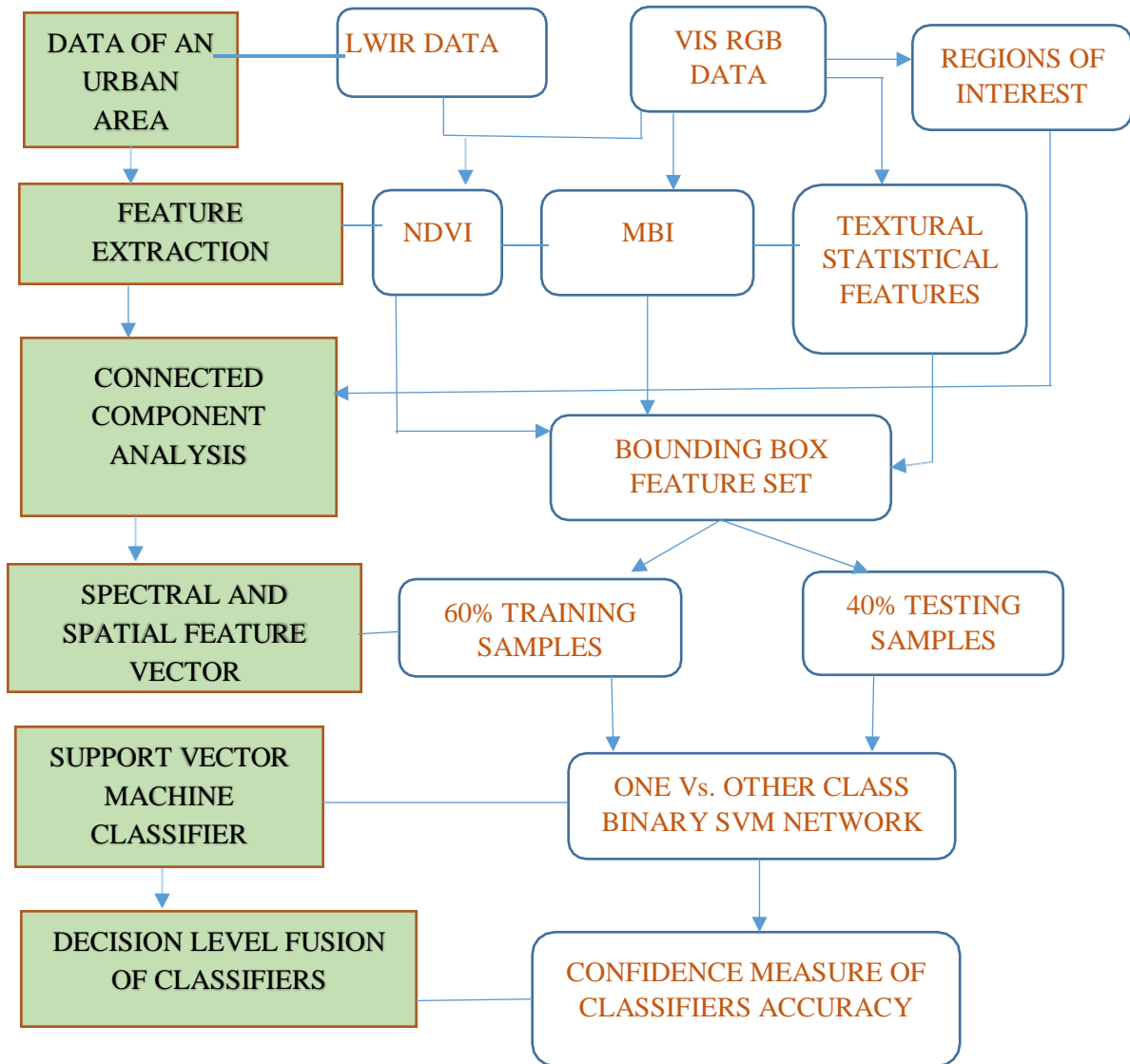
data (LWIR-84 spectral channels) without considering dimensional reduction algorithms and are also insensitive to the size of training samples and quality of the input data.

#### **4.4 Implementation**

A series of image processing steps have been framed for implementing various tasks in the present study for object-based classification of natural and man-made objects in an urban area using data shown in Figure-4.1. The flow chart of the implementation steps is given in Figure-4.3. The methodology includes the careful investigation of two types of datasets *i.e.*, LWIR HS and VIS RGB data for the extraction of significant attributes in spectral as well as spatial domain. In this regard, for the classification of natural and man-made objects from the data of an urban area, three sets of features are calculated *i.e.*, spatial, spectral and morphological features to generate the knowledge data base vector. In spatial domain, the textural second order statistical feature is computed for defining the contrast and homogeneity in the three bands of VIS RGB data. In addition to the textural features, spectral feature is computed using Normalised Difference Vegetation Index (NDVI) which is formulated by exploring the infrared bands from LWIR and red band from VIS RGB data. The mean of near infrared bands from LWIR data and red bands from VIS RGB data is used to compute the spectral index. Besides, textural feature and spectral feature index, spectral-structural feature is computed using Morphological Building Index (MBI) to highlight the characteristics of built up objects in high resolution VIS RGB data. Once, the feature vectors are built up, which contains the information of pixels either in the form of spatial intensities or the spectral values, they are extracted to form a knowledge data base for all classes in a unique way. For this purpose, regions of interest for all natural and man-made objects/classes are generated in the form of polygons. This is created to from the ground truth for all objects/classes from very high spatial resolution VIS RGB data. Connected component analysis is performed on each polygon of every object so that the

polygon only consists of the information of those pixels that hold certain level of connectivity with the neighbourhood pixels. This connectivity of pixels is labelled, and this way forms the connected object for each class of polygons. The features that are calculated consist of an information in the form of contrast, homogeneity, spectral reflectance and spectral-structural values. These feature vector values are then extracted in the bounding box around each connected polygon for all objects/classes. The feature vector values in a bounding box is a knowledge data base of each object/class. Bounding boxes of all classes of connected objects are of irregular size as the polygons (region of interest) captured have varied sizes, therefore, for computational purposes and for minimizing the mixed pixel issue, all bounding boxes are fixed to single size window *i.e.*, 25x25. Bounding box not only helps in identifying the objects of interest in an image but also provides the knowledge of position of the object in an image. The various spatial-spectral features extracted onto the bounding boxes have appreciable information on the edges/position of different objects/classes and each image object feature of the bounding box has a feature knowledge too of respective object/class. The feature segmented bounding box for each object/class is divided into training and testing samples. In this study, after certain trails, the ratio of training data is kept 60% and the ratio for testing data is 40%. It is so chosen as it seems to be an optimal ratio in concern to the classification accuracy of distinguished classes. The training samples are uniquely fed to Support Vector Machine (SVM) classifier for classification purpose. To classify natural and man-made objects/classes like building, vegetation, road, soil and trees multi-class SVM is applied. The SVM used here is non-linear SVM which separates the data in two classes by means of a classification hyperplane drawn in higher dimensional feature space. Classifier training uses the labelled data of bounding box feature samples for learning. For classification of  $n$ -class problem,  ${}^n C_2$  pairs of classifiers are created. An object feature thus gets  ${}^n C_2$  confidence measures for belonging

to various classes. In post-processing stage, fusion of features is done with classifiers decision, such that each classifier votes for a class label, and the majority class label is chosen.



**Figure 4.3 – Flowchart of object-based classification using LWIR HS and VIS RGB data**

All implementations are done using Matrix Laboratory (MATLAB-Version R2015a) and Environment for Visualizing Images (ENVI)-4.5 software.

## 4.5 Results and Discussions

Based on the above methodology, the discussion of results at each step of the implementation stage is given below,

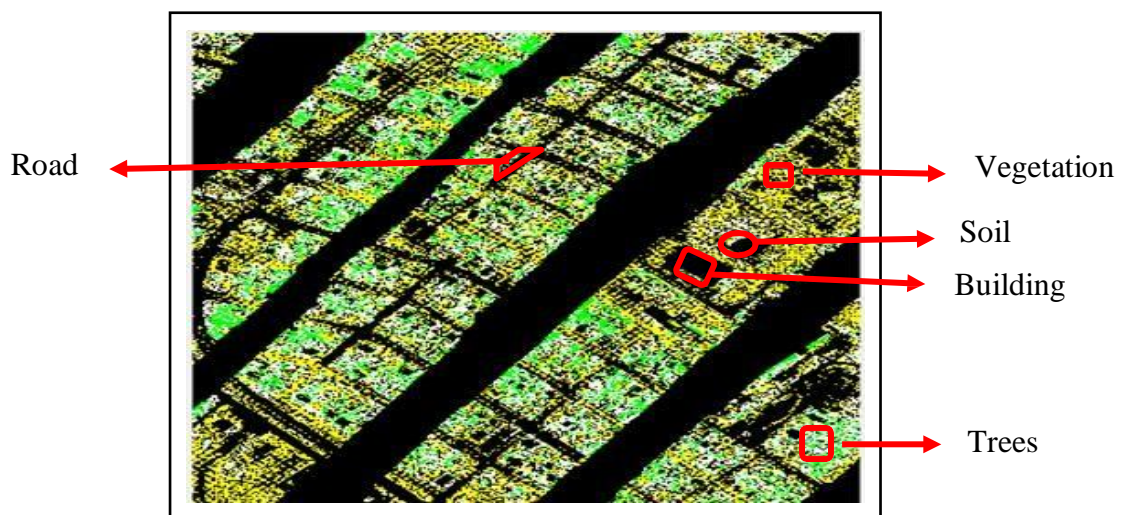
### 4.5.1 Spectral - Spatial Feature Extraction

The features are calculated in spatial and spectral domain which are obtained from LWIR and VIS RGB data. The images of the calculated features are shown below in Figure-4.4 (which represents Normalised Difference Vegetation Index (NDVI) spectral image) and Figure-4.5 (which represents Morphological Building Index (MBI) image). Along with this, textural second order statistical features are also calculated. All these features form the learning knowledge data base for SVM classifier. The information generated from these features in the form of feature vector matrix is incorporated on the regions of interest pixels which is further used for classification purpose. Following is a brief discussion on the results obtained from three sets of features.

- (i) The first set of features is the spectral feature which is obtained through popular spectral index *i.e.*, NDVI. NDVI calculations are done using LWIR hyperspectral and VIS RGB data. Hyperspectral data has bands in infrared range that extends from nominal red edge of the visible spectrum at 7800-nm to 11500-nm. The mean of all the bands is computed in order to gather the average spectral information of near infrared range for the computation of healthy vegetation. As LWIR data supports the infrared range information, therefore, the red band information for computing the vegetation index is extracted from VIS RGB data. For depiction of healthy vegetation, the maximum absorption is captured in red band and maximum reflectance captured in infrared band by the sensors, therefore, the spectral



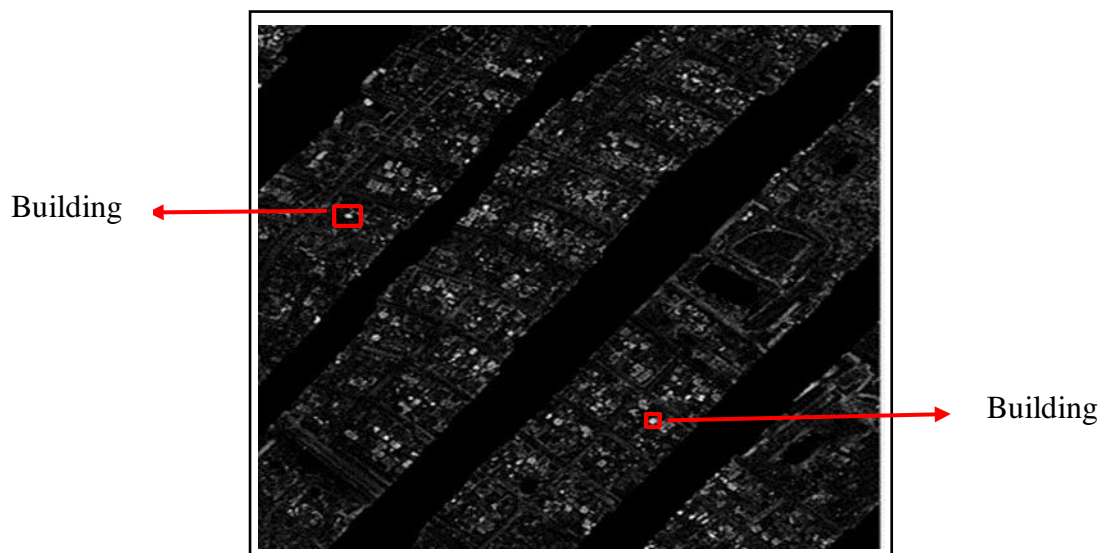
information of both bands is required for understanding the reflectance pattern for vegetation, hence, the fusion of average infrared bands from LWIR and red band from VIS RGB data has complemented the extraction of vegetation index by normalised difference of the spectral band information. The value of NDVI feature extracted in the experiment lies in the range from -0.549 to +1 (which is in the range -1 to +1 defined for NDVI in the literature and explained in Chapter-2 under the section-2.3.1.2.)) The values ranging from -0.1 to +0.1 is indicated as soil in NDVI class identification range. In the experiment, the values that lie between the above range is obtained from the NDVI matrix and is highlighted in red for class soil. Similarly, for other classes, the same information is observed and is highlighted in Figure-4.4 which is the false color composite image of the NDVI spectral index.



**Figure 4.4 - False color composite image of NDVI spectral Index**

- (ii) Another feature that is extracted contains the information of man-made structures such as, buildings in an urban area. The extraction of such structures is a challenging task because of its complexity in terms of shape,

size and brightness; and its spectral similarities with the surroundings *wrt* roads, parking lots and open areas. A recently developed algorithm for buildings *i.e.*, MBI is therefore used in this study which aims at describing the spectral-spatial properties of buildings (*e.g.*, contrast, size and directionality) by a set of morphological operators. The low and high contrast intensity numeric values in MBI matrix helps in identifying the buildings *wrt* natural objects/classes. Figure-4.5 shows the high low contrast image obtained from MBI calculations. The bright structures seen in an image are probable man-made structures. A subset of values obtained from MBI matrix is shown in Table-4.2 which highlights the sudden change in the values showcasing the low and high contrast values. The larger values indicate the pixel intensities for man-made structures as man-made structures tend to have larger values in most of the directions of white top-hat DMP, since they show high local contrast in these directions.



**Figure 4.5 – MBI Image**

**Table 4.2 – Subset of MBI Matrix**

4.500	17.568	17.068	14.431	10.477	12.727	10.795
4.840	18.272	18.090	16.909	12.931	12.045	0.886
6.590	18.113	18.250	19.545	18.977	0	0
9.227	18.204	19.568	21.113	2.799	0	0
10.295	19.454	21.113	21.113	0	0	0
12.295	18.068	18.590	0.954	0	0	0
12.409	16.863	0	0	0	0	0
13.068	13.704	0	0	0	0	0
15.818	0	0	0	0	0	0
18.045	0	0	0	0	0	0

- (iii) The third set of features extracted is the spatial feature which are second order textural features. The texture is a quantitative measure of the arrangement of intensities in a neighbourhood region. The second order textural statistical measures are calculated using gray level co-occurrence matrix (GLCM) approach. Two spatial statistical parameters are calculated - contrast and homogeneity for each visible band. A total of 486 statistical values are obtained, in which from each VIS band a textural feature vector space of 81 GLCMs are of contrast and another 81 GLCMs are homogeneity values. In the experiment, minimum value of contrast is 0 where the constant intensity values of the objects are seen. Maximum value of contrast is 0.667 which defines the difference in brightness levels of the man-made structures such as, buildings and roads within the same field of view. For homogeneity, the minimum value observed is 0.667 and the maximum value observed is 1. Homogeneity value is 1 for diagonal GLCMs which defines the closeness of the distribution of the pixel elements for buildings and roads.

Due to the large size of the matrices of calculated features, they have not been included here. As an example, a small matrix of numeric values obtained for “soil” in case of MBI, NDVI and textural features has been attached at an end in Appendix-I, II and III.

#### 4.5.2 Regions of Interest

The regions of interest pixels for natural and man-made objects from very high-resolution VIS RGB data are generated. Since, VIS RGB data contains five strips which does not contain any information, therefore, no regions of interest have been extracted from that portion of the data. The regions of interest pixels extracted for each class under natural and man-made objects are irregular shaped polygons which are shown in Figure-4.6. VIS RGB data has  $3769 \times 4386 = 16530834$  pixels and the polygons representing regions of interest for natural and man-made objects are captured from the entire site of an image. Table-4.3 shows the total number of pixels captured for each class under the category of natural and man-made objects.

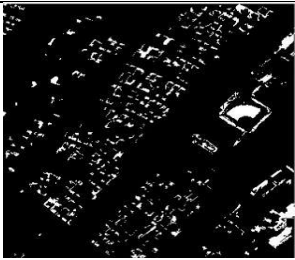

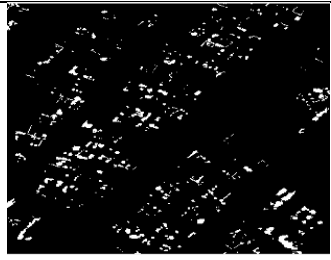


Objects	Class	Class	Class
Natural	 (a)Vegetation	 (b)Soil	 (c) Trees
	 (d)Buildings	 (e) Roads	

Figure 4.6 – Regions of interest polygons of natural and man-made objects

**Table 4.3 - Total number of pixels in each class of natural and man-made objects**

<b>Objects</b>	<b>Class</b>	<b>Total number of pixels</b>
Natural	Vegetation	1021428
	Soil	316798
	Trees	727620
Man-made	Buildings	1590235
	Roads	2514842

#### **4.5.3 Connected Component Analysis and Bounding Box**

Connected component analysis is performed to know the count of the connected components in each polygon of natural and man-made objects (which is shown in binary image, Figure-4.6) by 8-point neighbourhood system. The set of connected components partition an image into segments. The region property of the connected component which is used in this study is the bounding box. It is a small rectangle which not only identifies the objects of interest in an image but also their coordinate positions. Table-4.4 shows the total number of connected components obtained in the polygons containing the region of interest pixels for each class of natural and man-made objects.

**Table 4.4 - Total number of connected components in each class of natural and man-made objects**

<b>Objects</b>	<b>Class</b>	<b>Total number of connected components</b>
Natural	Vegetation	594
	Soil	140
	Trees	552
Man-made	Buildings	456
	Roads	363

#### **4.5.4 Extracting Features Knowledge Database in Bounding Box**

The spatial and spectral features computed from already existing mathematical formulations are then incorporated in the connected regions of bounding box. Hence, in this manner all the connected components in the bounding box will have all feature index

values for each class. This shows that the spatial intensity relationship of the neighbourhood pixels and spectral reflectance values of each feature is now extracted in the bounding box of connected components for all classes under the category of natural and man-made objects forming a complete knowledge data base in spectral as well as spatial domain.

#### 4.5.5 Resizing Bounding Box and Generation of Training and Testing Samples

The bounding box of connected objects of each class has different rectangular size due to irregular pattern of polygons. Therefore, for computational reasons the size of the bounding box is kept same and, in our experiment, the optimal size of 25x25 is taken. Further, the total number of connected objects/components in the bounding box containing the spatial and spectral feature knowledge is then divided into training and testing samples. From the total number of bounding boxes for each class, 60% of them are training samples and the remaining 40% are testing samples. Table-4.5 shows the number of training and testing bounding boxes for each class. As the feature window size of each connected component is 25x25 (which is 625) therefore, the training and testing sample size for all classes is 625 x number of connected components in training and testing sample. Table-4.6 shows the total size of feature sets for training and testing samples.

**Table 4.5 - Total number of training and testing bounding boxes for each class**

<b>Objects</b>	<b>Class</b>	<b>Training Bounding Box</b>	<b>Testing Bounding Box</b>
Natural	Vegetation	356x4	238x4
	Soil	84x4	56x4
	Trees	331x4	221x4
Man-made	Buildings	274x4	182x4
	Roads	218x4	145x4

**Table 4.6 - Feature size for training and testing samples for each class**

Objects	Feature	Class	Training Feature Sample Size	Testing Feature Sample Size
Natural	NDVI	Vegetation	625x356	625x238
		Soil	625x84	625x56
		Trees	625x331	625x221
Man-made		Buildings	625x274	625x182
		Roads	625x218	625x145
Natural	MBI	Vegetation	625x356	625x238
		Soil	625x84	625x56
		Trees	625x331	625x221
Man-made		Buildings	625x274	625x182
		Roads	625x218	625x145
Natural	TEXTURAL	Vegetation	486x356	486x238
		Soil	486x84	486x56
		Trees	486x331	486x221
Man-made		Buildings	486x274	486x182
		Roads	486x218	486x145

#### 4.5.6 SVM Classifier

Each training feature bounding box is given the class label and the system is trained using non-linear SVM classifier. For each pair of class, one SVM network is constructed. Thus, in the experiment, for a 5-class problem,  ${}^nC_2$  SVMs are trained to distinguish the samples of one class from the samples of another class. Classification of an unknown test bounding box samples is done according to maximum voting, where each SVM classifier network votes for one class. Following Tables-4.7 to 4.9 show the confidence measure of each class against the other class from SVM generated network which is based upon spectral and spatial feature set analysis.

**Table 4.7 - Confidence measure of one class against another class using NDVI feature**

<b>Accuracy (%)</b> <b>Class</b>	<b>Class</b>			
	Road (Column 1)	Soil (Column 2)	Tree (Column 3)	Vegetation (Column 4)
Building (Row1)	69.2	63.1	100	59.3
Road (Row2)	Building 62.0	Soil 36.5	Tree 67.5	Vegetation 66.9
Soil (Row3)	Building 82.1	Road 64.2	Tree 73.2	Vegetation 75.0
Tree (Row4)	Building 73.3	Road 75.5	Soil 57.9	Vegetation 57.9
Vegetation (Row5)	Building 87.3	Road 90.3	Soil 74.7	Tree 65.1

**Table 4.8 - Confidence measure of one class against another class using MBI feature**

<b>Accuracy (%)</b> <b>Class</b>	<b>Class</b>			
	Road (Column 1)	Soil (Column 2)	Tree (Column 3)	Vegetation (Column 4)
Building (Row 1)	100.0	100.0	93.4	100.0
Road (Row 2)	Building 53.7	Soil 36.5	Tree 46.9	Vegetation 53.7
Soil (Row 3)	Building 76.7	Road 66.0	Tree 73.2	Vegetation 75.0
Tree (Row 4)	Building 69.6	Road 68.7	Soil 47.0	Vegetation 60.1
Vegetation (Row 5)	Building 77.7	Road 75.6	Soil 70.1	Tree 68.9

**Table 4.9 - Confidence measure of one class against another class using Textural feature**

<b>Accuracy (%)</b> <b>Class</b>	<b>Class</b>			
	Road (Column 1)	Soil (Column 2)	Tree (Column 3)	Vegetation (Column 4)
Building (Row 1)	63.7	73.6	100.0	54.4
Road (Row 2)	Building 0.0	Soil 62.7	Tree 56.5	Vegetation 75.1
Soil (Row 3)	Building 51.7	Road 19.6	Tree 39.2	Vegetation 100.0
Tree (Row 4)	Building 75.5	Road 73.7	Soil 61.5	Vegetation 58.3



Vegetation (Row 5)	Building	Road	Soil	Tree
	72.6	64.2	60.0	0.02

#### 4.5.7 Decision Level Fusion on Multi-class SVM Classifier

To calculate the classification accuracy of SVM classifier network appropriate post-processing is required. In this study, decision level fusion of the classifiers is done. The decision of all testing class labels is done by the majority vote of each class of the testing sample from each feature set analysis. The resultant of this decision accounts for the best match or the maximum vote the class label obtained from learning the training set of the concerned feature set. Hence, the decision is done for one-against-one class by the majority vote rule. Each classifier votes for a class label, and the majority class label is chosen. Table-4.10 highlights the confidence measure of each class achieved from multi-class SVM classifier by decision level fusion of classifiers for each feature set.

**Table 4.10 - Confidence measure of natural and man-made objects by decision level fusion of SVM classifiers using NDVI, MBI and Textural features**

Class	Confidence Measure using NDVI feature (%)	Confidence Measure using MBI feature (%)	Confidence Measure using Textural feature (%)
<i>Column 1</i>	<i>Column 2</i>	<i>Column 3</i>	<i>Column 4</i>
Building	100.0	100.0	100.0
Road	79.3	66.9	66.8
Soil	91.0	85.7	57.1
Tree	82.8	75.1	83.7
Vegetation	91.6	84.8	75.6

A few important observations emerging from Tables-4.7 to 4.10 have been discussed and analysed below,

- (i) In Table-4.7 (row-2, column-2), it is seen that the classification of road against soil presents the least confidence measure *i.e.*, 36.5%. This may be because tropical soils and built environment generally have red band contribute to its

spectral signature. Since, classes such as road and soil show high reflectance in red spectral band, therefore, there spectral separability may be difficult to be addressed by NDVI feature alone and this may lead to low classification accuracy.

- (ii) From Table-4.7 (row-1, column-3), it can be seen that the confidence measure of class building against tree is 100%, the confidence measure of class soil against building (row-3, column-1) is 82.1%, the confidence measure of road against building and road (row-4, column-1 and column-2) is 73.3% and 75.5% and the confidence measure of class vegetation against building and road (row-5, column-1 and column-2) is 87.3% and 90.3% . The inference from the results show that SVM classification using NDVI feature analysis is recommended for classifying man-made objects and vegetation of an urban area using multisensory imageries.
- (iii) From Table-4.7 (row-4, column-1 and column-2), the confidence measure of natural vegetation against man-made objects *i.e.*, tree against building and road is 73.3% and 75.5%. The results show that the use of thermal data in NDVI feature calculation has given the advantage in classification of natural vegetation and metropolitan area. Since, thermal infrared uses emitted radiation instead of reflected radiation and man-made objects are significantly warmer than the natural vegetated areas, hence, this can be well interpreted by using thermal bands for NDVI feature calculations.
- (iv) Table-4.8 shows MBI feature analysis for classifying the data. From the results, it is seen that confidence measure of class building against all other classes is high (row-1, column-1, column-2, column-3 and column-4). This shows that

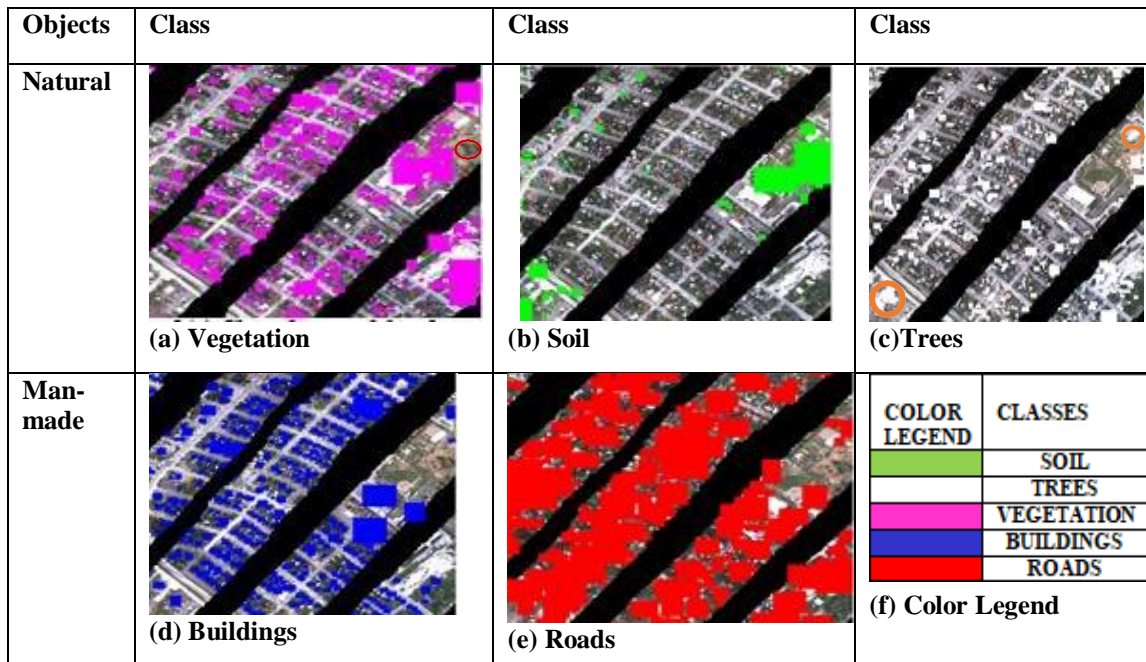
high resolution VIS RGB imagery is useful in depicting the class building from MBI feature.

- (v) From the low confidence measure of class road against building and soil (Table-4.8, row-2, column-1 and column-2) it is seen that MBI is subject to commission errors due to the similar characteristics between buildings, soil and roads. Hence, lower classification accuracy of roads is observed against building and soil.
- (vi) From Table-4.9 (row-5, column-1 and column-2) the confidence measure of vegetation against buildings (72.6%) and roads (64.2%) and also the confidence measure (row-4, column-1 and column-2) of trees against buildings (75.5%) and roads (73.7%) highlights that TEXTURAL features are beneficial for classification of vegetated and man-made objects. High contrast intensity values in textural statistics indicates the bright vegetated areas around buildings and roads which helps in delineating the vegetated portion from the man-made objects.
- (vii) From Table-4.10, it is seen that majority voting decision fusion generated from NDVI feature analysis (column-2) has resulted in best classification accuracy for natural and man-made objects as compared to results obtained from majority voting fusion of MBI (column-3) and textural (column-4) features.

#### **4.5.8 Classification Map**

Based upon the above calculations, the classification map of natural and man-made objects is best obtained from the results of NDVI feature set analysis and is shown in Figure-4.7. The classification of natural and man-made objects is done as per the color legend chosen (shown in Figure-4.7(f)) for all classes. Certain inferences from Figure-4.7 and Tables-4.6 and 4.10 can be made which are discussed below.

The high confidence measure of vegetation which is 91.6% (refer Table-4.10 (column-2)) shows the maximum regions of interest pixels have been mapped correctly. The red marked area in the image (Figure-4.7(a)) shows that the vegetated area is not identified in the classified results. The classification algorithm shows high confidence measure of soil which is 91% (refer Table-4.10 (column-2)) which shows almost all the regions of interest pixels (shown in Figure-4.6(b)) have been correctly identified. The confidence measure attained for trees is 82.8% (refer Table-4.10 (column-2)). The classification map shows certain mixed pixel classes mapped under this category which is highlighted in the image with orange circles (shown in Figure-4.7(c)). The misclassifications are supported from the calculations obtained in Table-4.7 (Confidence measure of one class against another class using NDVI feature). The confidence measure of tree obtained against soil and vegetation is quite low which is 57.9% for both the classes (row-4, column-3 and column-4). Hence, certain regions of pixels containing soil and vegetation have been identified as trees (marked as orange circles in Figure-4.7(c)) lowering the confidence measure. The confidence measure of building is 100% (refer Table-4.10 (column-2)) which shows all regions of interest pixels are correctly identified and the objects identified as buildings in classification map can be seen and matched from Figure-4.6(d). The confidence measure achieved for road is not highly appreciable *i.e.*, 79.3% (refer Table-4.10 (column-2)). The classification map of road (Figure-4.7(e)) shows mixed pixel mapping under this category.



**Figure 4.7 - Classification maps for natural and man-made objects**

#### 4.6 Summary

In the present Chapter, the potential use of multi-sensor data sets for classification of natural and man-made objects is presented. It has been seen that spectral and spatial features extracted from multi-sensor data have significant contribution in identification of objects in an urban area. The use of mean infra-red channels in thermal range for computing NDVI features has shown better effects not only in identification of natural objects but also contributed in obtaining good identification of man-made objects. In the experiment, MBI features has given an appreciable percentage in identification of soil *i.e.*, 85.7% along with effective depiction of buildings against other classes in the scene. The results show that the construction of MBI exhibits the spectral-structural characteristics of buildings and soil and these objects have shown larger values in the directions of the differential morphological profiles for their identification using a high-resolution VIS RGB data. Multiclass SVM classifier network built using textural features has shown good discrimination of natural and man-made objects because of the local contrast and homogeneity values in respect to

the neighbourhood pixels, thereby, highlighting the edges and enhancing the discrimination.

Many classification algorithms are followed by segmentation processes but here in this study, a significantly different approach has been evolved. For classification of natural and man-made objects using multi-sensor and multiresolution data, both spatial and spectral features are explored using connected component analysis and thereby, incorporating the knowledge feature set onto the bounding box of connected components of each class of interest. The knowledge feature set is used to train SVM classifier network and the validations for the testing samples are done using one-against-one class classification approach. Further, the decision of multi-class SVM classifier networks which are established using spectral and spatial features are fused together to explore the best suitable feature for classification. This approach has envisaged the potential use of high-resolution data for building up the region of interest pixels for identification of objects and exploring spectral and spatial features for object-based classification approach for an urban land-cover.

# *Classification of Natural and Man-made Objects Using Weighted Majority Voting Fusion*

### **5.1 Introduction to the problem**

In the field of data fusion, multi-sensor and multiresolution data have received remarkably higher attention. This has been achieved due to the availability of data from multiple sources. The data from different sources provide more information which increase the probability of better understanding the observed area. Planning and development of urban areas to meet the human developmental requirements is an ongoing process across the globe. This, in turn, requires continuous mapping of urban developmental patterns. Requirement of greater accuracy in mapping of urban areas has not only fuelled the development of better resolution remote sensing data but also of exploration of alternative image processing techniques for its analysis and interpretation.

Over the years, there have been significant advancements in the spectral, spatial and radiometric resolutions of remote sensing data [129]. The image processing techniques which form the basis of analysis and interpretation of remote sensing data too continue to be improved and evolved to meet the requirements of the enhanced resolution data as well as the requirements of the user/applications. Image classification facilitate remote sensing applications for grouping the pixels to represent various land cover features such as forests, urban, agricultural and other types of features. These classification techniques are broadly categorized as parametric or non-parametric depending upon whether statistical parameters are used to group pixels or other parameters such as artificial neural network and fuzzy parameters. The focus here however is only on non-parametric techniques which can be

further divided into two types namely, unsupervised and supervised [130]. Unsupervised classification involves clustering of the pixels based on the reflectance properties of the pixels. In the case of supervised classification, however, user selected reference data is considered for classification. Depending upon whether pixels or objects form the basis of classification, these are also referred as pixel or object-based classification.

Classification in urban areas is significantly different from classification of other natural classes because urban environment presents a complex mix of natural and man-made objects [131]. The classification in applications related with urban environment mostly deal with extraction of natural (such as, soil, water bodies, vegetation, trees *etc.*) and man-made objects/classes *e.g.* buildings, roads *etc.* The data usually available on the urban environments is a mosaic of small features of natural and manmade objects with different physical properties. Though, the classification of the objects/classes in the data related to urban environments is performed using pixel and object-based classification techniques but mostly with low classification accuracies [132]. Therefore, there exist greater demands for higher levels of classification accuracy in applications related to urban environments. This has stirred a great deal of interest amongst the researchers to continuously explore alternative methods to improve classification accuracy by data fusion.

Currently, a variety of remote sensing data is available which primarily includes, multispectral and hyperspectral data. While multispectral data consists of bands up to ten, the hyperspectral data consists of hundreds of contiguous spectral bands which make hyperspectral data more suitable for applications related to urban environment. The hyperspectral data may yield better classification of the objects/classes as the spectral signatures of the objects/classes can be utilized where the spatial adjacencies between the objects may degrade the classification accuracy of any object/class [133,134]. Therefore,



the knowledge of both the spatial as well as the spectral characteristics of natural and manmade objects in a scene can be explicitly used in discriminating the two classes.

Though, hyperspectral data may significantly improve classification of objects in remote sensing image, yet it may fail in the case of objects which may be shadowed or may have ambiguous shape/edges which are abundant in any urban environment. The classification of such objects/classes requires describing the spatial and spectral characteristics of the objects/classes simultaneously which may not be possible with the data from single source. It may, however, be improved by fusion of information drawn from multi-sensor and multiresolution data [135]. Fusion involves integrating complimentary multi-sensor data into one new set of data that contains enhanced information which cannot be achieved otherwise using set of image processing and mathematical techniques. In remote sensing, multi-sensor fusion is used to achieve higher spatial and spectral resolutions by combining the data from two sensors, one that has high spatial resolution and other having high spectral resolution. From the literature, it is evident that apart from other constraints, the type of fusion to be selected depends upon type of data and the application that the multisensory data is used for. In the case of object extraction, however, there are instances of decision level fusion having been used [136,137]. Decision level fusion makes use of specific criterion or algorithms to integrate the classified results from different classification techniques. Majority voting, max rule, min rule, average rule and neural networks are some of the algorithms reported in the literature [138] which can be applied in decision level fusion for object extraction in a scene.

In the literature, many examples of fusion of the LIDAR, microwave or panchromatic data with hyperspectral data for classification of urban land areas have been reported [139]. However, there exist ambiguities in object/class extraction that occur due to spectral

similarities and spatial adjacencies between various kinds of objects. These ambiguities may be resolved by classifying the objects/classes in land cover applications using decision level fusion on high dimensional data. In the present study, fusion of spectral and spatial attributes is presented on recent datasets *i.e.*, thermal infrared (TIR) and visible RGB data. TIR data affords the advantage that it highlights the object depending upon its material constituents. It examines the difference between emitted spectral radiance between two objects in the thermal infrared region and hence can perform detection and classification of these objects regardless of illumination conditions [119]. Besides, it is also effective in darkness and can be used for recognition of natural or man-made objects, therefore, well suited for urban environments. The other set of data *i.e.*, visible RGB data helps in studying the spatial characteristics of the objects in a scene. Hence, the characteristics from these two datasets can be studied for improving the classification accuracy of natural and man-made objects.

The objective of the present study is to carry out the object-based classification in urban environments by using fusion technique on multisensory data to classify natural and man-made objects. This Chapter discusses the various tasks that have been formulated and investigated. Following are the investigations/tasks that have been carried out,

- (i) To design the decision level fusion strategy for classification.
- (ii) To perform the comparative analysis to show the effects of using decision level fusion of spectral and spatial features.

## **5.2 Experimental Data Set**

In the present study, Data Set-1 is used which is mentioned in Chapter-3 under the section-3.1. The experimental data consists of two airborne data sets of an urban area at Thetford Mines, Canada that is acquired at different spectral ranges and spatial resolutions.

The images of the multi-sensor data *i.e.*, LWIR HS and VIS RGB data is presented in Figure-4.1 of Chapter-4. The data set includes the residential and commercial buildings, roads and green vegetated area in an urban area. The brief summary of salient features of the two data sets is listed in Table-4.1 of Chapter-4. The data set in this experiment is kept same so that the effects of using the decision level fusion strategy can be shown by comparing the results of fusion strategy with the results of the experiment derived in Chapter-4. In Chapter-4, the results of using multi-sensor data of an urban area by advanced classification algorithm is presented. In the present experiment, the fusion of spectral and spatial features in two stages is performed with the same data set to view the impact of the strategy in terms of the confidence measures of the classified classes under natural and man-made categories.

### **5.3 Theoretical Modelling**

Multi-sensor data fusion techniques aid in complimenting the data sets by combining different spatial and spectral characteristics of two different data sets [140]. The need for applying the fusion techniques in remote sensing arises because the information acquired from the sensors with high spectral resolution are characterized by spectral radiance patterns for different urban land-cover objects in large number of bands of the electromagnetic spectrum, but they provide inadequate information of the objects in spatial resolution [141]. On the other hand, a high spatial resolution data provides shape and geometric details of the urban land-cover objects but little spectral information. Consequently, individual sensor images may not provide enough information for classification, therefore, fusion techniques can enhance the classification accuracy of the objects in the scene. Multi-sensor fusion can be performed at three levels as discussed below,

- (i) In pixel level fusion, pixel by pixel information from different sensor data is merged to improve the detection of the objects/classes [142].
- (ii) Feature level fusion involves the fusion of the features from different sensors to create a feature vector for classifying the objects/classes [143].
- (iii) Decision level fusion is a higher level of integration of multi-sensor data. In this type of fusion, the classified results from the data of each sensor are merged by various criteria or algorithms to obtain the final classified data [144].

It has been reported that the use of single classifier network in classification has many a times led to wrong decision of samples in various experiments.

### 5.3.1 Majority Voting Rule

In the present paper, Majority Voting (MV) rule is applied to enhance the confidence measure of the classified results. The majority voting rule technique is defined on SVM classified results which are trained by spectral and spatial features by imposing a set of rules. Here, in the experiment, the class of sample  $s$  is determined by:

$$\text{Class}(s) = \text{mode}(\text{classified class label}) \quad (5.1)$$

The classifier predicts the labels of the testing samples and provides the information of the number of samples that voted for each label. This information is converted into proportions to interpret the probabilities for each class. The probability of the majority class is called the confidence measure. Majority voting rule is applied at the end of the classification stage to fuse the classifiers outputs to give the final decision. This rule is generally applied to rule out the probability of the minor class label in the classification and to calculate the probability of the class label of a class in a given set of classes that has more votes than other class labels [145]. This helps in extracting the object with maximum votes of class labels to fall under the class and thereby increases the classification accuracy.

### 5.3.2 Weighted Majority Voting

In Weighted Majority Voting (WMV), the decision of independent classifiers is weighted according to the evaluated accuracy on the training set. In the present study, the accuracy generated by the individual classifier of the specific class is adopted as the weights. This linearly combines the probabilistic predictions of multiple classifiers by weighting their posterior probabilities [146]. It can be defined as follows,

$$P(X \in C_i / X) = \frac{1}{k} \sum_{k=1}^N P(X \in C_i / X), i=1, 2, \dots, M \quad (5.2)$$

The class label is the decided as,

$$L(X) = \arg \max_{i=1, \dots, M} (P(X \in C_i / X)) \quad (5.3)$$

where  $P_k(X \in C_i / X)$  is probability of class  $i$  of pixel  $X$  in  $k^{th}$  classifier,  $M$  is the total number of classes,  $N$  is the total number of classifiers and  $L(X)$  is the class label of pixel  $X$ .

### 5.4 Methodology and Implementation

The decision level approach using fusion can be applied in two situations, one when decision of multiple classifiers is merged using the same dataset, and another is the merging of the decisions generated from multiple datasets. In the present study, a decision-based system is designed which explores the advantages of multi-sensor data for object-based classification to obtain the correct decisions of the class labels under natural and man-made category. The aim of the study is to design a decision level system computationally efficient to take advantage of the information provided by multiple data sources.

The methodological approach used in the present study have few similar initial implementation steps described in previous study of Chapter-4. Multiclass SVM classified results derived from spectral and spatial feature sets are used and further processed in this experiment. For the improvement in the classification results, multilevel decision fusion

technique is applied at the post processing stage of the earlier work. An alternative method using decision level fusion approach is designed for best possible match. For decision level fusion, weighted majority voting technique is used. The proposed methodological approach applies weighted majority voting at two levels, one for multiclass binary SVMs (using decision level fusion) at each independent feature set and other for multiclass binary SVMs (using decision level fusion) for combined feature set. This two-stage process for the classification is shown in Figure-5.1.

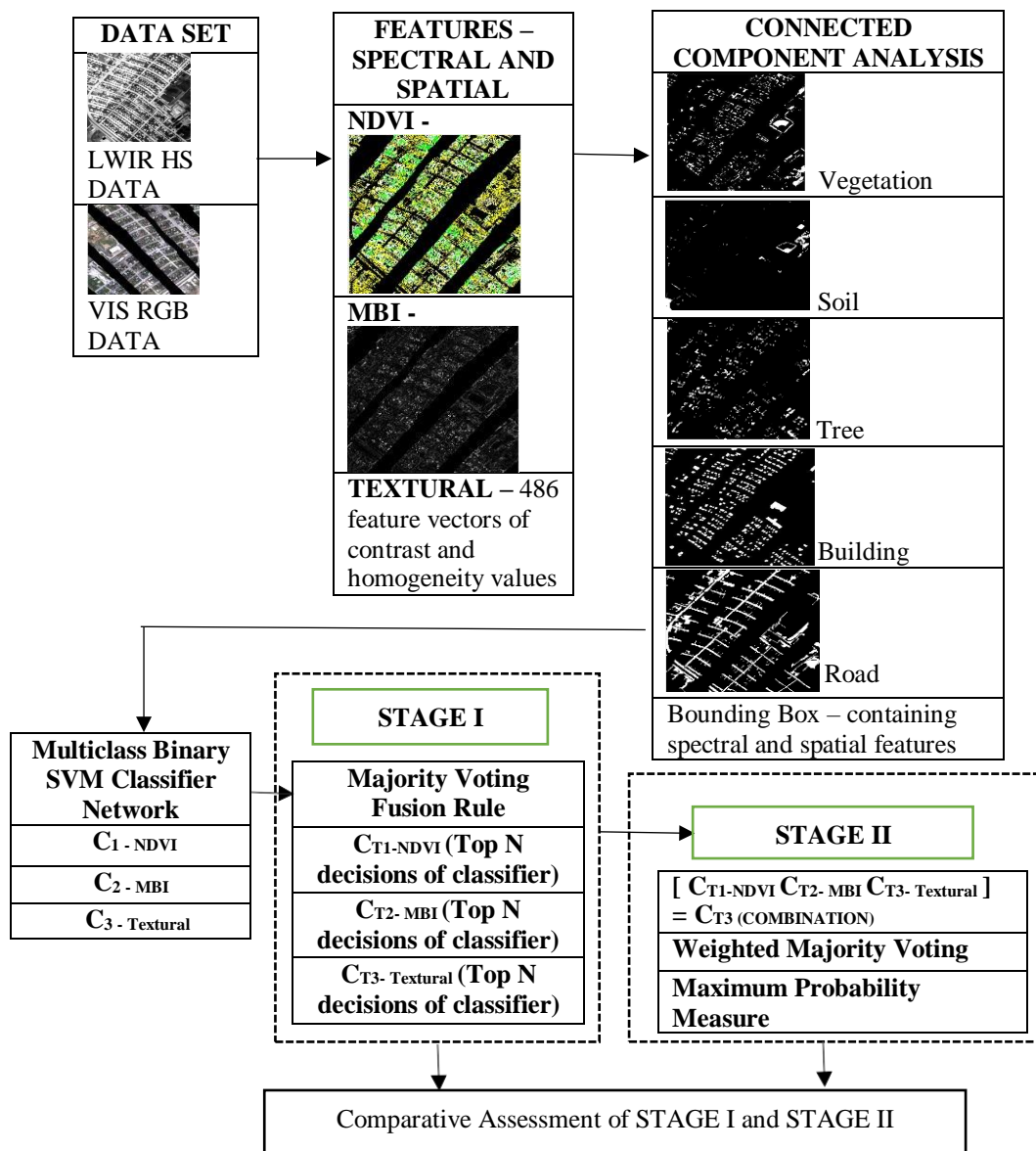


Figure 5.1 – Structure of multiclass classifier fusion

### 5.4.1 Fusion Strategy

To achieve the improvement in the classification accuracy of the natural and man-made objects/classes in multi-sensor remote sensing data, multilevel fusion approach is developed in this study. The methodology completely relies on the spatial and spectral aspects of multi-sensor data. TIR HS (thermal infrared hyperspectral) and VIS RGB (visible band) data are used to extract the features. Features are extracted in spatial and spectral domain for gathering the information of distinct objects/classes. Further, Support Vector Machine (SVM) is used to classify the class labels based on features extracted. The individual probabilities (confidence measures) from all such pair of binary SVMs are combined to uniquely represent the object feature to one of the classes. After summing up all the probabilities the class with highest probability value (confidence measure) represent the object. The benefit of using the weighted majority voting is that to decide the true class the decision from all possibilities are used. The max confidence from classifiers are the weights in weighted majority voting. Therefore, in case of noisy data if one or two pair of SVM classifiers comes with low probability, still the high probability of all other classifier pairs make it to fall into true class. It fails only if all the pair of classifiers come with low probability and an unstable decision. The novelty of the study lies in the methodological approach where instead of fusion of different classifiers for classification, different features are combined that form the knowledge data base for improvement in classification accuracy. The fusion of three different sets of features is the main highlight of the study which is done through weighted majority voting that acts as a local discrimination strategy at each classifier decision to clearly distinguish the class labels for object/class extraction.

#### 5.4.1.1 Stage 1 – Multiclass binary SVMs decision using individual features

There are many schemes of creating binary SVMs, however, in the present experiment, one-against-one approach is used for creating various possible pair of binary SVMs. Each pair classifies the object feature into one of classes with certain confidence measure. The confidence measure gives the probability of an object to belong to a class. The SVMs used here is linear kernel based which separates the data in two classes by means of a classification hyper-plane drawn in higher dimensional feature space. For 5-class problem,  ${}^5C_2$  such pairs of classifiers are created. In  $5(5-1)$  pair of classifiers, each one classifier distinguishes a pair of class i.e.,  $i$  and  $j$ . Let's say, if  $C_{ij}$  be the classifier, where class  $i$  is labelled as positives [+1] and class  $j$  is labelled as negatives [-1]. The training data for each classifier that comprises of three different feature vector values (i.e., NDVI, MBI and textural) contains the data from the two involved classes  $i$  and  $j$ . SVM classifier network finds an optimal separating hyperplane that discriminates the classes  $i$  and  $j$ . For  $C_{ij} (n-1*m$  (where  $m$  is the size of testing samples)) classified class labels result for each pair of classes, the major or max rule of majority voting is used to vote the class label in each row. The maximum votes for the class labels give the confidence measure. Hence, for all the testing object features there are  ${}^5C_2$  classified measures for belonging to various classes for all three feature sets and the max of class label in each pair of classifiers is the final decision. In this experiment  $k$  is a feature vector that ranges from 1 to 3. For  $k$  feature vectors, a set of decision fusion classified potential class labels for testing object features are expressed as  $C (f_{k=1 \text{ to } 3}) = [ C_{i1} C_{i2} C_{i3} C_{i4} ]_{4*5}$ . The structure of multiclass SVM classifier network of this stage is shown in Table-5.1.



**Table 5.1 – Structure of Stage I- Multiclass SVM classifier network**

Classes	One Class Vs. Other Class SVM Classifier Structure				Final Decision
Class1(L(X=1))	1 vs. 2	1 vs. 3	1 vs. 4	1 vs. 5	$L(X=1)= \arg \max_{i=1,\dots,M} (P(X \in C_i   X))$
Class2(L(X=2))	2 vs. 1	2 vs. 3	2 vs. 4	2 vs. 5	$L(X=2)= \arg \max_{i=1,\dots,M} (P(X \in C_i   X))$
Class3(L(X=3))	3 vs. 1	3 vs. 2	3 vs. 4	3 vs. 5	$L(X=3)= \arg \max_{i=1,\dots,M} (P(X \in C_i   X))$
Class4(L(X=4))	4 vs. 1	4 vs. 2	4 vs. 3	4 vs. 5	$L(X=4)= \arg \max_{i=1,\dots,M} (P(X \in C_i   X))$
Class5(L(X=5))	5 vs. 1	5 vs. 2	5 vs. 3	5 vs. 4	$L(X=5)= \arg \max_{i=1,\dots,M} (P(X \in C_i   X))$

**5.4.1.2 Stage 2 – Proposed strategy of multiclass binary SVMs decision using combined features**

The mathematical structure of the multiclass SVM classifier fusion is explained below,

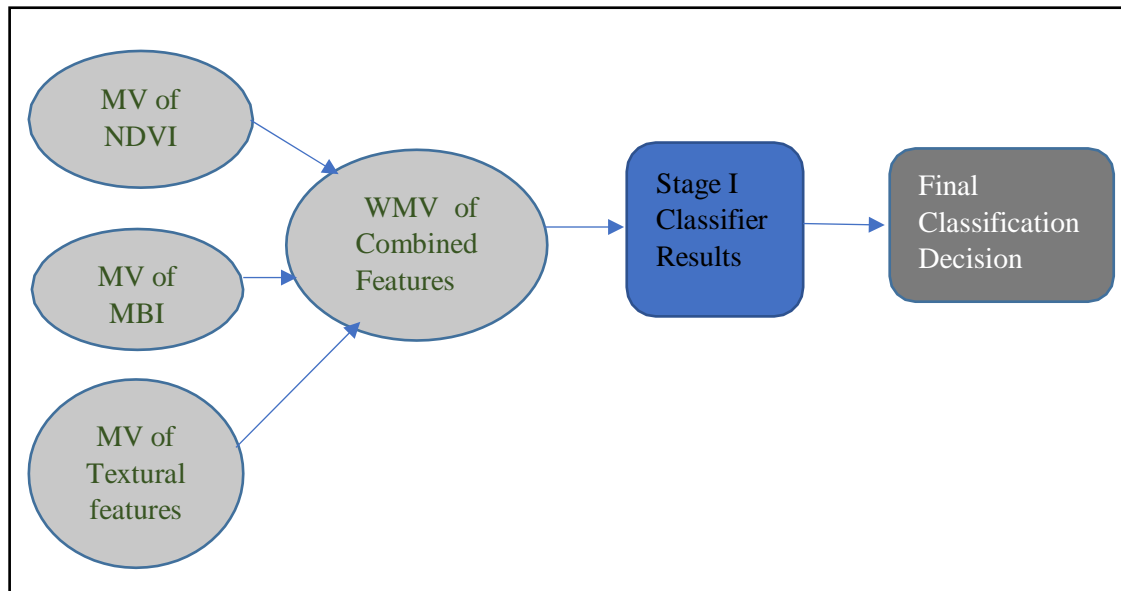
For  $n$ -dimensional feature space belonging to data  $R^n$ ;  $X = [x_1, x_2, \dots]^T$  is the  $n$ -dimensional feature vector values, such that,  $X \in R^n$ . If  $\Omega = \{\omega_1, \omega_2, \dots\}$  be the set of potential class labels;  $\mathcal{C} = \{C_1, C_2, \dots, l\}$  be the set of trained classifiers for decision fusion. For a given input pattern  $X$  (in the experiment  $X$  is the training spectral and spatial feature sets computed and discussed in Chapter 3), the output of the  $i^{\text{th}}$  classifier is denoted as in  $C_i(X) = [c_{i1}(X), c_{i2}(X), \dots, c_{im}(X)]^T$ , where  $c_{ij}(X)$ ,  $i = 1, 2, \dots, l$ ,  $j = 1, 2, \dots, m$ , represents the classification measure of SVM classifier  $C_i$  based on true positives considering that  $X$  belongs to class  $\omega_j$ . The outputs of  $l$  classifiers are fused and a decision is constructed as,  $\mathcal{C}(X) = F(C_1(X), C_2(X), \dots, C_l(X))$ , where  $F$  is the decision fusion rule.

The decisions (D) are constructed from the output generated from one class vs. another class classifiers for each feature vector values which can be represented as  $l \times m$  matrix,

$$D(X) = \begin{bmatrix} c_{1,1}(X) & \cdots & c_{1,j}(X) & \cdots & c_{1,m}(X) \\ \vdots & & \vdots & & \vdots \\ c_{i,1}(X) & \cdots & c_{i,j}(X) & \cdots & c_{i,m}(X) \\ \vdots & & \vdots & & \vdots \\ c_{l,1}(X) & \cdots & c_{l,j}(X) & \cdots & c_{l,m}(X) \end{bmatrix} \quad (5.4)$$

In the above matrix,  $l^{th}$  rows represent the measure of number of classifier networks for  $(X)$  and  $j^{th}$  columns are the possible measures of testing object features that  $l$  classifiers consider that the input pattern  $X$  belongs to class  $\omega_j$ . The decision is the fused outcome as  $(X)$  which is an  $m$ -dimensional vector that is denoted as in  $\mathcal{C}(X) = [d_1(X), d_2(X), \dots, d_m(X)]^T$ , where  $d_i(X)$ ,  $i = 1, 2, \dots, m$ , shows the confidence measure value that  $X$  belongs to class  $\omega_i$  after fusion. The max rule (which explained in equation (5.3)) deems that  $X \in \omega_k$ . This mathematical fusion model is applied on the proposed strategy shown in Figure-5.2, where the decision results obtained from Stage I is combined further with combined decision of all feature sets. Therefore, the outcome from this strategy predicts the confidence measure of the class label that has got the largest votes by fusing the outcomes of independent features along with the fused decisions of all feature sets. This strategy minimizes the ambiguity that may arise in prediction of class labels if both the class labels have equal votes or when there exists divergence in the decisions of individual classifiers.

All implementations are done using MATLAB R2015a and ENVI 4.5 software.



**Figure 5.2 – Structure of Stage II - Fusion strategy**

## 5.5 Results and Discussions

The confidence measure of class labels with correct decisions is very important in forming the classification results using one class vs. another class. It is dependent on the methodological approach defined for the development of the strategy to improve the classified results for minimizing the ambiguities that may arise in taking the decisions. In this Chapter, experiments are conducted to study the effects of fusion techniques on multisensory data. To achieve this, an alternative approach is designed by fusing the stage-I results obtained by independent features with the combined feature sets to improve the classification accuracy of natural and man-made objects using object-based classification algorithm. Based on the above methodology and implementation stages, the results are discussed below, and the statistics are shown in Table-5.2.

**Table 5.2 – Confidence measure of SVM classifier network for natural and man-made objects using weighted majority voting fusion strategy**

<b>Classes</b>	<b>SVM Classifier using Majority Voting on Vegetation Index (%)</b>	<b>SVM Classifier using Majority Voting on MBI (%)</b>	<b>SVM Classifier using Majority Voting on Textural Features (%)</b>	<b>SVM Classifier using Weighted Majority Voting on Combination of Features (%)</b>
<i>Column 1</i>	<i>Column 2</i>	<i>Column 3</i>	<i>Column 4</i>	<i>Column 5</i>
Building	100.0	100.0	100.0	100.0
Road	79.3	66.9	66.8	89.6
Soil	91.0	85.7	57.1	98.2
Trees	82.8	75.1	83.7	96.8
Vegetation	91.6	84.8	75.6	96.2

A few significant observations emerging from Table-5.2 have been analysed and are discussed below,

- (i) The results shown in Table-5.2 reveal that the classification accuracy of SVM classifier based on majority voting rule using spectral and spatial features lie in the range of 57% to 91% (can be seen from column-2 to column-4 of Table-5.2) for roads, soil, trees and vegetation, which is improved to 89-98% (can be seen in column-5 of Table-5.2) by applying SVM classifier using weighted majority voting fusion rule for all features.
- (ii) It is seen from Table-5.2 that for class “road” the majority voting rule on SVM using either of the spatial features *i.e.*, MBI or textural resulted in almost same classification accuracy (66.9% - can be seen in column-3 and column-4 of Table-5.2). But the fusion of spatial and spectral features has increased the

number of votes of class road against other classes and resulted in improvement of classification accuracy (89.6% - can be seen in column-5 of Table-5.2).

- (iii) From Table-5.2, it is seen that for the natural objects *i.e.*, soil and vegetation, NDVI feature contributed for better classification accuracies (column-2) as compared to MBI (column-3) and textural features (column-4). The fusion of spatial features with spectral features has improved the classification accuracy of soil from 91% (column-2) to 98% (column-5) and for vegetation it has improved from 91% (column-2) to 96% (column-5).
- (iv) Also, for natural object “tree”, through MV (stage-I), the textural features have resulted in accuracy of 83.7% (as recorded in Table-5.2, column-4) which is better than the results obtained as compared to MBI ( *i.e.*, 75.1%, column-3 of Table-5.2) and NDVI features ( *i.e.*, 82.8%, column-1 of Table-5.2). But, the fusion of all features using weighted majority voting has improved the classification accuracy of tree from 83.7% (column-4 of Table-5.2) to 96.8% (column-5 of Table-5.2).

The above observations have resulted in enhancement of the confidence measures of all classes. This shows that the decision strategy has strengthened the process of prediction of the class labels. The process of prediction of correct class label has been reinforced by the weighted voting of combined features extracted in spectral and spatial domain along with the largest votes that each class label attained at independent feature level. The strategy minimised the ambiguity decisions that may have arisen in the prediction of class labels otherwise. The decisions from the independent feature sets may not be enough to provide the correct number of votes in the prediction of the class label in certain cases. This case may arise if two class labels attain equal number of votes or if all class labels attain votes for different classes. In such situations, the convergence of the decision becomes difficult

and hence, results in lower accuracy. The combined weighted decision of the class label has helped in removing the above ambiguities and hence resulted in the enhancement in the statistics for confidence measure of each class which is discussed above in observations attained from Table-5.2.

## 5.6 Summary

In the present study, the complementary sources *i.e.*, very high-resolution VIS RGB and LWIR HS data have been explored for enhancing the urban land-cover object classification. VIS RGB data delineates the land-cover objects based on the knowledge spatial and structural attributes, while LWIR HS data provides rich spectral information for the identification of objects with dissimilar spectral signatures. In this experiment, decision fusion strategy is employed to extract and use the complimentary information provided by different sources for improving classification results of an urban area. The objective is to improve the classification accuracy of the extraction of natural and man-made objects from LWIR and VIS RGB dataset using multilevel fusion technique at two stages. At first stage, decision level rule is applied on the classified results of multi-class SVM network trained at each spatial and spectral feature. Then, at second stage, decision level performance is seen by combining the all features simultaneously and complementing these combined features with the stage-I results, forming a complete set of fused features and then again applying the decision rule to lower the misclassification effect on the judgement of the class labels. The proposed approach shows the improvement in the confidence measures of the classes. The comparative analysis of the results reveals that the overall confidence measure of the classified objects using SVM classifier have been improved from stage-I with minimum accuracy recorded for soil *i.e.*, 57.1% to 98.2% using weighted majority voting of combined spectral and spatial features derived stage-II. Even, for rest of the classes there is improvement in the accuracy which can be referred in Table-5.2. Hence, it can be

concluded from this experiment and its applicability in an urban area that fusing classifiers' decision based on combination of feature knowledge set in spectral and spatial domain can achieve better performance than the decision of classifier based on independent features.

# *Land-Cover Classification Using Non-Parametric Classifiers in Multisensory Images*

### 6.1 Introduction to the Problem

Requirements of higher accuracy in image and data analysis has not only fuelled the development of technologies in acquiring better resolution remote sensing data but also in exploring multiresolution and multi-sensor data [147]. Currently, a variety of multiresolution and multi-sensor remote sensing data is available which primarily includes, Multispectral (MS) and Hyperspectral (HS) data. Multispectral remote sensing data comprises of smaller number of spectral bands with larger bandwidth. Therefore, the data can be used for studying spatial characteristics of the ground objects. But the interpretation of multispectral data is difficult particularly, in land cover applications where intra-class variability is important. Hyperspectral remote sensing data includes large data sets comprising of 100 to 200 contiguous spectral bands that has ample spectral information of various intra-class ground objects in the scene. But the handling of large amount of data will, however, dramatically increase the complexity and processing time. Also, the effective and proper selection of relevant bands for the study of any application becomes the primary task while handling the hyperspectral remote sensing data. The correct interpretation of remote sensing data is very important in obtaining higher accuracies in classification applications.

The information derived from high resolution MS and HS data in the form of textural features, spectral indices, band ratios, Digital Elevation Model (DEM), or the information derived from other ancillary data may contribute in the improvement of



classification accuracies [148]. However, the increase in the number of spatial and spectral attributes from the multisource input data does not necessarily mean that these would enhance the performance of classification. In addition, a greater number of attributes may create large knowledge data base which may lead to noisy and redundant information, and thereby, may reduce the classification accuracy [149]. Multisource data may vary with each other in their effectiveness and reliability levels, that is, one data source may be appropriate in extracting one specific physical feature on the land surface while the other data source may be more useful in extracting some other feature. Hence, it is very important to understand the synergies between multisource datasets so that correct identification of significant input attributes may be extracted to aid high classification accuracy [150]. However, there exists a scope of insight for using multisource data sets for determining spectral and spatial features and exploring different methodological approaches in order to study their effects on classification accuracies [151]. In addition to the exploration of feature extraction techniques in spectral and spatial domain from multisource data, the classification algorithms also contribute effectively in improving the classification results. The effects of recently developed classification algorithms have not been well studied in classifying various multisource remote sensing data which could be interesting in addressing various issues and parameters related to the classification of land-cover features.

The choice of classification algorithms is important in classification. The correct selection of classification algorithms is essential as they result in considerable enhancement in the evaluation process of classified outcomes. Traditional classifiers can process the data in a short time span with relatively good classification results. However, the major limitation of these classifiers is their dependence on statistical assumptions which may not appropriately represent remote sensing data. Furthermore, it is difficult for statistical-based classifiers to assimilate varied sources of data for classification. Recently, non-parametric

classification techniques such as those based on machine learning theory *etc.* have been developed. Unlike conventional classifiers, the new classification algorithms, such as Artificial Neural Network (ANN), Support Vector Machine (SVM) or Self Organising Map (SOM) *etc.*, do not rely on statistical principles and therefore can handle a complex dataset more effectively [149,152]. Because of these properties, non-parametric classifiers are now considered as important alternatives to traditional methods, and the application of non-parametric classifiers to classify remotely sensed data has become an attractive subject for research. The classification performance could be enhanced further by applying a Multiple Classifier Systems (MCS) since it may take advantages of, and compensate weaknesses of, different classifiers. Despite the robustness of such techniques, few studies have been conducted on the application of these techniques for classifying combinations of different remote sensing datasets.

The traditional classification algorithms assume that all pixels or group of pixels of the training samples follow a normal distribution, hence, referred as parametric classification. In fact, it is not necessary that all remotely sensed images follow this sort of criterion, especially the complex data sets [153,154]. Another drawback of the parametric classifier is its difficulty in integrating spectral data with other kinds of data [147]. In the literature, [154] it has been reported that it is reasonable to weigh different input data sources for the classification process because of their different ability to discriminate land cover classes. However, these weighing factors are not applicable to the conventional parametric techniques. The non-parametric classifier does not require a normal distribution of the dataset and, consequently, no statistical parameters are needed to differentiate land-cover classes [147,148,153]. This property has made non-parametric classification techniques very attractive for land-cover classification. Previous studies have revealed that

non-parametric classification may give better classification results than parametric classification, particularly in complex study areas [155-158].

The integration of different remote sensing data could provide supplementary information and consequently improve the land-cover classification results. Interpretations from multiresolution and multi-sensor data can be enhanced with the knowledge of digital image fusion techniques [159,160]. Fusion of non-parametric classifiers decision on multiresolution and multi-sensor data may not only help in sharpening the details of low-resolution data but can also improve the classification results by enhancing the capability of classification algorithms [161]. Hence, with the improvement in classification algorithm techniques, the classification of land-cover objects using multisensory data has resulted in great deal of consideration amongst researchers to explore the possibilities in image processing and data fusion techniques for better results [162-164].

With respect to the discussion above, in this experiment, the classification of multisource datasets using two popular non-parametric classifiers have been evaluated. The objective here being the comparative analysis of performance of two non-parametric classifier algorithms *i.e.*, Support Vector Machine (SVM) and Artificial Neural Network (ANN) in classification of natural and man-made objects using multi-sensor and multiresolution hyperspectral LWIR and VIS RGB data. The single source data is not fully capable of extracting accurate ground objects either due to spectral similarities within different objects or due to spatial adjacencies between similar objects. In addition to spectral response, object characteristics, such as shape, size and structural relations also need to be interpreted. The use of complementary data observed from the same site with superior apprehension has resulted in increase of classification accuracy. The use of hyperspectral and multispectral data simultaneously seems to be a promising way for exploring the features related to spectral and spatial domain that can significantly improve

the accuracies and enhance the interpretations of remotely sensed data. Following are the investigations/tasks that have been carried out,

- (i) A multilevel fusion strategy developed in the previous study is explored using one more popular classifier algorithm for urban land-cover classification on hyperspectral and multispectral multiresolution, multi-sensor data to study the impact on classification accuracy of objects/classes. In this context, TIR HS (Thermal Infrared Hyperspectral) and VIS RGB data has been used to extract multiple features pertaining to natural and man-made objects/classes. For this purpose, salient features in spatial, textural and spectral domain are computed. Further, the multiple features generated through feature level fusion have been used to train two non-parametric classifiers *i.e.*, SVM and ANN.
- (ii) The comparative classification accuracy assessment of non-parametric classifiers is done through multi-level fusion strategy using spectral and spatial features. Multi-level fusion strategy is applied at two stages; one at classifier stage with each feature set and other while combining all the feature sets. The results show the effects of using feature approach on non-parametric classifiers for classification using multisensory data sets and the effects of using decision level fusion of features on classifiers.

The experiment highlights the performance of different classifiers on the study and experiments achieved in Chapter-4 and Chapter-5. In Chapter-4, the effects of using of multi-sensor data of an urban area by advanced classification algorithm *i.e.*, SVM is presented. In Chapter-5, the decision level fusion of spectral and spatial features is presented in two stages on the same data set (explored in Chapter-4) to view the impact of the decision strategy in terms of the confidence measures of the classified classes under

natural and man-made categories. In the present Chapter, the impact of all these features is foreseen using another popular non-parametric classifier. This experiment highlights the comparative performance of two classifiers using the methodological approach designed (in Chapter-4 and Chapter-5) for urban land-cover classification.

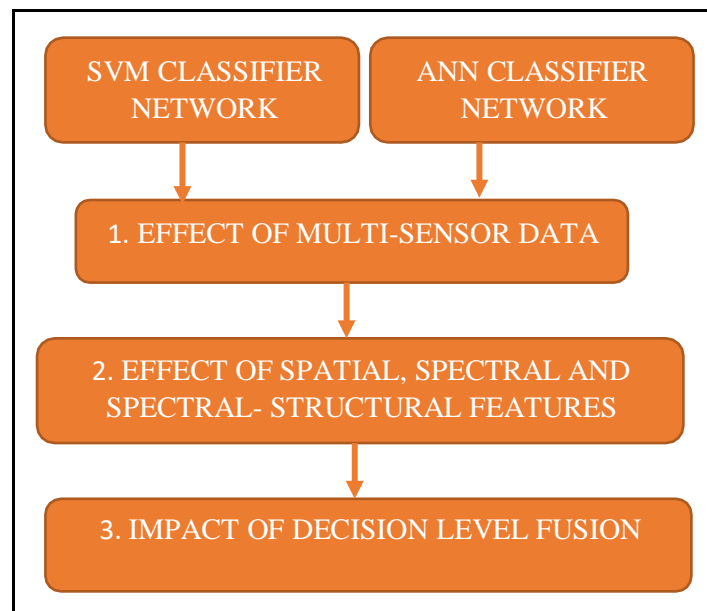
## **6.2 Experimental Data Set**

In the present study, Data Set-1 mentioned in Chapter-3 under Section-3.1 is explored. The experimental data consists of two airborne data sets of an urban area at Thetford Mines, Canada that is acquired at different spectral ranges and spatial resolutions. The images of the multi-sensor data *i.e.*, LWIR HS and VIS RGB data can be referred from Chapter-3 presented in Figure-3.2. The data set includes the residential and commercial buildings, roads and green vegetated area in an urban area. The brief summary of salient features of Data Set -1 is given in Table-4.1 of Chapter-4. The data set in this experiment is kept same to present the comparative performance of two non-parametric classifiers using decision level fusion of spectral and spatial features.

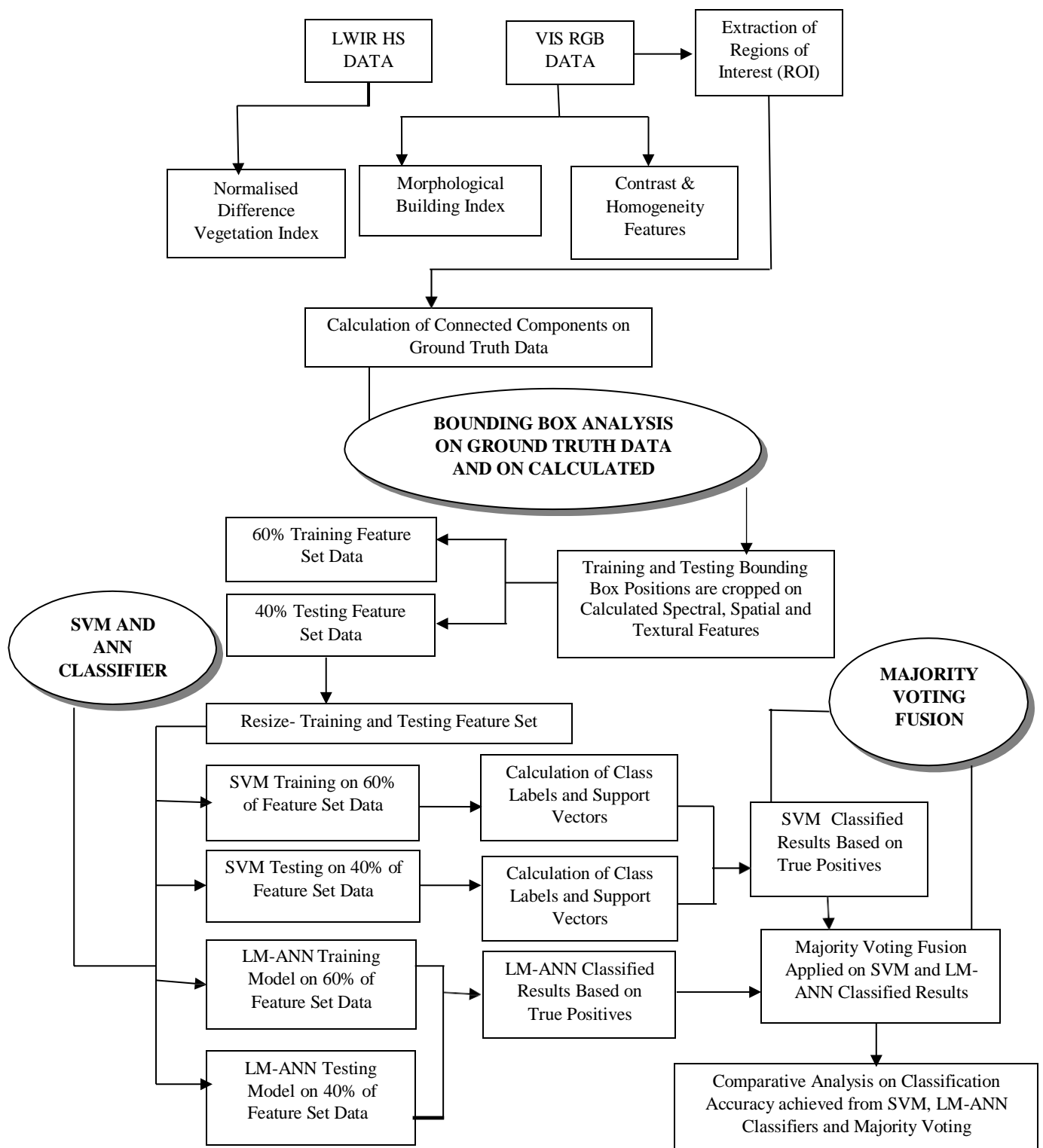
## **6.3 Methodology and Implementation**

The methodology deals in with the extraction of features in spectral, textural and spatial-structural domain from LWIR HS and VIS RGB imageries. The region of interest classes in the form of polygons of homogenous pixels are fetched from very high-resolution VIS RGB image. Connected component analysis is performed on every set of classes to obtain the total number of connected components in high resolution imagery. A bounding box is created around the set of connected components and the spectral and spatial features then extracted onto the connected component of each region of interest polygons. Bounding box data is divided into training and testing samples. The approach has been discussed in detail in Chapter-4. Here, in this experiment, two non-parametric classifier networks SVM

and ANN are built on the bounding box features. Further, decision level fusion is developed using independent and combined features on ANN network to evaluate its impact on the confidence measures of the classified objects. The comparative analysis is shown between the two non-parametric multi-class classifiers for classification of natural and man-made objects. Also, a study is presented to show the impact of using decision level fusion of combined features on ANN network by comparing its results with decision level fusion of combined features applied to SVM classifier network in the previous study. Figure-6.1 illustrates the parameters on which the classifier's study is performed and Figure-6.2 shows a complete flowline of the implementation of the methodology.



**Figure 6.1 – Parameters for study on two non-parametric classifiers**



**Figure 6.6 – Flowline of the implementation steps**

### 6.3.1 Artificial Neural Network

In the literature, many methods have been developed for training the neural networks. The significant techniques widely used are Steep Descent Algorithm (SDA), also known as Error Back-propagation Algorithm (EBA) and Gauss Newton Algorithm (GNA).

Both these algorithms are important source of least square optimization problems in data fitting but show some problem with convergence and computational speed. SDA shows slow final convergence and fails in finding the minimizer of second-degree polynomial whereas GNA shows quadratic convergence only if one or more measurement errors are small; otherwise large error components are difficult to handle and the speed of the final convergence declines. It has been found that for initial stages of neural network training SDA is preferred and for final stages where quadratic convergence is required GNA is preferred.

In present study, Levenberg Marquardt (LM) algorithm is used which blends these two minimization curve fitting algorithms. It adapts the fast speed characteristic of GNA and stability factor of SDA. Hence, LM algorithm [165] provides numerical solution to non-linear problems as it is fast and has stable convergence. The Levenberg-Marquardt algorithm is considered to operate explicitly with error functions which take the form of a sum of squared errors, therefore, also known as the damped least-squares method. The error function as a sum of squared errors is expressed as,

$$f = \sum_{i=1}^m e_i^2 \quad (6.1)$$

where  $m$  is the number of samples. The Jacobian matrix of the error function is defined as the derivatives of the errors with respect to the parameters,

$$J_{i,j} = \frac{\partial e_i}{\partial w_j} \quad (6.2)$$

for  $i=1, \dots, m$  and  $j=1, \dots, n$ ;  $m$  is the number of samples in the data set and  $n$  is the number of parameters in the neural network. Note that the size of the Jacobian matrix is  $m \cdot n$ . The gradient vector of the error function is computed as,



$$\nabla f = 2 J^T \cdot e \quad (6.3)$$

where  $e$  is the vector of all error terms. Finally, the Hessian matrix can be approximated as the following expression,

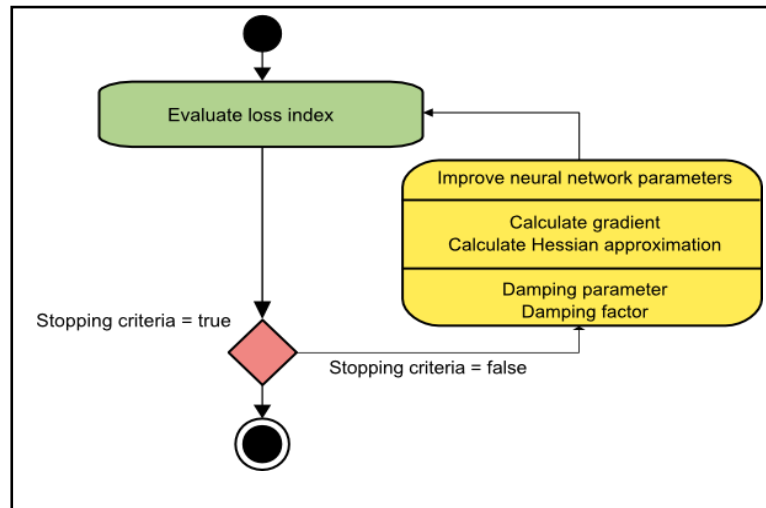
$$Hf \approx 2J^T \cdot J + \lambda I \quad (6.4)$$

where  $\lambda$  is a damping factor that ensures the positiveness of the Hessian and  $I$  is the identity matrix. The parameter improvement process with the Levenberg-Marquardt algorithm is defined as,

$$w^{(i+1)} = w^{(i)} - (J^{(i)T} \cdot J^{(i)} + \lambda^{(i)} I)^{-1} \cdot (2J^{(i)T} \cdot e^{(i)}), \quad (6.5)$$

for  $i=0, 1, \dots, n$  so on.

Different values of damping parameter  $\lambda$  leads to different expressions. When the value of damping parameter is zero, it equates to the Newton's method, using the approximate Hessian matrix. If the value of this parameter is large, the expression equates to gradient descent with a small training rate. Initially, the parameter  $\lambda$  is kept large so that primary updates are small steps in the gradient descent direction. In this process, if any iteration happens to result in a failure, then  $\lambda$  is increased by some factor. Otherwise, with decreasing error,  $\lambda$  is also decreased and Levenberg-Marquardt algorithm approaches the Newton's method. This procedure predictably speeds up the convergence to the minimum. Figure-6.3 shows a state diagram for the training process of a neural network with the Levenberg-Marquardt algorithm. The steps include the calculation of the error (*i.e.*, loss index), the gradient factor and the Hessian approximation expression. The damping parameter at each iteration is adjusted to reduce the error as explained above.



**Figure 6.3 – State diagram (Training) – LM Algorithm**

LM algorithm is an approach which is designed for error functions corresponding to sum-of-squares. These functions make the training neural network algorithm to process faster. However, the algorithm has some issues. The algorithm is not compatible with many error functions such as the root mean square errors, cross-entropy errors and regularization expressions. Also, the handling of large data sets and neural networks becomes difficult as they result in huge Jacobian matrix which leads to issues related to memory. Therefore, the Levenberg-Marquardt algorithm is not recommended for large data sets and/or neural networks.

All implementations are done using MATLAB R2015a and ENVI 4.5 software.

#### **6.4 Results and Discussions**

In this experiment, since the performance of two popular classifiers is studied for urban land-cover classification using LWIR and VIS RGB imageries. Therefore, the results of initial stages of extracting the features in spectral and spatial domain and the formation of feature knowledge set are obtained from earlier experiments. Here, the design parameter of LM-ANN classifier is presented.

#### 6.4.1 Design Parameters - LM-ANN

The network training function using the spectral and spatial feature information updates the weight and bias values according to LM optimization technique discussed above. Back propagation is used to calculate Jacobian parameters *wrt* weight and bias variables. Validation vector is used to stop the training if the performance of the network fails to improve or remains the same for maximum epochs. Table-6.1 shows the dimension parameters of LM ANN based on spatial and spectral feature sets.

**Table 6.1 - Dimensions of LM ANN based on NDVI, MBI and Textural Features**

Dimensions of LM ANN			
Number of Inputs	01		
Number of Hidden layers	02		
Number of Outputs	01		
Number of Weight Elements	NDVI	MBI	Textural
	1255	1255	977

#### 6.4.2 Design Parameters - Support Vector Machine

SVM is a non-parametric supervised learning classification technique, which have proven to be very robust and reliable in the field of machine learning [45-47]. The separation of two classes in SVM is determined by an optimal hyper-plane that maximises the margin between these classes in a multi-dimensional feature space. The training samples that are nearer to the hyper-plane known as ‘support vectors’ are used to determine the optimal hyper-plane. The samples that are close to the class boundary are considered for categorization in the algorithm. The support vectors obtained in this experiment for each feature *i.e.*, NDVI, MBI and textural is listed in Appendix-IV.

The confidence measures of the classification under natural and man-made category are discussed below,

- (i) Table-6.2 and Table-6.3 highlight the classification accuracy in terms of percentage confidence measure of correctly classified class label for natural and man-made objects. The results for each category in natural and man-made objects are studied and observed in two ways. One set of results are obtained on the decision of Majority Voting (MV) fusion of classifier networks based on each feature set. Other set of results are obtained on the decision of WMV fusion of classifier networks based on combination of the spatial and spectral feature set analysis.

**Table 6.2- SVM classifier results using majority voting fusion on spectral and spatial features**

Objects	Accuracy	SVM Classifier- MV using Vegetation Index (%)	SVM Classifier- MV using MBI (%)	SVM Classifier- MV using Textural Features (%)
	Classes			
	<i>Column 1</i>	<i>Column 2</i>	<i>Column 3</i>	<i>Column 4</i>
Man-made (Row 1)	Building	100.0	100.0	100.0
	Road	79.3	66.9	66.8
Natural (Row 2)	Soil	91.0	85.7	57.1
	Trees	82.8	75.1	83.7
	Vegetation	91.6	84.8	75.6

**Table 6.3– ANN classifier results using majority voting fusion on spectral and spatial features**

Objects	Accuracy	ANN Classifier-MV using Vegetation Index (%)	ANN Classifier-MV using MBI (%)	ANN Classifier-MV using Textural Statistics (%)
	Classes			
	<i>Column 1</i>	<i>Column 2</i>	<i>Column 3</i>	<i>Column 4</i>
Man-made (Row 1)	Building	62	81.3	54.9
	Road	28	66.9	53.9
Natural (Row 2)	Soil	100	100	100
	Trees	100	100	100
	Vegetation	100	100	100

(iii) Table-6.4 highlights the comparative analysis of classification accuracy achieved from Weighted Majority Voting (WMV) fusion of all the features using SVM and ANN classifiers.

**Table 6.4- Comparative assessment of classification accuracy of natural and man-made objects**

Objects	Classifier's Accuracy	SVM based WMV fusion using all features (%)	ANN based WMV fusion using all features (%)
	Classes		
	<i>Column 1</i>	<i>Column 2</i>	<i>Column 3</i>
Man-made (Row 1)	Building	100	55.4
	Road	89.6	67.9
Natural (Row 2)	Soil	98.2	100
	Trees	96.8	100
	Vegetation	96.2	100

The above results (Tables-6.2 to 6.4) lead to the following observations and analysis,

- (i) From the calculations shown in Table-6.3 (row-2: column-2, column-3 and column-4), it is seen that the classification accuracy is 100% for all the classes under natural object category. This may be because ANN's often converge on

local minima rather than global minima. Hence, ANN outperforms SVM classifier for classification of natural objects.

- (ii) The comparison of the ANN classifier results shown in Table-6.3 (row-1: column-1, column-2 and column-3) and Table-6.4 (row-1, column-3) show that the classification performance of building and road has not improved using decision of WMV fusion using combination of the spatial and spectral features. Hence, ANN's may not require fusion of classifiers decision based on multiple features to enhance the classification accuracy of the objects in urban land classification. This shows that ANN requires larger training feature sets to optimize the classification problem as the network fails in considering the structural risk from a limited set of training samples.
- (iii) The performance parameters shown in Table-6.3 (row-1 and row-2, column 3) obtained through WMV fusion of MBI features for classification of man-made and natural object classification has outperformed the results in comparison to the rest of the features *i.e.*, NDVI and textural feature sets (column-2 and column-4). This shows that in these experiments, ANN has shown better performance for classification of natural and man-made objects using spatial-spectral features analysis. The results show the effectiveness of high spatial resolution multispectral data and ANN in land-cover classification.
- (iv) The performance of SVM classifier network based on different features is shown in Table-6.2. From the analytical results, it is observed that MV fusion of NDVI feature (row-1 and row-2: column-1) has outperformed in classification of man-made and natural objects in comparison to the rest of the features *i.e.*, MBI and textural features (row-1 and row-2: column-3 and column-4). Hence, the

combination of LWIR channels and red channels have contributed significantly in delineating the land-cover features.

- (v) The comparative performance of two classifier networks is shown in Table-6.4. It shows that the classification accuracy of man-made objects *i.e.*, building and road achieved from SVM classifier network using WMV fusion of combination of features is 100% and 89.6% (row-1, column-2) which is more as compared to that obtained from ANN classifier network (which is 55.4% and 67.95% - row-1, column-3)). This shows that SVM outperforms ANN if classification results are based on decision level fusion of combined spatial and spectral feature sets. Hence, for the enhancement in classification accuracy of natural and man-made objects, SVM works well with combination of features in spatial and spectral domain. The increase in decisions does not show any significant effect on ANN classifier results.

## 6.5 Summary

Machine learning offers learning methods/algorithms which has high potential in classifying remotely sensed imagery effectively and efficiently. The robustness of machine learning classification algorithms includes the capacity to handle multi-dimensional and multi-source data of dynamic and uncertain environment. The experiment, therefore, provides an insightful study of relatively mature methods in machine learning for classification of complex urban area using support vector machines and artificial neural networks on multi-sensor imageries. The artificial neural network and support vector machine classifiers are used to extract land-cover classes of the urban area in Thetford Ford Mines, Canada. The comparative analysis of the two classifiers is presented to demonstrate the applied perspective of ANNs and SVMs for object-based classification using LWIR and VIS RGB imageries. The study area is categorized into two land types, *i.e.*, natural and

man-made objects. ROI training samples of the classes consist of the three types of features, *i.e.*, NDVI, MBI and textural. From the evaluations in terms of classification accuracy it emerges that SVM classifier network outperforms man-made object classification in comparison to non-parametric ANN classifier network. ANN classifier network outperforms natural object classification for the same urban land-cover. Also, the majority voting fusion of all set of features effect the performance measure of SVM classifier network more than ANN for enhancing the classification, whereas, this additional step is not required for ANN classifier network. SVM classifier shows a phenomenal change in the performance measures due to majority voting fusion of all the features. The methodological approach used in the present study for classification of LWIR and VIS RGB imageries shows that SVMs have better generalization capability than that of ANNs. The statistical results show that ANNs suffer from over-fitting problem and generate 100 percent classification accuracy in case of natural objects in an urban area while decreasing the identification of man-made objects in the scene. SVM tend to find global solution by learning the features in training samples and therefore minimise the conflict of analogous spatial and spectral characteristics of the objects in an urban area.



## ***Chapter 7***

# ***Identification of Optimal Spectral Wavelengths for Classification of Land Features using Hyperspectral Imagery***

### **7.1 Introduction to the Problem**

Identification of urban land-cover classes is essential for understanding the dynamics of urbanisation and modelling the urban ecosystem for developmental plans [166]. The urban land cover is a complex fusion of natural and man-built features such as water bodies, vegetation, man-built recreational parks, residential and industrial hub, open land *etc.* The feature extraction of urban land-cover is a complicated process since they are intricate mixture of numerous surface materials in relatively small regions.

Urban land-cover features are specified by various artificial and natural surface materials which are distinctive in their characteristics. The reflective radiance responses from urban surface materials influence the ecological and climatic balance/imbalance in the cities and effects the human health conditions of the people in the cities. Urban land-cover features include the blend of materials ranging from concrete, asphalt, wood, brick, slate, bitumen, metal, sand and stone. The manual categorization of the complex materials in an urban environment is time consuming, tedious and impractical these days.

Analysis and interpretation of reflected radiance from various urban materials captured by coarser multispectral sensors yield much less information as the number of spectral channels are limited; therefore, multispectral data is only useful in determining broad mineral and surface compositional classes [167]. Hyperspectral sensors have greater potential for mapping the features of urban land-cover. Hyperspectral data set is a cube

consisting of spectral bands covering a wide range of wavelengths. Since, it is a collection of recorded spectra with finer wavelength resolution, it has a higher potential for identifying and categorizing the surface materials of urban land-cover which aids in characterising the features of urban surface materials for variety of urban related applications. The spectral channels provide well-defined spectral properties which are suitable in determining the mineral type and its composition, vegetation sub-classes, rock types in the study of lithology *etc.* Hence, the spectral information contained in a hyperspectral imagery is a potential source for detecting/identifying all types of surface materials. However, the analysis of hyperspectral imagery is a challenging and difficult task. The interpretation of the data requires optimal methodology and there appears no standard approach to material classification of urban land-cover. Since, in urban environment numerous materials are present in relatively small regions, therefore, there exist issues related to within-class variability of many material which in turn affects the classification accuracy.

In order to classify the features of urban land-cover which are heterogeneous combination of materials ranging from concrete, wood, metal, sand, stone *etc.*, it is highly important to interpret the spectral signatures of the materials in an efficient way [168]. Spectral signature is a reflected radiance of a material at a particular wavelength that has significant information which may contribute in extracting the information about the feature than the spatial information of the material [168]. It is so because the spatial distribution of the materials is not regular and is composed by rapid temporal changes. The spectral property of the surface materials is studied in terms of reflectance pattern which is determined through various spectral analysis techniques [169].

From the literature, it is seen that color composite images are the most basic form of spectral analysis. The determination of optimum band display for discriminating the composition of materials was developed by Crippen in 1989 [170]. In this technique,

correlation matrix index is calculated which provides an objective method to determine best three bands for maximal spectral diversity in class identification but may not be best for enhancing the discrimination of sub class divisions. Another technique of spectral analysis is statistical transformation [171]. Several statistical approaches have been developed to maximize the spectral variance for sub class divisions of different surface compositional classes. The most widely used is Principal Component Analysis (PCA) which can be implemented through different strategies [172]. In [173], the study shows that in each analysis of possible spectral channel maximized the variance in input data and thus allowed a separation of classes based on those different spectral properties. In [174], the study developed the modification of PCA called Minimum Noise Fraction (MNF) transform in which noise covariance matrix is calculated first and then the reflectance data is rotated and scaled. The principal limitation of the statistical transforms is that they are data specific; therefore, the results and methodologies for interpretation are not easy [175].

Now a days, the popular spectral analysis technique for enhancing the spectral information of multiband spectral data is computation of spectral index. Spectral index is formed by the ratio between the reflectance of two and more wavelengths. The main advantage of using indices for identifying features is that they are easy to compute because of the simple algorithms and requires minimum computations. In literature, various vegetation indices have been explored for identifying the features of broadband greenness in urban land cover but the use of spectral indices for identifying other natural (soil, water, minerals *etc.*) and man-built (buildings, roads, pavements *etc.*) features is still limited. Also, multispectral sensor data have been used earlier for mapping the urban land classification in which spectral mixing is one of its limitation.

The spectral information available from multispectral/hyperspectral optical datasets is barely enough to distinguish certain closely resembling classes like vegetation and tree

clad areas, riverine sand and urban structures, salt affected land and dry sand, grass lands and croplands, scrub land and fallow land *etc.* Discerning these classes require an image with high spectral, spatial and radiometric resolutions. Urban land-cover classification is a vast and generalized field for hyperspectral data utilization. In this field, many research efforts are being made for utilizing the AVIRIS-NG data to examine the uniqueness of HS data over the multispectral data in identifying various land-cover classes. The current study presents the significance of airborne AVIRIS-NG hyperspectral data for detailed feature classification and characterisation of surface materials in urban landscape based on spectral index's technique. The use of hyperspectral data is still limited due to high dimensionality; that causes redundancy in the information and bear a limitation in terms of high processing time and storage. Hence, the identification of optimal wavelength regions for various land-cover classes attain significance for correct identification and for reducing the processing time during classification of individual land-cover features.

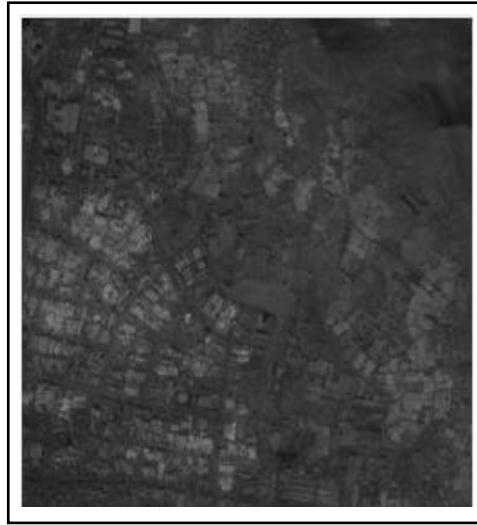
The current Chapter deals with the identification of significant spectral wavelengths for establishing various spectral indices for classification of urban land-cover classes using AVIRIS-NG remote sensing hyperspectral imagery. The exploration of potential wavelengths would help in identifying indices or assist in formulating the indices for maximal classes identification. The Chapter discusses various tasks that have been formulated and investigated in identification of optimal spectral wavelengths for classification. Following are the investigations/tasks that have been carried on for obtaining the desired results,

- (i) Pre-processing of data for atmospheric & geometric corrections and removal of bad bands.
- (ii) Field spectra collection for various land-cover classes using spectroradiometer.

- (iii) Identification of optimal band or wavelength region for recognition of land-cover classes.
- (iv) Spectral Index development for various land-cover classes of the considered study area.
- (v) Land-cover classification using spectral index image and field spectra and comparing their merits.

## **7.2 Experimental Data Set**

In the present study, AVIRIS-NG data has been used, the detailed acquisition of which has been explained in Chapter-3 under the section-3.2. AVIRIS-NG data has been collected under ISRO and NASA airborne campaign. AVIRIS-NG measures the spectral range 380-2510 nm at 5-nm intervals with high SNR (>2000 @ 600-nm and >1000 @ 2200-nm) and an accuracy of 95%. The Field-Of-View (FOV) is 34° and Instantaneous FOV (IFOV) is 1-milliradian. Ground Sampling Distance (GSD) varies from 4 to 8-m for flight altitude of 4-8 km with swaths ranging from 3-km to 6-km. AVIRIS-NG includes an INS/GPS system that enables full reconstruction of the airborne measurements to an ortho-rectified product. The details on the acquisition of the data set is explained in detail in Chapter-3 under the section-3.3.1. Table-3.2 of Chapter-3 shows the summary of the metadata information of AVIRIS-NG hyperspectral imagery of the captured site of urban land-cover of the city. In the current experiment, a subset of AVIRIS -NG HSI (shown in Chapter-3, Figure-3.5) is used. The size of the subset is 250x250 pixels with 387 bands. The grayscale display of the subset is shown in Figure-7.1. The positional coordinates of the clipped image from the original data is 133:127; 382:376.



**Figure 7.1 - Subset of the original AVIRIS-NG data**

*Ground Data Collection:* Field spectroscopic measurements have been carried out by using an instrument called Spectroradiometer, with spectral range (generally from 350-2500 nm) consisting of 2151 channels. The details of the ground data collection with its complete information has been described in Chapter-3 under the section-3.3.3. Along with the information of the spectras of different natural and man-made objects, positional data which included the latitude-longitude information of the objects, was acquired by G-tech device of spectroradiometer. The positional data information has been used to obtain the regions of interest pixels for the classes that needs to be classified in this experiment.

### **7.3 Theoretical Background**

The physical and chemical compositional properties of the surface materials can be studied based on the spectral information derived from multispectral and hyperspectral imageries. The processing of spectral information for varied natural and man-built classes is explored through the formulation of spectral indices. The level-wise categorization of features belonging to natural and man-built classes is prepared and shown below in Table-7.1. In the subsequent sections, the spectral indices for various categories listed in Table-7.1 have been discussed.

**Table 7.1 - Level-wise categorization of natural and man-built class features**

Level 1	Level 2	Level 3
Natural Class Features	Water	<ul style="list-style-type: none"> <li>• Open Water</li> <li>• Perennial Ice/Snow</li> <li>• Canopy Level</li> </ul>
	Barren Land	<ul style="list-style-type: none"> <li>• Bare Rock</li> <li>• Clay</li> <li>• Sand Quarries</li> </ul>
	Natural Vegetation	<ul style="list-style-type: none"> <li>• Grasslands</li> <li>• Forest Upland</li> <li>• Shrub land</li> </ul>
	Geological	<ul style="list-style-type: none"> <li>• Minerals</li> </ul>
Man-Built Class Features	Developed Land	<ul style="list-style-type: none"> <li>• Low and High Intensity Residential Areas</li> <li>• Commercial / Industrial Hub</li> </ul>
	Impervious Surface	<ul style="list-style-type: none"> <li>• Roads</li> <li>• Pavements</li> <li>• Transportation</li> </ul>

### 7.3.1 Spectral indices for depicting the features of natural class: Water

Based on the applicability, the water features can be studied at three levels: one for open water areas in urban land, second for identifying the water level content at canopy level and third for accessing the formation of ice or snow. In [176], proposed Modified Normalized Difference Water Index (MNDWI) is proposed to enhance open water features in urban land cover by suppressing the other land cover features such as soil, vegetation *etc.* This index finds its applicability in water turbidity estimations in urban land cover. Normalized Difference Water Index (NDWI) was proposed in [177] which got popularity in identifying the vegetation liquid water and finds its applicability in agricultural and forestry. In [178], Wilson proposed Normalized Difference Moisture Index (NDMI) which had identical band composite with Gao’s NDWI. They both developed the index to estimate leaf water content at canopy level. For depicting another feature of water *i.e.* perennial ice/snow, in [179] Hall proposed Normalized Difference Snow Index (NDSI) to study the characteristics of snow. This index also finds its applicability as snow/cloud discriminator

because cloud shows high reflectance in Short Wave Infrared band (SWIR) used in the index and there the reflectance of snow drops to near-zero values. Table-7.2 list out available spectral indices in literature for computing various types of water features.

**Table 7.2 - Spectral indices for computing features of water at different categorization level**

Features of Natural Class: Water	Spectral Index	Formulation	Wavelength (µm)	Reference
Open Water	MNDWI	$\frac{Green - SWIR}{Green + SWIR}$	Short Wave Infrared (SWIR): - Min:1.55; Mid:1.65; Max:1.75	[176,180]
Canopy Level	NDWI	$\frac{Green - NIR}{Green + NIR}$	Near Infrared (NIR): -	[180]
	NDMI	$\frac{\rho_{795} - \rho_{990}}{\rho_{795} + \rho_{990}}$	0.72-0.80; 0.83-0.99	[181]
Perennial Ice/Snow	NDSI	$\frac{Green - SWIR1}{Green + SWIR1}$	Green: - 0.5-0.6; SWIR1: - 1.55- 1.75	[182,183]

### 7.3.2 Spectral indices for depicting features of natural class: Barren land

Barren land is generally covered by two natural materials *i.e.*, soil and rocks. The texture of soil and rocks is characterized by the proportion of clay, sand and silt fractions present. Simple Ratio Clay Index (SRCI) and Normalized Difference Clay Index (NDCI) are widely used for studying soil clay content in Middle Infrared (MIR) and far IR regions. The combination of these regions contributes in understanding the spectral characteristics of soil texture, such that, the finer grain size clay particles have higher spectral reflectance than sand and silt [184]. The longer the wavelength the larger is the difference between the finer grain features and coarser grain features of the soil [185]. SWIR bands are used for computing clay ratio in hydrothermally altered rock formations with composites of clay and alunite [186]. Foreground area primarily covered with soil can be highlighted by Normalized Difference Soil Index [187]. Table-7.3 describes the spectral indices for computing various features of barren land.



**Table 7.3 - Spectral Indices for computing features of barren land at different categorization level**

Features of Natural Class: Barren Land	Spectral Index	Formulation	Wavelength ( $\mu\text{m}$ )	References
Soil	Normalized Difference Soil Index	$\frac{MIR - Green}{MIR + Green}$	MIR: -1.66; Green: - 0.56	[187]
Rock	Clay Ratio	$\frac{SWIR}{NIR}$	SWIR: - Min:1.55; Mid:1.65; Max:1.75 NIR: - 0.72-0.80; 0.83-0.99	[188,189]
Clay	SRCI	$\frac{SWIR1}{SWIR2}$	SWIR1:- 1.55-1.75 $\mu\text{m}$ SWIR2:- 2.08-2.35 $\mu\text{m}$	[189]
	NDCI	$\frac{\rho_{795} - \rho_{990}}{\rho_{795} + \rho_{990}}$	0.72-0.80; 0.83-0.99	[190]

### 7.3.3 Spectral indices for depicting features of natural class: Vegetation

Computation of spectral indices for natural vegetation detection has always been very popular in our literature. Various indices have been developed to identify different categories of natural vegetation. Different effects such as quality of photosynthesis, chlorophyll concentration, canopy leaf area, canopy leaf architecture etc. are considered to study different states of vegetation. Few indices derived from the reflectance measurements sensitive to different effects are given in Table-7.4 to evaluate healthy green vegetation, forest uplands, sparse vegetation and enhancing grassland vegetation while suppressing the soil.

**Table 7.4 - Spectral Indices for computing features of natural vegetation at different categorization level**

Features of Natural Class: Vegetation	Spectral Index	Formulation	Wavelength (µm)	References
Healthy Green Vegetation	NDVI	$\frac{NIR - Red}{NIR + Red}$	NIR: - 0.72-0.80; 0.83-0.99 Red: - 0.43-0.48	[191]
	Infrared Percentage Vegetation Index (IPVI)	$\frac{NIR}{NIR + Red}$	NIR: - 0.72-0.80; 0.83-0.99 Red: - 0.43-0.48	[192]
	Renormalized difference Vegetation Index (RDVI)	$\frac{NIR - Red}{\sqrt{NIR + Red}}$	NIR: - 0.72-0.80; 0.83-0.99 Red: - 0.43-0.48	[193]
Forest upland	Green Ratio Vegetation Index (GRVI)	$\frac{NIR}{Green}$	NIR: - 0.72-0.80; 0.83-0.99 Green:- 0.56	[194]
Sparse Vegetation	Soil Adjusted Vegetation Index (SAVI)	$\frac{1.5 * (NIR - Red)}{NIR + Red + 0.5}$	NIR: - 0.72-0.80; 0.83-0.99 Red: - 0.43-0.48	[195]
Grasslands	Optimised Soil Adjusted Vegetation Index (OSAVI)	$\frac{NIR - Red}{NIR + Red + 0.16}$	NIR: - 0.72-0.80; 0.83-0.99 Red: - 0.43-0.48	[196]
	Modified Non-linear Index (MNLI)	$\frac{(NIR^2 - Red) * (1 + L)}{NIR^2 + Red + L}$	NIR: - 0.72-0.80; 0.83-0.99 Red: - 0.43-0.48 Adjustment Factor L=0.5	[197]

### 7.3.4 Spectral indices for depicting features of natural class: Geological Minerals

To identify the features of mineralogy on surface and hydrothermally changed rocks significant regions of ElectroMagnetic (EM) spectrum are studied that display their spectral

characteristics. Table-7.5 highlights the geologically important wavelength regions in EM spectrum for detection of various transitional, hydroxyl and carbonate bearing mineral elements. From a literature review, amongst many minerals, the spectral indices used to detect the presence of iron-oxides and sulphates is listed in Table-7.6.

**Table 7.5 - Geologically important wavelength regions in EM spectrum**

Wavelength Region in EM Spectrum	Wavelength Range in nanometre	Mineralogy
Visible and Near Infrared (VNIR)	400-1100	Iron and Manganese Oxides, Rare Earths
SWIR	1100-2500	Hydroxyls, Carbonates, Sulphates, Micas, Amphiboles
TIR	8000-14000	Carbonates, Silicates

**Table 7.6 - Spectral Indices for computing features of minerals**

Features of Mineralogy	Spectral Index	Formulation	Wavelength ( $\mu\text{m}$ )	References
Iron-Oxide and Sulphide	Ferrous Minerals Ratio	$\frac{SWIR}{NIR}$	SWIR: - Min:1.55; Mid:1.65; Max:1.75 NIR: - 0.72-0.80; 0.83-0.99	[188,189]
	Iron Oxide Ratio	$\frac{Red}{Blue}$	Red:- 0.43-0.48; Blue:- 0.45-0.49	[198]
	World View New Iron Index	$\frac{Green * Yellow}{Blue * 1000}$	Green:- 0.54-0.58 Yellow:-0.51-0.54 Blue:- 0.45-0.49	[199]

### 7.3.5 Spectral indices for depicting features of man-built class: Developed Land and Impervious Surfaces

In the literature, spectral indices to automate the process of mapping built up and impervious surfaces have been formulated using Normalized Difference Built-up Index (NDBI), Built-up Area Extraction Index (BAEI), Normalized Built-up Area Index (NBAI),

and Normalized Difference Impervious Surface Index (NDISI). Table-7.7 presents the characteristics of these spectral indices.

**Table 7.7 - Spectral indices for computing man built-up features at different categorization level**

Features of Man-built Class	Spectral Index	Formulation	Wavelength ( $\mu\text{m}$ )	References
Built up Area	NDBI	$\frac{SWIR - NIR}{SWIR + NIR}$	SWIR: - Min:1.55; Mid:1.65; Max:1.75 NIR: - 0.72-0.80; 0.83-0.99	[200]
	BAEI	$\frac{Red + L}{Green + SWIR1}$	L is an arithmetic constant =0.3	[200]
	NBAI	$\frac{SWIR - TIRS}{SWIR + TIRS}$	TIRS: -10.6-11.19	[201]
Impervious Surface	NDISI	$\frac{T_b - (MNDWI + \rho_{NIR} + \rho_{SWIR1})/3}{T_b + (MNDWI + \rho_{NIR} + \rho_{SWIR1})/3}$ where, $MNDWI = \frac{\rho_{GREEN} - \rho_{SWIR1}}{\rho_{GREEN} + \rho_{SWIR1}}$	$T_b$ is brightness temperature of thermal band	[202]

#### 7.4 Methodology and Implementation

For correct identification of classes of urban land cover, it is necessary to identify the significant spectral bands that are sensitive to dissimilarities to various classes. Therefore, this study uses the significant identification of spectral wavelengths to discriminate the classes. The identified spectral wavelengths are then used to develop the band ratios that form the spectral indices to identify the class. However, the band ratio may be developed through numerous combinations of spectral wavelengths, therefore, it is necessary to calculate the Optimum Index Factor (OIF) to extract the best possible combinations of spectral wavelengths for the development of band ratio [203]. Next, for inter-class separation within the same class is obtained using SVM classifier network. To extract the classified parameters, the pixels lying in the regions of interest of categorized

classes are obtained from the latitudinal and longitudinal positions of the ground truth data. The pixels lying in regions of interest are then incorporated on the gray scale image obtained from formulated spectral indices. The region of interest pixels of the classes across the built-up spectral index are divided into training and validation samples. Support vector machine algorithm is used to classify the urban land-cover classes as well as their inter-class separation from the trained region of interest pixels.

#### **7.4.1 Implementation Steps of Methodological Approach**

The flow line of the implementation steps carried out in performing the above methodological approach is discussed in Figure-7.2. The stages of the implementation steps are discussed below.

##### ***7.4.1.1 Pre-processing of the Data Set***

The hyperspectral data is geometrically corrected to follow the World Geodetic System 84-datum. The radiometric correction is done using quick atmospheric correction module available in ENVI Software to retrieve spectral reflectance from AVIRIS-NG hyperspectral radiant image. Pan sharpening and removal of bad bands is performed after atmospheric correction using PANSHARP algorithm in order to enhance the visualization display of different sub-classes of the roof of the buildings. It is evident from the literature that bands near 1400-nm and 1900-nm are water absorption bands. These bad bands are identified by observing spectral signature along with statistical parameters *i.e.*, mean and standard deviation of different classes near aforesaid wavelengths. Some bands are also affected by noise with low Signal to Noise Ratio due to detectors overlap in AVIRIS-NG sensor. These bands have also been removed by observing SNR. In view of all the aforementioned facts, bands 196 to 207 (NIR Region) and bands 288 to 313 (SWIR Region) have been removed from AVIRIS -NG hyperspectral imagery in the pre-processing stage.

Thus, a total of  $12+26 = 38$  bad bands have been removed. The total number of bands left for further analysis are  $425-38 = 387$ , hence, the processing is carried on the imagery consisting of  $724 \times 9946$  pixels with 387 spectral channels.

#### 7.4.1.2 Spectral Indices Development from Field Spectroscopy Data

Band ratio is a numerical statistic that is the ratio of two significant spectral wavelengths, namely  $\lambda_1$  and  $\lambda_2$ , mathematically; it is given as  $(\lambda_1 / \lambda_2)$ . In hyperspectral data, the judgement of correct bands for the formation of any spectral indices is highly important. For this purpose, OIF is calculated for numerous spectral wavelengths to filter out the least effective spectral wavelength for the development of the concerned spectral indices. OIF is a simple statistic that is used to evaluate the most informative band ratio in terms of standard deviation and correlation between the two spectral bands. Since, it is the ratio of standard deviation and correlation between the two significant bands; therefore, it is necessary that best OIF can be evaluated if the significant information on variance of two spectral bands is present. Mathematically, OIF is given as,

$$OI = \frac{d_{\lambda_1} + Std_{\lambda_2}}{|Corr_{\lambda_1, \lambda_2}|} \quad (7.1)$$

where, *Std* is standard deviation of significant spectral wavelengths and *Corr* is the correlation coefficient between the spectral wavelengths. The spectral wavelengths for which the highest possible value of OIF is achieved are finally used for the development of band ratio. The possible band ratio is then converted into normalised difference for building up of spectral indices for the detection of the object. The main advantage of using indices for identifying features is that they are easy to compute because of the simple algorithms and requires minimum computations. The normalised difference value contains the

reflectance measurements that enhance the object detection. Mathematically, normalized spectral index formulation is defined as,

$$\text{Normalised Spectral Inde} = \frac{R(\lambda_2) - R(\lambda_1)}{R(\lambda_2) + R(\lambda_1)} \quad (7.2)$$

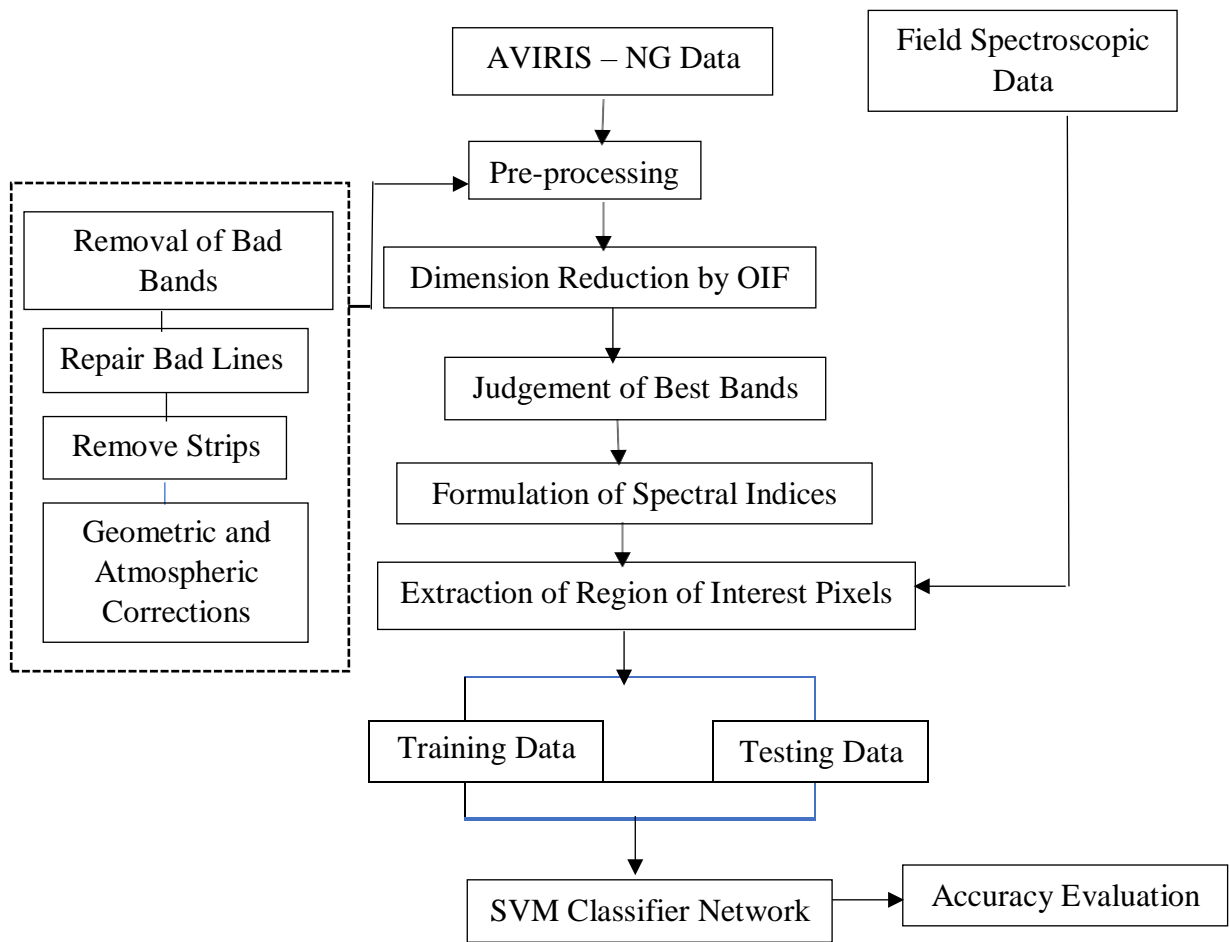
where,  $R(\lambda_1)$  indicates the reflectance measurements of the significant spectral band from the numerator of the band ratio and  $R(\lambda_2)$  indicates the reflectance measurements of another significant spectral band from the denominator of the band ratio. With normalised spectral index, various spectral indices of land-cover classes are formulated using the best rated OIF value.

#### **7.4.1.3 Training and Validation Data**

In this experiment, the identification of materials in man-built structures and soil is extracted from the latitudinal and longitudinal positions of the ground truth data and are incorporated as regions of interest pixels across the matrix obtained under NDBI and clay mineral index. They are further divided into training and validation samples.

#### **7.4.1.4 SVM classifier network**

Linear kernel SVM classifier network is made to learn the features for the concerned sub-classes. Based on the learning features, the materials for building roofs and the condition of the soil is obtained on validation samples.



**Figure 7.2 – Implementation of the methodological approach**

All implementations are done using MATLAB R2015a and ENVI 4.5 software.

## 7.5 Results and Discussions

The implementation steps described above define the approach used in obtaining the optimal wavelengths from hyperspectral remote sensing data. The informative bands are used to formulate the spectral indices which is further used for the classification of certain features in an urban environment. Since, the data consists of natural and man-built objects, therefore, in this experiment, the extracted informative bands are used to design spectral indices related to vegetation, building and soil (*i.e.*, NDVI, IPVI, DVI, NDSI, NDBI and Clay Mineral Index) found in the literature. From the formulated spectral



indices, only two (*i.e.*, NDBI and Clay Mineral Index) spectral indices have been further analysed for classifying the materials from the main class features.

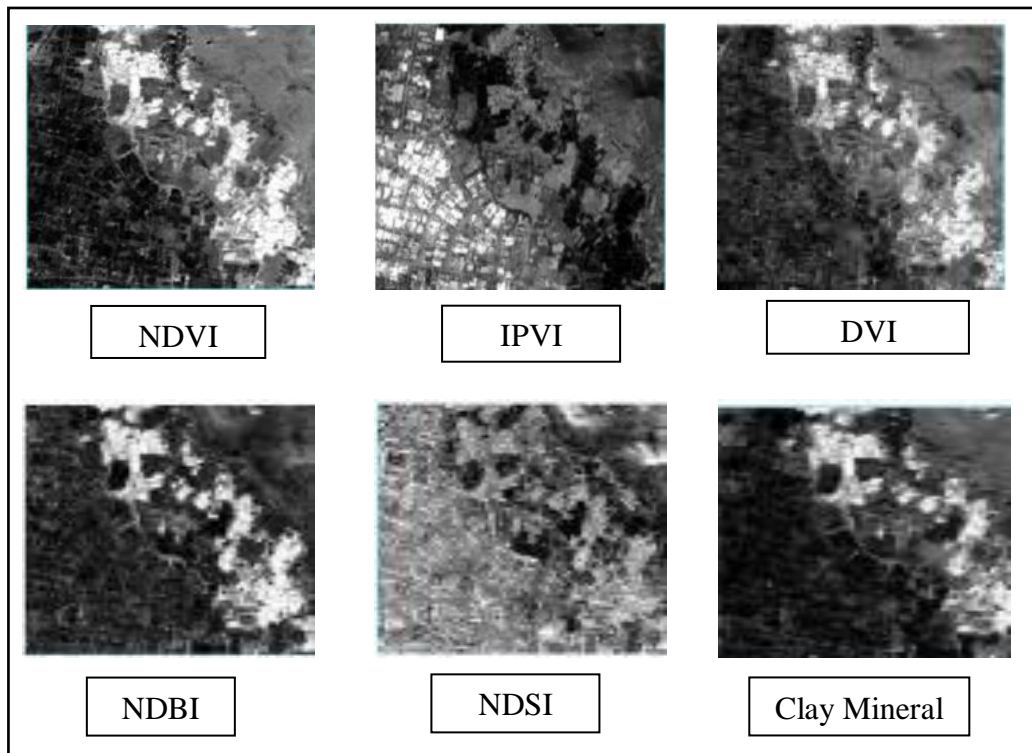
Based on the above approach discussed so far, the analysis of the results is as under,

- (i) The OIF is computed by evaluating different standard deviation and correlation values. The wavelength values for which the best OIF is obtained are selected to form the spectral indices. Table-7.8 highlights the wavelengths corresponding to informative bands and the best achieved values of OIF.

**Table 7.8 – Informative wavelengths and OIFs**

<b>Spectral Index</b>	<b>Wavelength 1 (nm)</b>	<b>Wavelength 2 (nm)</b>	<b>OIF</b>
Normalised Difference Vegetation Index (NDVI)	1077.65	666.94	0.2828
Infrared Percentage Vegetation Index (IPVI)	1077.65	666.94	0.2828
Difference Vegetation Index (DVI)	1077.65	666.94	0.2828
Normalised Difference Building Index (NDBI)	1788.88	892.33	0.3819
Normalised Difference Soil Index (NDSI)	1763.84	396.47	0.1718
Clay Mineral Index	2164.54	1713.75	0.1768

- (ii) The spectral indices are developed using informative wavelengths based on the above calculations described under the implementation stage. The gray-scale images are obtained for each computed spectral index. Figure-7.3 shows the images of the derived spectral indices indicated in Table-7.8 which are formed using informative wavelengths derived from OIF calculations.



**Figure 7.3 - Spectral index images**

- (iii) SVM classifier is built for NDBI and clay mineral index to extract the sub-division of materials in soil and man-built structures. Table-7.9 shows the total number of pixels that are used in the experiment in each sub-class division of two classes *i.e.*, soil and man-built structures.

**Table 7.9 - Total number of pixels for sub-classes**

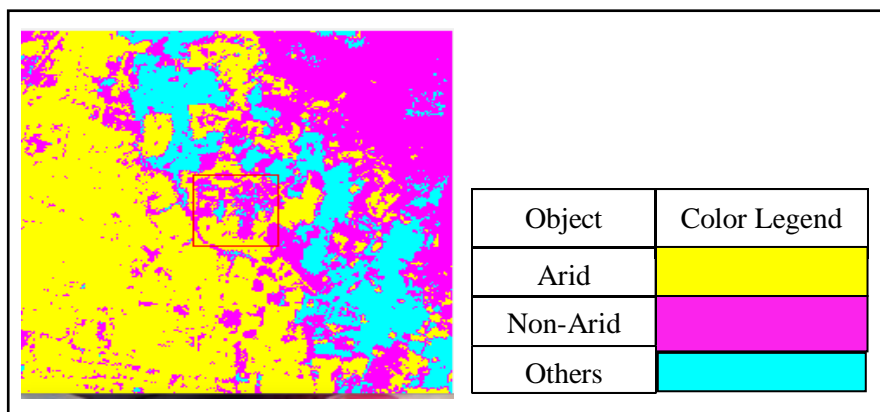
<b>Spectral Index</b>	<b>Sub-Class</b>	<b>Total number of pixels</b>
<i>Column 1</i>	<i>Column 2</i>	<i>Column 3</i>
Clay Mineral Index	Arid Soil	837
	Non-Arid Soil	1283
	Others	1326
NDBI	Concrete	1555
	Asphalt	1656
	Non-built up	2580

- (iv) Table-7.10 shows the division of total number of pixels (shown in Table-7.9, column 3) into training and testing samples. 60% of the total number indicates the training samples and 40% of the total number indicated the testing samples.

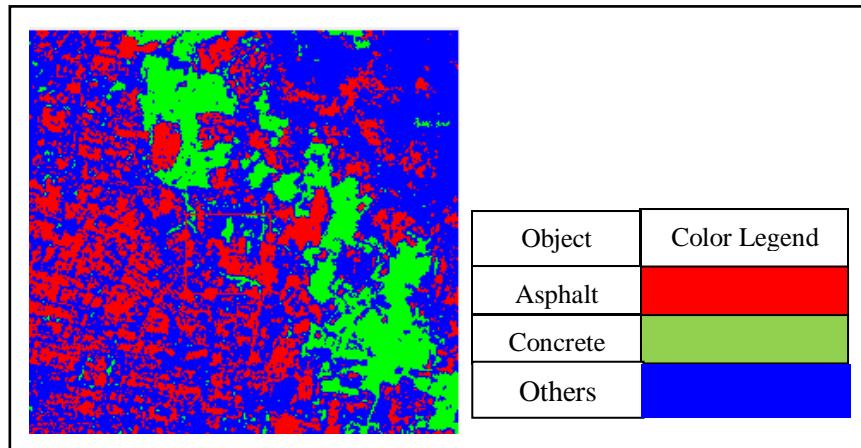
**Table 7.10 - Training and Testing Samples**

<b>Spectral Index</b>	<b>Sub-Class</b>	<b>Training pixels</b>	<b>Testing pixels</b>
Clay Mineral Index	Arid Soil	502	335
	Non-Arid Soil	769	514
	Others	795	531
NDBI	Concrete	933	622
	Asphalt	993	663
	Non-built up	1548	1032

- (v) Based on SVM network classifier results, the sub-division classification map of materials in man-built structures and soil is generated and are shown in Figure-7.4 and Figure-7.5.



**Figure 7.4 - Sub-division classified map of soil**



**Figure 7.5 - Sub-division classified map of materials in man-built structures**

- (vi) The classification accuracy of the sub-division classes is calculated and presented in Table-7.11.

**Table 7.11 - Classification accuracy of sub-classes obtained from Clay Mineral Index and NDBI**

<b>Spectral Index</b>	<b>Sub-Class</b>	<b>Producer's Accuracy (PA) (%)</b>	<b>User's Accuracy (UA) (%)</b>
<i>Column 1</i>	<i>Column 2</i>	<i>Column 3</i>	<i>Column 4</i>
Clay Mineral Index	Arid Soil	92.13	87.46
	Non-Arid Soil	93.84	92.02
	Others	91.77	96.42
NDBI	Concrete	83.41	83.27
	Asphalt	93.09	84.98
	Others	83.68	95.17

Following observations can be inferred from the results discussed above in Table-7.11,

- (i) It is seen that PA for “arid soil” (column-2) is 92.13% (column-3) while the UA is 87.46% (column-4). This means that even though 92.13% reference arid pixels have been correctly identified as “arid soil”, but actually 87.46% of the pixels identified as “arid soil” in the classification are present on ground. PA

of “arid soil” indicates the probability of “arid soil” in the reference data classified as the same in the viewpoint of the producer’s map.

- (ii) It is observed that for “non-arid soil” (column-2) PA is 93.84% (column-3) and UA is 92.02% (column-4). This shows that the correctly classified reference samples are nearly same as that of correctly classified samples. This indicates that the error of commission is low, *i.e.*, number of incorrect classified samples of non-arid soil are lesser, hence, the correctly classified samples of “non-arid soil” identified in the experiment seems to be present actually on ground data.
- (iii) For sub-class “concrete” PA is 83.41% (column-3) and UA is 83.27% (column-4). This shows that the correctly classified reference and identified data for sub-class “concrete” is almost same. This indicate that the proportion of the areas classified as “concrete” corresponds to same features in reference samples also. Hence, NDBI contributes in good identification of the material “concrete” in man-built structures.
- (iv) For “asphalt” (column-2) PA is 93.09% (column-3) and UA is 84.98% (column-4). High PA corresponds that the material “asphalt” on ground is correctly shown on the classified map.
- (v) Finally, from the results shown it is seen that PA for “other materials” (column-2) in class building is 83.68% (column-3) while the UA is 95.17% (column-4). High value of UA provides users with the probability that an area of the classified map of class “other materials” is also the same class on ground.

## 7.6 Summary

Soil is a composite material consisting of various constituents which are present in variable amount making its composition different in its physical and chemical terms. With the evolution in urbanisation, the presence of soil body or weathered rocks present on

barren lands keeps changing in situ or transferred to different areas due to dust storms, or human activity. The determination of the soil body that contains plant litter, roots, clay, minerals, micro fauna etc., is important for understanding the urban land-cover features in an urban environment for various applications. Clay minerals present in soil surface are inorganic, more complex and crystallized in nature, therefore, it is difficult to study their characteristics through X-ray diffractions. The clayey minerals are reactive and are exposed to visible–short wavelength infrared region (0.4-2.5  $\mu\text{m}$ ). Hence, airborne visible/infrared imaging spectroscopy seems to be an invaluable tool for capturing visible and near-infrared reflectance patterns for analysing soil properties in an urban area.

Urban land-cover is highly exposed to built-up area which generally consists of complex and crass arrangement of man-built structures. The information about building materials plays an important role in the evaluation of urban planning. The observations of man-built materials are constantly changing due to degradation and finally leading to urban feature heterogeneities. Therefore, the identification or classification of materials under man-built category is a concern in urban applications. It is studied that there exists an intrinsic law between man-built material types and their sunlight reflection characteristics. Hyperspectral remote sensing technology can acquire the reflection of sunlight emitted from the surfaces and can tap the information of those material types. The information in the form of spectral signatures can therefore help in determining the types of materials used in man-built structures.

This study aims to investigate the information about materials of natural (*i.e.*, soil) and man-built features from hyperspectral remote sensing image based on spectral measurements. Additionally, to classification of various materials under two effective classes of an urban area, the study also analyses the formulation of spectral indices by exploring the effective wavelengths for many other natural and man-made classes of an

urban area. This could be used for other high-level applications of remote sensing classification technology. The extraction of the characteristic information using HSI is a very complex process as it requires data pre-processing, corrections in geometric and radiometric domain and spectral reflectance calculation, removal of water vapour bands *etc.* The study integrates field spectroscopy and airborne hyperspectral remote sensing data to generate the spectral information of materials for classifying concrete and asphalt in man-built structures and identification of arid and non-arid regions in an urban area. The experiment determines the most suitable wavelengths for the formulation of various spectral indices using OIF technique. The spectral indices and the field spectroscopy data is explored for obtaining the classified information. The classification results obtained for identifying soil region and materials in man-built structures shows the importance of the selection of optimal wavelengths for fast and efficient extraction of material information in an urban area.

# *Spatial Shape Descriptors for Identification of Linear Objects in an Urban Area Using High Spatial Resolution Imagery*

### **8.1 Introduction to the Problem**

Research in analysing geographical regions of Earth's surface with the availability of spatial, spectral, temporal and radiometric resolution remote sensing data has increased manifolds. The resolution of remote sensing data defines the resolving power which not only includes the capability of identifying the various objects but also, provides the information for analysing the properties of these objects. Spectral resolution statistics is the medium of remotely sensed image for identifying materials in urban landscape for varied classification applications [204]. Temporal resolution helps in generating land-cover maps for environmental planning, land use change detection and transportation planning [205]. Spatial resolution influences the accuracy of the ground objects in urban land cover applications [206]. Urban land-cover is one of the major regions of the Earth's surface that leads to various physical, socio-economic and environmental phenomenon's [207]; therefore, high resolution remote sensing data plays a vital role in classifying diverse and complex urban landscape which is a mosaic of engineered and non-engineered objects. The engineered objects are the urban impervious surfaces used to describe the road intersections, building corners and other well-defined objects [208]. Engineered objects are constituted from composite materials that show similar physical and chemical properties, [209] therefore, their spectral information may not be sufficient to classify the objects with



high accuracy. Evidently, the classification of such objects needs to be addressed by spatial information in terms of their structure and shape [210]. It is well known from the literature that the spatial information can improve the classification accuracy of urban objects from high resolution remote multispectral data. Many effective models for obtaining the spatial features such as Gray Level Co-occurrence Matrix (GLCM) have been interpreted for spectral classification [211,212]. Segmentation techniques are employed which automatically group the neighbouring pixels into contiguous regions that exhibit similar spatial arrangement [213]. Another representative technique for extracting spatial information is Markov Random Field (MRF) model [214]. Wavelet Transform (WT) techniques are used to extract textural features at different approximation scales [215]. Differential Morphological Profiles (DMP) are used to extract spatial features for multi-scale geometry analysis [216]. Notably, Length–Width Extraction Algorithm (LWEA) [217] has been developed which measures the spatial features within spectrally similar neighbourhood pixels. In addition to LWEA, Pixel Shape Index (PSI) [63] has been developed that forms another spatial feature extraction algorithm to extract the spectrally similar objects. All these techniques deal with spatial analytical approach for extracting the statistical/geometrical/shape features for studying the homogeneity and heterogeneity of the neighbouring pixels. Well-defined computation of spatial arrangement of pixels is an important factor for consideration in calculating the features for delineation of objects in the data [218]. However, the classical shape features approach is based on extracting features by extending and measuring the length of each direction line. Consequently, this method does not provide sufficient contextual information around the central pixel of curved structures, and pixels in the shape features can be allocated to different values [64]. Another approach, of using morphological profiles [219] has been conducted but with limited accuracy. Although the integration of shape features by incorporating spatial

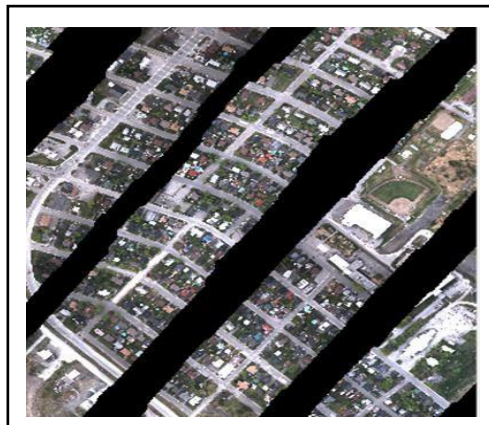
information [220] shows good performance in the extraction of roads, it is difficult to obtain universal shape feature extraction method for all situations, and therefore, further study is necessary. Based upon the above discussions, the paper investigates the parameters of spatial shape features for improving the classification accuracy of buildings and roads in urban landscape with two objectives as given below,

- (i) First objective pertains to delineation of buildings and roads using spatial shape features such as length, width and PSI. The paper implements the established mathematical formula of spatial structure features; however, it presents an improved way of calculating the directional lines. The novelty is in the methodology of computing local spatial structure feature for a window box on the bounding box, then extending it as an object and finally passing it to SVM classifier. To obtain this, first of all the bounding box of the buildings and roads are extracted from the dataset. Then, the features as direction line histograms are extracted from bounding boxes around the objects. These features are calculated at each box or window level. The features of each window box are concatenated and extended at object level. The inference of high-resolution images requires appropriate classifier for identifying the correct classes. SVM classifier which is fast and effective learning algorithm is used to interpret multiple spatial shape features.
- (ii) The other objective is to show the comparative assessment of classification accuracy of engineered objects using other spatial and spectral features. This is accomplished by performing a comparative analysis for classification of buildings and roads using proposed parameters for calculating spatial shape features with classical textural features. Further, the comparative analysis using only spectral features is also shown for delineating buildings and roads.

Multispectral classifiers such as spectral information divergence and spectral angle mapper are used to achieve the purpose.

## **8.2 Experimental Data Set**

The aerial data that is used in the present study is a high spatial resolution VIS RGB imagery. The details of the data have been explained in Chapter-2 in section-2.2. The image of VIS RGB data is again reproduced and is presented below as Figure-8.1.



**Figure 8.1 – VIS RGB imagery**

## **8.3 Theoretical Background**

For supervised classification of engineered objects, the accurate knowledge of features is highly important. The features aid in thematic feature extraction as they form the relevant and discriminative database necessary for separating one object/class from the other. Features are extracted by grouping similar characteristics of pixels in their spatial and spectral domain.

### **8.3.1 Homogeneity analysis in spatial domain**

Homogeneity analysis is the study of clusters of pixels in binary images that determine the connected regions. For each connected region, it provides the pixel properties or important features in the spatial domain such as color, area, perimeter, centroid and

bounding box. Connected components are those clusters of pixels in a binary image that hold the same intensity values which are connected to each other by *4-pixel* or *8-pixel* connectivity. The concept of connected component analysis has been explained in detail in Chapter-2 (section-2.2).

### **8.3.2 Spatial shape feature**

Shape features are indispensable in the context of each pixel in a spatial domain where the dominant shape of objects is rectangular. Therefore, in order to measure the spatial dimensions of spectrally similar connected pixels, the length and width direction line values for connected pixels are calculated. To discriminate objects such as buildings and roads, their size characteristics are of vital importance. These size features such as length and width direction line values are used to examine the contextual feature along the horizontal and vertical directions around the central pixel. Direction Line (DL) histograms are computed to evaluate the values of length and width of the spatially connected objects. The shape index of the central pixel is calculated which is total length of all direction lines. The mathematical abstraction is described in Chapter 2 (section 2.3.2.1).

### **8.3.3 Gray level co-occurrence matrix**

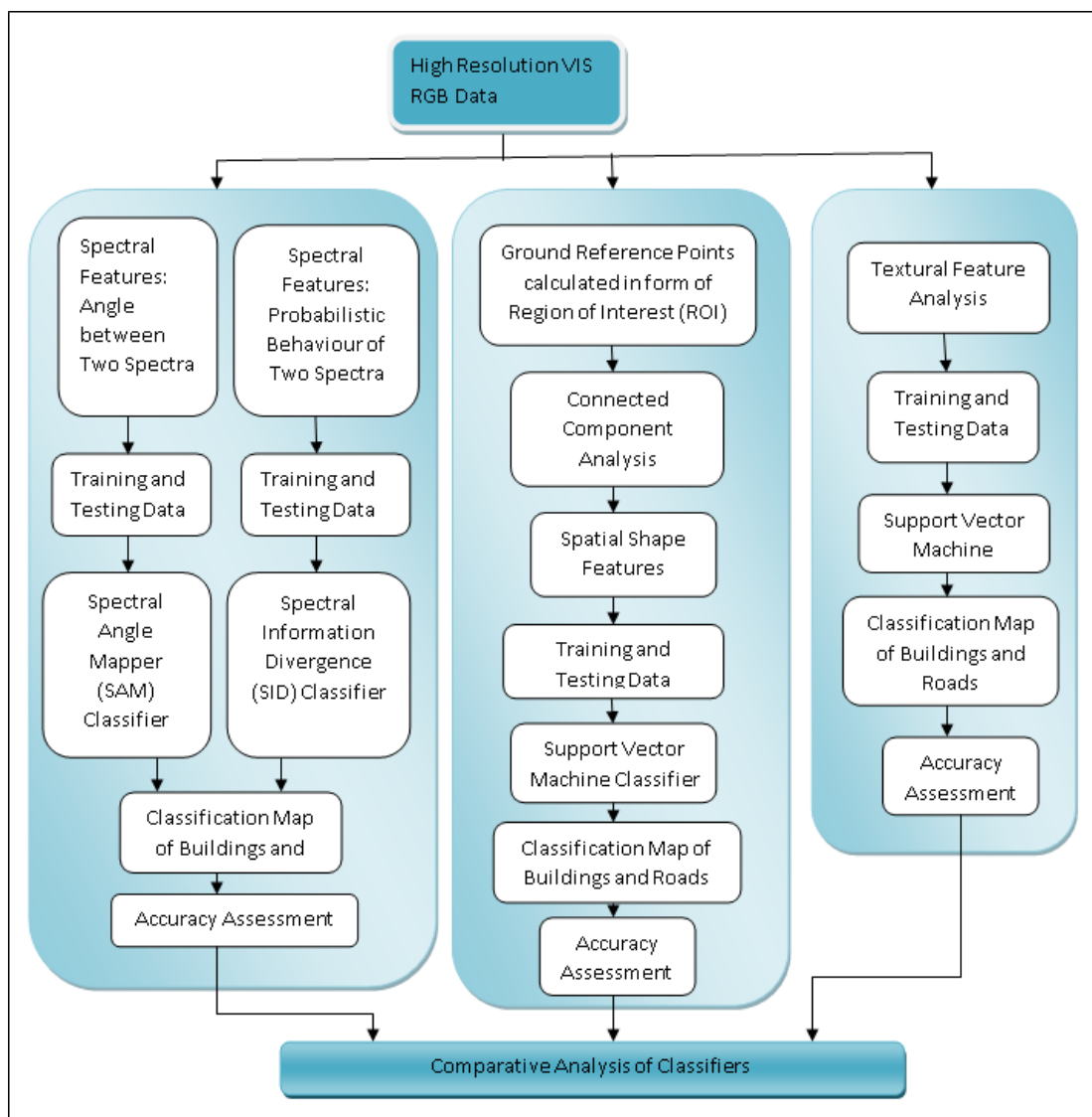
Gray level co-occurrence matrix is the most common second order statistical spatial feature technique. GLCM reveals statistical properties about the spatial distribution of the gray levels in the image. GLCM matrix calculates the frequency of occurrence of pixels '*i*' with gray-level intensity or a tone either horizontally, vertically, or diagonally to adjacent pixels with the value '*j*'. Once the matrix of GLCMs is created then several statistics listed in Table-2.3 in Chapter-2 can be deduced to obtain the information about the texture of an image. The statistical features are calculated by considering the pixels in pairs in a predefined neighbourhood around the current pixel. Each element of GLCM describes the

relative occurrence of two pixels within a predefined window size. The window size and the statistics used in this study are discussed under experiment section. These features are widely used in classification of images as high-resolution imagery can describe the texture of ground objects in detail.

#### **8.4 Methodology and Implementation**

The methodology includes the delineation of buildings and roads using spatial shape features such as length, width and pixel shape index. It is implemented using the established mathematical formula of spatial structure features however, an improved way of calculating these features from directional lines is presented in this study. For this purpose, local spatial structure feature is computed for a window size (discussed below in the experiments) on the bounding box and then extend as an object and finally passed it to SVM classifier. To do this, first the bounding box of the buildings and roads are generated from the dataset. Then, the features as direction line histograms are extracted from bounding boxes around the objects. These features are calculated at each box or window level. The features of each window box are concatenated to extend these features at object level. High-resolution images require appropriate classifier for identifying the correct classes. SVM classifier which is a fast and effective learning algorithm is used to interpret multiple spatial shape features. In order to observe the effects of using spatial shape features for classification of buildings and roads, the comparative assessment is performed using other spatial (*i.e.*, textural) and spectral (mean spectra of buildings and roads) features. For classification of spectral features classical classification algorithms are used in this study using *i.e.*, Spectral Information Divergence (SID) and Spectral Angle Mapper (SAM). Therefore, along with the effects of using different spatial and spectral features the effects of using different classifiers can also be seen.

The flowchart shown in Figure-8.2 gives the pipeline of the process carried out in this study. The flowchart presents the flow of the implementation steps designed to carry the comparative analysis on classification accuracy of the engineered objects by comparing the performance of various classifiers (*i.e.*, SVM, SAM and SID) trained on different spatial and spectral features (*i.e.*, spatial shape features, textural and mean spectra) for classification.



**Figure 8.2 – Flowline of the experiment conducted**

Two experiments have been performed to test the effectiveness of the proposed approach for calculating the shape features in the methodology. The first experiment is

designed to detect the influence of shape and size features on the extracted bounding box on connected regions of engineered objects *i.e.*, buildings and roads. The spatial shape features are used in classification of buildings and roads through a supervised classification algorithm. The second experiment is to compare the classification outputs using other spatial and spectral features.

#### 8.4.1 Experiment I – Influence of Parameters of Spatial Shape Features (SSF) on Bounding Box of Connected Regions

In this experiment the focus is on the extraction of two engineered objects *i.e.*, buildings and roads using SSF in urban areas. Although, these objects usually present analogous spectral features but have different shape and size characteristics, therefore these objects can be well identified by computing the spatial features.

##### Step 1: Generation of bounding box around the homogeneous pixels

The following flowchart in Figure-8.3 describes the pre-processing steps involved in generating the connected regions from VIS RGB data.

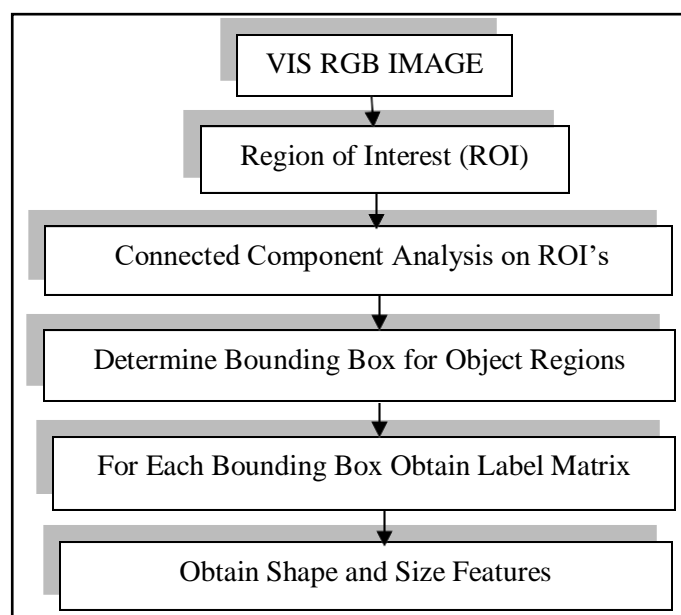


Figure 8.3 - Flowchart for depicting connected regions

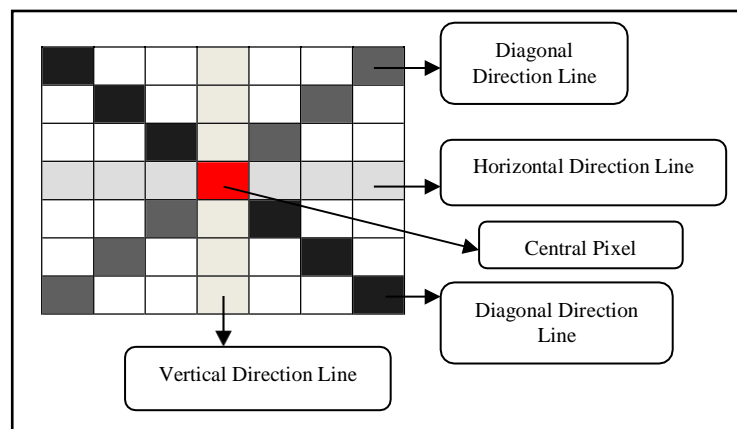
Generally, the roads have smaller width and larger lengths, so the length-width ratio will be greater, whereas, in contrast the buildings have smaller length-width ratio and diverse shape characteristics. In the dataset available, the buildings have multifarious rectangular polygon shape structures, therefore, in this experiment *8-pixel* connectivity is used to exploit the pixel properties which are connected horizontally, vertically and diagonally so that neighbour to every pixel is able to touch one of their edges or corners of multifarious structure. If  $CC_i$  be the  $i_{th}$  connected component of the binary image and  $CC_s$  be the set that includes all  $CC_i$ , then the bounding box feature of the connected component is defined as  $B(CC_i)$  which is exploited to obtain the coordinates of the connected region. Bounding Box is an important and relevant pixel feature of connected component which builds the multifarious structure of roads and buildings to an object region in rectangular shaped polygon, where  $(Xl_i, Yl_i)$  is the top left coordinate and  $(Xr_i, Yr_i)$  is the bottom right coordinate of the polygon. Bounding box property helps in segmenting objects with homogenous pixel properties from the background. For this, labelled components of a rectangular bounding box polygon are automatically cropped, and the image is displayed, which is shown in results section.

### **Step 2: Extraction of spatial shape features**

Spatial Shape Features (SSF) are obtained from the pixels associated with the bounding box of connected components. These spatial features are the length, width and PSI features. The features such as length and width are computed only in two directions around the central pixel which is inadequate to provide the essential information along the other directions. In this experiment, four directional lines for length and width measurements are proposed around the central pixel. The optimal choice of directional lines is highly important for describing the contextual structure around the central pixel. Two directions seem to be inadequate and more directions would unnecessarily add up spatial



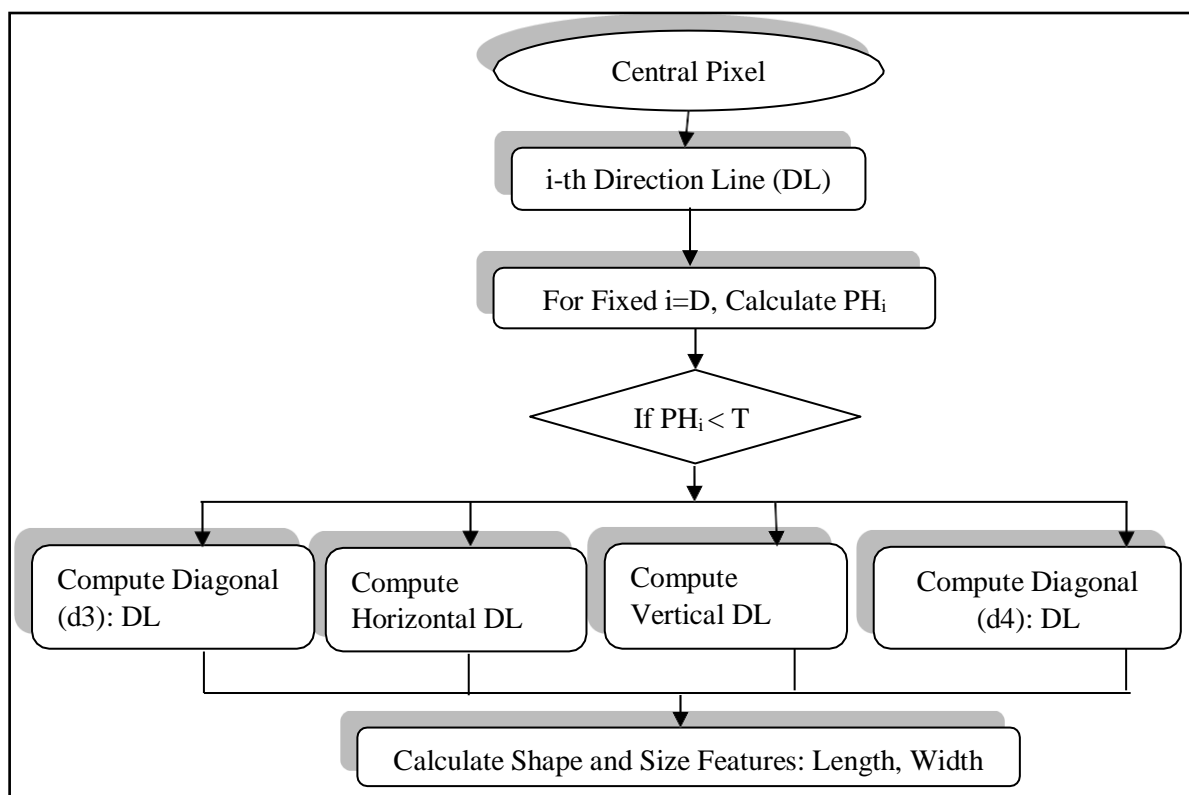
feature space generation leading to higher computations. Thus, the optimal feature sets of the central pixel in this experiment is formulated as  $d1$ : length and width values in horizontal direction,  $d2$ : length and width values in vertical direction,  $d3$ : length and width values diagonally at 45 degrees to the horizontal direction and  $d4$ : length and width values diagonally at 135 degrees to the horizontal direction around the central pixel. Figure-8.4 shows the proposed direction lines throughout the central pixel.



**Figure 8.4 - Direction lines**

The value of  $D$  (*i.e.*,  $D = 4$ ) is kept fixed in this experiment. Since, our problem is classification of buildings and roads that has diverse structural patterns in urban landscape, therefore, it is necessary to keep the feature length same. The total number of pixels for each direction line is determined by size of sliding window applied on the bounding box. Therefore, different sizes of sliding windows have been experimented with to assess the effect of spatial shape features in each direction. The outcome of this experiment is discussed in the results section. The pixel homogeneity is calculated along horizontal, vertical and diagonal direction lines around the central pixel if the threshold condition is satisfied. The histogram sum is calculated for pixel homogeneity values. The maximum value of the histogram gives the length feature and the minimum value of the histogram gives the width feature. PSI is calculated by summing up all the length and width values

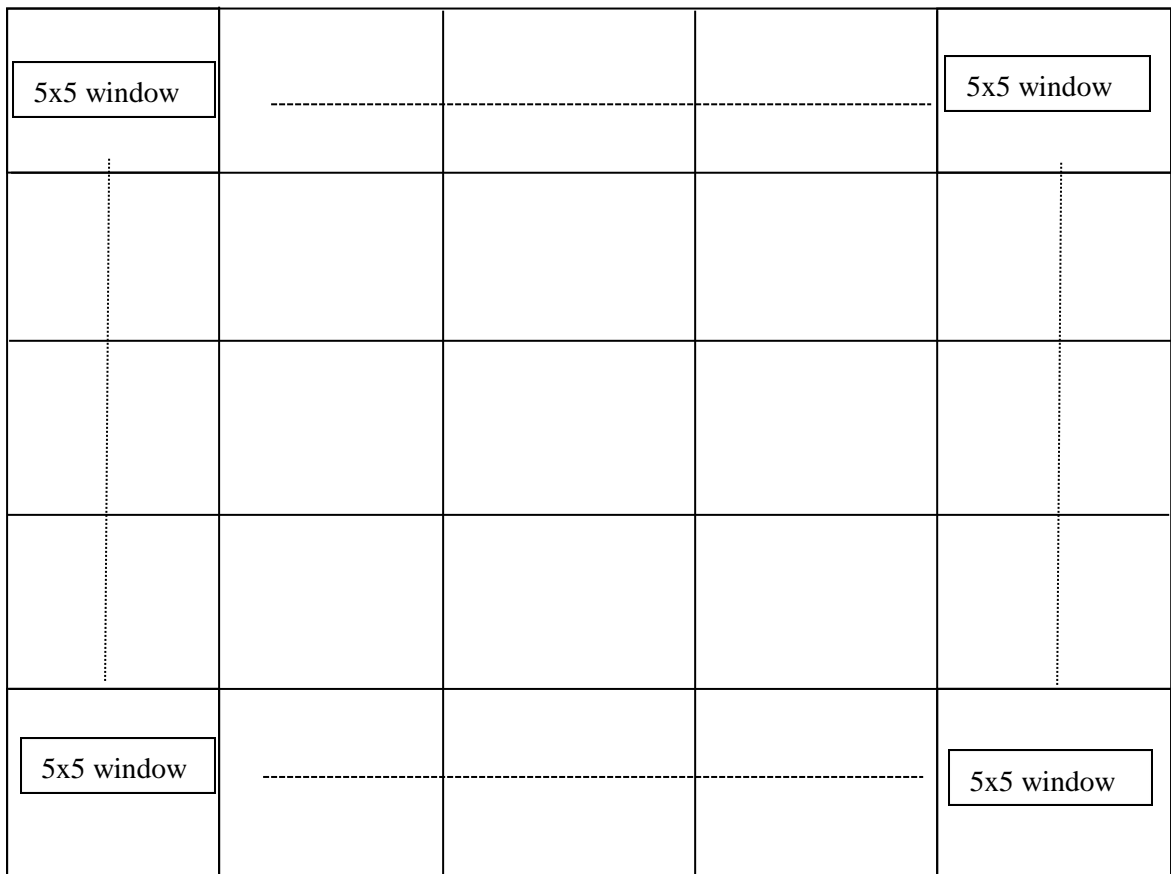
for a fixed value of number of directions. Figure-8.5 shows the step wise flow line of the parameters computed for proposed PSI shape feature.



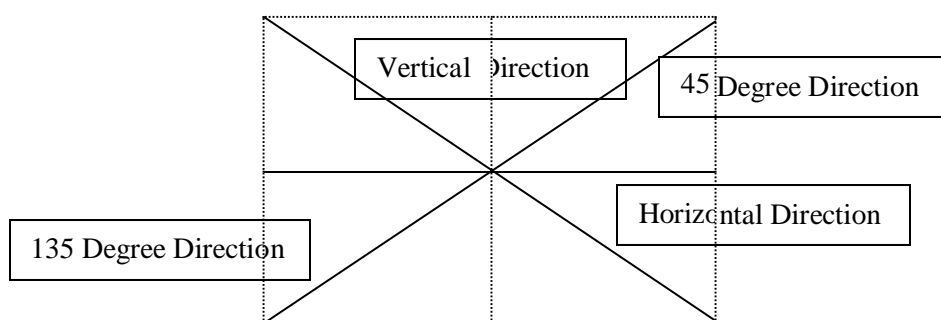
**Figure 8.5 - Flowchart for shape and size features calculation**

These calculated features are extracted from the bounding box of the connected regions in order to extract the shape and spatial arrangement of the objects in the image. The influence of the calculated features on the bounding box was determined through experiments. The shape and size features were calculated on each bounded box of the extracted number of the objects. It is seen that if the features are extracted once over the complete bounding box then the spatial arrangement and shape features are unable to provide enough contextual information of the objects. Therefore, in order to calculate the overall neighbourhood information within the bounding box the spatial shape features of an object are computed in a unique way. The bounding box of an object is divided in non-overlapping boxes in horizontal and vertical direction and then the local SSF features are computed for each box. The features of each box are concatenated and passed to SVM

classifier for classification. The concept has been explained using Figure-8.6. The directions for feature computation of each box is explained in Figure-8.7.



**Figure 8.6 - Dividing 25x25 bounding box in 5x5 boxes/windows**



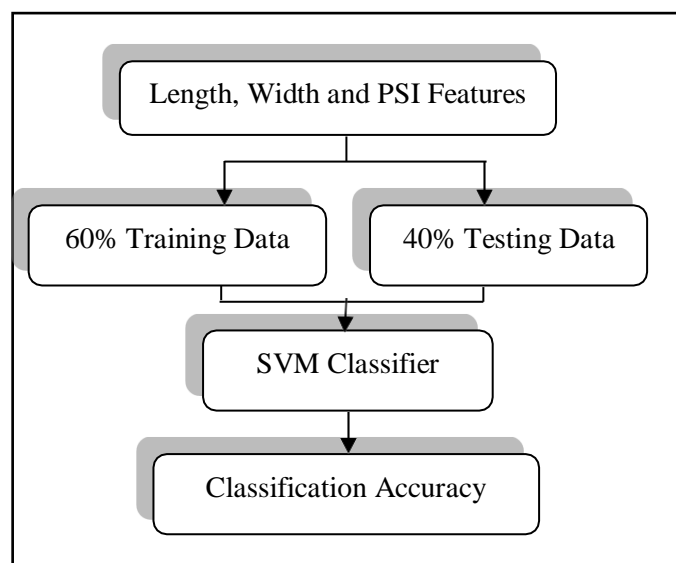
**Figure 8.7 – Directions for feature computation**

Figure-8.7 explains the SSF features computed considering the distribution of gray channel intensity in horizontal, vertical, 45-degree diagonal and 135-degree diagonal. To

reduce the computational complexity, in SSF calculations directional lines are not chosen explicitly, rather it assumes four directions of directional lines and these directions are horizontal, vertical, 45-degree and 135-degree. In each direction, only the pixels whose intensity is less than a threshold from central pixel is considered in the histogram vector and then this histogram vectors are used to further calculate features of SSF.

### **Step 3: SVM classification**

The extracted features are divided into training and testing samples which are fed to support vector machine classifier. To evaluate the classification performance of SVM, true positives of the concerned engineered objects are evaluated. Figure-8.8 shows the steps involved in classifying the engineered objects.



**Figure 8.8 - Flowchart for classification**

In this experiment, the features calculated on each window box in four directions around the central pixel for assessing the shape index for complete object are calculated which are shown in results section. These parameters form the pixel shape features which are incorporated on bounding box in different windowing styles. The features are calculated

on four different window sizes of bounding box and the effect of the shape features on each window style is shown in results section.

#### **8.4.2 Experiment II- To Compare the Classification Accuracy Obtained from Different Spatial and Spectral Features using Different Classifiers**

A second experiment is done to study the influence of spatial and spectral features on different classifiers. For this, the effect of three classifiers have been studied. SVM is trained and tested for textural and spatial shape features, whereas spectral features from the dataset are well explored using SAM and SID algorithms. The classification assessment is carried out in terms of Overall Accuracy (OA), Producer's Accuracy (PA) and Kappa Co-efficient ( $K_c$ ). Further, the overall comparison of all the three classifiers is shown in terms of PA for buildings and roads. The steps required to perform this experiment is shown in Figure-8.2. OA is the number of validated pixels that have been correctly classified to the total number of validated pixels used for all the classes. PA estimates the probability that the classifier has correctly labelled an image pixel.  $K_c$  is the proportion of correctly classified validated pixels after random agreements are removed.

### **8.5 Results and Discussions**

The regions of interest for two objects *i.e.*, buildings and roads have been extracted from VIS RGB data (and can be referred from Chapter-4, Figure-4.6 (d) & (e)) and the spatial shape features are incorporated in the bounding box of these features. The generation of bounding box for these two objects have been explained in Chapter-4 under the section-4.5.3. The results of two experiments are formulated using the extracted bounding box of connected components of engineered objects *i.e.*, buildings and roads.

### **8.5.1 Experiment I - SVM classification of engineered objects using spatial shape features on bounding box of connected regions**

The shape homogeneity parameters that are incorporated in the bounding box of the connected components are calculated in two ways. In the first, the shape homogeneity parameters are calculated over the entire area of each bounding box of an object of size 25x25. The length of direction lines around the central pixel are the pixel elements in the current row till the length of the edge of the bounding box. For each direction line, from the central pixel, the absolute values of shape homogeneity are evaluated in terms of length, width and PSI. In the second, different window box of sizes 5x5, 1x5 and 1x1 are moved over the original bounding box of each object of size 25x25. These windows are moved in rows and in columns across the bounding of each object as explained in Figure-8.6. For a combination of 25x25 bounding box and 5x5 window, a total of 25 non-overlapping window boxes are considered in horizontal and vertical direction. The shape features are computed from each 5x5 window box, likewise the features are calculated from rest of the combinations as well. The parameter T which indicates the maximum spatial distance between the central pixel and its neighbouring pixel in the gray channel representation needs to be evaluated. The threshold is a scaling factor in the algorithm and is pertinent to the spatial resolution of the data and the size of the bounding box on which the statistical features are evaluated. In this experiment, it is noted that as the parameter T increases from 10 to 120 the true positives for discriminating buildings and roads escalates. At T=100 it reaches the maximum, then after T=100 the true positives of the object “road” suddenly declines. Table-8.1 shows the calculation of correctly predicted objects *i.e.*, buildings and roads for various values of the threshold (this is calculated on testing feature sample size mentioned in Table-8.3). The value of threshold ought to be determined through

experiments as this parameter is related with the shape and spatial arrangement of objects in the data.

**Table 8.1 - Calculation of correctly predicted objects wrt threshold**

Threshold \ True Positive	T=10	T=20	T=30	T=40	T=50	T=60	T=70	T=80	T=90	T=100	T=110	T=120
Buildings	62	68	100	100	100	56	100	100	100	100	98	96
Roads	64	58	60	0	68	0	69	0	66	73	0	0

Table-8.2 shows the total number of training and testing bounding box of buildings and roads. The size of feature space is a vector of size  $75 \times 456$  for buildings and  $75 \times 363$  for roads. Computational complexity is of order  $n$ ,  $O(n)$ , where  $n$  is number of pixels, since the feature depends on the histogram at the core of computation. The total compute time for calculating spatial shape features is  $20.27ms$  and the average time for computing spatial shape features is  $0.81ms$ . The calculated features are divided into training and testing samples. Table-8.3 shows the number of training and testing spatial shape features obtained by moving non overlapping window of size  $5 \times 5$  on bounding box of connected components of buildings and roads. These spatial shape features are the input features for training SVM classifier.

**Table 8.2 - Training and testing samples**

Class \ Samples	Training Bounding Box	Testing Bounding Box	Total Number of Bounding Box
Buildings (60% of total number of bounding box)	274	182	456
Roads (40% of total number of bounding box)	218	145	363
<b>Total</b>	<b>492</b>	<b>327</b>	<b>819</b>

**Table 8.3 - Training and testing SSF**

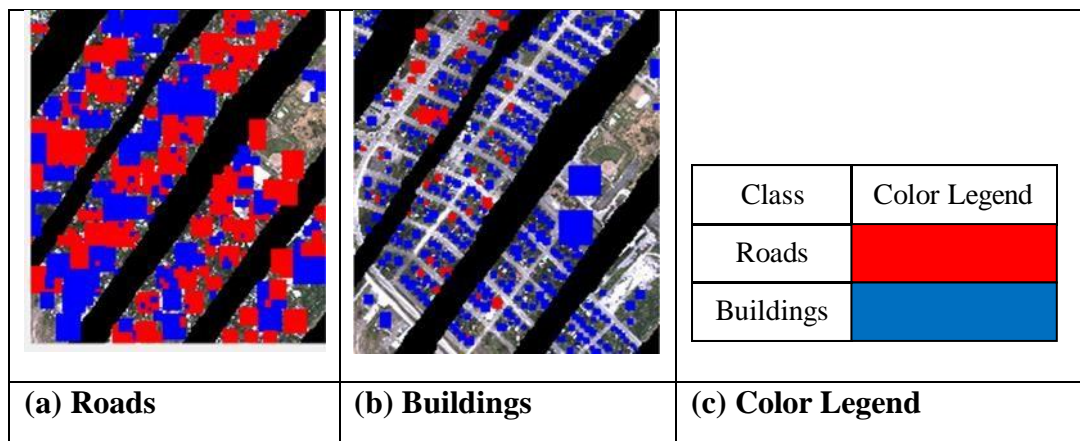
Objects	SSF_Training	SSF_Testing
Buildings	75x274	75x182
Roads	75x218	75x145

The SVM classifier network involves the assignment of class labels for each identified object in testing sample. The established parameters of the classifier network based on training samples is shown in Table-8.4.

**Table 8.4 - Design parameters of SVM for spatial shape features**

Design Parameters of SVM	Support Vector	Alpha	Bias	Kernel Function
Buildings	291x75	291x1	3.2196	Linear
Roads	311x75	311x1	-0.0161	Linear

The optimized hyperplane solutions are generated from the parameters listed in Table-8.4. The distinguished class labels belonging to buildings and roads are mapped on the classification map which is shown in Figure-8.9.



**Figure 8.9 - Classification map of engineered objects *i.e.*, buildings and roads generated using spatial shape features**



The classification accuracy of engineered objects *i.e.*, buildings and roads have been calculated in terms of PA and is shown in Table-8.5.

**Table 8.5 - Accuracy assessment for spatial shape features**

<b>Input: Shape Features</b>	<b>Bounding Box of size 25x25</b>	<b>Window (5x5) on Bounding Box</b>	<b>Window (1x5) on Bounding Box</b>	<b>Window (1x1) on Bounding Box</b>
<b>Accuracy Assessment (%)</b>	<b>SVM Classification</b>			
PA-Building	100	<b>100</b>	100	100
PA-Road	0	<b>97.3</b>	51	0
Shape Features are calculated by keeping the parameter D=4, direction lines at 0°, 45°, 90° and 135°, T=100				

The accuracy statistics in Table-8.5 shows that the SVM classifier results calculated using spatial shape features by running non overlapping window of size 5x5 on the bounding box of connected components show better results in comparison to other combinations of window sizes for the extraction of buildings and roads. The high accuracy of roads (*i.e.*, 97.3%) indicate that the stack of spatial shape descriptors enhances and exploit the structural characteristics of the elongated engineered objects in urban landscape. The information derived for accessing linearity for roads in terms of length, width and shape was not enough and led to lower accuracy in other combinations of window sizes.

### **8.5.2 Experiment II- To Compare the Classification Accuracy Obtained from Different Spatial and Spectral Features using Different Classifiers**

The textural features are calculated on the connected regions using GLCM approach. The parameters are calculated by applying window of size 3x3 onto the bounding box coordinates. Two spatial statistical parameters are calculated *i.e.*, contrast and homogeneity for each visible band. In total 486 features are obtained, in which textural

feature space of 81 GLCM contrast and homogeneity values on each visible band of the data is obtained. The range of the contrast between a pixel and its neighbor is given as,

$$\text{Range: } [0 \text{ (size (GLCM},1)-1) ^2] \quad (8.1)$$

In this experiment, the minimum value of contrast is 0 where the constant intensity values of the objects are seen. The maximum value of contrast is 0.667 which defines the difference in brightness of the buildings and roads within the same field of view. The range of homogeneity statistical parameter lies in the range of [0 1]. The minimum value of homogeneity is 0.667 and the maximum value observed is 1.

Textural features obtained from bounding box of buildings and roads form training and testing datasets. Table-8.6 shows the number of training and testing spatial textural features obtained. These spatial textural features are the input features for training linear SVM classifier.

**Table 8.6 - Training and testing textural features**

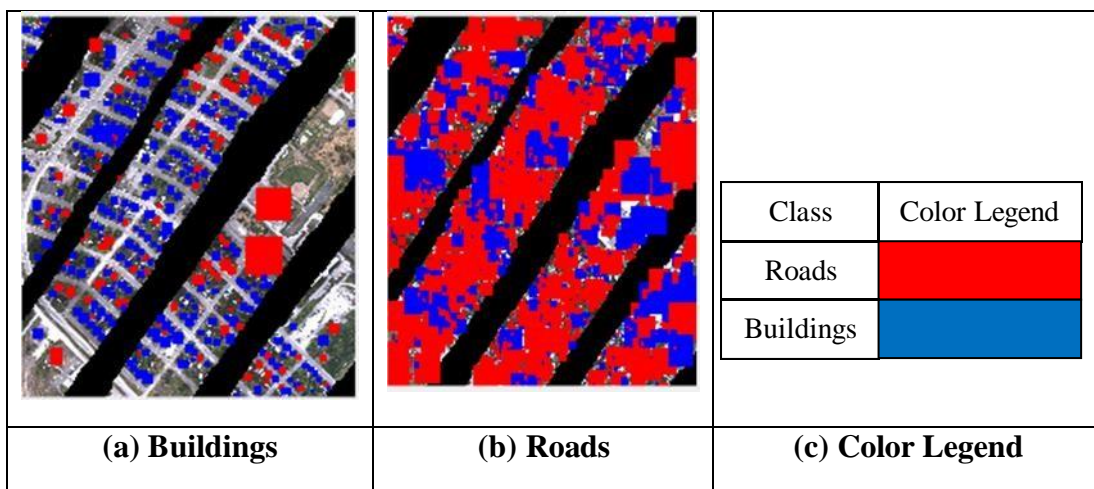
<b>Feature Training and Testing Samples for Engineered Objects</b>	<b>Textural Training Features</b>	<b>Textural Testing Features</b>
Buildings	486x274	486x182
Roads	486x218	486x145

The textural features are used to train SVM classifier network that establishes the support vector and bias parameters for the obtained textural features which is given in Table-8.7. The linear SVM trained classifier is applied to testing textural feature class labels and based on the optimized hyperplane generated from SVM classifier the engineered objects are distinguished.

**Table 8.7 - Design parameters of SVM for textural features**

Design Parameters-SVM	Support Vector	Alpha	Bias	Kernel Function
Buildings	701x486	701x1	-0.3839	Linear
Roads	701x486	701x1	-0.3839	Linear

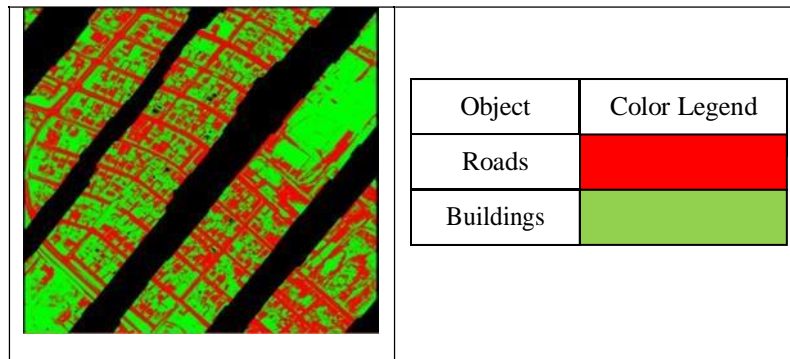
The classification map generated from SVM classified results based on textural features is shown in Figure-8.10.



**Figure 8.10 - Classification map of engineered objects *i.e.*, buildings and roads using textural features**

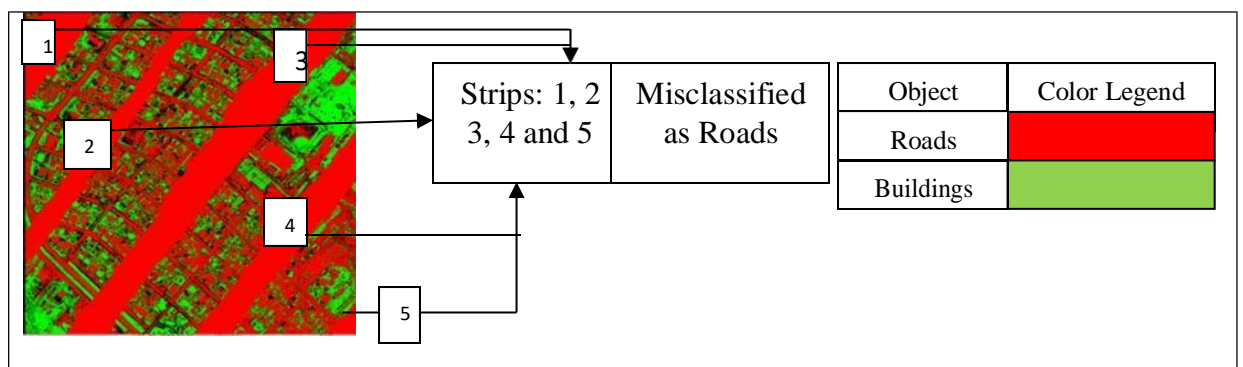
Another set of spectral features in the form of mean spectra for both the objects *i.e.*, buildings and roads are obtained from ENVI software. This training spectra is used in SAM and SID classifiers to obtain the angle and information measure for classifying the objects.

For SAM classification, based on the mean spectral signature generated for buildings and roads in this experiment, a single value of 0.3 radians is used as the maximum classification threshold value. This is selected after the careful consideration of different threshold angle values between the reference and testing spectrum based on the classification accuracy assessment. The classified image is shown in Figure-8.11. The color legend chosen for object-road is “red”, for object-building is “green”.



**Figure 8.11 – Classification map (SAM) of engineered objects *i.e.*, buildings and roads using mean spectra**

In SID classification, the similarity measure between the reference spectra and testing spectra is evaluated with the threshold value of cross entropy as 0.050. If the cross entropy of reference and testing pixels is less than 0.050 then the spectra have similar probabilistic measure and the testing pixels is classified to the reference pixel otherwise it is misclassified. If the probabilistic measure between the two pixels is more than 0.050, then lesser is the possibility of the matching of testing pixel with the reference pixel. Due to this reason, in this experiment, the strips in an image are misclassified as linear engineered object *i.e.*, road which can be seen in Figure-8.12. The classification map for engineered objects *i.e.*, buildings and roads based on spectral features is shown in Figure-8.12. The color legend chosen for object-road is “red” and for object-building is “green”.



**Figure 8.12 - Classification map (SID) of engineered objects *i.e.*, buildings and roads using mean spectra**

The assessment of classification (shown in Table-8.8) by spectral classifiers show that SAM classifier performs better than SID for classifying the engineered objects particularly buildings and roads. The overall accuracy and  $K_c$  parameters are high for SAM classification as this algorithm is based on the angular similarity between the reference and testing spectra of buildings and roads which may be different due to their structural dissimilarity. Table-8.8 shows the  $OA$  and  $K_c$  statistical assessment for both the classifiers. Even the classification map generated from SID classifier in Figure-8.12 clearly shows that the roads are highly misclassified for the strips in the data that has no information.

**Table 8.8 - Accuracy Assessment of Spectral Classifiers**

<b>Accuracy Assessment</b>	<b>SAM</b>	<b>SID</b>
$K_c$	0.6123	0.437
OA (%)	80.09	66.52

The classification accuracy of engineered objects from spatial shape features can be seen in Table-8.9. It shows the comparative analysis of SVM classifier with other conventionally existing spectral feature classifiers *i.e.*, SAM and SID. In Table-8.9, the comparison of different classifier networks with different features is shown. The results show that the classification accuracy of buildings and roads has been improved by the proposed methodological approach for computing spatial shape features.

**Table 8.9 - Classification Accuracy of Spatial and Spectral Features**

<b>Producers' Accuracy</b>	<b>Shape Features SVM</b>	<b>Spectral Features SID</b>	<b>Spectral Features SAM</b>	<b>Textural Features SVM</b>
<i>Column1</i>	<i>Column2</i>	<i>Column3</i>	<i>Column4</i>	<i>Column5</i>
Buildings	100	51.04	96.70	77.0
Roads	97.3	86.22	66.83	58.2

The high performance of SVM (refer Table-8.9, column-2) attributes to the higher capability of finding the optimal hyperplane for separating the similar characterised classes

using shape features. High classification accuracy of SVM also shows that it is the better class separation classifier for high spatial resolution data than SAM and SID classifiers though SAM and SID classifiers are easy and rapid in implementation.

From the results shown in Table-8.9 the following analysis emerges,

- (i) It is seen that classification accuracy of building and road using SID classifier (column-3) is 51.04% and 86.22% and by using SAM classifier (column-4) the classification accuracy is 96.7% and 66.83% for building and road. The performance parameter is less in comparison to the classification accuracy obtained using shape features which is 100% for building and 97.3% for road. This shows that only spectral features may be insufficient to identify buildings and roads in urban areas due to spectral homogeneity and similarity exhibited by them. Therefore, it is beneficial to explore the spatial features described in terms of shape descriptors to improve the classification accuracy of engineered objects.
- (ii) It is also seen that best classification accuracy of class road (97.3%, column-2) is achieved through this study in comparison to the results achieved so far even in earlier objectives. Hence, it may be concluded that the linear structured man-made objects can be well interfered through spatial shape features using very high- resolution spatial data.
- (iii) From Table-8.10 it is seen that the classification accuracy of building and road obtained by spatial feature using textural properties (column-5, is 77% and 58.2%) which is quite low in comparison to the classification accuracy obtained using spatial shape feature (column-2) which is 100% for buildings and 97.3% for roads. This shows that textural second order statistics may not be enough for the classification of structured man-made objects.

## 8.5 Summary

The main aim of the study is the use of spatial shape descriptors for the classification of man-made objects exhibiting similar spectral characteristics using high resolution remote sensing imagery. It is achieved by exploring the parameters and the methodological approach used in obtaining the pixel shape descriptors. The parameters used to obtain the shape descriptors include the number of direction lines (*i.e.*,  $D=4$ ), the extension of direction lines (in four directions) and the threshold ( $T=100$ ). The methodological approach includes the way of calculating the features on the connected components. The features deduced are used to train the SVM classifier network and is tested to obtain the classification accuracy. The results have shown an improvement in classification accuracy of the linear structured engineered object *i.e.*, road. Further, the classification accuracy of different classifiers based on textural and spectral features is also studied. The results confirm that only spectral features may not be enough in high spatial resolution remote sensing imageries for classifying engineered objects. SVMs have outperformed in identifying buildings by shape features in comparison to SAM and SID classifiers using spectral features. Although the classification accuracy of roads seems to be better in SID classifiers, but the lower values of kappa coefficient and overall accuracy has helped in determining that the higher producers' accuracy of roads is due to misclassification of pixels as roads. The erroneous judgement of roads may be due to similar angle and information measures in reference and testing spectra of pixels that are not actually roads. This verification has embarked the usefulness of spatial shape descriptors in identifying the linear engineered object *i.e.*, road in an urban area.

The findings in the study are relevant for urban planners as the correctness in identification of roads against buildings may aid them in proper planning and infrastructure

development. Further, the results show significant contribution in extraction of buildings and roads with the help of spatial shape descriptors.



# Conclusions and Major Contributions

### 9.1 General

The research presented in this thesis addresses some of the issues pertaining to object-based classification of urban land-cover features using thermal, VIS RGB and wide range hyperspectral data. The study emphasizes classification accuracy of natural and man-made objects by exploring features in spectral and spatial domain and combines the knowledge of these features at the time of decision level fusion keeping in mind the research gaps identified after an intensive literature review.

### 9.2 Objectives

The first part of this research has studied, explored and tested the ability of using multi-sensor and multiresolution remote sensing data to address the capability of spatial and spectral features for the object-based classification of natural and man-made objects in an urban land-cover. A methodological approach has been considered to explore decision level fusion of features at different stages. To achieve this, thermal hyperspectral (84 spectral channels, ranging from 7400-nm-11500-nm) and a very high spatial resolution (20-cm spatial resolution) VIS RGB data has been used which have not been explored much earlier. The two sets of land-cover objects *i.e.*, natural (trees, vegetation and soil) and man-made (buildings and roads) have been classified in this study from an urban area.

The second part of this research studies the responses of combining the spectral and spatial features at the classifiers' decision stage to improve the classification accuracy of urban land-cover objects. The experiments have been performed using two different

popular non-parametric classifiers for validating the response of exploring the fusion of different features on different classifier networks.

The third part of this research explores the benefit of using wide range hyperspectral data. The spectral channels of hyperspectral data ranging from 325-nm to 2500-nm have been explored for extracting the useful wavelengths for forming the spectral indices which in turn can be used for identifying the components /constituents of natural and man-made objects of an urban area.

The fourth part of this research focuses on improving the classification accuracy of linearly structured man-made object *i.e.*, road in an urban area by exploring the spatial shape attributes using a very high spatial resolution data.

A series of experiments have been conducted with the following objectives,

- (i) Extraction of natural and man-made objects using fusion of spectral and spatial features in multisensory thermal infrared hyperspectral and VIS RGB data.
- (ii) Enhancement in classification accuracy of land-cover objects using weighted majority voting fusion of spectral and spatial features in multisensory data.
- (iii) Comparative analysis for land-cover classification using two non-parametric classifiers in multisensory images.
- (iv) Formulation of spectral indices by identifying significant wavelengths from hyperspectral data for material classification.
- (v) Extraction of shape features for identification of linear structured man-made objects from a high spatial resolution remote sensing data.

### **9.3 Overview of Methodology**

For the outlined research objectives listed in above section, spatial and spectral features (*i.e.*, textural, MBI and NDVI) are calculated to form the knowledge database. For

classification of linear man-made structures *i.e.*, buildings and roads, the parameters forming the spatial shape features are also studied and explored. A novel way of multiresolution segmentation is proposed by using connected component analysis on bounding box of ground truth polygons extracted for each object/class. All spatial, shape and spectral features are then segmented using bounding box of connected components. These features form the training and testing samples for object-based classification. For classification of natural and man-made objects using spatial and spectral features the performance of four classifiers (*i.e.*, multi-class linear SVM, ANN, SAM and SID) are tested and studied in this study. The performance parameters of the classifiers have helped in outlining the various decisions on the classified results. In the study, to improve/enhance the classification accuracy of natural and man-made objects, a decision level fusion has been proposed. To achieve this, the decision level majority voting fusion of classifier results with each computed feature and with combination of all features is tested and studied. In addition to this, a separate study on spectral indices has been carried using AVIRIS-NG hyperspectral data in order to find the optimum bands for forming the band ratios and to explore the classification of inter-class variability for urban land cover using spectral band ratio features.

#### **9.4 Conclusions**

From the analysis of the results of the experiments, following specific conclusions have been drawn,

- (i) The results obtained from classification approach using decision level fusion of NDVI feature in SVM classifier network shows that the majority vote of NDVI feature has contributed in achieving a good confidence measures for classes, building (100%), vegetation (91.6%), soil (91%) and

road (79.3%). From these results, it can be inferred that NDVI feature has given better results for almost all classes, therefore, the mean spectral information from the thermal hyperspectral bands can be explored for studying the natural and man-made objects in urban land cover.

- (ii) The majority vote of MBI feature has resulted in appreciable confidence measure for class soil (85.7%), though MBI feature is largely used for extracting buildings. An appreciable confidence measure of class soil derived from decision level fusion of MBI feature leads to the conclusion that MBI feature may be explored for extracting information of those objects that show similar morphological profiles as observed for building structures using spectral structural feature from very high spatial resolution remote sensing data.
- (iii) The majority vote of textural feature has achieved better confidence measure for class tree (83.7%) in comparison to other two features belonging to the natural class. High confidence measure of tree obtained from textural feature indicates that a very high spatial resolution data can be explored for attaining better identification of natural objects. The use of spatial second order statistical feature can contribute significantly in classifying trees and vegetation in comparison to the spectral information.
- (iv) The comparative analysis of the results reveals that the overall confidence measure of the classified objects using SVM classifier have improved from 57.1% to 98.2% (for all classes except for building) by using proposed weighted majority voting strategy of combined spectral and spatial features derived from multisensory data.

- (v) From the experiments performed in this research, the results obtained from the comparative performance of two non-parametric classifiers show that SVM classifier network gives better generalisation results than ANN for identification of natural and man-made objects. The results show that in comparison to neural networks, SVM require less training data for decent performance.
- (vi) Various informative spectral wavelengths can be deduced using OIF technique. The important and significant wavelengths can be used in developing spectral indices. The two indices identified during this research, namely, clay mineral index and NDBI have resulted in significantly improving the classification of components/constituents in soil and man-built structures. The results have shown the importance of selecting optimal wavelengths for fast and efficient extraction of material information in an urban area. From the results, it can also be inferred that for inter-class variability, spectral band ratios can be well used for the study of the sub-class features in urban land-cover using AVIRIS-NG hyperspectral remote sensing imagery.
- (vii) From the research, it can be concluded that for linear man-made structures, particularly, the roads, it is beneficial to study the pixel shape features which can be extended to object level in order to improve the classification accuracy. The results have also shown that the use of very high spatial resolution VIS RGB data potentially contributes in improving the classification of man-made objects.

## 9.5 Major Contributions

The outcome of this research by way of various experiments discussed in this thesis lead to the following major research contributions,

- (i) A significant different approach has been evolved for classification of natural and man- made objects using multi-sensor and multi-resolution data in which both spatial and spectral feature domains have been explored using bounding box of connected objects for one-against-one class SVM classification.
- (ii) A new strategy for fusion of various features has been elucidated in Figure-5.2 of Chapter-5. The proposed strategy is based on decision level fusion using weighted majority voting of all spatial and spectral features has resulted in significant improvement in classification accuracy of natural and man-made objects in an urban land-cover.
- (iii) Certain wavelengths have been identified as shown in Table-7.8 from AVIRIS-NG HS data ranging from 385-nm to 2500-nm which have been used in formulation of various spectral indices. Two indices, namely Clay Mineral Index and NDBI have resulted in significantly improving the classification of components/constituents in soil and man-built structures.
- (iv) A new design approach has been proposed in section-8.4 for calculating the spatial shape features to improve the classification accuracy of linear structured man-made object in urban land cover *i.e.*, roads.

## 9.6 Recommendations

Several important recommendations can be made from the study.

First, the combination of finer spatial and spectral resolution data can be considered for land cover classification using the object-based classification approach.

Second, mean spectra of thermal LWIR data can be considered for the classification of natural and man-made objects by exploring NDVI features.

Third, decision level fusion of multiresolution and multi-sensor data using spatial and spectral features can be used to enhance the classification accuracy of physical features of urban land cover.

Fourth, for classifying the linear structured objects in urban areas, pixel shape parameters can be used by extending the features as objects for improvement in classification.

Fifth, the spectral indices can be used for obtaining the components/constituents of soil and man-built structures using appropriate wavelengths that can be identified using OIF technique.

Finally, it is recommended to make use of the combination of spatial and spectral attributes in multi-sensor and multiresolution data that improves the classification accuracy of natural and man-made objects in urban land-cover.

## **9.7 Further Work**

No research is said to be complete unless it does not lead to a few pointers for future research. The present study also, therefore, throws up some issues which may be investigated in future. Some of the specific issues emerging from the present research which need to be explored further are,

- (i) More spatial structural features can be explored using high spatial resolution data for identifying the man-made structure.

- (ii) The combination of various spectral and spatial features can be explored to identify the sub-classes or different level of categorizations in natural and man-made objects in an urban environment.
- (iii) Significant wavelengths can be explored from AVIRIS-NG HSI in order to enhance the material classification.
- (iv) New spectral indices can be formulated using important wavelengths from AVIRIS-NG HSI.
- (v) Fusion techniques can be explored to enhance the capabilities of multisensory datasets for classification of objects in urban areas.



## ***References***

- [1] Lillesand, T., Kiefer, R., and J. Chipman, *Remote Sensing and Image Interpretation*, 6th ed., New York, NY: John Wiley & Sons, 2008, pp. 756.
- [2] Navalgund, Ranganath & V, Jayaraman & Roy, Parth., “Remote sensing applications: An overview,” *Current science*, vol. 93(2), pp.1747-1766, 2007.
- [3] Rifaat Abdalla, *Introduction Chapter: From Land Surveying to Geomatics - Multidisciplinary Technological Trends*, *Trends in Geomatics - An Earth Science Perspective*, Rifaat Abdalla, IntechOpen, January 26, 2019.
- [4] Rustamov, Rustam B., Sabina Hasanova, and Mahfuza H. Zeynalova, eds. *Multi-purposeful Application of Geospatial Data*, BoD–Books on Demand, 2018.
- [5] Jong S.M., Meer F.D., Clevers J.G., *Basics of Remote Sensing*. In: Jong S.M.D., Meer F.D.V. (eds) *Remote Sensing Image Analysis: Including the Spatial Domain. Remote Sensing and Digital Image Processing*, vol 5, Springer, 2004, Dordrecht.
- [6] Liang, Shunlin, Xiaowen Li, and Jindi Wang, eds. *Advanced remote sensing: terrestrial information extraction and applications*, Academic Press, 2012.
- [7] Malgorzata, Verőné Wojtaszek, and Barsi Árpád, *Data acquisition and integration 6., 6 Remote Sensing*, Nyugat-magyarországi Egyetem, 2010.
- [8] Stojče Dimov Ilčev, *Global Satellite Meteorological Observation (GSMO) Applications*, vol. 2, Springer International Publishing, 2019.
- [9] Yang, C., Everitt, J.H. and Johnson, H.B., “Applying image transformation and classification techniques to airborne hyperspectral imagery for mapping Ashe juniper infestations,” *International Journal of Remote Sensing*, vol. 30(11), pp.2741-2758, 2009.
- [10] Miao Li, Shuying Zang, Bing Zhang, Shanshan Li & Changshan Wu, “A Review of Remote Sensing Image Classification Techniques: The Role of Spatio-contextual Information,” *European Journal of Remote Sensing*, vol. 47(1), pp.389-411, 2014.
- [11] Desheng Liu & Fan Xia, “Assessing object-based classification: advantages and limitations,” *Remote Sensing Letters*, vol.1(4), pp. 187-194, 2010.
- [12] Zerrouki, Nabil, and Djamel Bouchaffra, “Pixel-based or Object-based: Which approach is more appropriate for remote sensing image classification?,” *IEEE International Conference on Systems, Man, and Cybernetics (SMC)*, pp.864-869, 2014.
- [13] Yuji Murayama et al., “Pixel-based and object-based classifications using high-and medium-spatial-resolution imageries in the urban and suburban landscapes,” *Geocarto International*, vol. 30(10), pp.1113-1129, 2015.
- [14] Weiqi Zhou, “An Object-Based Approach for Urban Land Cover Classification: Integrating LiDAR Height and Intensity Data,” *IEEE Geoscience and Remote Sensing*, vol. 10(4), pp.928-931, 2013.
- [15] T. Blaschke, “Object based image analysis for remote sensing,” *ISPRS Journal of Photogrammetry and Remote Sensing*,” vol. 65, pp.2–16, 2010.

- [16] Inggit Sari et al., “Land Cover Classification using Object-Based Image Analysis of SPOT-6 Imagery for Land Cover and Forest Monitoring in Nagan Raya, Aceh – Indonesia, *International Journal on Advanced Science, Engineering and Information Technology*, vol.7(6), pp. 2139-2144, 2017.
- [17] Ruiliang Pu et al., “Object based urban detailed land cover classification with high spatial resolution IKONOS imagery,” *International Journal of Remote Sensing*, vol. 32(12), pp. 3285-3308, 2011.
- [18] Yu, Q., Gong, P., Clinton, N., Biging, G., Kelly, M. and Schirokauer, D., “Object-based detailed vegetation classification with airborne high spatial resolution remote sensing imagery,” *Photogrammetric Engineering and Remote Sensing*, vol. 72, pp. 799–811, 2006.
- [19] Hay, G.J. and Castilla, G., Geographic object-based image analysis (GEOBIA): a new name for a new discipline. In *Object-Based Image Analysis*, T. Blaschke, S. Lang and G. Hay (Eds.), pp. 75–90, New York: Springer, 2008.
- [20] Kux, H.J. and Arau´ Jo, E.H.G., Object-based image analysis using Quick-Bird satellite images and GIS data, case study Belo Horizonte (Brazil). In *Object-Based Image Analysis*, T. Blaschke, S. Lang and G. Hay (Eds.), pp. 571–588, 2008.
- [21] Ton, J.C., Sticklen, J. and Jain, A.K., “Knowledge-based segmentation of Landsat images,” *IEEE Transactions on Geoscience and Remote Sensing*, vol.29, pp. 222–232,1991.
- [22] Johnsson, K., “Segment-based land-use classification from SPOT satellite data,” *Photogrammetric Engineering and Remote Sensing*, vol. 60, pp. 47–53,1994.
- [23] Hill, R.A., “Image segmentation for humid tropical forest classification in Landsat TM Data,” *International Journal of Remote Sensing*, vol. 20, pp. 1039–1044,1999.
- [24] Herold, M., Liu, X.H. and Clarke, K.C., “Spatial metrics and image texture for mapping urban land-use,” *Photogrammetric Engineering and Remote Sensing*, vol. 69, pp. 991–1001,2003.
- [25] Carleer, A.P. and Wolff, E., “Region-based classification potential for land-cover classification with very high spatial resolution satellite data,” In *Proceedings of the 1st International Conference on Object-Based Image Analysis*, vol. 36, pp. 1682–1777, 2006.
- [26] Kong, C., Kai, X. and Wu, C., “Classification and extraction of urban land-use information from high-resolution image based on object multi-features,” *Journal of China University of Geosciences*, vol. 17, pp. 151–157, 2006.
- [27] Marchesi, A., Colombo, R. and Valentini, P., “Application of high spatial resolution satellite imagery for urban environment mapping, In *Proceedings of the 1st International Conference on Object-Based Image Analysis*,” vol. 36, pp. 1682–1777, 2006.
- [28] Mathieu, R., Aryal, J. and Chong, A.K., “Object-based classification of IKONOS imagery for mapping large-scale vegetation communities in urban areas,” *Sensors*, vol. 7, pp. 2860–2880, 2007.

- [29] Ren H, and Chang C I, "A Computer-Aided Detection and Classification Method for Concealed Targets in Hyperspectral Imagery," IEEE Remote Sensing Signal and Image Processing, 1998.
- [30] Know H and Nasrabasi N M, "Hyperspectral Target Detection using Kernel Spectral Matched Filter," Proceedings of IEEE Computer Society Conference on Computer Vision and Pattern Recognition Workshop, 2004.
- [31] Kruse FA, "Imaging Spectrometer Data Analysis-A Tutorial", Centre for the Study of Earth from Space (CSES) and Department of Geoscience, University of Colorado, Boulder, USA, 1994.
- [32] Manolakis D, Marden D and Shaw G A, Hyperspectral Image Processing for Automatic Target Detection Applications, Lincoln Laboratory Journal, vol. 14(1), 2003.
- [33] Yuehong Chen, Ya'nan Zhou, Yong Ge, Ru Anand Yu Chen, "Enhancing Land Cover Mapping through Integration of Pixel-Based and Object-Based Classifications from Remotely Sensed Imagery," Remote Sensing, vol. 10(77), 2018.
- [34] Lu, Dengsheng, Scott Hetrick, and Emilio Moran, "Land cover classification in a complex urban-rural landscape with QuickBird imagery," Photogrammetric Engineering & Remote Sensing, vol.76(10), pp. 1159-1168, 2010.
- [35] Zhang A., Tang P., "Fusion algorithm of pixel-based and object-based classifier for remote sensing image classification," IEEE International Geoscience and Remote Sensing Symposium, Melbourne, pp. 2740-2743, 2013.
- [36] Chan J.C.W., Bellens R., Canters F., Gautama S., "An assessment of geometric activity features for per-pixel classification of urban man-made objects using very high resolution satellite imagery," Photogrammetric Engineering & Remote Sensing, vol.75(4), pp. 397-411, 2009.
- [37] Pohl, C., Van Genderen, J.L., "Multi-sensor image fusion in remote sensing: Concepts methods and applications," International Journal of Remote Sensing, vol. 19(5), pp. 823-854, 1998.
- [38] Schmitt, M., and Zhu, X.X., "Data Fusion and Remote Sensing: An ever-growing relationship," IEEE Geoscience and Remote Sensing Magazine, vol. 4(4), pp. 6-23, 2016.
- [39] Loncan, L., Almeida, L.B., Bioucas-Dias, J.M., Liao, W., Briottet, X., Chanussot, J., Dobigeon, N., Fabre, S., Liao, W., Licciardi, G., Simoes, M., Tournet, J.-Y., Veganzones, M., Vivone, G., Wei, Q., and Yokoya, N., "Hyperspectral pansharpening: a review," IEEE Geoscience and Remote Sensing Magazine, vol. 3(3), pp. 27-46, 2015.
- [40] Fauvel, M., Benediktsson, J., Sveinsson, J., and Chanussot, J., "Spectral and spatial classification of hyperspectral data using SVMs and morphological profiles," Proc. IGARSS, pp. 4834-4837, 2007.
- [41] Wegner, J. D., Hänsch, R., Thiele, A., and Soergel, U., "Building detection from one orthophoto and high-resolution InSAR data using conditional random fields,"

- IEEE Journal of Selected Topics Applications Earth Observation and Remote Sensing, vol. 4, pp. 83-91, 2011.
- [42] Ban, Y., and Jacob, A., “Object-Based Fusion of Multitemporal Multiangle ENVISAT ASAR and HJ-1B Multispectral Data for Urban Land-Cover Mapping.,” IEEE Transactions on Geoscience and Remote Sensing, vol. 51(4), pp. 1998-2006, 2013.
- [43] Fauvel, M., Chanussot, J. and Benediktsson, J.A., “Decision fusion for the classification of urban remote sensing images,” IEEE Transactions on Geoscience and Remote Sensing, vol. 44(10), pp. 2828-2838, 2006.
- [44] Svatonova, Hana, “Analysis of Visual Interpretation of Satellite Data,” ISPRS - International Archives of the Photogrammetry, Remote Sensing and Spatial Information Sciences, pp. 675-681, 2016.
- [45] Campbell, J. B., Introduction to remote sensing. 4th ed., The Guilford Press, New York, 2007.
- [46] Lifeng He, Xiwei Ren, Qihang Gao, Xiao Zhao, Bin Yao, Yuyan Chao, “The connected-component labeling problem: A review of state-of-the-art algorithms,” Pattern Recognition, vol. 70, pp. 25–43, 2017.
- [47] Jahjah, Munzer, and Carlo Ulivieri, “Automatic archaeological feature extraction from satellite VHR images,” Acta Astronautica 66, vol. 9(10), pp. 1302-1310, 2010.
- [48] G.Meera Gandhi, S.Parthiban, Nagaraj Thummalu, A. Christy, “ NDVI: Vegetation change detection using remote sensing and GIS- A case study of vellore district,” Procedia Computer Science, vol. 57, pp. 1199-1210, 2015.
- [49] Xie Y, Zhao X, Li L, Wang H, “Calculating NDVI for LANDSAT 7-ETM data after atmospheric correction using 6s model: a case study in Zhangye City, China,” In proceeding IEEE Geo Informatics 18th international conference, pp. 1-4, 2010.
- [50] Hu Y, Ban Y, Zhang X, Liu J, Zhuang. D, “Spatial- temporal pattern of GIMMS NDVI and its dynamics in Mongolian Plateau,” In IEEE Proceeding on earth observation and remote sensing applications, pp.1-6., 2008.
- [51] Merwan Achibeta, Stefan Balevb, Antoine Dutotb, Damien Olivierb, “A Model of Road Network and Buildings Extension Co-Evolution Agent-based Modeling and Simulation of Cities,” Procedia Computer Science, vol. 32, pp. 828 – 833, 2014.
- [52] Shikhar Deep, Akansha Saklani, “Urban sprawl modeling using cellular automata,” The Egyptian Journal of Remote Sensing and Space Sciences, vol. 17, pp. 179–18, 2014.
- [53] Segl, Karl & Kaufmann, Hermann, “Detection of small objects from high-resolution panchromatic satellite imagery based on supervised image segmentation,” IEEE Transactions on Geoscience and Remote Sensing, vol. 39, pp. 2080 – 2083, 2001
- [54] Davis, L.S, “A survey of edge detection techniques,” Computer Graphical Image Processing, vol. 4, pp. 248–270, 1975.

- [55] Huang, D.S., Wunsch, D.C., Levine, D.S., Jo, K.H, “Advanced Intelligent Computing Theories and Applications,” In Proceedings of the Fourth International Conference on Intelligent Computing, Shanghai, China, 2008.
- [56] Manish H. Bharati, J.Jay Liu, John F. MacGregorb, “Image texture analysis: methods and comparison,” *Chemometrics and Intelligent Laboratory Systems*, vol. 72(1), pp. 57-71, 2004.
- [57] Xin Zhang, Jintian Cui, Weisheng Wang and Chao Lin, “A Study for Texture Feature Extraction of High-Resolution Satellite Images Based on a Direction Measure and Gray Level Co-Occurrence Matrix Fusion Algorithm,” *Sensors*, vol.17, 2017.
- [58] Haralick, Robert M., “Statistical and structural approaches to texture,” *Proceedings of the IEEE*, vol. 67(5), pp. 786-804, 1979.
- [59] Kiema, J.B.K., “Texture analysis and data fusion in the extraction of topographic objects from satellite imagery,” *International Journal of Remote Sensing*, vol. 23, pp. 767–776, 2002.
- [60] Myint, S.W., Lam, N.S.N. and Tylor, J.M., “Wavelets for urban spatial feature discrimination: comparisons with fractal, spatial autocorrelation, and spatial co-occurrence approaches,” *Photogrammetric Engineering & Remote Sensing*, vol. 70, pp. 803–812, 2004.
- [61] Shackelford, A.K. and Davis, C.H., “A combined fuzzy pixel-based and object-based approach for classification of high-resolution multispectral data over urban areas,” *IEEE Transactions on Geoscience and Remote Sensing*, vol. 41, pp. 2354–2363, 2003.
- [62] Chen, Yuanyuan, Quanfang Wang, Yanlong Wang, Si-Bo Duan, Miao Zhong Xu, and Zhao-Liang Li, “A Spectral Signature Shape-Based Algorithm for Landsat Image Classification,” *ISPRS International Journal of Geo-Information*, vol. 5(9), pp. 154, 2016.
- [63] Zhang, Liangpei, Xin Huang, Bo Huang, and Pingxiang Li, “A pixel shape index coupled with spectral information for classification of high spatial resolution remotely sensed imagery,” *IEEE Transactions on Geoscience and Remote Sensing*, vol.44(10), pp. 2950-2961, 2006.
- [64] Han, Youkyung, Hyejin Kim, Jaewan Choi, and Yongil Kim, “A shape–size index extraction for classification of high-resolution multispectral satellite images,” *International journal of remote sensing*, vol. 33(6), pp. 1682-1700, 2012.
- [65] Huang, X., Zhang, L. and Li, P., “Classification and Extraction of Spatial Features in Urban Areas Using High-Resolution Multispectral Imagery,” *IEEE Geoscience and Remote Sensing Letters*, vol. 4(2), pp. 260-264, 2007.
- [66] Hadiseh Hasani, Farhad Samadzadegan, “3D Object Classification Based on Thermal and Visible Imagery in Urban Area,” *The International Archives of the Photogrammetry, Remote Sensing and Spatial Information Sciences*, vol. XL-1/W5, 2015.
- [67] P. Soille, *Morphological Image Analysis—Principles and Applications*, 2nd ed. Berlin, Germany: Springer-Verlag, 2003.

- [68] J. Serra and P. Salembier, "Connected operators and pyramids," In Proceedings of SPIE Conference Non-Linear Algebra and Morphological Image Processing, vol. 2030, pp. 65–76, 1993.
- [69] J. Crespo, J. Serra, and R. Schafer, "Theoretical aspects of morphological filters by reconstruction," *Signal Processing*, vol. 47, pp. 201–225, 1995.
- [70] X. Huang and L. Zhang, "A multidirectional and multiscale morphological index for automatic building extraction from multispectral GeoEye-1 imagery," *Photogrammetric Engineering and Remote Sensing*, vol. 77(7), pp. 721–732, 2011.
- [71] Xin Huang and Liangpei Zhang, "Morphological Building/Shadow Index for Building Extraction from High-Resolution Imagery Over Urban Areas," *IEEE Journal of Selected Topics in Applied Earth Observations And Remote Sensing*, vol. 5(1), 2012.
- [72] Ma, Dan, Jun Liu, Junyi Huang, Huali Li, Ping Liu, Huijuan Chen, and Jing Qian, "Spectral similarity assessment based on a spectrum reflectance-absorption index and simplified curve patterns for hyperspectral remote sensing," *Sensors*, vol. 16(2), 2016.
- [73] Johnson, Brian, and Shahab Jozdani, "Identifying generalizable image segmentation parameters for urban land cover mapping through meta-analysis and regression tree modelling," *Remote Sensing*, vol.10(1), pp.73, 2018.
- [74] Aplin, P. and Atkinson, P.M., "Predicting missing field boundaries to increase per-field classification accuracy," *Photogrammetric Engineering and Remote Sensing*, vol. 70(1), pp. 141-149, 2004.
- [75] Keuchel, J., Naumann, S., Heiler, M. & Siegmund, A, "Automatic land cover analysis for Tenerife by supervised classification using remotely sensed data," *Remote Sensing of Environment*, vol. 86(4), pp. 530-541, 2003.
- [76] Jensen, J. *Introductory Digital Image Processing*, 3<sup>rd</sup> ed., 2005.
- [77] Vapnik, V. N., *The Nature of Statistical Learning Theory*, New York: Springer-Verlag, 1995.
- [78] Pal, Mahesh, "Multinomial logistic regression-based feature selection for hyperspectral data," *International Journal of Applied Earth Observation and Geoinformation*, vol. 14(1), pp. 214-220, 2012.
- [79] Knerr, S., Personnaz, L., and Dreyfus, G., *Single-layer learning revisited: A stepwise procedure for building and training neural network*. Neurocomputing: Algorithms, Architectures and Applications, NATO ASI, Berlin: Springer-Verlag, 1990.
- [80] Stergiou, C., and D. Siganos, *Introduction to neural networks*, Retrieved March 31 (1996):2004.
- [81] Richards, I A, and Jia, X, *Remote Sensing Digital Image Analysis - An Introduction*, 3<sup>rd</sup> Edition, Springer, 1996.
- [82] De Carvalho, O A and Meneses, P.R., "Spectral Correlation Mapper (SCM); An Improvement on the Spectral Angle Mapper (SAM)," 9th JPL Airborne Earth Science Workshop, JPL Publication, vol. 18, pp. 9, 2000.



- [83] Schwarz, I and Staenz, K, "Adaptive Threshold for Spectral Matching of Hyperspectral Data," *Canadian Journal of Remote Sensing*, vol. 27(3), pp. 216-224, 2001.
- [84] Hunter, El and Power, C H, "An Assessment of Two Classification Methods for Mapping Thames Estuary Intertidal Habitats Using CASI Data," *International Journal of Remote Sensing*, vol. 23(15), pp. 2989-3008, 2002.
- [85] Kruse F.A., Boardman J.W., Lefkoff A.B., Heidebrecht, K.B., Shapiro A.T., Barloon P.J., and Goetz A.F.H., "The Spectral Image Processing System (SIPS) - Interactive Visualization and Analysis of Imaging Spectrometer Data," *Remote Sensing of Environment*, vol. 44, pp. 145-163, 1993.
- [86] Chang, C.I., "An information theoretic-based approach to spectral variability, similarity and discriminability for hyperspectral image analysis," *IEEE Transaction on Information Theory*, vol. 46(5), pp. 1927–1932, 2000.
- [87] Cover and J. Thomas, *Elements of Information Theory*. New York:John Willey and Sons, 1991.
- [88] Kullback, S, *Information Theory and Statistics*. John Wiley & Sons, N.Y, 1959.
- [89] IEEE GRSS Data Fusion Contest, Presented to Image Analysis and Data Fusion Technical Committee, IEEE Geoscience and Remote Sensing Society (GRSS), 2014.
- [90] Space Applications Centre, Indian Research Organisation, Ahmedabad, Joint NASA-ISRO Campaign.
- [91] Varlyguin, Dmitry L., Robb Wright, Scott J. Goetz and Stephen D. Prince, "Advances in Land Cover Classification for Applications Research: A Case Study from The Mid-Atlantic, RESAC, 2001.
- [92] Schneider A., "Monitoring land cover change in urban and peri-urban areas using dense time stacks of Landsat satellite data and a data mining approach," *Remote Sensing of Environment*, vol. 124, pp. 689–704, 2012.
- [93] Li E., Du P., Samat A., Xia, J., Che M., "An automatic approach for urban land-cover classification from Landsat-8 OLI data," *International Journal of Remote Sensing*, vol.36, pp. 5983–6007, 2015.
- [94] Gong P., Howarth P.J., "The use of structural information for improving land-cover classification accuracies at the rural-urban fringe," *Photogrammetric Engineering of Remote Sensing*, vol. 56, pp. 67–73, 1990.
- [95] Herold M., Scepan J., Clarke K.C., "The use of remote sensing and landscape metrics to describe structures and changes in urban land uses," *Environment Planning*, vol. 34, pp. 1443–1458, 2002.
- [96] Voltersen M., Berger C., Hese S., Schmullius C., "Object-based land cover mapping and comprehensive feature calculation for an automated derivation of urban structure types at block level," *Remote Sensing of Environment*, vol. 154, pp. 192–201, 2014.

- [97] Agüera F., Aguilar F.J., Aguilar M.A., “Using texture analysis to improve per-pixel classification of very high-resolution images for mapping plastic greenhouses,” *ISPRS Journal of Photogrammetry Remote Sensing*, vol. 63, pp. 635–646, 2008.
- [98] Zhang, Ce, Xin Pan, Huapeng Li, Andy Gardiner, Isabel Sargent, Jonathon Hare, and Peter M. Atkinson, “A hybrid MLP-CNN classifier for very fine resolution remotely sensed image classification,” *ISPRS Journal of Photogrammetry and Remote Sensing*, vol.140, pp. 133-144, 2018.
- [99] Chaugule, Archana, and Suresh N. Mali, “Evaluation of texture and shape features for classification of four paddy varieties,” *Journal of Engineering*, 2014.
- [100] Pingel T.J., Clarke K.C., McBride W.A., “An improved simple morphological filter for the terrain classification of airborne LIDAR data,” *ISPRS Journal of Photogrammetry Engineering and Remote Sensing*, pp. 21–30, 2013.
- [101] Li M., Stein A., Bijker W., Zhan Q., “Urban land use extraction from very high resolution remote sensing images using a Bayesian network,” *ISPRS Journal of Photogrammetry Engineering and Remote Sensing*, vol.122, pp. 192–205, 2016.
- [102] Yichun Xie, Zongyao Sha, Mei Yu, “Remote sensing imagery in vegetation mapping: a review,” *Journal of Plant Ecology*, vol.1(1), pp. 9–23, 2008.
- [103] Walde I., Hese S., Berger C., Schmullius C., “From land cover-graphs to urban structure types,” *International Journal of Geographical Information Science*, vol. 28, pp. 584–609, 2014.
- [104] Tan Q., and Wang J., “Hyperspectral Versus Multispectral Satellite Data for Urban Land Cover and Land Use Mapping— Beijing, An Evolving City,” *ASPRS*, 2007.
- [105] C. Cilia, C. Panigada, M. Rossini, G. Candiani, M. Pepe, R.Colombo, “Mapping of asbestos cement roofs and their weathering status using hyperspectral aerial images,” *ISPRS International Journal of Geo-Information*, vol. 4, pp.928–941, 2015.
- [106] Justin George K, Vinay Kumar, Bhukya Tarun, Suresh Kumar, A Senthil Kumar, “Soil classification using airborne hyperspectral data employing various, ACRS, 2017.
- [107] Kupková, L, Červená, L, Suchá, R, Jakešová, L, Zagajewski, B, Březina, S & Albrechtová, J, “Classification of Tundra Vegetation in the Krkonoše Mts. National Park Using APEX, AISA Dual and Sentinel-2A Data,” *European Journal of Remote Sensing*, vol. 50(1), pp. 29–46, 2017 .
- [108] Raczko, E and Zagajewski, B, “Comparison of support vector machine, random forest and neural network classifiers for tree species classification on airborne hyperspectral APEX images,” *European Journal of Remote Sensing*, vol. 50(1), pp. 144–154, 2017.
- [109] Jung A., Kardevan P., and Tokei L., “Detection of urban effect on vegetation in a less built-up Hungarian city by hyperspectral remote sensing,” *Physics and Chemistry of the Earth*, vol. 30, pp. 255–259, 2005.
- [110] Alonzo M., Bookhagen B., and Roberts D.A., “Urban tree species mapping using hyperspectral and lidar data fusion,” *Remote Sensing of Environment*, vol. 148, pp. 70–83, 2014.



- [111] Ferreira M.P., Zortea M., Zanotta D.C., Shimabukuro Y.E., and de Souza Filho C.R., 2016, ‘Mapping tree species in tropical seasonal semi-deciduous forests with hyperspectral and multispectral data,’ *Remote Sensing of Environment*, vol. 179. pp. 66–78, 2016.
- [112] Dian Y., Pang Y., Dong Y., and Li Z., 2016, “Urban Tree Species Mapping Using Airborne LiDAR and Hyperspectral Data,” *Journal of the Indian Society of Remote Sensing*, vol. 44(4), pp. 595–603, 2016.
- [113] Liu L., Coops N.C., Aven N.W., and Pang Y., “Mapping urban tree species using integrated airborne hyperspectral and LiDAR remote sensing data,” *Remote Sensing of Environment*, vol. 200, pp. 170–182, 2017.
- [114] Huete A.R., Liu H., Batchily K., and Van Leeuwen, W., “A Comparison of Vegetation Indices Over a Global Set of TM Images for EOS-MODIS,” *Remote Sensing of Environment*, vol. 59(3), pp. 440–451, 1997.
- [115] Weiwei Ma, Cailan Gong, Yong Hu, Peng Meng, and Feifei Xu., “The Hughes phenomenon in hyperspectral classification based on the ground spectrum of grasslands in the region around Qinghai Lake,” *Proc. SPIE 8910, International Symposium on Photoelectronic Detection and Imaging, Imaging Spectrometer Technologies and Applications*, 2013.
- [116] Thenkabail P. S., Lyon J. G. and Huete A., “Hyperspectral Remote Sensing of Vegetation,” pp. 94-97, 2011.
- [117] Huang X., and Zhang L., “A multilevel decision fusion approach for urban mapping using very high-resolution multi/hyperspectral imagery,” *International Journal of Remote Sensing*, vol. 33(11), 2011.
- [118] Huang, X., Zhang, L., and Zhu, T., “Building change detection from multitemporal high resolution remotely sensed images based on a morphological building index,” *IEEE Journal of Selected Topics in Applied Earth Observations and Remote Sensing*, vol. 7(1), pp. 105–115, 2014.
- [119] Rodriguez-Galiano, V.F., et al., “Incorporating the downscaled Landsat TM thermal band in land-cover classification using random forest,” *Photogrammetric Engineering & Remote Sensing*, vol. 78 (2), pp. 129–137, 2012.
- [120] J Jinru Xue and Baofeng Su, “Significant Remote Sensing Vegetation Indices: A Review of Developments and Applications,” *Journal of Sensors*, 2017.
- [121] A.K. Mahlein, E.C. Oerke, U. Steiner, and H.W. Dehne, “Recent advances in sensing plant diseases for precision crop protection,” *European Journal of Plant Pathology*, vol. 133(1), pp. 197–209, 2012.
- [122] E.C. Oerke, A.K. Mahlein, and U. Steiner, “Proximal sensing of plant diseases,” in *Detection and Diagnostics of Plant Pathogens*, pp. 55–68, 2014.
- [123] A. Karnieli, N. Agam, R. T. Pinker et al., “Use of NDVI and land surface temperature for drought assessment: merits and limitations,” *Journal of Climate*, vol. 23(3), pp. 618–633, 2010.
- [124] R. P. Sripada, R. W. Heiniger, J. G. White, and R. Weisz, “Aerial color infrared photography for determining late-season nitrogen requirements in corn,” *Agronomy Journal*, vol. 97(5), pp. 1443–1451, 2005.

- [125] B. Zhang, D. Wu, L. Zhang, Q. Jiao, and Q. Li, "Application of hyperspectral remote sensing for environment monitoring in mining areas," *Environmental Earth Sciences*, vol. 65(3), pp. 649–658, 2012.
- [126] Farid Melgani, "Classification of Hyperspectral Remote Sensing Images with Support Vector Machines," *IEEE Transactions on Geoscience and Remote Sensing*, vol. 42(8), pp. 1778-1790, 2004.
- [127] Xin Huang, Liangpei Zhang, "An SVM Ensemble Approach Combining Spectral, Structural, and Semantic Features for the Classification of High-Resolution Remotely Sensed Imagery," *IEEE Transactions on Geoscience and Remote Sensing*, vol. 51(1), pp. 257-272, 2013.
- [128] Luo, Shezhou, Cheng Wang, Xiaohuan Xi, Hongcheng Zeng, Dong Li, Shaobo Xia, Pinghua Wang, "Fusion of Airborne Discrete-Return LiDAR and Hyperspectral Data for Land Cover Classification," *Remote Sensing*, vol. 8(1), pp. 3-12, 2015.
- [129] Li Miao, Zang Shuying et al., "Spatial and temporal variation of the urban impervious surface and its driving forces in the central city of Harbin," *Journal of Geography Science*, vol. 28, pp. 323–336, 2018.
- [130] Lei Ma, Yongxue Liu, "A review of supervised object-based land cover image classification," *ISPRS Journal of Photogrammetry and Remote Sensing*, vol. 130, 277-293, 2017.
- [131] Konštantín Rosina, Monika Kopecká, "Mapping of Urban Green Spaces Using Sentinel-2a Data: Methodical Aspects," *Proceedings, 6th International Conference on Cartography and GIS*, pp. 562-568, 2016.
- [132] Mustafa Neamah Jebur, Helmi Zulhaidi Mohd Shafri, Biswajeet Pradhan & Mahyat Shafapour Tehrani, "Per-pixel and object-oriented classification methods for mapping urban land cover extraction using SPOT 5 imagery," *Geocarto International*, vol. 29, pp.792-806, 2014.
- [133] Christopher Small, "Projecting the Urban Future: Contributions from Remote Sensing," *Spatial Demography*, vol. 4(1), pp. 17-37, 2016.
- [134] Lefei Zhang, Dacheng Tao, "On Combining Multiple Features for Hyperspectral Remote Sensing Image Classification," *IEEE Transactions on Geoscience and Remote Sensing*, vol. 50, pp. 879-893, 2012.
- [135] B. Khaleghi, A. Khamis et al., "Multi-sensor data fusion: A review of the state-of-the-art," *Information Fusion*, vol. 14, pp. 28–44, 2013.
- [136] Mookambiga, A. and V. Gomathi, "Comprehensive review on fusion techniques for spatial information enhancement in hyperspectral imagery," *Multidimensional System of Signal Processing*, vol. 27, pp. 863-889, 2016.
- [137] Federico Castanedo "A Review of Data Fusion Techniques," *The Scientific World Journal*, 2013.
- [138] L.O. Jimenez, A. Morales Morell et al., "Classification of hyper-dimensional data based on feature and decision fusion approaches using projection pursuit, majority voting, and neural networks," *IEEE Transaction on Geoscience Remote Sensing*, vol. 37, pp. 1360-1366, 1999.

- [139] Huang, X., and L. Zhang, "A multilevel decision fusion approach for urban mapping using very high-resolution multi/ hyperspectral imagery," *International Journal of Remote Sensing*, vol. 33, pp. 3354–3372, 2012.
- [140] Ghasem Abdi et al., "A decision-based multi-sensor classification system using thermal hyperspectral and visible data in urban area," *European Journal of Remote Sensing*, vol. 50(1), pp. 414-427, 2017.
- [141] González-Audicana M., Saleta J., Catalan R. & Garcia R., "Fusion of multispectral and panchromatic images using improved IHS and PCA mergers based on wavelet decomposition," *IEEE Transactions on Geoscience and Remote Sensing*, vol.42(6), pp.1291-1299, 2004.
- [142] D. Lu & Q. Weng , "A survey of image classification methods and techniques for improving classification Performance," *International Journal of Remote Sensing*, vol. 28, pp. 823-870, 2007.
- [143] Behnaz Bigdeli, Farhad Samadzadegan and Peter Reinartz, "A decision fusion method based on multiple support vector machine system for fusion of hyperspectral and LIDAR data," *International Journal of Image and Data Fusion*, vol. 5, pp. 196–209, 2014.
- [144] Linhai Jing, Qiuming Cheng, and Wenlei Wang, "A Fusion Method for Mixed Pixels Based on Classification of Panchromatic Image," *IEEE International Geoscience and Remote Sensing Symposium*, pp. 8-11, 2008.
- [145] Li J., Zhang H., Guo M., Zhang L., Shen H., & Du Q., "Urban classification by fusion of thermal infrared hyperspectral and visible data", *Photogrammetry Engineering and Remote Sensing*, vol. 81(12), pp. 901-911, 2015.
- [146] Giacinto G., Roli F., "Design of effective neural network ensembles for image classification," *Image Vision of Computing Journal*, vol. 19, pp. 697–705, 2001.
- [147] Yang, Bo, Zhong-liang Jing, and Hai-tao Zhao, "Review of pixel-level image fusion," *Journal of Shanghai Jiaotong University (Science)*, vol.15(1), pp. 6-12, 2010.
- [148] Tso B., Mather P.M., "Classification methods for remotely sensed data," London: Taylor and Francis, pp. 332, 2001.
- [149] Waske, B., and J. A. Benediktsson, J. A., "Fusion of Support Vector Machines for classification of multisensor data," *IEEE Transactions on Geosciences & Remote Sensing*, vol. 45(12), pp. 3858-3866, 2007.
- [150] Peddle D. R., and Ferguson D.T., "Optimization of multisource data analysis: an example using evidence reasoning for GIS data classification," *Computers & Geosciences*, vol. 28, pp. 45-52, 2002.
- [151] Li G., Lu D., Moran, E., Heteick S., "Land-cover classification in a moist tropical region of Brazil with Landsat TM imagery," *International Journal of Remote Sensing*, vol. 32, pp.8207-8230, 2011.
- [152] Pal M. and Mather P.M., "Support vector machines for classification in remote sensing," *International Journal of Remote Sensing*, vol. 26(5), pp. 1007–1011, 2005.

- [153] Dixon B., and Candade N., “Multispectral land-use classification using neural networks and support vector machines: one or the other, or both,” *International Journal of Remote Sensing*, vol. 29(4), pp. 1185–1206, 2008.
- [154] Waske B. & Braun M., “Classifier ensembles for land cover mapping with multispectral SAR imagery,” *International Journal of Photogrammetry and Remote Sensing*, vol. 64(5), pp. 450-457, 2009.
- [155] Berberoglu S., Lloyd C. D., and Atkinson P. M., Curran P. J., “The integration of spectral and textural information using neural networks for land cover mapping in the Mediterranean,” *Computer & Geosciences*, vol. 26, pp.385-396, 2000.
- [156] Foody G.M., “Status of land cover classification accuracy assessment,” *Remote Sensing of Environment*, vol. 80, pp. 185–201, 2002.
- [157] Kavzoglu T., and Mather, P. M., “The use of backpropagating artificial neural network in land cover classification,” *International journal of Remote sensing*, vol. 24(23), pp. 4907-4938, 2003.
- [158] Kavzoglu T., “Increasing the accuracy of neural network classification using refined training data,” *Environmental Modelling & Software*, vol. 24 (7), pp. 850-858, 2009.
- [159] Xiaoqing Luo, Zhancheng Zhang, Xiaojun Wu, “A novel algorithm of remote sensing image fusion based on shift-invariant Shearlet transform and regional selection,” *AEU- International Journal of Electronics and Communication*, vol. 70(2), pp. 186-197, 2016.
- [160] Berger, Christian, Frank Riedel, Johannes Rosentreter, Enrico Stein, SörenHese, and Christiane Schmallius, “Fusion of Airborne Hyperspectral and LiDAR Remote Sensing Data to Study the Thermal Characteristics of Urban Environments,” *Computational Approaches for Urban Environments*, pp. 273-292, 2015.
- [161] Jiayi Ma, Yong Ma, Chang Li, “Infrared and Visible Image Fusion Methods and Applications: A survey,” *Information Fusion*, vol. 45, pp. 153-178, 2018.
- [162] Eslami M., & Mohammadzadeh A., “Developing a spectral-based strategy for urban object detection from airborne hyperspectral TIR and visible data,” *IEEE Journal of Selected Topics in Applied Earth Observations and Remote Sensing*, vol. 9(5), pp. 1808–1816, 2015.
- [163] Rashinkar, Pratiksha, and V. S. Krushnasamy, “An overview of data fusion techniques,” *International Conference on Innovative Mechanisms for Industry Applications (ICIMIA)*, pp. 694-697, 2017.
- [164] Liao, W., Huang, X., Van Coillie, F., Gautama, S., Pizurica, A., Philips, W., ... Tuia, D., “Processing of multiresolution thermal hyperspectral and digital color data,” *Outcome of the 2014 IEEE GRSS data fusion contest, IEEE Journal of Selected Topics in Applied Earth Observations and Remote Sensing*, vol.8(6), pp. 2984–2996, 2015.

- [165] Libin Zhou and Xiaojun Yang, "Training algorithm performance for image classification by neural networks," *Photogrammetric Engineering & Remote Sensing*, vol.76(8), pp. 945-951, 2010.
- [166] Li N., Liu F., Chen Z., "A texture measure defined over intuitionistic fuzzy set theory for the detection of built-up areas in high-resolution SAR images," *IEEE Journal of Selected Topics in Applied Earth Observations and Remote Sensing*, vol. 7(10), pp. 4255–4265, 2014.
- [167] Bhaskaran S. and Datt B., "Applications of hyperspectral remote sensing in urban regions," ACRS, 2000.
- [168] Segl K., Heiden U., Mueller M. and Kaufmann H., "Endmember detection in urban environments using hyperspectral HyMap data," *Third EARSeL Workshop on Imaging Spectroscopy*, Herrschin, 2003.
- [169] C. Chisense, "Classification of Roof Materials Using Hyperspectral Data," *International Archives of the Photogrammetry, Remote Sensing and Spatial Information Sciences*, vol. XXXIX-B7, ISPRS, 2012.
- [170] Crippen R.E., "Selection of Landsat TM band and band-ratio combination to maximize lithological information in color composite displays," *Proceedings of the 7th Thematic Conference on Remote Sensing and Exploration Geology*, pp.917-921, 1989.
- [171] Keshava N., Mustard J.F., "Spectral unmixing," *IEEE Signal Proceedings for Exploit Hyperspectral Imaging*, vol. 19: pp. 44–57,2002.
- [172] David G.G., Andrew D., Niemann K.O., et al, "Processing HY- PERION and ALI for forest classification," *IEEE Transaction of Geoscience and Remote Sensing*, vol. 41(6), pp. 1321–1331, 2003.
- [173] Crosta, A. and J.M. Moore, "Enhancement of Landsat Thematic Mapper imagery for residual soil mapping in SW Minas Gerais State, Brazil: a prospecting case history in Greenstone belt terrain," *Proceedings of the 7th ERIM Thematic Conference: Remote sensing for exploration geology*, pp. 1173-1187, 1989.
- [174] Green A.A., Berman M., Switzer P., Graig M.D., "A Transformation for ordering Multispectral data in terms of quality with implications for noise removal," *IEEE Transaction of Geoscience and Remote Sensing*, vol. 26, pp. 65-74, 2012.
- [175] Liu X, Zhang B, Gao L R, et al., "A maximum noise fraction transform with improved noise estimation for hyperspectral images," *Sci China Ser F-Inf Sci*, vol. 52(9), pp. 1578–1587, 2009.
- [176] Xu H., "Modification of Normalised Difference Water Index (NDWI) to Enhance Open Water Features in Remotely Sensed Imagery," *International Journal of Remote Sensing*, vol. 27(14), pp. 3025-3033, 2006.
- [177] Gao B.C., "NDWI—a normalized difference water index for remote sensing of vegetation liquid water from space," *Remote Sensing of Environment*, vol. 58, pp. 257–266, 1996.
- [178] Wilson, E.H. and Sader, S.A., "Detection of forest harvest type using multiple dates of Landsat TM imagery," *Remote Sensing of Environment*, 80, pp. 385–396, 2002.

- [179] Hall D.K., Foster J.L., Chien J.L., & Riggs G.A., "Determination of actual snow-covered area using Landsat TM and digital elevation model data in Glacier National Park, Montana," *Polar Record*, vol. 31(177), pp.191-198, 1995.
- [180] McFeeters S., "The use of Normalized Difference Water Index (NDWI) in the Delineation of Open Water Features," *International Journal of Remote Sensing*, vol. 17, pp. 1425-1432, 1996.
- [181] Bernstein L.S., X. Jin, B. Gregor, and S. Adler-Golden, "Quick Atmospheric Correction Code: Algorithm Description and Recent Upgrades," *Optical Engineering*, vol. 51(11), 2012.
- [182] Hall D., G. Riggs, and V. Salomonson, "Development of Methods for Mapping Global Snow Cover Using Moderate Resolution Imaging Spectroradiometer Data," *Remote Sensing of Environment*, vol. 54(2), pp. 127-140, 1995.
- [183] Salomonson, V., and I. Appel, "Estimating Fractional Snow Cover from MODIS Using the Normalized Difference Snow Index," *Remote Sensing of Environment*, vol. 89, pp. 351-360, 2004.
- [184] Curran P.J., *Principles of Remote Sensing*. London: Longman, pp. 21-23, 1985.
- [185] Khasanah A.N. and Danoedoro P., "Mapping Clay Fraction Using Hyperion Imagery in Relation to Different Kind of Parents Material in D.I.Yogyakarta," *Asian Conference on Remote Sensing*, 2013.
- [186] Jensen, J.R., *Remote sensing of the environment: An Earth resource perspective*. Prentice Hall, Upper Saddle River, N.J, 2007.
- [187] M.M.Waqar, J.F.Mirza, R.Mumtazard, E. Hussain, "Development of new indices for Extraction of Built-Up Area and Bare Soil on Landsat Data," *Open Access Scientific Reports*, 2012.
- [188] Segal D., "Theoretical Basis for Differentiation of Ferric-Iron Bearing Minerals, Using Landsat MSS Data," *Proceedings of Symposium for Remote Sensing of Environment, 2nd Thematic Conference on Remote Sensing for Exploratory Geology*, Fort Worth, pp. 949-951, 1982.
- [189] Drury S., *Image Interpretation in Geology*. London: Allen and Unwin, pp. 243, 1987.
- [190] Shabou, Marouen, Bernard Mougnot, Zohra Chabaane, Christian Walter, Gilles Boulet, Nadhira Aissa, and Mehrez Zribi, "Soil clay content mapping using a time series of Landsat TM data in semi-arid lands," *Remote sensing*, vol. 7(5), pp. 6059-6078, 2015.
- [191] Rouse J., R. Haas, J. Schell, and D. Deering, "Monitoring Vegetation Systems in the Great Plains with ERTS," *Third ERTS Symposium, NASA*, pp. 309-317, 1973.
- [192] Crippen R., "Calculating the Vegetation Index Faster," *Remote Sensing of Environment*, vol. 34, pp. 71-73, 1990.
- [193] Roujean, J., and F. Breon, "Estimating PAR Absorbed by Vegetation from Bidirectional Reflectance Measurements," *Remote Sensing of Environment*, vol. 51, pp. 375-384, 1995.



- [194] Sripada R., et al., "Aerial Color Infrared Photography for Determining Early In-season Nitrogen Requirements in Corn," *Agronomy Journal*, vol. 98, pp. 968-977, 2006.
- [195] Huete A., "A Soil-Adjusted Vegetation Index (SAVI)," *Remote Sensing of Environment*, vol. 25, pp. 295-309, 1988.
- [196] Rondeaux G., M. Steven, and F. Baret, "Optimization of Soil-Adjusted Vegetation Indices," *Remote Sensing of Environment*, vol. 55, pp. 95-107, 1996.
- [197] Yang Z., P. Willis, and R. Mueller, "Impact of Band-Ratio Enhanced AWIFS Image to Crop Classification Accuracy," *Proceedings of the Pecora 17 Remote Sensing Symposium*, 2008.
- [198] Wolf A., "Using World View-2 Vis-NIR MSI Imagery to Support Land Mapping and Feature Extraction Using Normalized Difference Index Ratios," Unpublished report, Longmont, CO: Digital Globe, 2010.
- [199] Zha Y., J. Gao, and S. Ni., "Use of Normalized Difference Built-Up Index in Automatically Mapping Urban Areas from TM Imagery," *International Journal of Remote Sensing*, vol. 24(3), pp. 583-594, 2003.
- [200] Bouzekri S., Lasbet A.A., Lachehab A., "A New Spectral Index for Extraction of Built-Up Area Using Landsat-8 Data," *Journal of Indian Society Remote Sensing*, vol. 43(4), pp. 867-873, 2015.
- [201] Hongmei Zhao, Xiaoling Chen, "Use of normalized difference bareness index in quickly mapping bare areas from TM/ETM+," *Proceedings of IEEE International Geoscience and Remote Sensing Symposium*, pp. 1666-1668, 2005.
- [202] Xu H., "Analysis of impervious surface and its impact on urban heat environment using the normalized difference impervious surface index (NDISI)," *Photogrammetry Engineering and Remote Sensing*, vol.76, pp. 557-565, 2010.
- [203] Samsudin, Sarah Hanim & Shafri, Helmi & Hamedianfar, Alireza, "Development of spectral indices for roofing material condition status detection using field spectroscopy and WorldView-3 data. *Journal of Applied Remote Sensing*," vol.10(2), 2016.
- [204] Weng, Q., "Remote sensing of impervious surfaces in the urban areas: requirements, methods, and trends," *Remote Sensing of Environment*, vol. 117, pp. 34- 49, 2012.
- [205] M. Usman, R. Liedl, M.A. Shahid, A. Abbas, "Land use/land cover classification and its change detection using multi-temporal MODIS NDVI data," *Journal of Geographical Science*, vol. 25(12), pp. 1479-1506, 2015.
- [206] Wei, Chunzhu, Thomas Blaschke, Pavlos Kazakopoulos, Hannes Taubenböck, and Dirk Tiede, "Is spatial resolution critical in urbanization velocity analysis? Investigations in the Pearl River Delta," *Remote Sensing*, vol. 9(1), pp. 80, 2017.
- [207] Bumairiyemu Maimaiti, Jianli Ding, Zibibula Simayi, Alimujiang Kasimu, "Characterizing Urban Expansion of Korla City and its spatial-temporal patterns using remote sensing and GIS methods," *Journal of Arid Land*, vol. 9(3), pp. 458-470, 2017.

- [208] Li Miao, Zang Shuying et al., “Spatial and temporal variation of the urban impervious surface and its driving forces in the central city of Harbin”, *Journal of Geographical Sciences*, vol. 28(3), pp. 323–336, 2018.
- [209] Luca Demarchi et al., “Assessing the performance of two unsupervised dimensionality reduction techniques on hyperspectral APEX data for high resolution urban land-cover mapping,” *ISPRS Journal of Photogrammetry and Remote Sensing* 87, 166–179, 2014.
- [210] Im J., Lu Z., Rhee J., Quackenbush L.J., “Impervious surface quantification using a synthesis of artificial immune networks and decision/regression trees from multi-sensor data,” *Remote Sensing of Environment*, vol. 117, pp. 102–113, 2012.
- [211] Ouma Y.O., Tetuko, J. And Tateishi, R. (2008), “Analysis of co-occurrence and discrete wavelet transform textures for differentiation of forest and non-forest vegetation in very-high resolution optical-sensor imagery,” *International Journal of Remote Sensing*, 29, 3417–3456, 2008.
- [212] Zhang Y., “Optimisation of building detection in satellite images by combining multispectral classification and texture filtering,” *ISPRS Journal of Photogrammetric and Remote Sensing*, vol. 54, pp. 50–60, 2009.
- [213] Sebastian van der Linden, Andreas Janz, B.Waske, et al., “Classifying segmented hyperspectral data from a heterogeneous urban environment using support vector machines,” *Journal of Applied Remote Sensing*, vol. 1(1), 2007.
- [214] Y. Dong, B.C. Forster, and A.K. Milne, “Segmentation of radar imagery using Gaussian Markov random field model,” *International Journal of Remote Sensing*, 20(8), 1617-1639, 2009.
- [215] S.W. Myint, N.S.N. Lam, and J.M. Taylor, “Wavelets for urban spatial feature discrimination: Comparisons with fractal, spatial autocorrelation, and spatial co-occurrence approaches,” *Photogrammetry Engineering of Remote Sensing*, vol. 70(7), pp. 803-812, 2004.
- [216] J.A. Benediktsson, M. Pesaresi, and K. Arnason, “Classification and feature extraction for remote sensing images from urban areas based on morphological transformations,” *IEEE Transaction on Geoscience and Remote Sensing*, vol. 41(9), pp. 1940-1949, 2003.
- [217] Shackelford, A.K. and Davis, C.H., “A combined fuzzy pixel-based and object-based approach for classification of high-resolution multispectral data over urban areas,” *IEEE Transactions on Geoscience and Remote Sensing*, vol. 41, pp. 2354–2363, 2003.
- [218] S. Nithya, S. Ramakrishnan, “Local line directional neighbourhood pattern for texture classification,” *EURASIP Journal on Image and Video Processing*, 2018.
- [219] Zhi Yong Lv et al., “Morphological Profiles Based on Differently Shaped Structuring Elements for Classification of Images with Very High Spatial Resolution,” *IEEE Journal of Selected Topics in Applied Earth Observations and Remote Sensing*, vol. 7(12), pp. 4644-4652, 2014.



- [220] Wenzhong Shi, Zelang Miao, Qunming Wang, & Hua Zhang, "Spectral–Spatial Classification and Shape Features for Urban Road Centerline Extraction," *IEEE Geoscience and Remote Sensing Letters*, vol. 11(4), pp. 788–792, 2014.

## ***Web References***

1. <https://gisgeography.com/obia-object-based-image-analysis-geobia>
2. [https://en.wikipedia.org/wiki/Remote\\_sensing](https://en.wikipedia.org/wiki/Remote_sensing)
3. [https://ars.els-cdn.com/content/image/1-s2.0-S0031320317301693-gr1\\_lrg.jpg](https://ars.els-cdn.com/content/image/1-s2.0-S0031320317301693-gr1_lrg.jpg)
4. <https://www.e-education.psu.edu/geog480/node/493>
5. <http://www.seos-project.eu/modules/remotesensing/remotesensing-c01-p05.html>
6. [https://shodhganga.inflibnet.ac.in/bitstream/10603/24460/10/10\\_chapter5.pdf](https://shodhganga.inflibnet.ac.in/bitstream/10603/24460/10/10_chapter5.pdf)
7. [https://www.brainkart.com/article/Spectral-Signature-Concepts-Typical-Spectral-Reflectance-Charactristics-Of-Water,-Vegetation-And-Soil\\_4470/](https://www.brainkart.com/article/Spectral-Signature-Concepts-Typical-Spectral-Reflectance-Charactristics-Of-Water,-Vegetation-And-Soil_4470/)
8. <https://medium.com/data-science-group-iitr/support-vector-machines-svm-unraveled-e0e7e3ccd49b>
9. [https://www.sig.ac.in/assets/student\\_proect\\_pdf/MarciaChenThesis.pdf](https://www.sig.ac.in/assets/student_proect_pdf/MarciaChenThesis.pdf)
10. <https://aviris-ng.jpl.nasa.gov/aviris-ng.html>
11. <https://www.e-education.psu.edu/geog480/node/523>
12. <https://eos.com/panchromatic/>
13. <https://gisgeography.com/multispectral-vs-hyperspectral-imager>
14. <https://www.geoimage.com.au/satellite/TerraSar>

## Appendix-I

### *MBI Numeric Values of Soil (Listed Training Samples-113X20)*

#### *(Actual Training Feature Size of Soil-625X84)*

	1	2	3	4	5	6	7	8	9	10	11	12	13	14	15	16	17	18	19	20
1	0.142039	1.199632	1.099732	0.703518	1.6042	0.298789	2.672115	1.512066	0.728156	0.076191	0.528389	2.118081	0.304812	0.442515	1.053013	0.113587	0.363107	2.96975	1.13741	3.038843
2	0.155129	1.514435	1.002815	0.939092	1.250731	1.305888	1.238549	1.296382	9.369744	0.111901	0.520491	2.479414	0.268141	0.965783	2.460119	0.280317	0.563528	0.995482	2.13494	5.051048
3	0.467468	2.011394	1.390618	0.988794	1.014057	1.236174	2.89475	2.390127	16.80333	0.251431	0.333307	2.302791	0.535498	0.574791	1.270442	0.86953	0.715601	4.002158	1.70703	4.426598
4	0.797789	4.084522	1.137954	0.108523	0.740658	1.040649	2.714588	3.330541	12.16976	0.321921	0.535729	2.520497	0.517886	1.260886	0.558436	0.695978	0.421377	4.528564	-0.12349	1.273588
5	0.470067	3.450183	0.818031	4.81986	0.58437	1.378943	0.244214	2.843158	0.974944	0.305543	1.817261	2.534069	0.146972	3.532732	0.583026	0.577445	0.12151	1.430124	2.476612	1.480977
6	0.396003	2.345891	0.828658	6.938542	0.133021	4.437651	0.409834	1.196179	0.841193	0.062182	1.91527	2.599552	0.345458	0.806195	0.780308	0.528099	0.144447	0.927959	5.06678	1.207738
7	0.451779	2.391439	1.224296	7.829191	2.568639	3.303058	3.829098	1.835772	0.890345	0.089426	1.343654	2.596476	0.352769	1.301813	0.625436	0.569517	0.129423	0.955971	1.721409	1.7561
8	0.499658	1.21776	1.453092	7.664247	0.552902	0.833058	3.088291	1.507343	0.862562	0.075383	0.832639	2.489578	0.359067	1.492422	0.690389	0.498864	0.220795	1.361918	0.751657	3.397852
9	0.370707	2.072657	1.710757	7.217169	1.051455	0.516194	3.864169	3.095243	1.068542	0.127567	4.200309	2.346628	1.206514	4.709114	0.362055	0.577623	1.038834	1.305643	0.75948	5.741342
10	0.19308	2.93674	1.351622	6.784763	1.409018	0.455285	1.759458	1.926098	0.94295	0.028973	6.163346	2.566362	1.23776	4.298673	0.506996	2.846526	1.67776	2.209982	0.617261	4.851414
11	0.301257	2.830536	0.949442	6.644084	1.86585	0.612719	1.340398	2.752442	0.551922	0.037495	3.084688	3.179402	0.671202	6.409954	0.33372	0.962289	1.417051	3.953617	0.302747	2.527725
12	0.179495	0.434523	0.358375	4.193728	2.356696	0.505758	0.100965	2.78766	0.682272	0.060543	0.914524	3.330987	0.469719	6.626056	0.259976	1.820886	1.214516	0.093748	0.084766	2.778305
13	0.214567	0.087316	0.172129	4.747618	3.922335	0.347496	1.346567	0.988116	0.73386	-0.02607	0.196329	3.065197	0.087488	4.704039	0.513978	5.579993	0.52582	1.878153	0.237438	2.288677
14	0.665215	0.27039	0.533023	7.620458	1.089102	1.030898	2.32724	1.086434	0.743585	0.685429	0.507593	1.003375	0.012548	7.792699	0.629251	0.695797	0.359205	3.32701	0.373945	4.458864
15	1.598935	0.28485	0.765796	7.105921	1.270244	2.596124	3.086583	3.136733	1.307807	1.595968	0.190803	0.192376	2.806514	3.375682	0.779179	0.100696	0.756856	2.334111	0.570066	3.985926
16	1.398075	6.468476	0.905454	7.570924	0.984697	2.201689	2.289587	3.562148	0.929621	3.14987	0.635774	0.316201	4.984263	6.776897	1.109162	0.17847	0.83504	2.627178	0.574656	4.551939
17	2.051841	8.68875	1.022336	7.86262	0.95864	0.575362	2.019318	1.810921	-0.02654	2.783208	0.916159	0.395173	5.734292	2.371664	1.327133	0.201541	1.617059	1.683703	2.078117	4.762996
18	3.612843	8.431869	0.821623	5.1505	0.702568	0.81165	0.366482	3.774303	0.121513	1.799465	1.032458	0.195183	6.149355	1.437914	1.054642	0.265061	2.022346	1.941903	1.764956	3.106509
19	4.434456	10.34393	0.959224	6.792462	0.041124	3.202615	1.129599	2.416134	0.862598	1.614957	1.415173	0.398702	4.816307	2.392988	0.290934	4.611359	1.939434	2.59455	1.343908	2.405552
20	4.725275	10.39374	1.398129	9.76641	0.121536	4.031847	1.645766	1.004788	0.520249	1.49852	1.482378	0.638619	3.275966	1.745509	0.138665	2.726791	1.59568	1.953146	1.48102	1.851866
21	4.545743	11.33228	0.741426	10.23053	0.259933	3.228134	0.902293	2.411038	0.520317	3.552574	1.950306	0.616329	3.017108	1.906014	0.289149	1.012384	1.360018	3.447199	1.111721	1.777692
22	5.112381	3.366874	0.380825	2.505705	1.625252	2.578814	1.965341	3.402135	1.924869	5.651998	2.395273	0.507762	2.919795	3.37929	0.151309	1.064387	1.83525	2.661453	4.229614	1.795566
23	5.354493	7.417503	3.385903	0.732976	2.008413	2.277074	4.282161	1.257574	0.632919	5.621148	2.520577	0.847176	4.393644	15.19884	0.534466	0.794958	1.129363	1.885416	0.87934	1.889273

24	3.226097	9.554976	3.630186	1.709914	3.065832	0.989237	2.142447	0.648334	1.990384	4.76752	2.118496	2.186748	3.563965	9.833867	0.583713	1.477551	0.194907	0.738727	0.026219	1.904765
25	1.219017	10.36297	2.270046	2.075851	3.063527	0.439235	1.008975	0.206289	1.926779	3.363448	1.762811	2.518472	0.050065	-0.0022	1.883837	2.686434	0.545678	0.481077	1.052913	2.062117
26	0.130767	1.563911	1.103353	0.80556	1.429512	2.308583	0.907137	0.808126	5.157297	0.035498	0.458101	2.771128	0.306305	1.439629	0.638144	0.168917	0.486525	4.445238	0.585802	4.185029
27	0.185453	2.779277	1.03	0.914478	1.116325	0.66858	1.412226	2.744682	16.38639	0.112455	0.506807	2.515024	0.276344	0.732712	1.780901	1.049273	0.663808	1.30304	2.273585	4.078686
28	0.415868	4.569311	1.153844	0.595227	0.85043	0.464912	2.591792	3.702759	16.66171	0.169491	0.233269	2.814911	0.616851	0.793395	1.414921	1.088615	0.766977	1.802432	2.222837	4.226284
29	0.623025	3.014813	1.303119	-0.07784	0.564698	0.816913	2.112041	2.945832	16.79283	0.355394	1.44902	2.592726	0.604554	1.379086	0.506594	0.694673	0.456805	2.905354	0.185403	2.805203
30	0.762517	0.945223	1.178915	3.511795	0.256422	0.671195	0.706764	2.791463	6.274151	0.324854	1.833631	2.249596	0.027922	3.95635	0.813644	0.623894	0.188695	0.692017	3.201671	2.128236
31	0.749855	1.601161	0.764016	5.54275	0.24785	1.480738	0.385291	1.826348	0.363675	0.057761	0.897971	2.945858	0.451012	2.47579	0.605224	0.660199	0.34817	2.336953	3.119162	2.179327
32	0.660976	2.104497	1.104364	8.471511	0.673358	4.441643	5.583338	2.231008	1.052631	0.046243	0.299434	3.372025	0.714862	3.108081	0.445507	0.633344	0.510161	1.856827	1.640039	2.789426
33	0.374579	1.34266	1.438677	9.478434	0.307214	2.468382	4.71398	0.479644	0.985955	0.077251	0.907738	2.9364	1.017243	6.10403	0.253475	0.556841	0.554947	2.45747	1.249418	9.445736
34	0.321838	2.035298	1.825278	7.571927	0.554793	1.903616	2.424283	0.03145	0.748248	0.128927	2.657898	2.802822	1.249189	6.194055	0.148491	0.315884	0.962282	3.811689	1.692251	13.98971
35	0.316879	3.176191	1.607985	7.333685	0.358383	2.311449	2.25411	1.137053	0.307076	0.126467	4.797487	2.867763	0.848093	2.337787	0.374588	1.08484	1.561446	3.066466	2.595877	5.033082
36	0.411026	2.604415	0.908732	8.950629	1.199619	2.112772	1.759105	3.207791	0.446997	0.037639	4.079727	3.425231	0.234372	5.222627	0.57744	1.099269	1.142695	3.15501	1.964945	1.167488
37	0.335705	1.59743	0.414956	5.219274	1.785374	1.809292	0.302288	1.686249	0.839052	-0.04979	1.586991	3.306994	0.036432	7.459516	0.394924	-0.13351	0.669085	3.587493	0.916543	1.831269
38	0.807193	0.081575	0.700714	5.068755	4.503278	1.213297	0.502282	0.896279	0.948544	1.205132	0.422502	0.753308	0.326164	6.733751	0.191855	3.582655	0.322705	4.702238	0.392652	3.936975
39	1.235064	0.084533	0.869409	7.031838	2.312695	1.050442	2.02252	1.751344	0.882049	3.936639	0.289062	0.087523	2.608282	7.530543	0.476767	4.314463	0.151435	2.896048	0.288059	3.709139
40	1.434581	1.25455	1.041236	6.84436	0.986157	1.111265	1.644461	2.261058	0.97713	2.988794	1.145091	0.468982	5.574592	5.27325	1.037272	0.179277	0.551149	1.971321	0.439451	3.741771
41	1.683047	7.151908	1.269476	6.708673	1.173028	1.900371	2.335246	3.901934	1.23143	2.025237	1.653028	0.221985	6.603985	9.841606	1.303571	0.142535	1.002455	1.452364	0.664936	5.11679
42	1.782915	8.323065	1.619857	7.265503	0.711938	1.869197	1.873612	1.874088	0.04001	2.153726	1.464386	0.319347	6.710501	3.670644	1.631087	-0.10078	1.732766	1.047636	1.71018	4.299112
43	2.496077	10.03286	1.80612	6.228244	0.074022	2.168001	1.887045	2.993513	0.06747	1.613385	1.365448	0.471459	6.618087	1.306745	1.069559	1.951991	2.424397	1.294719	2.009776	2.820634
44	4.206038	10.15918	1.011808	6.665041	0.136193	3.106677	2.207985	2.752219	0.867906	2.035515	1.571509	0.575838	5.323961	0.693545	0.319929	4.052333	2.272911	1.949228	2.479668	3.66202
45	4.626525	8.800247	1.324321	8.378474	-0.18923	1.969123	1.902469	1.553733	0.720543	2.145373	1.327479	0.619822	4.462202	1.83975	0.078894	4.166862	1.891213	1.965583	2.635429	3.020987
46	4.879693	6.039871	0.599134	10.5154	1.01661	1.394481	3.1409	2.052072	0.2008	1.520533	0.839277	0.755831	3.834456	1.442292	0.221575	2.534199	1.413084	2.587811	1.975009	2.047407
47	6.238586	0.769637	0.267193	3.657869	5.194125	0.975489	4.44487	0.685807	1.696132	2.17969	2.249296	1.712653	3.044763	4.951369	0.72648	0.901946	1.818594	3.347028	7.153346	2.008869
48	5.987497	2.78771	2.770305	0.949767	2.374754	1.334979	1.867055	0.27683	0.801835	4.811112	3.344754	2.408445	3.552897	19.26119	1.714655	1.401828	1.100224	2.101355	7.917919	1.244858
49	5.419528	10.65391	4.019615	1.820774	3.078025	0.48797	0.958139	0.763537	0.928034	4.734222	2.465335	2.9185	3.592987	13.43189	1.303731	1.094707	0.316603	0.762919	-0.27996	0.818659
50	3.479522	10.55801	3.167706	1.698166	2.986173	0.160975	0.867446	0.848006	2.383006	3.273818	1.925891	3.308106	0.310327	1.76327	1.105453	2.685309	0.505035	0.632695	0.226848	1.045767
51	0.160922	3.919621	0.831344	0.815952	1.569598	3.672375	1.432987	5.496749	9.208875	0.168067	0.56589	2.463467	0.343852	0.705772	0.485467	0.893823	0.63025	3.758013	2.109366	5.653059
52	0.140341	4.017331	0.738867	0.791652	0.962015	1.277282	1.062629	5.481504	17.62853	0.178716	0.369207	2.731631	0.228869	3.447531	1.143483	1.164226	0.705836	2.369763	4.030693	2.885044
53	0.578587	2.409934	0.955262	0.42599	0.879383	0.159007	2.095033	3.741143	16.65968	0.118502	0.880324	2.683888	0.502988	3.46999	1.197962	0.854123	0.593136	1.206355	1.988974	1.982961

54	0.569112	1.492312	1.338726	0.33091	0.290634	0.658664	1.990114	2.116509	17.03677	0.213304	1.723027	2.696859	0.679995	0.680754	0.813247	0.663167	0.527158	2.847996	0.057061	2.206846
55	0.478804	2.207057	1.428082	2.182978	0.281738	0.938158	0.917536	1.456701	10.633	0.194468	1.309668	2.429594	0.375322	2.525215	0.701691	0.595442	0.376622	1.493062	2.331401	1.831191
56	0.437381	1.689553	1.186865	4.612634	0.403686	0.684214	1.77883	2.197033	-0.01362	0.032251	0.158074	2.868001	0.743297	4.18835	0.478996	0.483565	0.265501	3.660711	1.797367	2.752349
57	0.422431	2.058933	0.932547	8.948805	0.419426	1.63381	1.854965	3.168159	0.832443	0.082697	0.820084	2.969011	1.215376	4.870121	0.196925	0.268307	1.152001	4.468206	1.407349	4.168209
58	0.328853	1.908206	1.349081	9.613332	0.130141	4.38174	2.003849	0.709362	0.507992	0.13642	1.757581	2.608722	1.51774	2.608352	0.21378	0.298061	1.414028	3.182221	1.962882	3.84067
59	0.184686	1.039895	1.832007	7.791743	0.336406	3.526741	2.057484	0.152874	0.268784	0.130596	2.207569	2.452182	1.197842	0.879259	0.364815	0.435211	1.204498	1.784451	2.132801	2.560062
60	1.983316	1.882689	1.637501	7.451451	0.153901	3.124871	2.309107	1.301827	1.006832	0.115033	2.333342	3.138221	0.306528	0.793771	0.362382	0.266132	1.595977	2.453104	2.98627	0.111994
61	3.076043	1.785872	0.868862	9.030889	0.521396	2.728947	1.452565	3.800434	0.680942	-0.09187	3.404795	4.168516	0.024484	3.069829	0.290676	1.778847	1.059755	5.52819	3.887447	0.307561
62	1.10175	1.682439	0.581234	5.281892	0.447203	1.409119	0.73196	1.219969	0.853665	1.466659	2.148066	1.480219	0.895708	5.130828	0.218154	1.349557	0.345637	8.759141	2.386585	1.533539
63	1.361345	0.650772	1.022326	4.675434	4.071565	0.709339	0.174258	1.163461	0.825016	5.403808	0.652579	0.39337	3.145248	6.763986	0.29405	0.218687	0.279382	8.594385	1.162229	1.283108
64	1.953837	0.186784	1.306995	7.103868	4.567634	0.6813	1.578652	1.327056	0.612528	3.822517	1.147845	0.433037	5.827404	7.79812	0.504713	5.254208	0.473163	1.299118	0.372477	3.153502
65	2.356951	0.599813	1.444828	6.516917	0.971224	1.537792	1.109043	2.205445	0.904202	1.987532	2.520446	0.188516	6.848373	5.547178	0.914332	2.841616	1.134861	2.26945	0.608999	3.435657
66	3.17239	1.976173	1.76595	7.420662	1.334673	2.381837	1.470075	2.928792	1.060121	1.958853	2.934424	0.125008	6.93348	0.693759	1.149265	-0.20858	1.501421	2.127573	0.912372	5.481654
67	3.468818	6.695604	2.104797	7.277506	0.15068	2.663462	1.393687	3.08028	0.191926	2.198041	2.685031	0.094306	6.450192	0.619723	1.278101	1.196725	2.08417	1.299958	1.15081	5.27904
68	4.268505	6.292091	2.354879	6.589677	0.108725	2.455515	3.880507	1.620887	-0.00114	1.792205	2.026784	0.320367	6.293721	0.959952	0.746687	4.299818	2.454499	3.844144	1.745884	2.376007
69	4.942264	1.525725	1.516345	7.488318	-0.06305	1.278784	4.064486	1.562472	0.618316	2.022683	1.869361	0.404167	5.224509	1.728794	0.171993	4.043994	2.458465	1.245865	2.832369	2.706899
70	6.132626	1.087242	1.470707	7.246618	1.872627	0.885836	4.117206	0.966571	0.767229	1.943364	0.974664	0.756389	4.885633	1.313304	0.305063	5.572507	2.119114	2.884571	2.701001	3.927148
71	6.958957	0.695035	0.648463	8.290159	5.316552	0.441912	3.262503	2.870214	0.205577	1.658476	0.597963	1.681639	4.155806	1.304332	0.675108	4.641244	1.377059	2.68452	3.502378	4.30286
72	6.806594	4.042785	0.376568	2.760773	5.671619	0.282567	1.586746	0.855631	1.523045	1.088382	5.250594	2.716881	2.361736	1.19617	1.037825	1.930418	1.719058	1.46362	4.558819	2.66369
73	6.650635	4.468638	2.527735	1.09308	3.60258	0.272585	0.839899	0.310717	1.36233	0.744332	6.220726	2.675985	2.461346	3.958382	2.842555	0.80634	1.192894	1.255458	3.820235	1.13337
74	5.017187	7.912878	4.586214	1.595811	2.812176	0.683836	1.067141	0.170859	0.264417	4.396622	3.986745	2.919177	4.409797	4.93349	2.680252	0.878811	0.229922	1.240474	0.314599	1.278235
75	4.414109	12.65093	3.846324	1.401836	2.823978	0.973656	1.614505	0.901909	2.547857	5.393348	2.529935	3.136682	2.105062	9.220805	0.948303	1.625056	0.156395	0.912339	0.327922	0.902676
76	0.823328	2.1663	0.93953	0.727121	1.726788	3.961244	1.852682	3.104165	11.88549	0.260765	0.328716	5.380157	0.510931	1.182757	0.809458	1.151905	0.566357	1.930309	3.089113	5.753892
77	0.135346	0.772179	0.895752	0.433886	1.073776	2.393513	2.426661	3.012394	17.69743	0.311588	0.871715	2.88558	0.457661	3.250908	1.184802	0.671053	0.571246	3.040717	3.2214	3.016163
78	0.409749	1.833233	1.310874	0.256633	0.531938	1.039616	1.317521	4.423495	16.42293	0.134912	1.607041	3.163943	0.536629	5.127619	0.975158	0.692106	0.329347	1.146966	0.686875	2.289541
79	0.477558	3.412069	1.642598	1.256035	0.271579	0.280575	1.860817	1.558903	16.79857	0.121746	1.534613	3.254374	0.471008	2.983085	0.50106	0.594969	0.415364	1.98587	2.839383	2.323351
80	0.353588	2.740425	1.477548	3.38251	0.621903	0.387091	1.127119	0.55165	13.20617	0.052888	0.272901	2.304822	0.560241	0.650504	0.455954	0.49438	0.260259	2.002848	2.021826	1.857216
81	0.275919	1.988246	1.16072	4.843216	0.388462	0.715931	1.161959	2.18009	0.819045	-0.00213	0.375985	2.886259	0.839204	2.785848	0.368059	0.370264	0.19725	2.178424	1.155873	1.173102
82	0.273696	1.197256	0.689836	8.634981	0.117866	0.548059	2.559371	2.468209	0.571015	0.010779	1.529537	2.984245	1.029654	2.266308	0.518011	0.160395	1.181053	3.527071	1.500606	1.361114
83	-0.03798	2.282977	1.100114	8.301145	0.344839	1.789491	2.284318	1.732568	0.242298	0.05064	1.671916	2.741711	0.854958	0.858675	0.392532	0.177681	1.283602	1.590332	2.123182	1.341552

84	1.189562	0.815239	1.550786	7.394951	0.665351	4.84186	1.6743	-0.10631	0.764441	0.055771	2.034618	3.296184	0.444006	0.768005	0.331974	0.274093	1.154828	2.746203	2.811586	0.428112
85	4.979965	0.892265	1.425489	8.153175	0.103632	1.889833	1.034305	4.393095	1.259439	-0.02091	1.828249	3.288012	-0.04304	1.442165	0.445015	0.288898	0.998126	4.029117	4.967873	1.092738
86	2.795094	1.511321	0.883265	8.658883	1.073232	0.791547	1.007816	10.01871	0.936818	2.514694	1.898849	1.471038	0.827879	2.957612	0.437521	0.895802	0.680085	5.867262	2.062554	1.401342
87	1.108326	1.801165	1.03622	5.88929	0.623764	1.03279	2.884569	2.707484	0.728593	7.299047	1.157013	0.349283	3.125125	3.726837	0.61212	2.014685	0.390655	10.47546	1.609568	2.952253
88	1.354513	1.808875	1.469656	6.314198	1.933128	0.856563	0.955068	1.026396	0.745222	8.881317	0.90923	0.498481	5.471143	8.366266	0.451375	-0.02889	0.638876	11.40424	1.229515	3.314603
89	2.342416	0.397183	1.828889	6.585634	5.772608	1.419932	0.633746	1.526432	0.553193	7.227005	2.000572	0.122016	7.234095	6.80944	0.849605	1.554353	1.294316	4.856741	1.048801	0.669216
90	2.985941	0.376202	1.862446	7.172585	1.285668	2.015013	1.231904	2.900674	0.894757	4.075524	3.040243	0.189941	7.510707	1.575242	0.722546	7.244703	1.722717	2.822599	0.785614	2.722063
91	3.759189	4.093014	2.364603	6.762869	0.177319	1.971143	1.452232	1.436295	1.189798	2.764253	3.237915	0.275149	7.432046	4.339779	0.905036	3.869356	1.933782	4.171934	0.677153	2.392126
92	4.818644	2.690007	2.368685	7.802082	0.139031	0.984572	2.304387	3.853176	0.369337	2.96638	3.172493	0.33737	6.372088	1.393799	0.946056	3.915417	2.291628	3.72434	0.795455	5.022477
93	5.060159	0.107844	2.170186	6.723891	0.04279	0.7073	1.10803	4.488757	0.100927	2.466447	2.418856	0.361276	5.904274	0.480527	0.386833	3.895126	2.387097	4.069885	0.788015	4.903404
94	5.12254	4.495803	1.841535	7.220603	0.908381	0.298185	1.290969	2.27632	0.20372	2.338978	1.811353	0.778011	5.401288	1.37663	0.330492	5.31715	2.32719	1.790491	1.369768	3.887189
95	6.21333	3.127419	1.677336	6.335887	7.801578	0.352686	2.303939	1.780469	0.547798	2.012957	1.598233	2.090251	5.221737	1.669326	0.429569	5.997815	2.453533	2.480513	2.113771	3.886336
96	6.318774	1.999944	1.0172	2.07307	8.501622	0.395242	1.580212	2.424039	0.33741	1.439685	7.255698	2.696748	4.724865	0.889518	1.239007	6.441185	1.762705	1.818072	2.529047	5.283929
97	6.400441	8.827693	0.817708	0.590896	3.793027	0.479552	1.147393	1.101433	1.236872	1.078467	11.90469	2.887088	2.129208	1.331624	1.473163	3.989489	1.591354	2.40091	2.16028	4.272632
98	6.515113	5.610917	2.554424	1.108874	2.964516	0.557135	1.160276	0.247709	1.837679	0.404706	10.98201	3.040286	1.647446	1.003863	0.851512	0.822496	1.290981	1.292511	3.647377	3.308959
99	4.636818	2.549278	4.834271	1.11469	3.027894	0.47782	1.744657	0.151023	0.229636	2.502889	7.545881	3.165902	4.579717	9.449577	2.509553	0.463672	0.101891	1.752848	5.365146	2.772888
100	4.438862	4.235011	4.120151	1.271497	2.470759	0.501242	1.357769	0.472996	2.596029	5.484808	3.312897	2.309718	3.320963	11.2915	2.970761	1.026209	0.093123	1.138854	0.159758	1.420069
101	1.549997	0.783422	0.79003	0.96077	1.697065	1.41239	3.821481	2.110892	12.96396	0.310749	0.635532	5.962995	0.765584	1.356095	2.039241	0.997711	0.387348	1.026254	4.849794	2.964138
102	0.738064	1.08462	0.86842	0.626102	1.057183	4.063948	5.946703	1.213899	17.37843	0.26259	1.447399	2.979793	0.778753	1.431694	0.952847	0.588958	0.373439	3.099313	1.881427	3.609864
103	0.214834	2.099903	1.230773	0.617924	0.220397	2.626144	6.586389	2.742406	16.45092	0.135813	1.600663	2.81722	0.715308	3.782692	0.539442	0.503172	0.204089	1.736398	2.58466	4.193554
104	0.640066	4.394012	1.667477	1.197199	0.705287	1.089585	7.685083	0.554121	16.80724	0.003638	0.727912	3.120505	0.477332	3.737203	0.329386	0.537446	0.318144	1.12202	1.864766	4.560524
105	0.539962	2.334564	1.350074	5.941079	0.773736	0.254198	0.722927	1.233599	13.99144	0.024783	0.716623	1.960881	0.618485	0.863019	0.799301	0.432615	0.211309	2.493288	0.880473	4.878497
106	0.310311	1.401431	0.901785	5.170755	0.516542	0.289935	0.437726	1.285633	1.899166	0.015758	1.387297	2.24624	0.915339	0.849083	0.780903	0.28565	0.386328	-0.0483	1.129702	3.728971
107	0.208886	0.877796	0.741151	8.57182	0.465184	0.679458	2.74027	1.758953	0.460787	0.064709	1.557266	3.334099	0.647728	1.845899	0.54066	0.190642	0.883121	3.787772	1.486874	1.999175
108	1.844225	1.845273	0.923078	8.909482	1.072075	0.962486	2.489647	3.438588	0.457897	-0.01264	1.59725	4.903577	0.052243	3.608933	0.336845	0.215978	0.628128	4.906222	1.52137	1.052826
109	3.605439	1.608624	1.208993	8.935566	0.217458	2.82859	0.810962	0.208797	0.881545	0.073467	1.59717	2.724194	-0.14577	0.482073	0.229829	0.264805	0.654288	3.496918	2.815616	1.451348
110	2.199984	0.51406	1.164895	8.386509	0.179033	4.812391	0.604875	3.707795	1.103696	2.502183	1.272095	0.118791	1.257774	4.695096	0.682224	0.295543	0.47649	3.198065	4.79722	3.137044
111	0.982681	1.341082	1.203472	9.127461	1.236731	1.058166	1.395756	4.822266	0.958639	6.571127	0.725262	0.050945	3.574584	4.888784	0.839149	0.27023	0.47167	2.413973	6.708626	3.962314
112	1.172128	1.367161	1.610438	7.795499	0.973361	1.104027	3.723843	1.045467	0.758828	8.197126	0.839171	0.268693	5.018089	1.880475	0.756961	0.750241	0.767906	10.38862	5.203322	0.553028
113	2.118986	1.680818	1.767962	8.489569	1.173713	1.492072	3.384234	1.648907	0.730187	8.365014	1.425239	0.088906	6.878316	2.332107	0.365837	0.452877	1.376554	11.11236	1.956932	1.045793

## Appendix-II

### NDVI Numeric Values of Soil (Listed Training Samples-113X20)

#### (Actual Training Feature Size of Soil-625X84)

	1	2	3	4	5	6	7	8	9	10	11	12	13	14	15	16	17	18	19	20
1	0.227565	-0.17485	0.097794	0.383886	-0.0273	0.381595	0.427978	0.478616	-0.0485	0.303399	0.377677	-0.07397	0.46913	-0.30935	0.386685	0.503002	0.213028	-0.15458	-0.25602	-0.11521
2	0.211372	-0.18721	0.046587	0.328627	-0.03791	0.041832	0.35893	0.225245	-0.11599	0.382597	0.389518	-0.04262	0.441659	-0.24798	0.438886	0.307293	0.074064	-0.20662	-0.1481	-0.09589
3	0.279487	-0.26705	0.17806	0.42554	0.012485	-0.03605	0.388764	0.209595	-0.09494	0.449156	0.338738	-0.04648	0.325887	-0.24062	0.513965	0.349106	0.100516	-0.09836	0.099841	0.340955
4	0.383165	-0.26178	0.282647	0.000938	-0.02419	-0.05868	0.595513	0.114838	0.310158	0.481736	0.167768	-0.07119	0.221591	-0.14827	0.499214	0.32514	0.263621	0.163392	-0.0034	0.39098
5	0.401906	-0.23423	0.281033	-0.13867	0.195325	-0.17175	0.548421	0.328202	0.343447	0.476238	0.165272	-0.10122	0.173207	0.092892	0.491145	0.384502	0.391256	0.159963	-0.12137	0.377074
6	0.322722	-0.22139	0.145883	-0.19915	-0.09196	-0.10661	0.248167	0.318964	0.370958	0.416446	0.250271	-0.09633	0.262584	0.071369	0.531089	0.376041	0.456611	-0.0223	-0.03608	0.27921
7	0.221128	-0.16776	-0.01037	-0.23761	0.126946	-0.00177	0.267441	0.363267	0.339099	0.329698	0.296589	-0.05565	0.33735	0.055889	0.527217	0.361247	0.425154	-0.1025	0.063992	0.191913
8	0.230951	-0.19046	-0.01157	-0.19283	0.048	0.033695	0.175807	0.293242	0.354175	0.256733	0.151246	-0.02114	0.310125	-0.21301	0.529002	0.393831	0.289824	-0.11401	0.10143	0.153091
9	0.364014	-0.21616	0.167994	-0.16744	0.08887	0.053376	0.272758	0.354626	0.382749	0.282128	0.03865	-0.03613	0.232644	-0.2813	0.46594	0.126451	0.125341	-0.14174	0.072157	0.044215
10	0.44359	-0.18644	0.299677	-0.20231	0.178949	0.034722	0.395366	0.205601	0.408322	0.353939	0.225411	-0.10406	0.170358	-0.31072	0.470267	0.269572	0.056258	0.011336	0.198312	0.152409
11	0.43571	0.21972	0.346034	-0.19297	0.069101	0.055512	0.508529	0.192838	0.359633	0.464413	0.311205	-0.14043	0.125327	-0.30003	0.435086	0.100107	0.140352	0.491723	0.285327	0.159554
12	0.311125	0.347779	0.255511	-0.13487	0.120458	0.112085	0.23776	0.278689	0.308281	0.548281	0.319982	-0.05431	0.22975	-0.10865	0.393248	0.011436	0.307192	0.362861	0.329344	0.25397
13	0.141955	0.372776	0.099859	-0.14514	0.175049	0.143996	-0.04996	0.106481	0.315149	0.444582	0.306182	0.268736	0.298397	-0.2311	0.335796	0.221899	0.392502	0.210019	0.350673	-0.01872
14	0.058947	0.360997	0.099612	-0.20999	0.291795	0.115555	-0.17351	-0.01711	0.338152	0.211126	0.426685	0.381425	0.148076	0.081539	0.265367	0.346472	0.372782	0.293857	0.329602	-0.33347
15	0.146644	0.02467	0.195258	-0.21977	0.278141	0.179608	-0.16339	-0.03814	0.422845	-0.05884	0.373223	0.343449	0.007527	0.030415	0.219225	0.233672	0.285852	0.282121	0.346224	-0.30425
16	0.181986	-0.21161	0.245744	-0.13926	0.269949	0.327968	-0.15069	0.136251	0.507288	-0.06884	0.251647	0.328062	-0.12122	0.268441	0.170087	0.351109	0.105335	0.346734	0.148131	-0.28792
17	0.111468	-0.25061	0.196492	-0.10048	0.352436	0.439569	0.015791	0.05359	0.462258	-0.06433	0.187811	0.32218	-0.24075	0.26975	0.227102	0.189427	-0.05478	0.237728	0.119087	-0.35066
18	-0.00248	-0.32105	-0.01894	-0.23746	0.367088	0.403756	0.022976	0.071053	0.366874	-0.02207	0.13966	0.336739	-0.22859	0.22702	0.356222	0.003546	-0.1122	0.206485	0.142317	-0.28584
19	-0.15515	-0.34869	-0.18451	-0.22986	0.508136	0.318628	-0.08148	0.042481	0.375786	-0.01657	0.153499	0.331089	-0.12649	0.302254	0.487108	0.081322	-0.022	0.316001	0.122901	-0.33694
20	-0.18574	-0.25417	-0.11388	-0.0868	0.416554	0.242212	-0.12374	-0.25174	0.329863	-0.12242	0.057943	0.322283	-0.0546	0.340759	0.426648	0.172448	0.090831	0.206616	0.209505	-0.33895
21	-0.07721	0.19063	0.013966	0.185157	0.418787	0.200525	-0.16413	-0.27498	0.074521	-0.20964	-0.05639	0.268935	-0.09084	0.308033	0.330902	0.086278	0.082182	0.045056	0.307251	-0.32254
22	0.031972	-0.03081	-0.02568	0.156557	0.2293	0.252404	-0.26749	-0.20591	0.063825	-0.19312	-0.04288	0.186953	-0.22487	-0.20126	0.221152	0.107938	0.051978	-0.16746	0.535015	-0.37386
23	0.136032	-0.19391	-0.07826	0.138525	0.113476	0.431696	-0.18692	-0.27683	-0.09286	-0.16519	-0.04069	0.108962	-0.27804	0.032443	0.202836	-0.00605	-0.04295	-0.12388	0.569811	-0.27883

24	0.130922	-0.25672	-0.13074	0.209226	0.227651	0.509012	-0.14014	-0.33315	-0.10309	-0.15166	-0.07284	0.119583	-0.22046	0.514033	0.140023	-0.20799	-0.15131	-0.11466	0.447086	-0.28697
25	0.325886	-0.18549	0.221253	0.402568	-0.02101	0.112015	0.400766	0.365105	0.092407	0.353299	0.313578	0.018379	0.390934	-0.29813	0.561276	0.508948	0.294589	-0.23091	-0.25316	-0.19165
26	0.27323	-0.22328	0.103793	0.322219	0.0224	-0.01335	0.426731	0.298347	-0.03699	0.361632	0.285869	-0.01066	0.483975	-0.22746	0.443153	0.332316	0.207219	-0.16522	-0.27676	-0.1523
27	0.258058	-0.29655	0.071667	0.381396	0.015059	-0.01577	0.383635	0.150581	0.115575	0.385185	0.315176	-0.13978	0.42927	-0.21523	0.439344	0.366941	0.104462	-0.17755	-0.14366	-0.10057
28	0.311415	-0.19546	0.155932	0.512562	0.020659	-0.00861	0.42564	0.273997	0.105287	0.391988	0.223378	-0.18307	0.326838	-0.20903	0.518074	0.358838	0.136624	-0.09441	0.106824	-0.03548
29	0.340426	-0.14282	0.240573	0.052469	0.094412	-0.00985	0.520171	0.245304	0.043174	0.409822	0.239507	-0.08211	0.221819	-0.2745	0.496827	0.368827	0.266245	0.005688	0.020224	0.067935
30	0.342696	-0.18981	0.269887	-0.17069	0.071793	-0.05128	0.560091	0.333569	0.397103	0.428901	0.370008	-0.00525	0.150986	-0.07854	0.504772	0.359284	0.361202	-0.13016	-0.07829	0.141098
31	0.301537	-0.18843	0.149727	-0.18017	0.065803	-0.18556	0.105003	0.322858	0.318943	0.397865	0.411971	-0.00403	0.24239	-0.00352	0.511801	0.373223	0.395934	-0.16048	-0.01912	0.214897
32	0.256678	-0.14298	0.01898	-0.23327	0.054839	-0.11352	0.032474	0.439588	0.366284	0.353048	0.302585	-0.06421	0.309015	-0.11983	0.521423	0.380498	0.385739	-0.21027	-0.00502	-0.05213
33	0.276616	-0.17484	-0.0015	-0.2409	0.075287	-0.0868	0.145876	0.462457	0.361527	0.343317	0.18571	-0.12798	0.276957	-0.13874	0.524214	0.39149	0.284633	-0.25712	0.017895	-0.2483
34	0.353698	-0.20832	0.147639	-0.23172	0.167364	-0.07208	0.116419	0.346321	0.443353	0.366211	0.098535	-0.13892	0.248425	-0.11779	0.459363	0.352318	0.134926	-0.21576	-0.02311	0.155875
35	0.392892	-0.22316	0.287007	-0.21691	0.192065	-0.06225	0.251637	0.198616	0.384059	0.393059	0.167819	-0.06489	0.200426	-0.2654	0.381748	0.263381	0.116738	-0.13076	0.01649	0.272489
36	0.355293	-0.04986	0.320186	-0.19034	0.188036	-0.0319	0.488413	0.271274	0.314439	0.421194	0.34857	0.068183	0.175097	-0.31492	0.404218	0.394429	0.20089	0.181117	0.152298	0.129107
37	0.221673	0.300907	0.207926	-0.20168	-0.00315	0.019935	0.367572	0.335026	0.321766	0.327431	0.39023	0.37789	0.163681	-0.31802	0.396197	0.101001	0.323702	0.177584	0.202593	0.119335
38	0.104609	0.342213	0.08617	-0.16003	0.195373	0.13517	0.195442	0.135079	0.2675	0.052823	0.335755	0.376266	0.089752	-0.27981	0.272236	0.068724	0.388619	0.259311	0.315617	0.0977
39	0.064347	0.307646	0.093613	-0.14833	0.270956	0.29613	-0.08388	0.021571	0.34631	0.018275	0.271321	0.234762	0.01309	-0.06816	0.196746	0.274141	0.350765	0.347343	0.386334	-0.21443
40	0.117173	-0.05039	0.168353	-0.15362	0.290165	0.335311	-0.19026	-0.07384	0.323783	0.083101	0.172775	0.339888	-0.03899	-0.08662	0.165605	0.336625	0.26428	0.393626	0.270874	-0.32518
41	0.206221	-0.18123	0.20827	-0.18148	0.329461	0.251198	-0.18232	0.129935	0.557642	0.036978	0.146285	0.431833	-0.14416	0.17415	0.155951	0.32227	0.103507	0.39136	0.068256	-0.33171
42	0.170034	-0.27547	0.140318	-0.1628	0.433511	0.278673	-0.10566	0.130324	0.428754	0.012172	0.193732	0.436482	-0.25274	0.296173	0.198733	0.151828	-0.04179	0.261638	0.056722	-0.28957
43	-0.00319	-0.25788	-0.00685	-0.17183	0.457203	0.303722	-0.10758	0.092748	0.382372	-0.00109	0.216641	0.352416	-0.25495	0.349342	0.278535	0.000468	-0.06948	0.218827	0.014894	-0.32707
44	-0.12034	-0.13859	-0.15832	-0.21359	0.516285	0.29653	-0.16462	0.072387	0.284533	-0.00138	0.262728	0.239877	-0.14702	0.227285	0.411531	0.02877	-0.00097	0.231586	0.047593	-0.30382
45	-0.15494	0.110486	-0.10176	-0.2053	0.520025	0.302533	-0.2377	-0.15753	0.364494	-0.02044	0.228831	0.215899	-0.05407	0.298927	0.355464	0.082135	0.074869	0.144061	0.085427	-0.3189
46	-0.1371	0.368704	0.014582	0.071151	0.186547	0.398211	-0.28609	-0.22926	0.081131	-0.0772	-0.06546	0.194157	-0.08152	0.260148	0.300026	0.155042	0.065404	0.001176	0.049834	-0.31252
47	-0.03154	0.238698	-0.01932	0.222558	0.251892	0.397945	-0.19065	-0.28643	0.056526	-0.22371	-0.17128	0.199535	-0.18946	-0.37282	0.181366	0.029397	0.040612	-0.11646	0.189743	-0.2237
48	-0.00848	-0.19416	-0.10487	0.153608	0.155315	0.442325	-0.16954	-0.34	-0.02316	-0.2277	-0.08555	0.178529	-0.29297	-0.12252	0.163045	0.034509	-0.03056	-0.1395	0.541088	-0.25574
49	0.012913	-0.2727	-0.15964	0.135166	0.150446	0.472532	-0.15188	-0.33899	-0.16859	-0.1358	-0.03011	0.078938	-0.2304	0.358137	0.171338	-0.11639	-0.11925	-0.12133	0.568225	-0.26451
50	0.356805	-0.26005	0.22697	0.391476	-0.08514	-0.08099	0.421976	-0.07069	-0.00353	0.438427	0.275933	0.027681	0.385094	-0.21122	0.579842	0.458891	0.253431	-0.16073	-0.27491	-0.23062
51	0.40727	-0.26716	0.172441	0.28106	0.041596	0.014102	0.460192	0.002144	0.049234	0.409048	0.215657	-0.0306	0.452842	-0.28315	0.495014	0.30623	0.213324	-0.20372	-0.32265	-0.15855
52	0.370192	-0.10146	0.129559	0.407424	0.046751	0.034053	0.433531	0.128197	0.070643	0.375823	0.148266	-0.13253	0.413565	-0.27901	0.463388	0.385467	0.187266	-0.14803	-0.05882	-0.12335
53	0.31713	0.05265	0.154434	0.489297	0.040947	-0.00702	0.444631	0.286091	0.137416	0.324414	0.145934	-0.18211	0.311328	-0.19824	0.501564	0.35706	0.206474	-0.20609	0.28629	-0.07243



54	0.262166	-0.11878	0.185566	0.068215	0.128452	-0.02474	0.4494	0.375571	0.033358	0.300106	0.356413	-0.08837	0.215666	-0.23711	0.512327	0.383505	0.27007	-0.1016	0.034544	0.061365
55	0.265226	-0.13647	0.20094	-0.19224	-0.02757	-0.01791	0.370476	0.271547	0.326184	0.326126	0.545762	-0.00473	0.162799	-0.20807	0.499108	0.342965	0.339223	-0.17299	-0.0278	0.135137
56	0.325311	-0.1664	0.17009	-0.1827	0.105298	-0.06546	0.315021	0.241709	0.33132	0.344151	0.404531	-0.00194	0.199048	-0.1524	0.473493	0.35435	0.291972	-0.26123	-0.04104	0.078401
57	0.362242	-0.18661	0.096757	-0.18504	0.031614	-0.15238	0.158265	0.418119	0.381089	0.394038	0.213685	-0.04454	0.254229	0.032632	0.47969	0.385948	0.256857	-0.23659	-0.05795	0.114397
58	0.367362	-0.15023	0.067069	-0.28172	0.090834	-0.13935	0.131503	0.449814	0.401872	0.441185	0.17152	-0.11887	0.252374	0.219658	0.455003	0.362936	0.238826	-0.19694	-0.02333	0.252116
59	0.200853	-0.19369	0.153483	-0.27718	0.149551	-0.12382	0.141807	0.340304	0.358002	0.442953	0.231851	-0.10656	0.254911	0.183825	0.397854	0.431809	0.160398	-0.20855	-0.05206	0.361468
60	0.006489	-0.20331	0.250643	-0.1707	0.152455	-0.10452	0.196223	0.168027	0.339928	0.378262	0.211181	0.043146	0.216176	-0.14279	0.388657	0.197147	0.184418	-0.2156	-0.01297	0.322902
61	0.160528	-0.2019	0.267066	-0.14779	0.308801	-0.02479	0.392152	0.326249	0.313142	0.191309	0.367617	0.429778	0.090789	-0.28881	0.351135	0.291157	0.264676	-0.33774	0.044258	0.230771
62	0.204386	0.123039	0.192472	-0.18977	-0.01035	0.026652	0.463624	0.320377	0.312994	-0.12921	0.456745	0.422765	-0.03764	-0.33876	0.290495	0.324646	0.309091	-0.18979	0.078988	0.175362
63	0.184457	0.298375	0.110078	-0.21858	0.119332	0.241372	0.17312	0.210963	0.30594	-0.09434	0.297386	0.29874	-0.08253	-0.37172	0.20187	0.046731	0.322215	0.475098	0.230111	-0.09215
64	0.147519	0.339809	0.091863	-0.09428	0.237626	0.334111	-0.14788	0.041361	0.317528	0.074733	0.108644	0.307333	-0.07287	-0.02662	0.18016	0.07192	0.275906	0.332967	0.186215	-0.15989
65	0.08533	0.32538	0.133279	-0.13685	0.249696	0.207796	-0.19816	0.019229	0.339326	0.09428	0.019707	0.394237	-0.08359	0.281142	0.151545	0.365317	0.204058	0.334941	0.072704	-0.22953
66	0.025034	0.077718	0.139906	-0.23678	0.438051	0.175264	-0.18231	0.062894	0.508569	0.086547	0.063358	0.488274	-0.13665	0.316697	0.143828	0.199662	0.104173	0.362432	0.010178	-0.30145
67	-0.03256	0.090965	0.070295	-0.19442	0.415091	0.251321	-0.25978	0.268095	0.479113	0.063423	0.204663	0.426595	-0.22486	0.326238	0.174194	0.042497	0.019584	0.182487	-0.03871	-0.28076
68	-0.02194	0.349068	0.007238	-0.13419	0.532367	0.314452	-0.27615	0.222979	0.377592	0.029547	0.281187	0.353791	-0.22685	0.236959	0.265081	-0.01131	0.002351	0.247572	-0.03982	-0.27956
69	-0.03361	0.328987	-0.09756	-0.19549	0.458634	0.388533	-0.27027	0.146107	0.306897	-0.01189	0.33513	0.216585	-0.15029	0.257057	0.271918	-0.07036	0.032002	0.089468	-0.03222	-0.30674
70	-0.08648	0.365644	-0.07146	-0.232	0.262678	0.424948	-0.25288	-0.16955	0.327614	-0.04247	0.227789	0.103337	-0.08031	0.216924	0.262217	-0.03201	0.063358	0.092047	0.012025	-0.2993
71	-0.11053	0.238925	-0.00921	0.089186	0.125971	0.438953	-0.18619	-0.29997	0.097881	-0.05678	-0.21521	0.12346	-0.08127	0.317973	0.244935	0.099863	0.028684	0.189165	-0.00234	-0.24875
72	-0.14491	0.203453	-0.05198	0.276322	0.193181	0.433007	-0.16483	-0.33252	0.032117	-0.09954	-0.32666	0.204136	-0.1637	0.301567	0.124308	0.077218	0.018717	0.063507	0.174874	-0.23207
73	-0.09761	0.043545	-0.15581	0.186267	0.198341	0.386921	-0.17116	-0.32609	0.010298	-0.26029	-0.1652	0.190546	-0.29516	0.212152	0.102031	0.042685	-0.00974	-0.16405	0.437823	-0.24607
74	-0.05138	-0.25629	-0.16373	0.048219	0.110225	0.327896	-0.19459	-0.33882	-0.16071	-0.23937	-0.01341	0.109868	-0.26419	-0.11604	0.169213	-0.0117	-0.06176	-0.12136	0.467084	-0.2625
75	0.32497	-0.20803	0.202525	0.391174	-0.02748	-0.08608	0.161421	0.07742	-0.00519	0.480264	0.302718	-0.2159	0.353905	-0.23684	0.567231	0.30989	0.226299	0.020979	-0.20849	-0.23108
76	0.461906	-0.17032	0.20974	0.300744	-0.01942	-0.0541	0.175386	0.163762	0.012515	0.432839	0.130346	-0.11712	0.376011	-0.28165	0.480297	0.417618	0.24191	-0.2466	-0.17712	-0.17016
77	0.440305	-0.17488	0.168998	0.402896	0.042245	-0.00472	0.447345	0.121043	0.063243	0.367041	0.025795	-0.07592	0.370737	-0.33354	0.473904	0.324421	0.288188	-0.15434	0.208255	-0.15006
78	0.333016	-0.19571	0.135751	0.365198	0.077608	0.035793	0.351284	0.346538	0.04957	0.264052	0.212703	-0.06885	0.321702	-0.26579	0.523365	0.377596	0.29329	-0.18238	0.043631	-0.13345
79	0.19601	-0.16043	0.136383	-0.0365	0.038875	0.007839	0.38171	0.392537	0.07913	0.197835	0.498742	-0.04429	0.255024	-0.18834	0.484963	0.344488	0.31264	-0.14645	-0.06008	-0.08861
80	0.208368	-0.15205	0.158942	-0.23693	0.069266	-0.05163	0.402342	0.285854	0.213096	0.255071	0.522498	-0.12344	0.207622	-0.20876	0.436959	0.361573	0.306496	-0.06966	-0.07781	0.023664
81	0.333971	-0.16465	0.204255	-0.17125	0.029565	-0.02972	0.230097	0.272102	0.366239	0.377535	0.308273	-0.13703	0.224152	-0.15977	0.407753	0.346216	0.221663	-0.1907	-0.08874	0.015938
82	0.433135	-0.20324	0.193743	-0.1193	0.08362	-0.08013	0.131954	0.329395	0.368342	0.4731	0.225497	-0.06188	0.237835	0.109782	0.430948	0.335874	0.197864	-0.1618	-0.09748	-0.00919
83	0.31287	-0.14738	0.170371	-0.26144	0.038455	-0.1918	0.178394	0.433857	0.373197	0.497452	0.158004	-0.0268	0.238341	0.268695	0.413535	0.39858	0.204702	-0.2075	-0.06613	0.184882

84	-0.09014	-0.157	0.17959	-0.30164	0.093808	-0.07348	0.251905	0.086797	0.306273	0.456836	0.238205	0.129918	0.233454	0.239358	0.351902	0.357514	0.228609	-0.17092	-0.01554	0.273078
85	-0.06021	-0.18438	0.200649	-0.12253	0.100027	-0.02649	0.256619	-0.18371	0.312177	0.140853	0.326234	0.373977	0.163442	0.07909	0.286946	0.371954	0.26858	0.011838	0.078657	0.332029
86	0.107543	-0.19646	0.187996	-0.1177	0.178435	-0.04026	0.21137	0.200298	0.333494	-0.22541	0.459758	0.314737	-0.00194	-0.13722	0.257419	0.100192	0.294544	-0.32388	0.090233	0.287679
87	0.204074	-0.12003	0.172972	-0.23607	0.195249	0.000566	0.399104	0.30722	0.297371	-0.35761	0.411386	0.286384	-0.11258	-0.3021	0.248807	0.413144	0.268896	-0.3522	0.060699	0.245047
88	0.228182	0.21948	0.140457	-0.2296	-0.0359	0.010434	0.294911	0.21946	0.356831	-0.2892	0.229202	0.411032	-0.14795	-0.04037	0.164952	0.175399	0.221406	0.266879	0.029118	0.223395
89	0.188408	0.329776	0.094722	-0.11309	0.226716	0.048333	-0.13777	0.07103	0.277681	-0.09884	0.067602	0.394999	-0.14854	0.303595	0.178842	-0.0452	0.177605	0.306547	-0.00843	-0.07978
90	0.042105	0.209385	0.060421	-0.09643	0.3411	0.153586	-0.1847	0.151497	0.340845	0.052468	-0.00309	0.356244	-0.14988	0.030938	0.162234	0.020887	0.143855	0.160466	-0.03071	-0.0385
91	-0.14165	0.302536	0.053005	-0.27836	0.425154	0.366043	-0.1892	0.041593	0.43137	0.095735	0.044905	0.318624	-0.14535	0.270267	0.15831	0.053962	0.106301	0.146698	-0.0362	-0.14578
92	-0.15869	0.411019	0.034362	-0.1803	0.463711	0.457352	-0.1688	0.066387	0.521887	0.101306	0.189916	0.280525	-0.1703	0.350479	0.202462	0.013006	0.087243	0.105104	-0.05971	-0.24092
93	-0.02639	0.188314	0.031188	-0.10393	0.546852	0.463083	-0.19007	0.16954	0.34814	0.067274	0.273602	0.277993	-0.16723	0.245329	0.227202	-0.01736	0.075388	0.157321	-0.08126	-0.24497
94	0.03413	0.242122	-0.00995	-0.13219	0.223262	0.451436	-0.21759	-0.03109	0.352668	0.009043	0.235865	0.21567	-0.14879	0.256255	0.25486	-0.15785	0.045617	0.117748	-0.01918	-0.26614
95	0.019914	0.286352	-0.03604	0.021823	0.015943	0.441747	-0.1843	-0.29956	0.272615	-0.02568	-0.10836	0.174077	-0.13019	0.316788	0.19311	-0.11487	0.02881	0.167494	-0.00816	-0.26122
96	-0.08098	0.012168	-0.04859	0.189707	0.274829	0.4093	-0.17552	-0.32913	0.116037	-0.04315	-0.40752	0.139319	-0.11408	0.223303	0.207555	-0.03133	-0.01848	0.179765	0.124144	-0.21587
97	-0.20983	0.155392	-0.11551	0.31956	0.199096	0.410614	-0.17885	-0.32673	0.00406	-0.01412	-0.42114	0.093356	-0.15316	0.31732	0.210528	0.13407	-0.02473	0.188048	0.248911	-0.26437
98	-0.16169	0.264088	-0.19085	0.213365	0.136085	0.424747	-0.2112	-0.33426	-0.01745	-0.12572	-0.25822	0.10675	-0.25585	-0.07415	0.085306	0.139886	-0.00958	-0.1322	0.176106	-0.22993
99	-0.04	0.209238	-0.15304	0.03897	0.2235	0.416037	-0.1948	-0.33397	-0.1631	-0.24676	-0.0305	0.209763	-0.24246	-0.18014	0.072653	0.000402	-0.01652	-0.13874	0.444518	-0.13214
100	0.234136	-0.18086	0.208561	0.377807	-0.0012	0.12294	-0.23595	0.16258	-0.06603	0.459675	0.249651	-0.27947	0.316533	-0.14481	0.448733	0.38389	0.207925	0.180862	-0.1464	-0.1722
101	0.352064	-0.18021	0.252094	0.336518	-0.06774	-0.12111	-0.29811	0.31353	-0.01578	0.437701	0.076141	-0.09281	0.293726	-0.23951	0.551968	0.375736	0.276558	-0.21863	-0.01839	-0.19086
102	0.397465	-0.13683	0.231785	0.3587	0.011071	-0.08487	-0.17315	0.261087	-0.03387	0.382155	0.109921	-0.00369	0.299947	-0.30924	0.509266	0.390321	0.356887	-0.20099	-0.02347	-0.1936
103	0.309886	-0.16705	0.148019	0.337585	0.067936	-0.01865	-0.06605	0.414581	0.032765	0.292598	0.325689	-0.00593	0.322475	-0.28713	0.498847	0.342569	0.356466	-0.17393	-0.08582	-0.23132
104	0.235291	-0.16197	0.104035	-0.17055	-0.02129	0.031538	0.348324	0.304495	0.02796	0.276814	0.388013	-0.04133	0.310976	-0.19335	0.405963	0.345615	0.336311	-0.1813	-0.10312	-0.24435
105	0.246737	-0.13058	0.133811	-0.21995	0.112564	0.001225	0.437004	0.298844	0.205769	0.350682	0.308054	-0.1727	0.282237	-0.18787	0.384272	0.370337	0.262681	0.04108	-0.06872	-0.21661
106	0.315118	-0.14268	0.21133	-0.16194	-0.05571	-0.03615	0.254385	0.279423	0.336355	0.442986	0.27457	-0.22421	0.258498	-0.17842	0.393699	0.369314	0.18195	-0.07791	-0.12114	-0.1171
107	0.245891	-0.18532	0.268462	-0.13543	0.066281	-0.04352	0.149416	0.217761	0.35231	0.48581	0.253014	-0.17079	0.233319	-0.10306	0.372908	0.352594	0.186479	-0.17541	-0.11186	-0.00665
108	0.030032	-0.16903	0.258818	-0.27319	0.063313	-0.12611	0.288791	0.363793	0.359138	0.456502	0.240004	0.124204	0.201736	0.193212	0.357808	0.349163	0.205405	-0.05939	-0.0533	0.105528
109	0.09976	-0.12257	0.206729	-0.24968	0.075031	-0.17301	0.311482	0.119812	0.321537	0.195448	0.286778	0.485198	0.100887	0.117502	0.278359	0.373824	0.285767	-0.00068	0.016592	0.176245
110	0.18079	-0.17535	0.123756	-0.14856	0.099429	-0.03238	0.277167	0.091772	0.313521	-0.1268	0.368503	0.413016	0.018199	0.165638	0.203231	0.374883	0.322835	0.200268	-0.00768	0.179332
111	0.152183	-0.16578	0.101496	-0.15737	0.065324	-0.052	0.176988	0.296628	0.331066	-0.25682	0.351479	0.212383	-0.03239	0.159422	0.192806	0.292776	0.296433	-0.17202	0.011582	0.298101
112	0.18079	-0.17535	0.123756	-0.14856	0.099429	-0.03238	0.277167	0.091772	0.313521	-0.1268	0.368503	0.413016	0.018199	0.165638	0.203231	0.374883	0.322835	0.200268	-0.00768	0.179332
113	0.152183	-0.16578	0.101496	-0.15737	0.065324	-0.052	0.176988	0.296628	0.331066	-0.25682	0.351479	0.212383	-0.03239	0.159422	0.192806	0.292776	0.296433	-0.17202	0.011582	0.298101

### Appendix-III

#### Textural Features of Soil (Listed Training Samples-113X17)

#### (Actual Training Feature Size of Soil-625X84)

	1	2	3	4	5	6	7	8	9	10	11	12	13	14	15	16	17
1	0.333333	1.833333	0	0.166667	0.333333	2.166667	0.166667	2	1.666667	0	0	0	0.166667	0.666667	0	0.5	0
2	0	1.666667	0	0	0	1.833333	0.333333	1	2	0	0	0.166667	0	1.166667	0	0.166667	0
3	0	0.666667	0	0	0	2.666667	0.166667	1	2.333333	0	0.166667	0	0.166667	0.666667	0.166667	0.333333	0
4	0.833333	0.527778	1	0.916667	0.833333	0.541667	0.916667	0.625	0.611111	1	1	1	0.916667	0.666667	1	0.75	1
5	1	0.611111	1	1	1	0.708333	0.833333	0.722222	0.444444	1	1	0.916667	1	0.638889	1	0.916667	1
6	1	0.666667	1	1	1	0.513889	0.916667	0.722222	0.680556	1	0.916667	1	0.916667	0.666667	0.916667	0.833333	1
7	0.666667	0	0	0	0.333333	0.333333	0.333333	0.166667	0	0	0.166667	1	0	0.666667	0.166667	0	0
8	0.833333	0.166667	0	0.166667	0.166667	0.333333	0.166667	0	0.166667	0.166667	0.166667	0.833333	0	0.5	0	0	0
9	1.5	0	0	0	0.5	0.166667	0.333333	0.5	0	0.166667	0.5	0.666667	0.166667	0.5	0	0	0.333333
10	0.666667	1	1	1	0.833333	0.833333	0.833333	0.916667	1	1	0.916667	0.722222	1	0.666667	0.916667	1	1
11	0.805556	0.916667	1	0.916667	0.916667	0.833333	0.916667	1	0.916667	0.916667	0.916667	0.805556	1	0.75	1	1	1
12	0.694444	1	1	1	0.75	0.916667	0.833333	0.75	1	0.916667	0.75	0.666667	0.916667	0.75	1	1	0.833333
13	0.833333	0.166667	0	0.5	0.166667	0.666667	0.333333	0.333333	0.333333	1.5	0.166667	1.333333	0.666667	0.5	0	0	0
14	0.833333	0.333333	0	0.5	0.166667	0.5	0.333333	0.333333	0.166667	0.833333	0.166667	1.833333	0.666667	0.166667	0	0	0
15	0.833333	0.166667	0	0.833333	0	0	0.333333	0.166667	0	2	0.333333	1.833333	1.333333	0.333333	0.166667	0	0
16	0.583333	0.916667	1	0.75	0.916667	0.666667	0.833333	0.833333	0.833333	0.472222	0.916667	0.555556	0.666667	0.75	1	1	1
17	0.583333	0.833333	1	0.75	0.916667	0.75	0.833333	0.833333	0.916667	0.583333	0.916667	0.527778	0.666667	0.916667	1	1	1
18	0.583333	0.916667	1	0.805556	1	1	0.833333	0.916667	1	0.444444	0.833333	0.527778	0.555556	0.833333	0.916667	1	1
19	0.166667	1.166667	0.166667	0.333333	0	0.166667	1	0.666667	0	0.666667	0.5	0	0.166667	0.333333	0.333333	0.166667	0
20	0	1.666667	0.166667	0.333333	0	0.5	0.833333	1.166667	0	0.5	0.5	0	0	0.333333	0.333333	0.166667	0
21	0.333333	1.833333	0.333333	0.5	0.166667	0.166667	1	0.333333	0	0.333333	0.5	0.166667	0	0.5	0.166667	0.166667	0.333333
22	0.916667	0.638889	0.916667	0.833333	1	0.916667	0.5	0.666667	1	0.666667	0.75	1	0.916667	0.833333	0.833333	0.916667	1
23	1	0.611111	0.916667	0.833333	1	0.75	0.583333	0.638889	1	0.75	0.75	1	1	0.833333	0.833333	0.916667	1

24	0.833333	0.708333	0.833333	0.75	0.916667	0.916667	0.5	0.833333	1	0.833333	0.75	0.916667	1	0.75	0.916667	0.916667	0.833333
25	0.333333	0.166667	0	0.5	0.333333	1.833333	0.5	0.333333	0.166667	0	0	0.166667	0.166667	2.333333	0	0.166667	0
26	0.166667	0.166667	0	1	0.333333	0.833333	0.5	0.333333	0.333333	0.166667	0	0.166667	0.166667	2.166667	0.166667	0.166667	0
27	0.333333	0.333333	0	1.166667	0.333333	1.166667	0.333333	0.166667	0.166667	0.333333	0.333333	0.166667	0	3	0	0	0.166667
28	0.833333	0.916667	1	0.75	0.833333	0.527778	0.75	0.833333	0.916667	1	1	0.916667	0.916667	0.5	1	0.916667	1
29	0.916667	0.916667	1	0.722222	0.833333	0.583333	0.75	0.833333	0.833333	0.916667	1	0.916667	0.916667	0.583333	0.916667	0.916667	1
30	0.833333	0.833333	1	0.638889	0.833333	0.638889	0.833333	0.916667	0.916667	0.833333	0.833333	0.916667	1	0.388889	1	1	0.916667
31	0	0.333333	0	0	0.166667	0.166667	0.5	1.5	0.666667	0	0	0.166667	0	1	0.166667	0	0
32	0	0.333333	0	0	0.5	0.333333	0.333333	0.833333	0.5	0	0	0	0	0.333333	0	0	0
33	0	0.166667	0	0	0.166667	0.333333	0.5	1.833333	0.333333	0	0	0.333333	0.333333	1	0.166667	0	0
34	1	0.833333	1	1	0.916667	0.916667	0.75	0.694444	0.666667	1	1	0.916667	1	0.722222	0.916667	1	1
35	1	0.833333	1	1	0.75	0.833333	0.833333	0.583333	0.75	1	1	1	1	0.833333	1	1	1
36	1	0.916667	1	1	0.916667	0.833333	0.75	0.527778	0.833333	1	1	0.833333	0.833333	0.722222	0.916667	1	1
37	0.333333	0.666667	0	0	0	0.5	0	1.5	0	0	0.166667	0.5	0	1.333333	0	0.166667	0.166667
38	0.333333	0.333333	0	0	0.333333	0.333333	0	1.5	0	0	0.166667	0.166667	0	0.833333	0	0.166667	0.166667
39	0	0.666667	0	0	0	0.333333	0.333333	1	0.5	0.166667	0	0.166667	0.166667	2.333333	0.333333	0	0
40	0.833333	0.666667	1	1	1	0.75	1	0.694444	1	1	0.916667	0.75	1	0.555556	1	0.916667	0.916667
41	0.833333	0.833333	1	1	0.833333	0.833333	1	0.694444	1	1	0.916667	0.916667	1	0.583333	1	0.916667	0.916667
42	1	0.666667	1	1	1	0.833333	0.833333	0.722222	0.75	0.916667	1	0.916667	0.916667	0.5	0.833333	1	1
43	0.5	0.5	0	0	0	0.333333	0.666667	0.666667	0.333333	0	0	0.166667	0	0.666667	0.166667	0.333333	0.333333
44	0.666667	0.5	0	0	0.333333	0.666667	0.333333	1	0.5	0	0.333333	0.333333	0	0.333333	0.333333	0.333333	0.166667
45	0.166667	0.5	0	0	0	0.666667	0.5	0.666667	0	0.166667	0	0	0	0.833333	0	0.166667	0
46	0.75	0.75	1	1	1	0.833333	0.666667	0.888889	0.833333	1	1	0.916667	1	0.666667	0.916667	0.833333	0.833333
47	0.666667	0.75	1	1	0.833333	0.666667	0.833333	0.722222	0.75	1	0.833333	0.833333	1	0.833333	0.833333	0.833333	0.916667
48	0.916667	0.75	1	1	1	0.666667	0.75	0.888889	1	0.916667	1	1	1	0.805556	1	0.916667	1
49	0.166667	0	0	0	0	0.666667	3	1	0	0.333333	1.333333	0.5	0	1.333333	0	0.166667	0
50	0	0.166667	0	0	0.166667	0	2	1	0	0.666667	1.166667	0.5	0	0.166667	0.5	0.166667	0.333333
51	0.5	0.166667	0	0	0	0.666667	3	1.166667	0	0.5	1.333333	0.5	0	0.666667	0.166667	0	0
52	0.916667	1	1	1	1	0.666667	0.388889	0.722222	1	0.833333	0.555556	0.75	1	0.555556	1	0.916667	1
53	1	0.916667	1	1	0.916667	1	0.444444	0.722222	1	0.666667	0.638889	0.75	1	0.916667	0.75	0.916667	0.833333

54	0.75	0.916667	1	1	1	0.666667	0.388889	0.638889	1	0.75	0.555556	0.75	1	0.666667	0.916667	1	1
55	0	1.166667	0	0.333333	0	0.166667	0.166667	0.333333	0.833333	0	0.166667	0	0	0.333333	0	0	0
56	0	1.166667	0	0.333333	0	0.166667	0.166667	0.166667	0.833333	0.333333	0.166667	0	0	0.666667	0	0.333333	0.166667
57	0.333333	1.833333	0	0.5	0.166667	0.166667	0	0.833333	1	0.333333	0.166667	0	0.166667	1.166667	0.333333	0	0.166667
58	1	0.638889	1	0.833333	1	0.916667	0.916667	0.833333	0.805556	1	0.916667	1	1	0.833333	1	1	1
59	1	0.638889	1	0.833333	1	0.916667	0.916667	0.916667	0.583333	0.833333	0.916667	1	1	0.666667	1	0.833333	0.916667
60	0.833333	0.527778	1	0.75	0.916667	0.916667	1	0.583333	0.722222	0.833333	0.916667	1	0.916667	0.638889	0.833333	1	0.916667
61	0.666667	0	0	0	0.333333	0.333333	0.333333	0.166667	0	0	0.166667	1	0	0.666667	0.166667	0	0
62	0.833333	0.166667	0	0.166667	0.166667	0.333333	0.166667	0	0.166667	0.166667	0.166667	0.833333	0	0.5	0	0	0
63	1.5	0	0	0	0.5	0.166667	0.333333	0.5	0	0.166667	0.5	0.666667	0.166667	0.5	0	0	0.333333
64	0.666667	1	1	1	0.833333	0.833333	0.833333	0.916667	1	1	0.916667	0.722222	1	0.666667	0.916667	1	1
65	0.805556	0.916667	1	0.916667	0.916667	0.833333	0.916667	1	0.916667	0.916667	0.916667	0.805556	1	0.75	1	1	1
66	0.694444	1	1	1	0.75	0.916667	0.833333	0.75	1	0.916667	0.75	0.666667	0.916667	0.75	1	1	0.833333
67	0.833333	0.166667	0	0.5	0.166667	0.666667	0.333333	0.333333	0.333333	1.5	0.166667	1.333333	0.666667	0.5	0	0	0
68	0.833333	0.333333	0	0.5	0.166667	0.5	0.333333	0.333333	0.166667	0.833333	0.166667	1.833333	0.666667	0.166667	0	0	0
69	0.833333	0.166667	0	0.833333	0	0	0.333333	0.166667	0	2	0.333333	1.833333	1.333333	0.333333	0.166667	0	0
70	0.583333	0.916667	1	0.75	0.916667	0.666667	0.833333	0.833333	0.833333	0.472222	0.916667	0.555556	0.666667	0.75	1	1	1
71	0.583333	0.833333	1	0.75	0.916667	0.75	0.833333	0.833333	0.916667	0.583333	0.916667	0.527778	0.666667	0.916667	1	1	1
72	0.583333	0.916667	1	0.805556	1	1	0.833333	0.916667	1	0.444444	0.833333	0.527778	0.555556	0.833333	0.916667	1	1
73	0.166667	1.166667	0.166667	0.333333	0	0.166667	1	0.666667	0	0.666667	0.5	0	0.166667	0.333333	0.333333	0.166667	0
74	0	1.666667	0.166667	0.333333	0	0.5	0.833333	1.166667	0	0.5	0.5	0	0	0.333333	0.333333	0.166667	0
75	0.333333	1.833333	0.333333	0.5	0.166667	0.166667	1	0.333333	0	0.333333	0.5	0.166667	0	0.5	0.166667	0.166667	0.333333
76	0.916667	0.638889	0.916667	0.833333	1	0.916667	0.5	0.666667	1	0.666667	0.75	1	0.916667	0.833333	0.833333	0.916667	1
77	1	0.611111	0.916667	0.833333	1	0.75	0.583333	0.638889	1	0.75	0.75	1	1	0.833333	0.833333	0.916667	1
78	0.833333	0.708333	0.833333	0.75	0.916667	0.916667	0.5	0.833333	1	0.833333	0.75	0.916667	1	0.75	0.916667	0.916667	0.833333
79	0.333333	0.166667	0	0.5	0.333333	1.833333	0.5	0.333333	0.166667	0	0	0.166667	0.166667	2.333333	0	0.166667	0
80	0.166667	0.166667	0	1	0.333333	0.833333	0.5	0.333333	0.333333	0.166667	0	0.166667	0.166667	2.166667	0.166667	0.166667	0
81	0.333333	0.333333	0	1.166667	0.333333	1.166667	0.333333	0.166667	0.166667	0.333333	0.333333	0.166667	0	3	0	0	0.166667
82	0.833333	0.916667	1	0.75	0.833333	0.527778	0.75	0.833333	0.916667	1	1	0.916667	0.916667	0.5	1	0.916667	1
83	0.916667	0.916667	1	0.722222	0.833333	0.583333	0.75	0.833333	0.833333	0.916667	1	0.916667	0.916667	0.583333	0.916667	0.916667	1

84	0.833333	0.833333	1	0.638889	0.833333	0.638889	0.833333	0.916667	0.916667	0.833333	0.833333	0.916667	1	0.388889	1	1	0.916667
85	0	0.333333	0	0	0.166667	0.166667	0.5	1.5	0.666667	0	0	0.166667	0	1	0.166667	0	0
86	0	0.333333	0	0	0.5	0.333333	0.333333	0.833333	0.5	0	0	0	0	0.333333	0	0	0
87	0	0.166667	0	0	0.166667	0.333333	0.5	1.833333	0.333333	0	0	0.333333	0.333333	1	0.166667	0	0
88	1	0.833333	1	1	0.916667	0.916667	0.75	0.694444	0.666667	1	1	0.916667	1	0.722222	0.916667	1	1
89	1	0.833333	1	1	0.75	0.833333	0.833333	0.583333	0.75	1	1	1	1	0.833333	1	1	1
90	1	0.916667	1	1	0.916667	0.833333	0.75	0.527778	0.833333	1	1	0.833333	0.833333	0.722222	0.916667	1	1
91	0.333333	0.666667	0	0	0	0.5	0	1.5	0	0	0.166667	0.5	0	1.333333	0	0.166667	0.166667
92	0.333333	0.333333	0	0	0.333333	0.333333	0	1.5	0	0	0.166667	0.166667	0	0.833333	0	0.166667	0.166667
93	0	0.666667	0	0	0	0.333333	0.333333	1	0.5	0.166667	0	0.166667	0.166667	2.333333	0.333333	0	0
94	0.833333	0.666667	1	1	1	0.75	1	0.694444	1	1	0.916667	0.75	1	0.555556	1	0.916667	0.916667
95	0.833333	0.833333	1	1	0.833333	0.833333	1	0.694444	1	1	0.916667	0.916667	1	0.583333	1	0.916667	0.916667
96	1	0.666667	1	1	1	0.833333	0.833333	0.722222	0.75	0.916667	1	0.916667	0.916667	0.5	0.833333	1	1
97	0.5	0.5	0	0	0	0.333333	0.666667	0.666667	0.333333	0	0	0.166667	0	0.666667	0.166667	0.333333	0.333333
98	0.666667	0.5	0	0	0.333333	0.666667	0.333333	1	0.5	0	0.333333	0.333333	0	0.333333	0.333333	0.333333	0.166667
99	0.166667	0.5	0	0	0	0.666667	0.5	0.666667	0	0.166667	0	0	0	0.833333	0	0.166667	0
100	0.75	0.75	1	1	1	0.833333	0.666667	0.888889	0.833333	1	1	0.916667	1	0.666667	0.916667	0.833333	0.833333
101	0.666667	0.75	1	1	0.833333	0.666667	0.833333	0.722222	0.75	1	0.833333	0.833333	1	0.833333	0.833333	0.833333	0.916667
102	0.916667	0.75	1	1	1	0.666667	0.75	0.888889	1	0.916667	1	1	1	0.805556	1	0.916667	1
103	0.166667	0	0	0	0	0.666667	3	1	0	0.333333	1.333333	0.5	0	1.333333	0	0.166667	0
104	0	0.166667	0	0	0.166667	0	2	1	0	0.666667	1.166667	0.5	0	0.166667	0.5	0.166667	0.333333
105	0.5	0.166667	0	0	0	0.666667	3	1.166667	0	0.5	1.333333	0.5	0	0.666667	0.166667	0	0
106	0.916667	1	1	1	1	0.666667	0.388889	0.722222	1	0.833333	0.555556	0.75	1	0.555556	1	0.916667	1
107	1	0.916667	1	1	0.916667	1	0.444444	0.722222	1	0.666667	0.638889	0.75	1	0.916667	0.75	0.916667	0.833333
108	0.75	0.916667	1	1	1	0.666667	0.388889	0.638889	1	0.75	0.555556	0.75	1	0.666667	0.916667	1	1
109	0.166667	0.333333	0	0.166667	0.166667	0.5	0.666667	0.333333	0	0	0.5	0	0	1.5	0	0	0
110	0	0.166667	0	0	0	0.833333	0.166667	0.166667	0	0	0.5	0	0.333333	1.333333	0	0	0
111	0	0.5	0	0.333333	0.333333	0.5	0	0.333333	0	0.166667	0	0	0	2.333333	0.333333	0	0.333333
112	0.916667	0.833333	1	0.916667	0.916667	0.75	0.666667	0.833333	1	1	0.75	1	1	0.472222	1	1	1
113	1	0.916667	1	1	1	0.583333	0.916667	0.916667	1	1	0.75	1	0.833333	0.555556	1	1	1

## Appendix-IV

### SVM Classifier Network- Support Vector of Features

#### 1. SVM generated training database by Vegetation Index-NDVI

<b>Building</b> <i>(Class 1)</i>	<b>SVM Training Data</b>	<b>Road (1,2)</b>	<b>Soil (1,3)</b>	<b>Trees (1,4)</b>	<b>Vegetation (1,5)</b>
	<b>Support Vector</b>	247	151	21	251
	<b>Class Labels</b>	492	358	605	630
<b>Road</b> <i>(Class 2)</i>	<b>SVM Training Data</b>	<b>Building (2,1)</b>	<b>Soil (2,3)</b>	<b>Trees (2,4)</b>	<b>Vegetation (2,5)</b>
	<b>Support Vector</b>	247	196	248	213
	<b>Class Labels</b>	492	302	549	574
<b>Soil</b> <i>(Class 3)</i>	<b>SVM Training Data</b>	<b>Building (3,1)</b>	<b>Road (3,2)</b>	<b>Trees (3,4)</b>	<b>Vegetation (3,5)</b>
	<b>Support Vector</b>	151	196	209	201
	<b>Class Labels</b>	358	302	415	440
<b>Tree</b> <i>(Class 4)</i>	<b>SVM Training Data</b>	<b>Building (4,1)</b>	<b>Road (4,2)</b>	<b>Soil (4,3)</b>	<b>Vegetation (4,5)</b>
	<b>Support Vector</b>	359	248	209	394
	<b>Class Labels</b>	605	549	415	687
<b>Vegetation</b> <i>(Class 5)</i>	<b>SVM Training Data</b>	<b>Building (5,1)</b>	<b>Road (5,2)</b>	<b>Soil (5,3)</b>	<b>Trees (5,4)</b>
	<b>Support Vector</b>	252	213	201	394
	<b>Class Labels</b>	630	574	440	687

## **2. SVM generated training database by Textural Features**

<b><i>Building</i></b> <b><i>(Class 1)</i></b>	<b>SVM Training Data</b>	<b>Road (1,2)</b>	<b>Soil (1,3)</b>	<b>Trees (1,4)</b>	<b>Vegetation (1,5)</b>
	<b>Support Vector</b>	290	163	413	420
	<b>Class Labels</b>	492	358	605	630
<b><i>Road</i></b> <b><i>(Class 2)</i></b>	<b>SVM Training Data</b>	<b>Building (2,1)</b>	<b>Soil (2,3)</b>	<b>Trees (2,4)</b>	<b>Vegetation (2,5)</b>
	<b>Support Vector</b>	392	142	281	456
	<b>Class Labels</b>	492	302	549	574
<b><i>Soil</i></b> <b><i>(Class 3)</i></b>	<b>SVM Training Data</b>	<b>Building (3,1)</b>	<b>Road (3,2)</b>	<b>Trees (3,4)</b>	<b>Vegetation (3,5)</b>
	<b>Support Vector</b>	174	173	256	150
	<b>Class Labels</b>	358	302	415	440
<b><i>Tree</i></b> <b><i>(Class 4)</i></b>	<b>SVM Training Data</b>	<b>Building (4,1)</b>	<b>Road (4,2)</b>	<b>Soil (4,3)</b>	<b>Vegetation (4,5)</b>
	<b>Support Vector</b>	280	281	256	449
	<b>Class Labels</b>	605	549	415	687
<b><i>Vegetation</i></b> <b><i>(Class 5)</i></b>	<b>SVM Training Data</b>	<b>Building (5,1)</b>	<b>Road (5,2)</b>	<b>Soil (5,3)</b>	<b>Trees (5,4)</b>
	<b>Support Vector</b>	420	390	253	346
	<b>Class Labels</b>	630	574	440	687



### **3. SVM generated training database by MBI**

<b><i>Building</i></b> <b><i>(Class 1)</i></b>	<b>SVM Training Data</b>	<b>Road (1,2)</b>	<b>Soil (1,3)</b>	<b>Trees (1,4)</b>	<b>Vegetation (1,5)</b>
	<b>Support Vector</b>	92	166	385	137
	<b>Class Labels</b>	492	358	605	630
<b><i>Road</i></b> <b><i>(Class 2)</i></b>	<b>SVM Training Data</b>	<b>Building (2,1)</b>	<b>Soil (2,3)</b>	<b>Trees (2,4)</b>	<b>Vegetation (2,5)</b>
	<b>Support Vector</b>	282	203	310	288
	<b>Class Labels</b>	492	302	549	574
<b><i>Soil</i></b> <b><i>(Class 3)</i></b>	<b>SVM Training Data</b>	<b>Building (3,1)</b>	<b>Road (3,2)</b>	<b>Trees (3,4)</b>	<b>Vegetation (3,5)</b>
	<b>Support Vector</b>	199	203	253	245
	<b>Class Labels</b>	358	302	415	440
<b><i>Tree</i></b> <b><i>(Class 4)</i></b>	<b>SVM Training Data</b>	<b>Building (4,1)</b>	<b>Road (4,2)</b>	<b>Soil (4,3)</b>	<b>Vegetation (4,5)</b>
	<b>Support Vector</b>	382	310	253	357
	<b>Class Labels</b>	605	549	415	687
<b><i>Vegetation</i></b> <b><i>(Class 5)</i></b>	<b>SVM Training Data</b>	<b>Building (5,1)</b>	<b>Road (5,2)</b>	<b>Soil (5,3)</b>	<b>Trees (5,4)</b>
	<b>Support Vector</b>	298	288	245	357
	<b>Class Labels</b>	630	574	440	687

## ***Biodata***

**Rubeena** was born on 11<sup>th</sup> August 1981 in Ludhiana (Punjab), India. She received her B.Tech degree in Electronics and Communication Engineering from Lala Lajpat Rai Institute of Engineering and Technology, Punjab Technical University, Jalandhar in 2003. She topped the four years course of Engineering and was awarded with Topper Certificate. She received her M.Tech degree in Electronics and Communication Engineering from Indira Gandhi Institute of Technology, Guru Gobind Singh Indraprastha University, New Delhi in 2011. She was awarded with a Gold Medal for securing first position during her course. She holds the position of Assistant Professor in Department of Electronics and Communication Engineering at Bharati Vidyapeeth's College of Engineering since 2009. She joined Delhi Technological University, New Delhi as part time Ph.D Scholar in Civil Engineering Department under the supervision of Dr. K.C. Tiwari in 2013. Her research focuses on multisource data fusion strategies for improvement in classification /extraction of urban objects.